SOIL HYDRIC-SALINE BALANCE IN MANGROVE SWAMP RICE IN GUINEA BISSAU

JUAN GABRIEL GARBANZO LEÓN

SCIENTIFIC ADVISORS:

Professor Ph.D. Maria do Rosário da Conceição Cameira

Professor Ph.D. Paula Cristina Santana Paredes

Ph.D. Tiago Cunha Brito Ramos

THESIS PRESENTED TO OBTAIN THE DOCTORAL DEGREE IN SUSTAINABLE LAND USE, **specialty ENVIRONMENTAL SCIENCE AND ENGINEERING**

2025

SOIL HYDRIC-SALINE BALANCE IN MANGROVE SWAMP RICE IN GUINEA BISSAU

JUAN GABRIEL GARBANZO LEÓN

SCIENTIFIC ADVISORS:

Professor Ph.D. Maria do Rosário da Conceição Cameira
Professor Ph.D. Paula Cristina Santana Paredes
Ph.D. Tiago Cunha Brito Ramos

THESIS PRESENTED TO OBTAIN THE DOCTORAL DEGREE IN SUSTAINABLE LAND USE, **specialty ENVIRONMENTAL SCIENCE AND ENGINEERING**

Jury:

President:

Doutor Carlos Manuel Antunes Lopes, Professor Associado com Agregação do(a) Instituto Superior de Agronomia da Universidade de Lisboa.

Members:

Doutora Maria da Conceição Pinto Baptista Gonçalves, Investigadora Coordenadora do(a) Instituto Nacional de Investigação Agrária e Veterinária, I.P.

Doutor Mário Manuel de Miranda Furtado Campos Cunha, Professor Associado com Agregação do(a) Faculdade de Ciências da Universidade do Porto;

Doutor José Manuel Monteiro Gonçalves, Professor Coordenador Principal do(a) Escola Superior Agrária do Instituto Politécnico de Coimbra;

Doutora Marina Augusta Pereira Padrão Temudo, Investigadora Auxiliar com Agregação do(a) Instituto Superior de Agronomia da Universidade de Lisboa;

Doutora Paula Cristina Santana Paredes, Professora Auxiliar do(a) Instituto Superior de Agronomia da Universidade de Lisboa, orientadora.

Financial Institutions:

European Commission through the DeSIRA Program "Mangroves, mangrove rice and mangrove people: sustainably improving rice production, ecosystems and livelihoods" (Grant Contract FOOD/2019/412-700).
Fundação para a Ciência e a Tecnologia, I.P. (FCT) through the project UIDB/04129/2020 of LEAF - Linking Landscape, Environment, Agriculture and Food.
University of Costa Rica

2025

Acknowledgments

Completing this doctoral thesis has been a long journey, filled with challenges, concerns, moments of demotivation, and numerous obstacles. However, this achievement would not have been possible without the support of many individuals, to whom I would like to express my deepest gratitude.

First and foremost, I want to express my heartfelt gratitude to my family, who have always provided me with unwavering support. I am incredibly thankful for my beloved mother, Auxiliadora, as well as Isabel, Lucía, Leiner, Rodolfo, Claudia, Jaime, and Adila, for teaching me the importance of hard work and perseverance, values that have become the foundation of my long academic journey. I would also like to thank my late father, Jesús, who inspired me to strive for this goal. Then, I dedicate this achievement to my bases of inspiration: Saúl, Mila, Levi, Eric, and Luna, who have been a constant light source in my life.

I am deeply grateful to Professor Marina Temudo, the principal investigator of this project, for giving me the opportunity to participate in this research. Her valuable recommendations and ideas were instrumental in the development of this thesis. I would also like to thank Professor Ramon Sarro, his help and kindness were truly important in this process. I would also like to thank Professor Sjoerd E.A.T.M. van der Zee, who welcomed me on this significant project and guided me through the conceptualization of this work. May he rest in peace.

I want to express my heartfelt gratitude to my advisors, Professor María do Rosario Cameira, Professor Paula Paredes, and Doctor Tiago Ramos. Thank you for your insightful ideas, patience, and unwavering support throughout every stage of this process. Your valuable suggestions and the trust you placed in my abilities have been essential to the success of this project. Thank you to Professor Paul Struik for his support at Wageningen University, as well as to Harm Gooren, Tang Darrell, and Professor Coen Ritsema for their help in the Soil Hydro Physics Laboratory.

I am genuinely grateful to my friends Jesús Céspedes, Merlin Leunda, and Filipa Zacarias for their continuous communication and support throughout every phase of this work. Your advice and friendship have been invaluable, significantly

contributing to various aspects of the research. Your collaboration and companionship have made this journey much more enriching and motivating.

I want to express my gratitude to the research team and my colleagues: Orlando Mendes, Matilda Merkohasanaj, Viriato Cossa, Joseph Sandoval, Sofia Conde, Giovanni Maucieri, Eduino Mendes, Adriano Barbosa, Alqueia Intchama, Adinane Jalo, Paulina, Poncho, Ronny, Emilio, and Suliman. Thank you all for your dedication and the countless hours working together, laying the groundwork for many of the ideas developed during this journey. Your support, both in the Tabancas and field, and willingness to share knowledge were essential throughout this stage.

A special thanks also goes to my dear friends Daniela Soares, Antonia Ferreira, Daniel García, Razieh Ebadati, Eric Sequeira, Sebastián Sanders, Cassio Ferrazza, Vanessa de Arruda, Diogo Pinto, Diogo Simão, Luis Catarino and from the Department of Rural Engineering, as well as to Henry Mavisoy. Thank you for your constant motivation during the countless hours we spent writing articles together, and for the many smiles and memorable moments we shared. Also, my colleagues in Costa Rica; Luis Cordero, Karol Cordero, Sisgo Acuña, Victor Carmona, Manuel Zuñiga, Roger Fallas, Bryan Aleman, Claudio Vargas, Manuel Camacho, Mario Villatoro, Juan Carlos Méndez, Michael Gonzáles, María Fernanda Campos, Patricia Gutiérrez and Karol Espinoza who have been supported me in several processes throughout this Ph.D.

Also, I would like to express my sincere gratitude to the staff of the Academic Division, especially Catarina Cruz and Maria do Carmo Alves, for their dedication and assistance. Their professionalism and kindness have been deeply appreciated throughout this process.

Lastly, I would like to dedicate this thesis to all the mangrove swamp rice farmers (https://www.malmon-desira.com/farmer-researchers) who have accompanied me on this journey in various ways. Thank you for trusting me, your support, the meals you provided, and being by my side during every task we undertook together. To all of you, I express my deepest gratitude.

Resumo

Esta tese, desenvolvida no âmbito do projeto europeu "Mangroves, Mangrove Rice, and Mangrove People", visou a caracterização do cultivo de arroz nos ecossistemas de mangal da Guiné-Bissau, onde a segurança alimentar depende de sistemas agrícolas muito sensíveis à variabilidade climática e às condições de salinidade dos solos. O objetivo principal foi quantificar o balanço hídrico-salino nesses sistemas de produção de arroz, visando melhorar as práticas de gestão do solo, da água e da cultura. Para tal, aplicaram-se metodologias interdisciplinares, incluindo ensaios de campo, entrevistas sobre conhecimentos locais, amostragem e análise de solos, caracterização biofísica, modelação geoespacial, utilização de índices de vegetação, técnicas de aprendizagem automática, estimativas da evapotranspiração de referência (ET_o) em condições de escassez de dados, dados meteorológicos usando, observações ou de reanálise (AgERA5, MERRA-2), e simulações das dinâmicas hídrico-salinas com HYDRUS-1D. Os resultados revelaram maior eficiência na captação de água da chuva no norte (16%) em comparação com o sul (15%), bem como condições ótimas de plasticidade do solo para mobilização em Elalab (18,6%) e Cafine-Cafal (35,5%). As zonas salinas foram mapeadas com um conjunto de índices incluindo o *normalized difference salinity index* (RNDSI), o *normalized salinity index* (NDSI), *normalized difference water index* (NDWI), e o índice de textura (Limo), com o modelo Random Forest a apresentar a maior precisão preditiva (RMSE = 25,49 dS m^{-1}). A aproximação simplificada baseada nos dados de temperatura para estimar a ET_o demonstrou maior precisão (RMSE < 26%), do que a utilização dos dados de reanálise, mesmo quando após correção de viés. A modelação hídrico-salina permitiu estimar os impactos potenciais a salinidade na produtividade do arroz, que poderão levar a reduções de até 60%. Concluiu-se que os fatores-chave no controlo da salinidade no solo são a quantidade da precipitação sazonal, a profundidade do nível freático e a qualidade da água subterrânea. Este estudo oferece uma base técnica sólida para apoio à produção de arroz de mangal, destacando a necessidade de inovação na infraestrutura hídrica e conservação ecológica perante as alterações climáticas.

Palavras-chave: Adaptação climática, salinização do solo, produção sustentável, aprendizagem automática, modelação.

Abstract

This thesis, developed within the framework of the European project "Mangroves, Mangrove Rice, and Mangrove People," focused the characterization of the rice cultivation in the mangrove ecosystems of Guinea-Bissau, where food security relies on agricultural systems highly sensitive to climate variability and hypersaline soil conditions. The main objective of the study was to quantify the hydro-saline balances within the mangrove rice production system, aiming to improve soil, water, and crop management practices. To achieve this, a range of interdisciplinary methodologies were applied, including field trials, interviews on indigenous knowledge and technological innovation, soil sampling and analysis, biophysical characterization, geospatial modeling, the use of vegetation indices, machine learning techniques, estimating reference evapotranspiration (ET_o) under data-scarce conditions, using observed, meteorological variables or reanalysis datasets (AgERA5, MERRA-2), and hydro-saline dynamic simulations using HYDRUS-1D. The results revealed more efficient rainwater harvesting in the north (16%) compared to the south (15%), along with optimal soil plasticity conditions for tillage in Elalab (18.6%) and Cafine-Cafal (35.5%). Saline zones were mapped using normalized difference salinity index (RNDSI), normalized salinity index (NDSI), normalized difference water index (NDWI) indices, and Silt texture, with Random Forest achieving the highest predictive accuracy (RMSE = 25.49 dS m^{-1}). The temperature-based approach for ET_o estimation showed higher accuracy (RMSE < 26%) than either reanalysis data set even after a bias correction was applied. Hydro-saline modeling enabled the estimation of potential impacts on rice yields, which could decline by up to 60%. It was concluded that the key factors for soil salinity control included the amount and distribution of seasonal rainfall, groundwater depth, and groundwater quality. This study provides a solid technical background for more resilient rice production in mangrove agroecosystems, highlighting the urgent need for innovation in water infrastructure and ecological conservation in the face of climate change.

Keywords: Climate adaptation, Soil Salinization, Sustainable production, Machine-Learning, Modeling.

Resumen

Esta tesis, enmarcada en el proyecto europeo *"Mangroves, Mangrove Rice, and Mangrove People"*, analizó el balance hídrico-salino del cultivo de arroz en manglares de Ginea-Bissau, donde la seguridad alimentaria depende de sistemas agrícolas altamente sensibles a la variabilidad climática y a las condiciones de los suelos. El objetivo principal fue cuantificar el balance hídrico-salino dentro del sistema de producción de arroz en zonas de manglar, con el fin de mejorar las prácticas de manejo del suelo, del agua y del cultivo. Para ello, se emplearon diversas metodologías interdisciplinarias, incluyendo ensayos en campo, análisis de suelos, caracterización biofísica, modelado geoespacial, uso de índices satelitales, técnicas de aprendizaje automático, estimación de la evapotranspiración de referencia del cultivo (ET_o) en condiciones de escasez de datos, uso de reanálisis (AgERA5, MERRA-2) y simulaciones de dinámicas hídrico-salinas mediante HYDRUS-1D. Los resultados mostraron una eficiente recolección de agua de lluvia en el norte (16 %) en comparación con el sur (15 %), con condiciones de plasticidad óptimas de labranza en Elalab (18.6 %) y Cafine-Cafal (35.5 %). Los índices normalized difference salinity index (RNDSI), normalized salinity index (NDSI), normalized difference water index (NDWI) índices, y el limo permitieron mapear las zonas salinas utilizando Random Forest (RMSE = 25.49 dS m^{-1}). La aproximación simplificada con base a los datos de temperatura para estimar la ET_o, demostró mayor precisión (RMSE < 26 %) que la utilización de los datos de reanálisis, mismo cuando fue aplicado una corrección por sesgo (Bias). El modelado hídrico-salino permitió identificar los posibles impactos sobre los rendimientos de los cultivos, los cuales podrían disminuir hasta en un 60 %. Se concluye que los factores clave en el control de la salinidad del suelo fueron la cantidad y distribución de las lluvias estacionales, la profundidad del agua subterránea y su calidad. Este estudio proporciona una base técnica sólida para una producción de arroz más resiliente en suelos de manglar, destacando la necesidad de innovación en infraestructura hídrica frente al cambio climático.

Palabras clave: Adaptación Climática, Salinización del Suelo, Producción Sostenible, Aprendizaje Automático, Modelización.

Resumo estendido

Esta tese, faz parte do projeto "Mangroves, Mangrove Rice, and Mangrove People: Sustainably Improving Rice Production Ecosystems and Livelihoods." Este projeto, financiado pela União Europeia, especificamente no âmbito do programa de Inovação Inteligente para o Development Smart Innovation through Research in Agriculture (DeSIRA), visa desenvolver ferramentas e práticas que permitam enfrentar os desafios da produção de arroz em sistemas de mangais na Guiné Bissau.

A produção de arroz nos sistemas de mangal (MSRPS, na sigla em inglês) na Guiné-Bissau (GB) é essencial para a segurança alimentar e nutricional das populações costeiras do país. Este sistema, que é caracterizado pela modificação antropogénica dos solos de mangal, e enfrenta graves desafios devido à variabilidade nos padrões e quantidade de precipitação e ao aumento da salinidade do solo.

Estes fatores afetam negativamente a produtividade do arroz, tornando imprescindível identificar as principais limitações na gestão da água e do solo. Os solos de mangal no país dependem do armazenamento de água doce (proveniente da chuva) para a lavagem dos sais do perfil do solo e tornar as terras produtivas. No entanto, a variabilidade de precipitação tem vindo a diminuir a adequada lixiviação dos sais, afetando o crescimento e produtividade do arroz. A variabilidade climática tem vindo a agravar-se pelas mudanças climáticas, pelo que é vital implementar ferramentas e estratégias que visam para melhorar a eficiência no uso da água e a gestão do solo, essenciais para a sustentabilidade deste sistema agrícola.

Este estudo abordou os desafios da produção de arroz em mangal através de metodologias interdisciplinares que integram a caracterização biofísica do sistema, o diagnóstico da salinidade do solo e a melhoria das práticas de gestão da água.

Como primeira abordagem, foram recolhidas informações meteorológicas e dados sobre a produtividade do arroz, obtidos junto dos Ministérios da Agricultura e da Meteorologia do país, embora com níveis variáveis de precisão. Os documentos analisados estavam redigidos em diversas línguas (inglês, francês, português e espanhol) complementados com entrevistas centradas no conhecimento endógeno e na inovação tecnológica, conduzidas na língua própria dos agricultores (crioulo). Para além da revisão bibliográfica, esta tese integrou investigação empírica, incluindo transeptos realizados

para observações das características morfológicas do solo as quais foram realizados com agricultores, com descrições in situ das diferentes agroecologias dos arrozais.

Seguidamente, realizaram-se amostragens sistemáticas de solo em várias zonas de cultivo e procedeu-se à caracterização biofísica de MSRPS em três aldeias da Guiné-Bissau, utilizadas como estudo de caso. Foram realizadas diversas análises, nomeadamente a medição da consistência/plasticidade dos solos e dos níveis de salinidade. Adicionalmente, recorreram-se a modelos geoespaciais e técnicas de aprendizagem automática (Random Forest, Support Vector Machines, and Convolutional Neural Networks) para elaborar mapas de salinidade dos solos. Estes modelos permitiram identificar áreas hipersalinas, essenciais para melhorar a gestão agrícola e mitigar os efeitos da salinização.

A estimativa das necessidades hídricas das culturas é geralmente realizada utilizando o método dos coeficientes culturais da FAO, que consiste na multiplicação da evapotranspiração de referência (ET_o) por um coeficiente cultural (K_c). O método FAO-PM para o cálculo da ET_o depende de um conjunto de dados meteorológicos, que, em países como a Guiné-Bissau, muitas vezes estão indisponíveis, incompletos ou apresentam qualidade insuficiente, devido à manutenção inadequada dos equipamentos de medição. Esta tese avaliou abordagens alternativas, conforme descrito nas diretrizes revistas do FAO56, para estimar a ET_o utilizando apenas dados de temperatura. Os resultados indicaram que o método Penman-Monteith baseado somente em dados de temperatura (PMT) é geralmente preciso, com um RMSE que não excede 26% da média diária da ET_o. Relativamente à radiação de onda curtao comprimento de onda, a utilização da diferença de temperatura como preditor, em combinação com equações de regressão linear múltipla focadas em agrupamentos (clusters) para estimar o coeficiente de ajustamento da radiação (k_{Rs}), produziu resultados precisos. Além disso, os resultados destacam que o método PMT apresentou estimativas de ET_o mais precisas do que os dados de reanálise provenientes de diferentes fontes (AgERA5 e MERRA2), mesmo após terem sido objeto de uma correção de viés. No entanto, na ausência de dados observados de temperatura, os dados AgERA5 podem ser utilizados com precaução como fonte alternativa, embora seja necessário cautela devido aos erros desvios e incertezas associados à estimativa de ET_o com este produto de reanálise. Estes resultados apresentam uma abordagem prática para melhorar a gestão da água na agricultura em

agroecossistemas tropicais da África Ocidental, especialmente em regiões com acesso limitado a dados meteorológicos fiáveis.

A ET_o é um dos dados de entrada do modelo de fluxos HYDRUS-1D o qual foi usado para simular a dinâmica da salinidade e o balanço hídrico do solo, considerando múltiplos cenários de chuva, a profundidade do nível freático e salinidade de solo, o que ajudou a prever o impacto na produção do arroz.

Os resultados mostram que os níveis de salinidade nas zonas de cultivo de arroz na GB dependem, em grande medida, da quantidade e distribuição das chuvas sazonais, bem como da qualidade e profundidade do lençol freático. As simulações demonstraram que as variações na precipitação e nas profundidades do lençol freático são os principais fatores que contribuem para a salinização do solo, o que, por sua vez, afeta os rendimentos do cultivo de arroz. Por exemplo, registaram-se eficiências de recolha de água da chuva de 15% na região sul e 16% na região norte.

Relativamente aos índices de plasticidade, os valores obtidos foram de 18,6% para Elalab e 35,5% para Cafine-Cafal, em humidade gravimétrica, indicando os momentos ideais para o início das operações de mobilização do solo. Além disso, a utilização de modelos preditivos facilitou a identificação de áreas com elevadas concentrações de salinidade. Por exemplo, o modelo Random Forest demonstrou a maior precisão na previsão da salinidade (R^2 = 0,80, dS m^{-1}, RMSE = 25,49 dS m^{-1}, NRMSE = 51 %), com o índice de salinidade de diferença normalizada (RNDSI, calculado com red edge), evidenciando a sua precisão no mapeamento e previsão de regiões hipersalinas.

Foram também identificadas estratégias eficazes para contrariar os efeitos da salinidade nos MSRPS, incluindo a melhoria da gestão de diques e estruturas de drenagem para evitar a entrada de água salgada durante as épocas de produção de arroz, o uso de variedades de arroz mais tolerantes à salinidade nas zonas mais afetadas, e a adoção de variedades de ciclo longo em áreas com melhores condições hídricas.

O sistema de produção de arroz nos sistemas de mangal no país é altamente dinâmico e complexo, influenciado por vários fatores, incluindo a salinidade do solo, a variabilidade climática e a falta de infraestrutura adequada para a medição e gestão da água. Os resultados obtidos nestas investigações sublinham a importância de implementar tecnologias de diagnóstico de solos e modelos preditivos para otimizar a gestão hídrica e

a eficiência no uso dos recursos naturais. A adoção destas ferramentas permitirá aos agricultores da GB uma primeira abordagem para mitigar os efeitos negativos da salinização no crescimento do arroz, garantindo uma produção de arroz mais sustentável e resiliente face aos impactos das variações nas chuvas, decorrentes das alterações climáticas. É crucial continuar a explorar inovações na infraestrutura de gestão da água e promover a conservação dos mangais, o que contribuirá para a estabilidade ecológica e produtiva do sistema.

No entanto, persistem desafios importantes. As pressões sociais e económicas levam muitas comunidades a expandir as áreas de cultivo para zonas sensíveis, agravando a degradação ambiental e aumentando o risco de falhas produtivas (caso das bolanhas novas). A ausência de mecanismos de compensação pelo governo de GB que sejam adequados para estas populações vulneráveis dificulta a conservação dos serviços ecossistémicos. Além disso, os projetos de desenvolvimento frequentemente carecem de alinhamento com as necessidades reais dos agricultores, resultando em fraca eficácia e pouca sustentabilidade porque trabalham com informações desenvolvidas externas ao país. A escassez de programas de restauração de campos salinizados ou abandonados também compromete a resiliência do sistema. Em sínteses, esta tese faz uma aproximação multidisciplinar donde oferece uma orientação sólida para melhorar a produtividade do sistema de arroz em mangal e apoiar as comunidades costeiras na adaptação às condições climáticas em mudança.

Contents

RESUMO **4**

ABSTRACT 5

RESUMEN 6

RESUMO ESTENDIDO 7

CHAPTER 1 ..... **16**

GENERAL INTRODUCTION 16

1. Introduction *17*

1.1. Context *17*

1.2. Salinity effect in soil and rice yield *19*

1.3. Water and modeling *20*

1.4. Agricultural Resilience to Salinization and Migration *21*

2. Research questions *22*

3. General and specific aims *24*

4. Thesis framework *26*

CHAPTER 2 ..... **31**

MANGROVE SWAMP RICE PRODUCTION SYSTEM OF GUINEA BISSAU: IDENTIFICATION OF MAIN CONSTRAINTS ASSOCIATED WITH SOIL SALINITY AND RAINFALL VARIABILITY ... 31

1. Abstract *32*

2. Introduction *33*

3. Rice production in Guinea Bissau *39*

3.1. Rice production systems in GB *39*

3.2. MSRP and typologies of fields *41*

3.3. Areas and yields *48*

3.4. Rice crop species and varieties *50*

4. Salinity and salt management in the MSRPS in GB *56*

4.1. Base concepts *56*

4.2. Salinity in the bolanhas of MSRPS *59*

4.3. Salinity and water productivity in the MSRPS *63*

5. General soil properties, taxonomy, and topography in MSR fields *68*

5.1. Soil taxonomy in associated - tidal mangrove fields and tidal mangrove terrace *69*

5.2. Acidity formation in tidal mangrove soils. *73*
6. Rainfall patterns and farmers' agronomic practices related to water management in the MSRPS..... *74*
6.1. The use of dikes, bunds and rigdes for water management in the paddies *77*
7. Key issues overview and future research *80*

CHAPTER 3..... **85**

MOVING TOWARD THE BIOPHYSICAL CHARACTERIZATION OF THE MANGROVE SWAMP RICE PRODUCTION SYSTEM IN GUINEA BISSAU: EXPLORING TOOLS TO IMPROVE SOIL- AND WATER-USE EFFICIENCIES 85
1. Abstract..... *86*
2. Introduction *87*
3. Materials and Methods..... *91*
3.1. Location and Main Characteristics of the Study Sites *91*
3.2. Experimental Observations and Data Collection..... *94*
3.3. Data Treatment..... *96*
3.3.1. Water Harvesting Efficiency..... *96*
3.3.2. Soil Consistency and Chemical Analysis..... *97*
3.3.3. Statistical Data Analysis..... *98*
4. Results..... *100*
4.1. Precipitation and Temperature *100*
4.2. Soil Chemical Properties..... *101*
4.3. Effective Planting Areas and Number of Plots..... *103*
4.4. Water-Harvesting Efficiency *104*
4.5. Soil Consistency Limits..... *106*
5. Discussion..... *111*
6. Conclusions *115*

CHAPTER 4..... **117**

ADVANCES IN SOIL SALINITY DIAGNOSIS FOR MANGROVE SWAMP RICE PRODUCTION IN GUINEA BISSAU, WEST AFRICA..... 117
1. Abstract..... *118*
2. Introduction *119*
3. Materials and methods *124*
3.1. Location and main characteristics of the study sites..... *124*

3.2. Field data collection and analysis ... *126*
3.3. Compilation of remote sensing data ... *127*
4. Theory and Calculation ... *128*
4.1. Data preparation and models training ... *130*
5. Results ... *138*
5.1. Soil salinity in the study sites ... *138*
5.2. Selection of salinity predictors ... *141*
5.3. Soil salinity models ... *145*
6. Discussion ... *149*
6.1. Soil salinity and texture in MSRP ... *149*
6.2. Spatial distribution of hypersalinity in MSRP fields ... *152*
6.3. Consideration regarding the utilized model ... *154*
7. Conclusions ... *156*
8. Appendix ... *158*
8.1. Appendix A. Sampling point map and geostatistical analysis and validation for soil texture raster. ... *158*
8.2. Appendix B. Bands and indices used in soil salinity studies. ... *160*
8.3. Appendix D. Confusion matrix of EC_e data with salinity indices and soil texture raster. ... *162*
8.4. Appendix E. Importance of features in modeling. ... *163*
8.5. Appendix F. General computational flow of the CNN ... *164*

CHAPTER 5 ... **165**

ADDRESSING WEATHER DATA GAPS IN REFERENCE CROP EVAPOTRANSPIRATION ESTIMATION: A CASE STUDY IN GUINEA BISSAU, WEST AFRICA ... 165
1. Abstract ... *166*
2. Introduction ... *167*
3. Material and methods ... *171*
3.1. Climate ... *171*
3.2. Data ... *172*
3.2.1. Ground truth weather data ... *172*
3.2.2. Reanalysis weather data ... *173*
3.3. Computation of the FAO-Penman Monteith ET_o ... *175*
3.4. Calculation of ET_o using only temperature data (FAO-PMT) ... *177*

3.5. Data quality assurance and quality checking (QAQC) *180*
3.6. Bias correction of reanalysis-based ET_o estimates *182*
3.7. Accuracy assessment *184*
3.8. Spatial variability of ET_o in Guinea-Bissau *185*
4. Results and discussion *186*
4.1. QAQC assessment *186*
4.2. Meteorological characteristics of the studied sites *188*
4.3. FAO-PM ET_o using temperature data only *191*
4.4. ET_o estimation using different reanalysis datasets *203*
4.5. ET_o mapping *208*
5. Conclusions *210*
6. Supplementary material *212*
6.1. Supplementary S1. Numerical method for deriving the cluster-focused multiple linear regression (MLR) equations to estimate k_{Rs} (Eq. 4) *212*
6.2. Supplementary B. Climate characterization and data QAQC. *213*
6.3. Supplementary C. Goodness of fit indicators and standard deviation for predicting ET_o in sites. *214*
6.4. Supplementary D. Correlation between ET_o estimated with weather observations and with AgeERA5 and MERRA-2 reanalysis data. *217*
6.5. Supplementary E. Spatial distribution of annual ET_o in GB. *219*

CHAPTER 6 ..... **220**

MODELING SOIL WATER AND SALINITY DYNAMICS IN MANGROVE SWAMP RICE PRODUCTION SYSTEM OF GUINEA BISSAU, WEST AFRICA 220
1. Abstract *221*
2. Introduction *222*
3. Material and methods. *226*
3.1. Study area *226*
3.2. Modeling approach *233*
3.2.1. Model description *233*
3.2.2. Model setup, calibration, and validation *235*
3.3. Modeling scenarios *238*
4. Results and discussion *241*
4.1. Model performance *241*

4.2. Salinity impact on rice yields ... *249*
4.3. Rainfall and groundwater depth scenarios ... *253*
4.4. Driving mechanisms for salinity build-up in MSRP ... *261*
4.5. Soil salinity management in MSRP systems ... *263*
5. Conclusions ... *265*
6. Supplementary material ... *266*
6.1. Supplementary A. Sensor Calibration ... *266*
6.2. Supplementary B. Rainfall correction ... *267*
6.3. Supplementary C. Modeling conditions at the Cafine Tidal site. ... *268*
6.4. Supplementary D. Modeling conditions at the Cafine Associated site. ... *269*
6.5. Supplementary B. Modeling conditions at the Elalab Associated site. ... *270*

CHAPTER 7 ... **271**

GENERAL DISCUSSION AND CONCLUSIONS ... 271
7. Discussion ... *272*
7.1. Integrating Chapter Findings: understanding of Soil Properties, Water Management, and Salinity in MSRP ... *272*
7.2. Addressing knowledge Gaps: Spatial variability and salt accumulation in MSRP *277*
7.3. Study limitations and implications for future research in MSRP ... *279*

CONCLUSIONS AND FUTURE RESEARCH ... **281**

REFERENCES LIST ... **285**

References for Chapter 1 ... *285*
References for Chapter 2 ... *288*
References for Chapter 3 ... *301*
References for Chapter 4 ... *308*
References for Chapter 5 ... *323*
References for Chapter 6 ... *335*
References for Chapter 7 ... *343*

Chapter 1

General introduction

1. Introduction

1.1. Context

This thesis was conducted within the framework of the DeSIRA project, a major initiative aimed at improving the sustainably of rice production, preserving mangrove ecosystems, and enhancing the livelihoods of local communities in Guinea-Bissau. Funded by the EU DeSIRA program, a key instrument supporting agricultural research for development (R4D) in the agricultural innovation, the project holds relevance in Guinea-Bissau, where rice production plays a vital role in food security and rural development. The program's financial and institutional support was essential in enabling a research agenda that adopted a problem-solving and participatory approaches, and action-research methodologies.

The PhD research design was developed over several months of immersive fieldwork, during which time the researcher lived and worked alongside farmers in their fields. This close engagement enables an understanding of, and response to, the daily challenges they face in mangrove swamp rice cultivation, a cropping system that is facing major salinity issues, exacerbated by climate change and social transformations that reduce labor availability.

Guinea-Bissau (GB), a small country in West Africa, relies heavily on rice production to ensure the food security, feed its population and balance the economy. There are three main rice production systems in the country: Mangrove Swamp Rice (MSR), Upland (slash-and-burn), and inland valley (lowland freshwater swamp). Additionally, a small area is cultivated under irrigated conditions (Ministry of Natural Resources and Environment, 2006). Rice is the staple food for most of the population’,

with an annual per capita consumption estimated ranging from 91 kg to 136.9 kg (Balasubramanian et al., 2007; Fofana et al., 2014).

Mangrove swamp rice is a distinctive rainfed cropping system that relies exclusively on rainfall both to meet crop water requirements and to leach salts from the rootzone (Écoutin et al., 1999; Espírito-Santo, 1949; Schwarz, 1993; Temudo, 2011). It originates from the slashing of mangrove trees and the construction of dykes to create plots (e.g., Temudo & Cabral, 2017). Thus, it represents the primary driver of mangrove deforestation in Guinea-Bissau (Lourenço et al., 2009; Temudo & Cabral, 2017). Among the West African countries where mangrove swamp rice cultivation is practiced (approximately 200 000 ha), Guinea-Bissau has the largest area occupied (approximately 102 100 ha) by this cropping system (Adefurin & Zwart, 2016; Cormier-Salem, 1999; Temudo, 2011).

This unique agri-fish-livestock farming system relies on the ability to mobilize specialized knowledge, including the construction and maintenance of dikes and dams, water management, controlling of soil fertility and toxicity, selecting appropriate rice varieties, and the availability of substantial labor at key moments in the agricultural cycle. Labor-intensive tasks include clearing the mangrove, constructing dikes and canals, desalinating soil, and preparing it for sowing the rise using a long wooden plow tipped with an iron edge (Temudo, 2011; Van Ghent & Ukkerman, 1993).

This cropping system requires no additional inputs beyond the use of appropriate seeds. However, in some sites pesticides are occasionally applied. Fertilization and weed control are assured through plowing, by cattle roaming while pasturing the rice stubble, as most mangrove swamp rice farmers are also herders, and, until recently, through the regular tidal flooding of the lower fields with brackish sea water during the dry season.

However, this sustainable balance has been disrupted by climate change, which has compromised the natural flooding regime. This has resulted in an increased toxicity of acid-sulfate soils, which are transformed under aerobic soil conditions. Proper water and soil management has thus become critical to maintaining the sustainability of rice production (Fofana et al., 2014; Mendes & Fragoso, 2023), high concentration of soluble salts in the soil solution directly affects plant growth and productivity (https://www.youtube.com/shorts/UH4SErYaY_U).

1.2. Salinity effect in soil and rice yield

High soil salinity typically leads to osmotic stress in plants, which hampers water uptake, increases ion toxicity, and causes imbalances in the accumulation of cations in the plant. As soil salinity reduces the available water for plants, more energy and assimilates are required to sustain water and nutrients uptake. In response to water stress, plants often close their stomata to limit transpiration, which in turn reduces CO_2 exchanges and photosynthetic activity (Agurla et al., 2018; Bazrafshan et al., 2020). Furthermore, evapotranspiration exacerbates this problem by drawing cations from deeper to upper layers near the rhizosphere, intensifying salinity.

The cations K^+, Mg^+, Ca^{2+}, and Na^+ are the main nutrients involved in the osmotic effect in soil and plant but the problem begins when monocations like Na^+ increase the concentration in soils (Kronzucker et al., 2013; Sparks, 2003a). In clay particles, it can interchange space with essential nutrients by plants (K^+, Mg^{+2}, Ca^{+2}, Zn^{+2}, and others) between the negative clay charge and soil solution, in other words, clay particles could be filled by Na^+ and the other nutrient pass to the soil solution (Sparks, 2003b). It increases the possibility of losses by leaching and nutrient deposition to a deep soil horizon. Then, the combined effect of high temperature, low relative humidity, salt

presence, and crop transpiration increases the water requirement in the field. Likewise, external cation such as Na^+ in high concentration may perhaps increase antagonism with K^+, Mg^+, Ca^+, Zn^+, and this effect adds to another nutritional problem in crops. Therefore, plants spend energy on water uptake for physiological function, and the mass flow could accumulate toxicity ions in intercellular space, increase the nutriment competition, create plant toxicity, and reduce yield. In synthesis, it causes nutrients deficiency in crops, soil structure loss, and water availability reduction in salinity soil.

1.3. Water and modeling

Transient-state models have proven to be a valuable tool for simulating the dynamic interactions of water and salts in the soil. These models account for temporal and spatial variability, allowing for the assessment of salt accumulation processes over time, and understanding and managing salinization in vulnerable agricultural systems (Ragab, 2002; Šimůnek et al., 2016; van Dam et al., 2008). Several models are included in this group such as Hydrus -1D, - 2D - 3D, Drainmod, RZWQM2, RZWQM2, SWAT, SWATRE, Modflow and SWAP (Anugrah et al., 2020; Dokoohaki et al., 2016; Middleton et al., 1992; Shelia et al., 2018; Singh, 2021; Van de Craats et al., 2020). Simpler models, such as steady-state approaches, can also be used. However, they present limitations, as they assume minimal variation in salt concentrations over time and space within a field. This assumption can lead to inaccuracies in soil water balance calculations, particularly in dynamic environments like coastal rice systems where salinity levels fluctuate significantly (Corwin, 2021; Letey and Feng, 2007).

On the other hand, there are simulation models used to assess the impacts of salinity and water stress on crop yield (e.g. SIMDualKc model, (Rosa et al., 2016)). Several studies have employed mechanistic models capable of estimating biomass and crop

yields, which also serve as valuable tools for evaluating irrigation strategies and crop management practices. These models are very demanding in terms of parameterization and data, particularly on soil hydraulic properties, crop and nutrients data. Several models are included in this group such as SALTMOD WOFOST and AquaCrop.

1.4. Agricultural Resilience to Salinization and Migration

Climate variability exacerbated by clime change poses an increasing threat to the sustainability of mangrove swamp rice (MSR) cultivation. Rising sea levels and intensified tidal surges cause seawater intrusion, leading to an increase of soil salinization and acidification, which reduces rice yields. Altered rainfall patterns, characterized by shorter, more intense rainy seasons, disrupt traditional water management, exacerbating soil degradation. Labor shortages due to youth migration hinder the maintenance of protective dikes, further compromising cultivation. Mangrove degradation, often driven by economic pressures, reduces natural coastal protection and increases vulnerability to erosion and storm surges. These combined factors threaten food security and the livelihoods of coastal communities that depend on MSR. Climate change, therefore, poses a critical threat to MSR sustainability in West Africa, particularly in Guinea-Bissau.

Further research on water and soil management in mangrove swamp rice production, MSRP, is essential to enhance the resilience of this traditional farming system and to provide more effective support for local farmers. Strengthening scientific knowledge in this domain does not only contribute to mitigating the impacts of climate change but also help safeguard food security and the sustainable use of natural resources in Guinea-Bissau's coastal regions.

2. Research questions

This thesis investigates the physicochemical characteristics of soils, water and land management, and rice crop development through case studies conducted in two villages located in the northern and southern regions of Guinea-Bissau. The primary objective is to enhance rice production by improving efficient water use under the specific constraints of mangrove swamp rice systems. The research was carried out in real-world agronomic context ─ farmers' fields ─ and was guided by the following key research questions:

- ✓ What are the physicochemical properties of soil and the prevailing water conditions in mangrove swamp rice fields in Guinea-Bissau?

- ✓ What is the current knowledge regarding rice sowing in mangrove environments, particularly in relation to climate variability, soil toxicity, and crop development?

- ✓ How much water in needed to prevent yield loss due to salinity stress, and what strategies can be adopted to rehabilitate soils that are currently unproductive or showing reduced productivity?

- ✓ Under which conditions can brackish water be allowed into the fields during the dry and/or the rainy season without jeopardizing crop yields due to increased soil salinity?

To address these questions, the study began with a detailed characterization of the farmers' knowledge and local practices in the selected villages. Building on this understanding, several models of salt and water transport in the soil were calibrated and validated. The resulting insights were then used to design improved sowing strategies, water management, and agronomic practices tailored to the local context.

3. General and specific aims

The main objective of this thesis was to quantify the hydro-saline balances within the mangrove swamp rice production system, with the aim of improving land, water and crop management practices in Guinea-Bissau. By understanding of the dynamics of water and salt in this traditional cropping system, the findings of this research also provide practical recommendations for optimizing land, water, and crop production management in Guinea-Bissau.

The specific aims of this thesis were as follows:

1) To develop a conceptual framework for understanding the constraints imposed by the hydro-saline balance within the MSR production system (MSRPS);

2) To contribute to the biophysical characterization of the MSRPS in both the northern and southern regions of Guinea-Bissau, with a focus on improving the understanding of the soil–water–salinity interactions for more effective plots management;

3) To characterize soil chemical composition, and develop a predictive model for assessing spatial distribution, and propose targeted recommendations for soil salinity management in MSR;

4) To develop tools for estimating the climate demand conditions, i.e. the reference crop evapotranspiration (ET_o) using the FAO Penman-Monteith equation, using

exclusively temperature data and reanalysis datasets, thereby enhancing water management under data-scarce conditions;

5) To calibrate and validate the HYDRUS-1D model for simulating soil-water dynamics and salt transport in both tidal plots (lower areas near the mangroves) and associated upland mangrove plots (higher areas along the catena);

6) To compute the soil-water balance and evaluate the impact of soil-water management on rice yields at each study site;

7) To evaluate the effects of changing groundwater dynamics and rainfall variability on rice production.

4. Thesis framework

This dissertation is structured around five scientific articles, developed in a chronological sequence to progressively gather the data required to address each research objective. In other words, the findings and insights from each article informed and supported the development of the subsequent one, creating a coherent and cumulative research trajectory. The research involved a combination of field and analytical methodologies, including field reconnaissance, semi-structured interviews with farmers, soil sampling and profile characterization, laboratory analysis of soil physical and hydraulic properties, continuous monitoring of in-field sensors, rice growth observations, weather monitoring, remote sensing, and data analysis. A comprehensive literature review was also conducted, including books, national databases, peer-reviewed scientific articles, academic thesis, and meta-analyses from reputable sources such as the World Bank, the Food and Agriculture Organization of the United Nations (FAO), and official data from the Government of Guinea-Bissau (GB), among others. This provided a description of the baseline knowledge on the research topics to be addressed throughout the thesis.

Soil samples and plant samples were collected throughout the three rice seasons. These were analyzed and processed in three different laboratories: the Soil Laboratory of the Agriculture Department of Guinea-Bissau, the Soil Physics and Hydrology Laboratory at Wageningen University, and the Soil and Foliar Laboratory at the University of Costa Rica. These laboratories were selected based on the availability of specialized equipment and the suitability of each facility for carrying out specific analyses. The soil laboratory of the Rural Engineering Department of the Ministry of

Agriculture in Bissau was used to develop the physical analysis of the collected soil samples. In summary, the thesis is structured as follows:

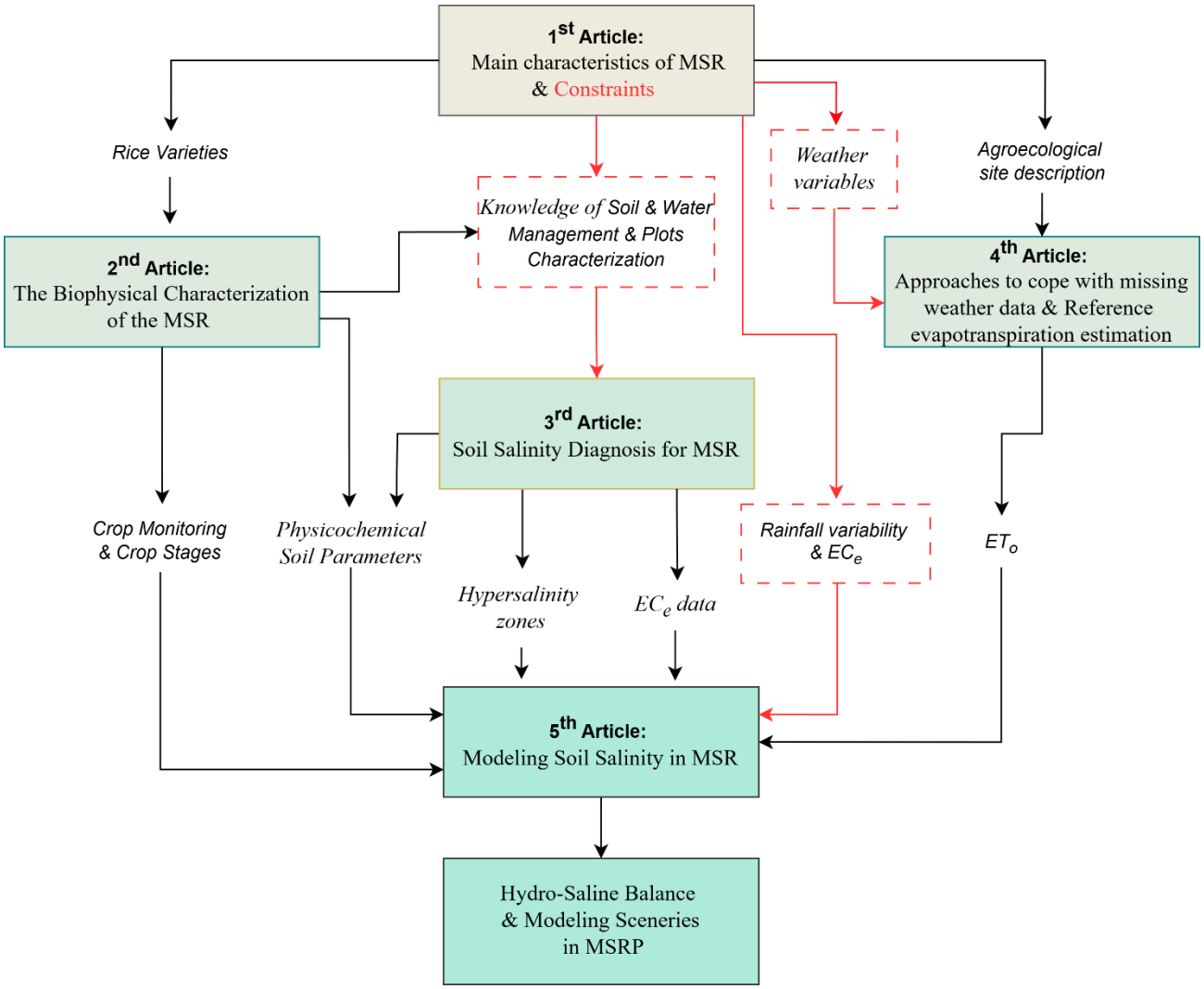

Figure 1.1. Structural framework of the thesis

Chapter 2, corresponding to the first scientific article, presents a comprehensive literature review enriched with data information from institutional databases, interviews with farmers, and field surveys. It also included site description along transects and detailed fields observations, which enabled the identification of the key challenges related to soil salinity in mangrove environments. The article offers an in-depth description of the different rice production systems found in Guinea-Bissau, with a particular focus on

the Mangrove Swamp Rice Production (MSRP) system. The study defines the structural and functional characteristics of MSRP and explores the local classification of rice fields (Bolanhas in Creole) into plots, highlighting their correlation with high-salinity areas. It also provides a technical and visual characterization of the sites, supported by photographic documentation of field plots, local rice varieties, and the vernacular terminology used by farmers. This first article identifies and synthesizes the key constraints limiting agricultural performance and rice productivity in Guinea-Bissau, thus laying the groundwork for the subsequent chapters.

Chapter 3 (second article) focuses on the characterization of plots and bunds, assessing the number of plots per unit area, their dimensions, and their influence on water retention and soil moisture, with particular attention to the soil plasticity limits. A comparative analysis was conducted between two villages, one located in the southern region of the GB and the other in the northern region, based on the evaluation of the impacts of the rainfall variability and the biophysical characteristics of each site on the agricultural practices and land management strategies. The findings in this study highlight the need to adapt farming practices to the spatial and temporal distribution of water, particularly in terms of the timing of tillage operations. Water management was shown to be more efficient in smaller plots, due to the reduced variability in waterlogging depth. Finally, to optimize tillage operations and mitigate salinity-related issues, the use of gravimetric moisture content and soil consistency mapping is recommended. Additionally improving drainage infrastructure, conducting a comprehensive analysis of salt composition, developing salinity distribution maps and establishing a hydro-saline balance are key strategies for enhancing the sustainability of mangrove swamp rice systems.

Chapter 4, which corresponds to the third scientific article, examines the chemical composition and spatial distribution of salts within the MSRP system at the field level. The study was conducted in three case study villages and employed machine learning techniques to generate high-resolution soil electrical conductivity maps (EC_e) with a high degree of accuracy. These maps allowed for the identification of hypersaline zones and the assessment of salinity patterns in relation to land use and water management practices. The article underscores the importance of understanding the interplay between agricultural practices, water management, and the role of sodium in shaping soil salinity and rice cultivation and productivity within the MSRP. It proposes targeted interventions to enhance water distribution infrastructure and restore mangrove forests in currently unproductive areas. It validates the findings from the first and second articles by reinforcing the link between soil physicochemical properties and spatial salinity patterns. Moreover, the study highlights the need for long-term monitoring to gain a deeper understanding of water and salt dynamics in the soil to support the development of sustainable and resilient rice production systems in mangrove environments.

Chapter 5, corresponding to the fourth scientific article, focuses on the estimation of reference crop evapotranspiration (ET_o) within the MSRP. ET_o corresponds to climatic demand conditions and is essential for estimating crop water use (ET_c) when the FAO approach is used. It is therefore a mandatory input for many tools, such as soil water balance and flux models such as HYDRUS-1D. This article provides a baseline estimate that serves as a foundation for calculating crop evapotranspiration in the subsequent article. The study explores alternative methods for estimating ET_o using only temperature data. The analysis includes a comparison of reanalysis datasets, namely AgERA5 from the Copernicus project and MERRA-2 from NASA, which differ in spatial resolution and temporal consistency. This article delivers a key tool for estimating ET_o in Guinea-Bissau

and provides a viable alternative for regions with limited meteorological data. Its relevance is particularly significant for institutions and stakeholders engaged in improving water use efficiency and managing salinity in MSRP. Furthermore, it highlights the necessity of refining global models to better suit tropical regions characterized by high climatic variability, fostering more efficient and resilient agricultural practices.

Chapter 6, corresponding to the fifth scientific article, presents a hydro-saline balance analysis of the MSRP, modelling with the HYDRUS-1D the observed condition and potential scenarios based on historical rainfall data. It integrates multiple data sources, including the soil physicochemical characterization, biophysical parameters of the rice fields, ET_o estimates for calculating crop transpiration (ET_c), and agronomic information on rice varieties and yields. The hydro-saline modelling confirms earlier findings regarding salt-free periods essential for rice production (Guei et al., 1997) while also identifying critical constraints, particularly the systems dependence on rainfall to maintain salinity within tolerable limits. The study proposes several management strategies to address soil salinization, such as the identification and use of salt-tolerant rice varieties adapted to local conditions, the improvement of drainage infrastructure, and the implementation of long-term research programmed to assess salinity tolerance across different environmental contexts in Guinea-Bissau. These recommendations aim to support the development of sustainable rice production systems in mangrove environments, enhancing the resilience of local agriculture in the face of climate variability and soil degradation.

Chapter 2

Mangrove swamp rice production system of Guinea Bissau: Identification of main constraints associated with soil salinity and rainfall variability

This chapter was published in *Agronomy*.

Garbanzo, G., Cameira, M., Paredes, P., 2024. The Mangrove Swamp Rice Production System of Guinea Bissau: Identification of the Main Constraints Associated with Soil Salinity and Rainfall Variability. Agronomy 14, 468. https://doi.org/10.3390/agronomy14030468

Keywords: Soil Salinity; West Africa; Tropical Polders; *Oryza* spp; Agronomic Practices; Water Management; Typologies of Paddies; Associated Mangrove; Tidal Mangrove.

1. Abstract

Mangrove swamp rice production (MSRP) stands for rice cultivation in former mangrove soils that were anthropogenically modified for food production. They utilize the largest possible storage of freshwater to desalinate the soils and make them productive. However, temporal variability in rainfall patterns causes loss of efficiency in production, impacting crop growth and reducing productivity. To improve MSRP in the country, it is necessary to identify the primary constraints associated with salinity, enhancing, and maximizing freshwater storage efficiency and water productivity. This study provides a general description of the MSRP system in both the northern and southern regions of Guinea-Bissau aiming at the identification of the main water management limitations. The description involves the use of typologies and the identification of zones within the paddies with specific characteristics. Furthermore, this review includes an analysis of the physicochemical characteristics of soils related to salinity issues, a description of agronomic management, rice varieties and the significance of dikes and bunds management for improving mangrove swamp rice water management. It shows how the MSRPS is characterized by dynamism and complexity, involves a wide range of constraints associated with salinity features, cultural influences, and microclimatic conditions that are subject to temporal variations.

2. Introduction

Rice (*Oryza sativa* L. and *O. glaberrima*) is one of the most important staple foods on the Asian, African, and American continents. Global rice production is estimated at approximately 540 million tons over the past decade (Food and Agriculture Organization of the United Nations., 2018; Kraehmer et al., 2017).

The rice crop grows primarily in the humid and seasonally dry tropics of the world, in most cases with irrigation or freshwater harvesting systems (Mallareddy et al., 2023). Flood irrigation is the most widely used irrigation method for rice cultivation worldwide (Nie and Peng, 2017). Rice paddy fields are usually permanently flooded, but with the aim of reducing water use, several flooding variants have been introduced such as dry seeding (Alberto et al., 2014; Diaz et al., 2019), anticipated cut-off, and intermittent water application (Oue and Laban, 2020). Due to the increase of water shortage and scarcity aerobic rice is being implemented using sprinkler or surface irrigation (Choudhury et al., 2013; Clerget et al., 2014; Fukai and Mitchell, 2022; Moratiel and Martínez-Cob, 2013).

Most rice cultivars show remarkable adaptability to thrive in flooded agricultural systems (Chauhan et al., 2017), especially in regions characterized by abundant sunlight and access to freshwater resources (Mallareddy et al., 2023). Recent plant breeding led to the development of modern cultivars adapted to aerobic conditions (Farooq et al., 2023). Rice productivity primarily depends on soil fertility, climatic factors, efficient water management, agronomic practices, weed control, and the adaptability of rice varieties (Bos et al., 2006; Kraehmer et al., 2017; Mallareddy et al., 2023). It has been reported that rice productivity can reach values of 10 Mg ha^{-1} under optimal climatic and agronomic conditions and with the support of agrochemical inputs (Chauhan et al., 2017; van Oort and Zwart, 2018), but climate change calls for the adoption of agroecological pathways especially among smallholders living in marginal regions.

In the north-western regions of Africa, upland (slash-and-burn), inland lowland swamp and mangrove swamp rice production can be found, all of which are rainfed. It is estimated that African rice production systems began 3000 to 2000 years ago (Da Silva, 1993; W Hawthorne, 2001; Linares, 2002; Penot, 1994). Reports from overseas travelers during early colonization (between the years 1400 - 1600) indicated that the population from countries such as Senegal, Gambia, Guinea-Bissau, Guinea-Conakry and Sierra Leone practiced rice cultivation (Kyle, 2015; Lea, 1993; Teeken et al., 2012). This implies that the indigenous population developed technological knowledge for rice production in different agroecological conditions, and domesticated wild ancestors (*Oryza glaberrima*) and adapted exogenously introduced rice varieties (*O. sativa*) for these different conditions over many centuries (Linares, 2002). In a context of high agro-ecological and cultural diversity, limited labor availability and access to agrochemicals, and a strong tradition of self-sufficiency farmers' rice varieties in West Africa are the result of a long breeding process shaped by both ecological and social factors (Nuijten et al., 2013, 2009).

The yields of farmers' varieties therefore vary greatly depending on location, year, and production system, but as would be expected in the marginal regions where rice is grown without external inputs and/or irrigation, they often outperform the so-called high-yielding or "modern" varieties because they are well adapted to those harsh conditions (Teeken et al., 2012; Temudo, 2011). In addition, it was reported that local farmers selected rice varieties based on several characteristics besides productivity, including fragrance, taste, digestion time, swelling during cooking, ease of harvesting and threshing (Teeken and Temudo, 2021; Temudo, 1998).

Guinea-Bissau (GB) is a small West African country (Figure 1.1) with a population of approximately two million people and an area of 37 500 square kilometers (Cooper and McConkey, 2005; Röhrig et al., 2021; The Republic of Guinea-Bissau., 2018), having

borders with Senegal to the north and Guinea-Conakry to the south. The country has extensive mangrove forests that extend across the entire national territory from south to north (Cooper and McConkey, 2005), and a total of 88 islands, 20 of which are inhabited (Fernandes, 2012; Secretary of State for Environment and Tourism., 2014). In the mangrove regions, there are large areas of deforested land that are used for rice production. There are also upland areas where rainfed rice, vegetables, fruit trees (namely cashews) are grown (Cooper and McConkey, 2005; Dias et al., 2022; The Republic of Guinea-Bissau., 2018).

Rice production is crucial to GB as it forms the basis of the population's diet. There are three rice production systems in the country: mangrove swamp rice, upland (slash-and-burn) rice and lowland swamp rice (rainfed and irrigated) (Ministry of Natural Resources and Environment., 2006). The annual per capita, rice consumption is estimated to be around 91 - 136.9 kg (Balasubramanian et al., 2007; Fofana et al., 2014; Soullier et al., 2020). Nevertheless, daily rice consumption can vary significantly, ranging from 400 to 700 grams, depending on the location (rural or urban), the time of the year (dry vs. rainy season; after harvest vs. hunger period) and the changing eating habits (1 to 3 meals per day; inclusion or not in the diet of other cereals and root crops) of different ethnic groups (e.g., Balanta, Manjaco, Felupe, Baiote, Pepel versus Fula and Mandinga) and households.

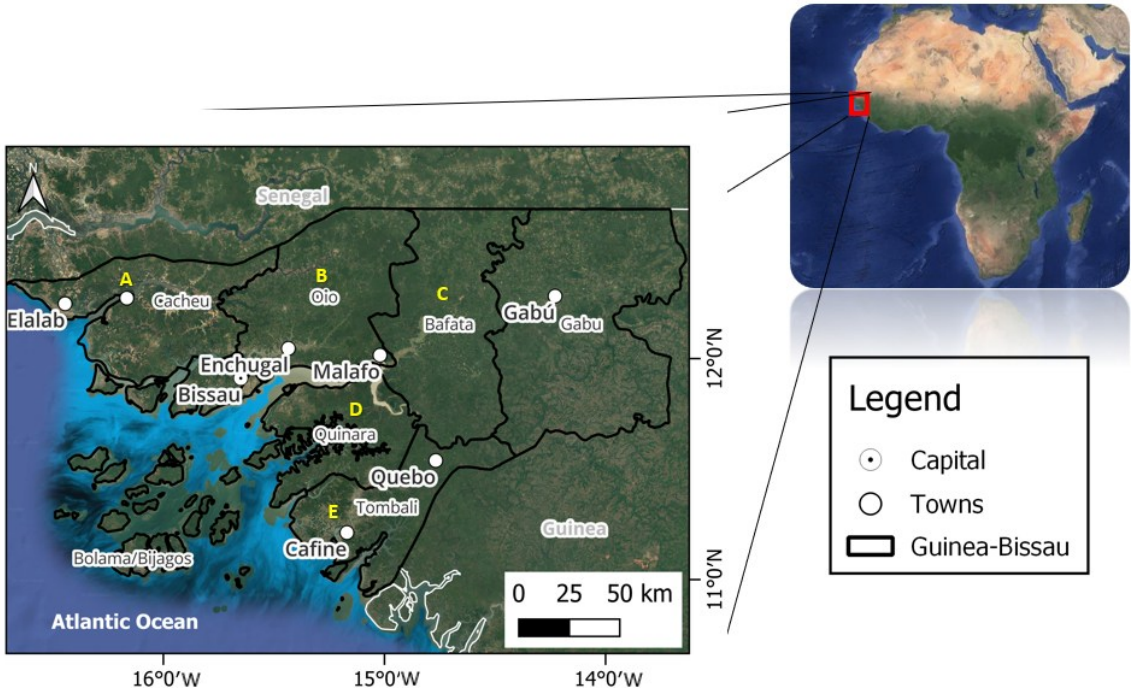

Figure 2.1. Location of Guinea-Bissau and main regions (Cacheu = A, Oio = B, Bafata = C, Quinara = D, Tombali = E) where swamp rice is cropped.

The mangrove swamp rice production system (MSRPS) is governed by soil salt concentration, and in some cases soil acidity, as well as the need for freshwater availability for plants. MSRPS belongs to a rainfed wetland rice ecosystem, specifically within the sub-ecosystems that are prone to drought and flooding; thus, highly vulnerable to rainfall patterns, needing water harvesting in the plots to ensure rice production (Andriesse and Fresco, 1991; Balasubramanian et al., 2007). Rice sowing coincides with the start of the rainy season, when plots typically have low salt concentrations that favor the growth of salt-tolerant rice varieties (Penot, 1994; Temudo, 1998). The decision of when to sow is related with the timing that salinity in the plots is low. Decision making is based on traditional knowledge without the support of agronomic tools and has become more difficult due to increased rainfall variability (distribution and quantity) (Cossa, 2023). The timing of sowing has become unreliable, especially in the northern regions where rainfall is already scarce. To date, no studies on the dynamics of salt and water

movement in the soil have been carried out for the MSRPS. The lack of sufficient knowledge about rainfall timings and salts dynamics often leads to inadequate crop development due to problems such as water shortages, toxicity and acidity, which in some cases leads to complete crop loss (Sylla, 1994). Furthermore, MSRP is strongly influenced by spring tides, which often lead to saltwater intrusion (Mendes and Fragoso, 2023), and a partial or total loss of rice production.

The MSRPS is dynamic and constantly changing due to its vulnerability to rainfall variability, that modifies freshwater storage, and forces annual/seasonal adaptation of agronomic practices (Andrieu, 2018; Temudo et al., 2020), through the active improvisation/innovation of farmers (Martiarena and Temudo, 2023). Consequently, appropriate water management is essential to support farmers in reducing the high salinity of the soils in the plots on an annual basis.

Nowadays, temporal and spatial variability of rainfall in the country have become increasingly uncertain due to climate change (Dore, 2005; Idris et al., 2022; Nuijten et al., 2013). It is well documented that certain regions of the world are more vulnerable to climate change, and GB is one such vulnerable country (Martiarena and Temudo, 2023; Mendes and Fragoso, 2023; Sousa et al., 2023; van Oort and Zwart, 2018). This susceptibility arises from its location in a transition zone between the African tropics and the Sahara Desert and its low-lying topography. The country's agricultural production is highly dependent on rainfall, accounting for approximately 90% of its output (Cabral, 1954a; World Bank Group., 2019). Long-time average annual rainfall ranges from 1200 to 5000 mm depending on the region; further information will be provided in Section 5.

The temporal variability of rainfall has a potential influence on the food security of the population producing rice for subsistence purposes. Currently, rainfall is concentrated

in a shorter period, limiting the production window for MSRP (Mendes and Fragoso, 2023). Additionally, heavy rainfall over a short period can lead to the destruction of MSRP infrastructures (dams and bunds) resulting in the loss of the production and further productivity of the rice fields. This issue will be further dealt with in Section 5. Another constraint to agricultural production in GB is the lack of necessary infrastructures, such as deep wells and dams, to support irrigation (Machado and Serralheiro, 2017; Mallareddy et al., 2023; The Republic of Guinea-Bissau., 2018).

The global aim of the present review article is to provide a conceptual framework for understanding the hydric-saline balance constraints of the MSRPS in GB. A systematic review could not be carried out due to the small number of available articles on the subject, and the need to include old (since the 1950s) and grey literature (e.g. books, governmental and project reports) that was not digitally accessible through the search engines (Agris, Scopus, ScienceDirect, Springer, Google academic) used in this review. The meteorological information and rice yield datasets were accessed from the agricultural and meteorological ministries of the country but have variable accuracy. The documents used were in various languages (English, French, Portuguese, and Spanish) along with the characterization of the sites in the Kriol dialect. Additionally, to the literature review, this article also comprised some empirical research, which included transects conducted with farmers with on-site descriptions of the paddies' diverse agroecologies, on-farm trials, soil sampling and analysis, biophysical characterization, and interviews to farmers about endogenous knowledge and technological innovation. In sum, the comprehensive research covers various essential aspects: (a) biophysical description of the MSRPS; (b) agronomic management of the MSRPS (c) key constraints, such as salinity and rainfall variability, and their impacts on water availability and rice yield; and (d) future research needs.

3. Rice production in Guinea Bissau

3.1. Rice production systems in GB

Rice in GB is produced in several ecologies with diverse techniques of cultivation. The less productive rice system is performed in the uplands on former forests or savanna woodlands after slash-and-burn, and less frequently under palm oil groves (Figure 2.2). The degree of crop association is quite variable as well as the length of the crop-fallow periods (Temudo et al., 2015; Temudo and Santos, 2017). Upland rice is known in GB as "*N'pam-pam*" or "*arroz de lugar*" (in Kriol language) and is a rainfed production system. The sowing of *N'pam-pam* is usually carried out after the first rains of the year, as the production period is limited by rainfall and the soil water availability (Medina, 2008). Within the total land area used for rice cultivation (14.7% of the country agricultural area), upland rice accounted for 37% only (Ferreira, 1968; The Republic of Guinea-Bissau., 2018), while MSRP and lowland freshwater production ("*Lalas*" in Kriol) accounted for the remaining 63% (The Republic of Guinea-Bissau., 2018). However, the expansion of cash crop cultivation areas, particularly cashew, in recent years has led to a drastic reduction in the area occupied by the upland rice system (Temudo et al., 2015).

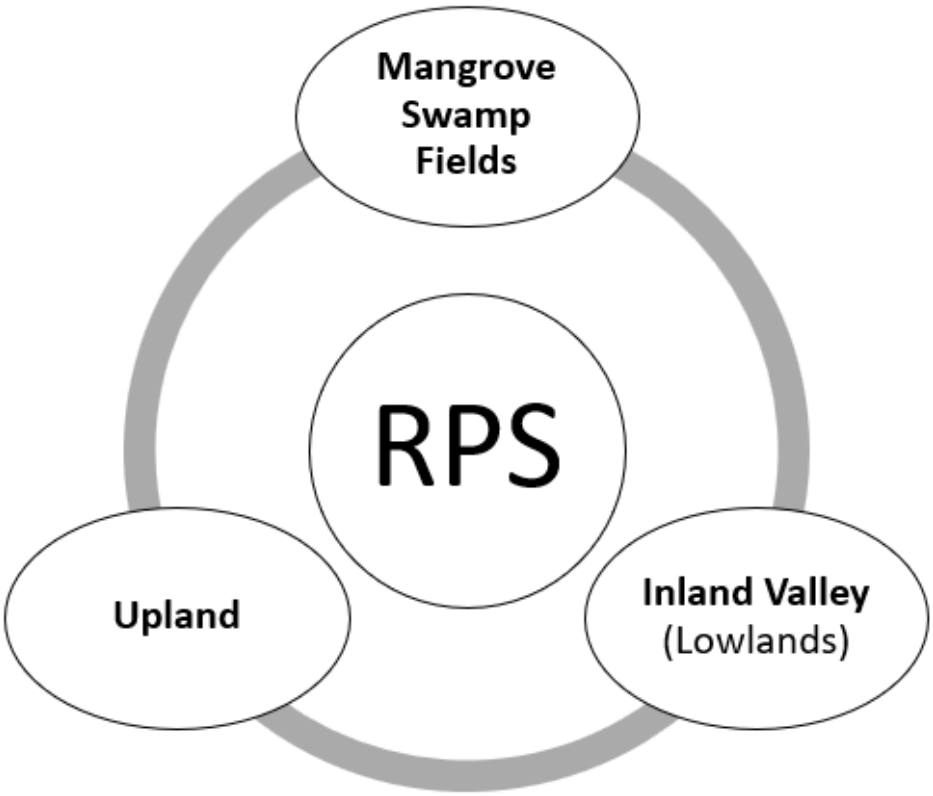

Figure 2.2. Rice production systems (RPS) of Guinea-Bissau.

The other rice production systems, in contrast, are carried out in the lowlands and include two different traditional systems of rice swamp cultivation called in Kriol "*bolanha doce*" (inland freshwater swamp fields) and "*bolanha salgada*" (mangrove swamp fields). The local term "*bolanha*" refers to the fact that rice is cultivated with a permanent depth of water (permanent flooded paddies) until or almost until the end of the rice cycle. The freshwater swamps where rice is cultivated are located in inland valleys where there is a shallow water table or an impermeable soil layer that allows water storage and thus assures fresh-water harvest (Marzouk, 1991). This system is characteristic of North-Eastern GB and is essentially performed by women belonging to the Fula and Mandinga ethnic groups, who plow with a hoe after burning the grasslands and are not used to build dikes (Temudo, 1998). In the other regions of the country (Cacheu, Oio, Quínara and Tombali), men from other ethnic groups (such as the Balanta, the Manjaco,

the Felupe, the Nalu and the Beafada) can also produce freshwater swamp rice in wet savannah grasslands (”*lalas*” in Kriol) but using a long plow (“*radi*” in Kriol) with which they build dikes, ridges and furrows (Mota, 1954) improving fresh water management. Freshwater rice production systems do not present salinity constraints and fields are usually far from mangrove forests. This rice production system accounts for approximately 10% of the 63% of rice cultivation area in lowlands and saltwater plots (The Republic of Guinea-Bissau., 2018). In some areas of the Bafatá region of Eastern GB, supplement irrigation is used with water being pumped from the river or using gravity-based drainage systems.

3.2. MSRP and typologies of fields

In the coastal areas, near the mangrove forests, we can find the “*bolanha salgada*” rice paddies (MSR fields) (Figure 2.3, 2.4). This system is characterized by the former presence of mangrove forests, which over the years have been invaded by the tides in part or the whole area of the rice fields. Farmers slash the mangroves, build the main dike to prevent saltwater intrusion and create plots of land for freshwater storage by dividing the area with bunds, which have been mentioned in previous literature as secondary dikes (Linares, 1981). Coastal ethnic groups use these locations due to their high rice productivity compared to the uplands and inland swamp valleys. At the top of the weak slope that links the villages to the mangroves, there may exist a grassland area (“*lala”* in Kriol) where rainwater accumulates naturally due to the existence of a depression. As previously mentioned, farmers can use their MSRPS techniques to create a “*bolanha doce*” (freshwater swamp rice fields) associated with the mangrove rice swamp fields which have higher fertility, less weeds, but also salinity issues.

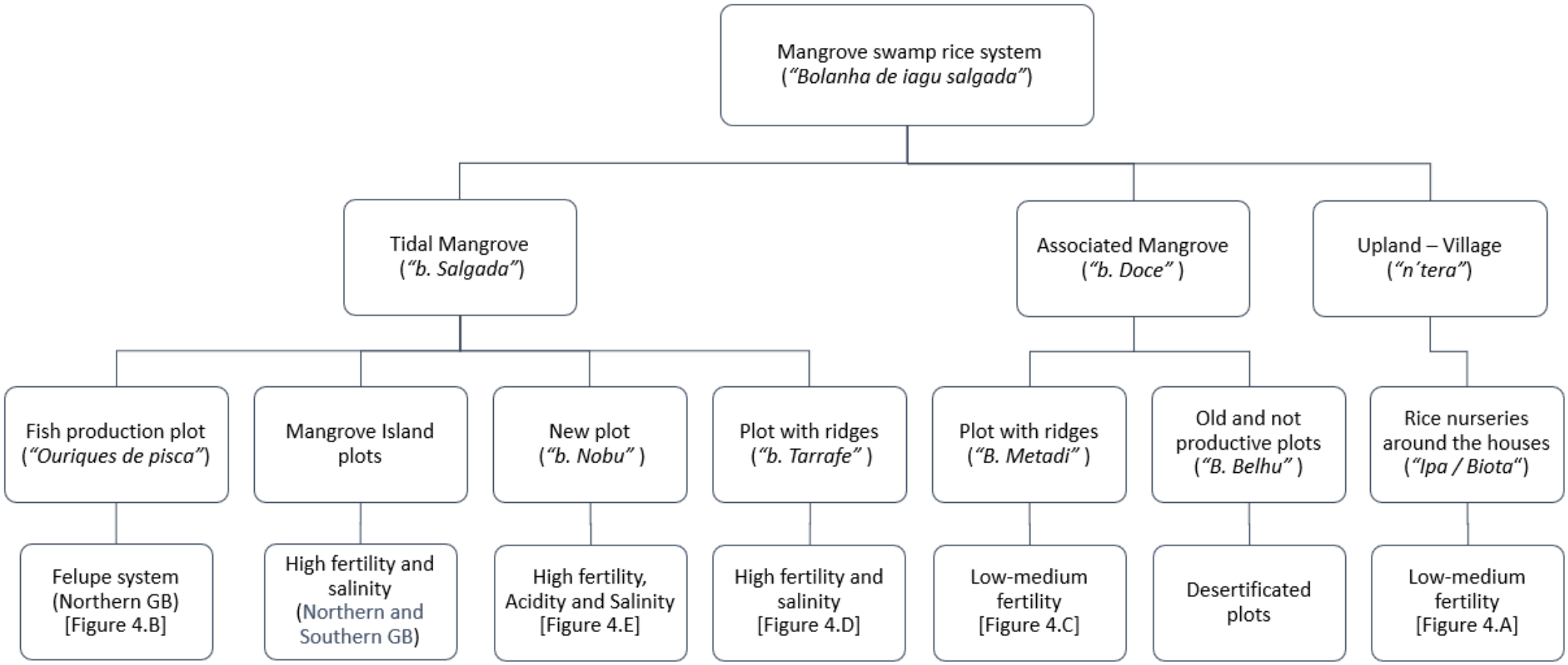

Figure 2.3. Some characteristics of the "*bolanhas"* of mangrove swamp rice system (MSRPS) of Guinea-Bissau.

The rice fields which result from the destruction of the mangroves and that are periodically invaded by the tides are called in the literature tidal mangrove fields (*bolanha de* tarrafe in Kriol), while the upper fields where only the brackish groundwater induces soil salinity during the dry season are called associated mangroves (bolanha de metadi in Kriol meaning middle swamp fields) (Figure 2.3). This part of the rice fields has generally weed species with low salinity tolerance, and a wide diversity of grasses from the Poaceae family during the rainy season (Merkohasanaj et al., 2022).

At the upper end of the associated mangroves' area are the old swamp fields ("bolanha belhu"); these can be abandoned due to low fertility or be cultivated with short cycle upland rice varieties for the hungry season when there is land scarcity (namely in Oio among the Balanta ethnic group). Farmers frequently abandon these plots because their productivity is very low, and they do not provide sufficient returns on labor investments. The creation of new plots is triggered by decreasing fertility and, in the long-term, to the occurrence of a desertification process (i.e. degraded land resources) (Andreetta et al., 2016). Evidence of desertification problems has long been observed in the Casamance region of Senegal (Linares, 1981), which borders the GB's Cacheu region (Figure 2.1), where areas of low fertility and high salinity predominate. This highlights an inherent sustainability problem as producers fail to replenish nutrients depleted by crop growth through the incorporation of weeds and rice stubs during plowing. As farmers strive to sustainably meet their families' rice self-sufficiency production needs, they are compelled to create new plots where they can achieve higher rice yields. Then, within each category, farmers from the northern, central, and southern regions divide the plots based on specific characteristics that increase their fertility and rice yields.

A possible cause of desertification in the mangrove swamp rice abandoned fields ("*bolanha behlu*"), is sodicity (Na^+ accumulation) and loss of soil organic carbon concentration (Andreetta et al., 2016). Some authors have suggested that the osmotic effect observed in plants is due to a combination of salinity, iron toxicity, and soil acidification in hydromorphic soils of GB (Ministry of Natural Resources and Environment., 2006; Secretary of State for Environment and Tourism., 2014; Sylla, 1994; Sylla et al., 1995; The Republic of Guinea-Bissau., 2018; van Oort, 2018). Nevertheless, this is not sufficiently proven as the literature does not provide data demonstrating concentration of sulfur (S) and Iron (Fe) in the first horizon of the plots' soil. Some studies conducted specifically in mangrove soils indicate the presence of acidity caused by sulfuric acids, but this information refers specifically to soils previously covered by mangroves (D'Amico et al., 2023; Naidoo, 2023; Oosterbaan and Vos, 1980; Sylla, 1994; van Oort, 2018). On this basis, it is possible that soils with significant concentrations of toxicity (such as Na and Fe) and acidity (SO_3) occur predominantly in new mangrove fields (*bolanha novo* in Kriol) and to a lesser extent in older fields of the tidal mangrove area (*bolanha de tarrafe* in Kriol). This is due to their proximity to soils still covered with mangroves and their status as newly created sites for MSRP.

The scientific categories of tidal mangrove's and associated mangrove's fields are linked to the relative influence of the tides and of the brackish groundwater on rice production (Oosterbaan and Vos, 1980; Penot, 1992; Sylla et al., 1995). Likewise, Guinea-Bissau farmers categorize tidal mangroves' fields in different sub-classes based on their specific age, function, fertility level (empirically assessed), and location in relation to the mangroves and the village (Figure 2.3, 2.4). Although all tidal mangrove fields could be called "*bolanhas de Tarrafe*", at present farmers only apply this concept to the high fertile lower fields near to the main dike and the mangroves where high

concentrations of salts can be found. The recently opened tidal fields of "*bolanhas de Tarrafe*" where mangrove roots and stubs can still be found and thus cannot be plowed, are called new swamp fields ("*bolanha novo*" in Kriol). In these plots, there are generally no concerns about soil acidity, due to sulfuric acids, in the first soil horizons (D'Amico et al., 2023). This is attributed to the extensive oxidation process in the soil profile, which leads to the formation of pyrite, resulting in the release of sulfuric acid and H^{+} through the oxidation of Fe^{+2} (details are provided in Section 4.2).

Additionally, over time, leaching of anions and cations to deeper soil horizons occurs (Sylla et al., 1995; Ukpong, 1995). The new swamp fields ("*bolanha novo*") are the newest areas where farmers start planting (or sowing directly high salt tolerant rice varieties) 3 to 5 years after slashing the mangroves and building a main dike; this period is needed for rainfall to leach salts, thus naturally reducing salinity and toxicity caused by seawater cations. These are the most fertile locations among all plots of a paddies (Merkohasanaj et al., 2022). However, these are the only sites that suffer from acidity problems caused by sulfuric acid due to their limited exposure to oxygen and leaching of cations and anions (D'Amico et al., 2023). The start of ploughing of the new *bolanha* also depends upon the dominant mangrove species, as roots constituted with physical barriers, mainly the ones of *Aviccenia germinans* and *Languncularia sp.* that take longer to rotten (Cossa, 2023).

There are two less common sub-categories of tidal mangroves, primarily used among Felupe and Baiote ethnic groups in some northern islands of GB (Figure 2.3, 2.4), known as "*Nhatabas*", and "*Ouriques de pisca*". The "*Nhatabas*" (called "*ilhas*" by the Balanta) are tidal mangrove fields ("*bolanhas de Tarrafe*") in terms of the soil physicochemical properties, located in remote islands, requiring the use of canoes for the transport of both workers and the rice harvest (Temudo and Cabral, 2023). Finally, the

fishing dikes ("*ouriques de pisca*" in Kriol) are ponds surrounded by dikes, reserved exclusively for the reproduction and growth of fish (Van der Knaap, 2019) (although they might have been former rice plots). Farmers facilitate the entry of saltwater, shrimps, and fish into these ponds by opening drainage pipes made from palm trunks (Cooper and McConkey, 2005; Oosterbaan and Vos, 1980).

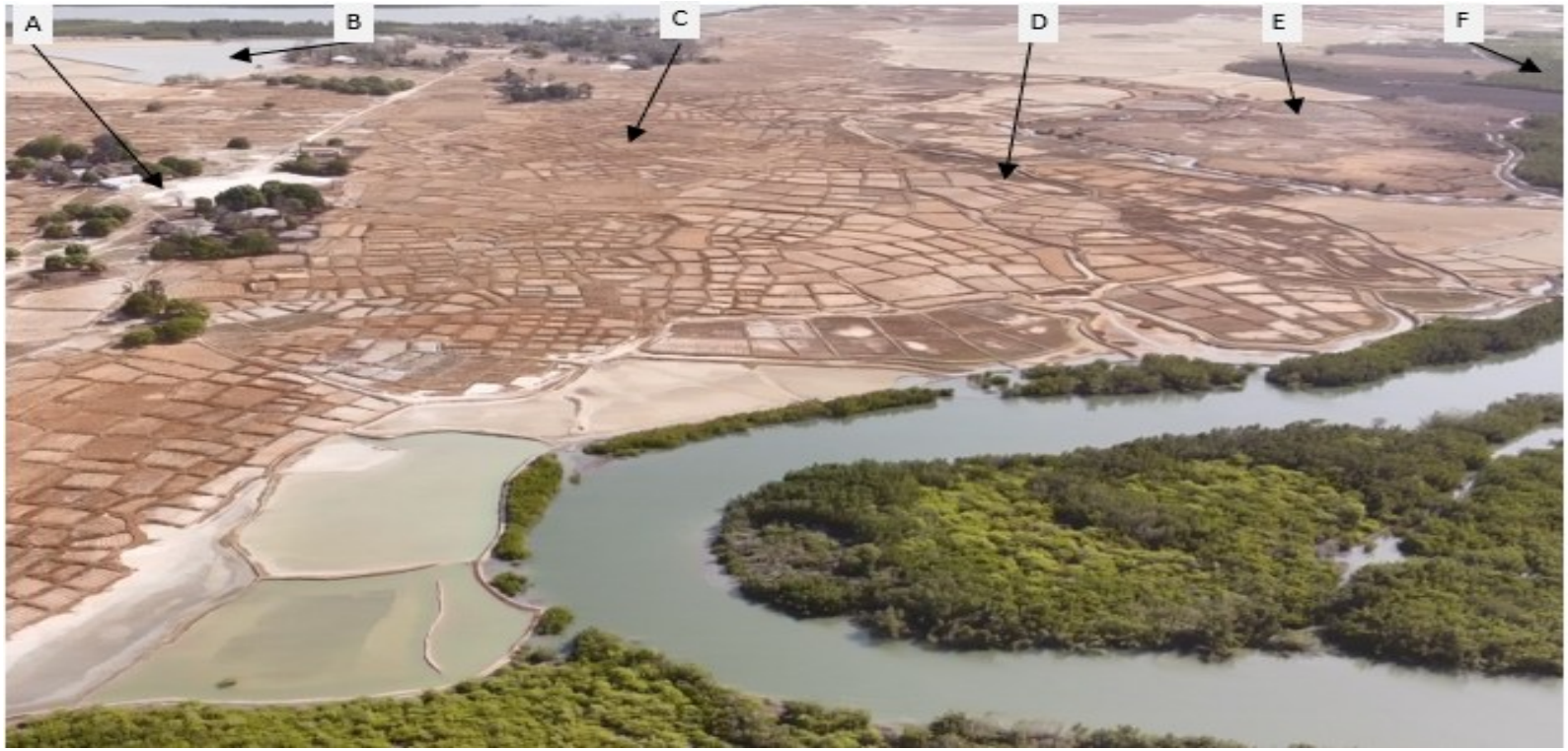

Figure 2.4. Plots of mangrove swamp rice production system in mangrove of Elalab, Guinea-Bissau. A) Village (*Tabanca*), B) fish production plot in the Felupe/Baiote system (*Orike de pisca*), C) Associated mangrove (*bolanha doce*), D) Tidal mangrove (*bolanha salgada*), E) New mangrove plots (*bolanha novo*), F) Mangroves (*Tarrafe*).

In some villages there is also an “associated terrace” (*cabeça de bolanha* in Kriol, meaning head of the rice swamp field) covered by wet or dry grassland. In the upland savannah woodlands/grasslands surrounding the households, where cattle, pigs and goats roam, some farmers sow the rice nurseries at the beginning of the rainy season. Farmers can also use the mangrove fields to create nurseries, as in the south of GB, or more seldom perform direct sowing as in the southern GB (Balanta ethnic group of the Cafine region and the Felupe/Baiote ethnic groups of the Cacheu region).

3.3. Areas and yields

The official international statistics (Food and Agriculture Organization of the United Nations, 2023; The World Bank, 2023) show that in the last 60 years, total rice production in GB has been on an upward trend (Figure 2.5). However, these statistics are based upon rough estimates for the entire country. According to FAO and the World Bank estimates (Food and Agriculture Organization of the United Nations, 2023; The World Bank, 2023), rice production was lower in the 60s and 70s than in the last decade (Koehring, 1980). In the last 10 years, the average total area under rice cultivation in the country was 112 564 ha, with an annual average production of 180 749 Mg of rice. This is in line with the estimates of the African Union, which currently forecasts an approximate production of 182 544 Mg for the period 2010-2020 (African Union., 2023). A similar increasing trend can be observed in relation to the rice harvested area (Food and Agriculture Organization of the United Nations, 2023; The World Bank, 2023). This indicates an active and strong expansion of rice production areas, despite the continuing dependence on rice imports (Food and Agriculture Organization of the United Nations, 2023). This is likely due to a combination of factors, ranging from the active rebuilding of mangrove swamp rice fields’ infrastructures after the liberation war (1963-1974) and

the expansion of new planting areas with higher soil fertility and water availability (Temudo and Cabral, 2017; Vasconcelos et al., 2015).

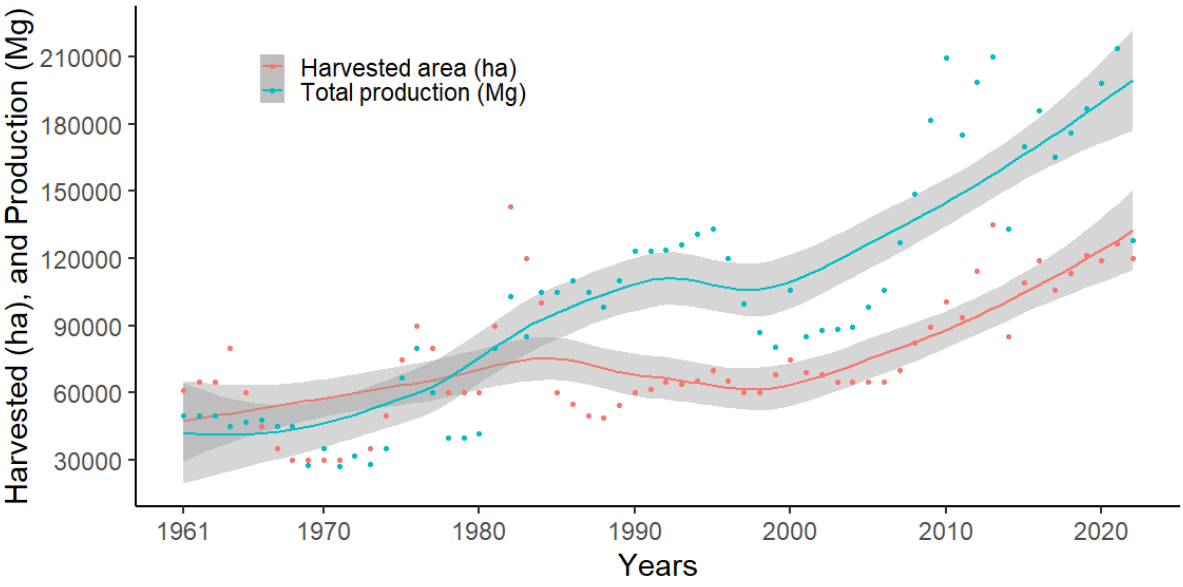

Figure 2.5. Smoothed conditional means plots of the harvested area (ha) and national production (Mg) of rice from 1961 to 2022 (Food and Agriculture Organization of the United Nations, 2023).

The rice yields in GB exhibit considerable temporal and spatial variability, the latter depending on the region and the rice production system. Table 2.1 shows the rice yield reported in several studies about rice cropped in upland locations and MSRP fields. The results show that the MSRPS outperforms the upland rice in all studies, with differences ranging from 15% to 60%. These differences indicate that the yield of the diverse rice production systems in GB is extremely different, largely due to the strong differences in agro-ecological characteristics between upland, inland valleys, and MSRP fields.

3.4. Rice crop species and varieties

Two species of rice plants have been identified in GB since colonial times, *Oryza glaberrima* and *O. sativa*. The first is a species native to Africa, where farmers have been domesticating and selecting varieties for 2000 and 3000 years (Cormier-Salem, 1999; Da Silva, 1993; W Hawthorne, 2001; Linares, 2002). On the contrary, *O. sativa* is a species native to Asia and was introduced by the Portuguese and/or the Arabs during the colonial period in the 17th century (Linares, 2002; Teeken et al., 2012). These species have significant advantages and disadvantages in terms of their adaptability to the MSRPS (Table 2.2). The main reasons for their adoption are their productivity (sensu lato), their adaptation to social and cultural factors, and their tolerance to biotic and abiotic factors (Kyle, 2015; Temudo, 2011). Over the years, farmers in GB have selected varieties from both species with the most suitable organoleptic and agronomic characteristics.

Table 2.1. Literature reported rice yields in upland and mangrove swamp system (MSRPS).

Year/System	Yield ranges (kg ha^{-1})		References
	Upland	MSRPS	
1947	-	2060 - 3000	(Castro, 1950)
1948	–-	1620 - 2680	(Castro, 1950)
1949	-	1040 - 1960	(Castro, 1950)
1953	300 - 600	1800 - 2000	(Ferreira, 1968)
1968	1098	1832	(Ferreira, 1968)
1970	600 - 800	1000 - 3000	(WALTER Hawthorne, 2001)
1982	-	1900	(Seidi, 1998)
1983	-	2700	(Seidi, 1998)
1986	270 - 950	1020 - 3750	(Van Ghent and Ukkerman, 1993)
1987	-	1305 - 2700	(Rodrigues and Carrapiço, 1990)
1988	-	1714 - 3033	(Rodrigues and Carrapiço, 1990)
1990	400 - 600	-	(Cormier-Salem, 1999)
1991	300 - 600	600 -1500	(Da Silva, 1993)
1994	-	1960	(Seidi, 1998)
1995	-	2800	(Adesina and Seidi, 1995)
1999	500	1500 - 4000	(Cormier-Salem, 1999)
2001	1000	3000	(Chauhan et al., 2017)
2008	400 - 800	-	(Kyle, 2015)
2008	400 - 800	-	(Kyle, 2015)
2010	-	1584	(African Union., 2023)
2014	-	1700 - 2600	(Secretary of State for Environment and Tourism., 2014)
2015	-	1120 – 2870	(Tesio et al., 2021)
2017	-	1000	(Chauhan et al., 2017)
2021	-	1600	(Röhrig et al., 2021)
2023	-	1180 - 1910	(Cossa, 2023)

A significant number of rice varieties have been reported in GB over the last 70 years (Table 2.3). These varieties possess genetic characteristics of the *O. sativa and O. glaberrima* species, and even of inter-specific hybrids (J. Espírito-Santo, 1949). The literature reports a total of 54 varieties (both farmers' varieties and "improved" ones) identified in MSRP (Table 2.3) over the last 12 years (Teeken et al., 2012; Temudo, 2011;

Tesio et al., 2021). There is a wealth of information that still needs to be thoroughly explored to accurately determine whether different names correspond to the same rice varieties and the same name can correspond to different varieties. This is a challenge the country faces due to its wide diversity of ethnic groups with completely different languages, making it difficult to properly identify a variety.

Table 2.2. Characteristics of *Oryza glaberrima* and *Oryza sativa* used for rice production system in mangrove reported in West Africa.

Species	History and adaptability	Phenotypic characteristics	Genotypic characteristics
Oryza glaberrima	• Indigenous African rice • Wild ancestor *O. Brevilugata* • Domesticated 2000 – 3000 years ago • Dryland and wetland rice cultivation • High adaptability in water depth fluctuations • Some varieties have high salinity tolerance • Some varieties have high draught tolerance	• Small grain • Dark seed color • Pear-shaped grains • Grain with red, olive to black seedcoat • Straight panicles • Panicles with simple branches • Short-rounded ligules • Wide leaves • Seeds scatters easily • The grain is brittle • Difficult to mill	• Short and medium cycle • Tolerance to diseases and pests • Tolerance to iron toxicity • Tolerance to acidity • Tolerance to low fertility soils • Salt or drought tolerance • Good acclimatization.
Oryza sativa	• Asiatic origins • Two strains (*O. japonica*, *O. indica*) • Introduced early 1600s by Portuguese and/or Arabs • Dryland and wetland rice cultivation • Lower tolerance in water depth fluctuations • Slowly compete with weeds • Some varieties have high and low salinity tolerance	• Bigger grains • General white seed color • Pear shaped grains • Panicles are not upright • Pointed ligules • Panicles bend after flowering and have more ramifications	• Short, medium and long cycles • More susceptible to diseases and pests • Scatter lees seed on the ground
References	(Adesina and Seidi, 1995; Cormier-Salem, 1999; W Hawthorne, 2001; Linares, 2002, 1981; Teeken et al., 2012)		

The wide diversity of rice varieties in GB (Table 2.3), are continually being selected based on farmers' changing needs over time. The vast majority of farmers do not carry out mass selection before harvesting the grain to be used as seed for the next cropping season, and farmers permanently access and adopt seeds of new varieties through informal channels. Furthermore, natural interspecific hybrids were found in smallholders' fields as a result of spontaneous cross pollination (Nuijten et al., 2009). Varieties are usually adopted by farmers based on agroclimatic conditions (soil physico-chemical conditions, climate), post-harvest quality and nutritional considerations (Penot, 1995; Temudo, 2011, 1998). Various local criteria are used when selecting rice varieties including: (1) nutritional quality and post-harvest characteristics (duration of digestion time, swelling capacity during cooking, taste, difficulty in threshing, processing characteristics (de-husking), time required for a given volume of rice to be fully consumed) and; (b) both phenotypic and genotypic traits of the variety (growth cycle, yields, salt tolerance, plant height, tillering capacity, flood tolerance, drought tolerance, susceptibility to lodging and shedding, susceptibility to pests and diseases) (Temudo, 2011, 1998). In most villages these two main sets of criteria are used, with the first category having more weight than the second. Furthermore, these criteria may vary depending on the topographical characteristics of the plots and the cultural practices in different villages across the country

Table 2.3. Rice varieties' common names reported in the literature for Guinea-Bissau since 1948 to 2023.

Years	1948 - 1973	1974 - 1990	1991 - 2010	2011 - 2023	
Varieties	• Adusta • Amaura • Americano • Atanha • Atrobrunnea • Bandjulô • Cuncú béle • Cycliana • Cristal (Angola) • Dichroa • Dinqueri • Elongata • Feluge • Gambiel • Gilanica • Iacá • Ioncubá • Italica • Jambaram • Jambaram branco • Landjau • Malanotrix • Malicoió • Ménè • Mohóbè • Mutica • Ruio (Angola) • Openê • Poupa • Santi • Selho • Senco • Sepica • Some (Thome) • Tanha	• BG 400 SLR • BG-380-2 • BG400-2 • BG400-SRI • Cablack • Iaca • IR15-19 • IR2035-120-3 • Rd15 • RD15 • RG380-2 • ROHIB 15 • ROHYB 6 • Rok5 • WAR1 • WAR77 • WAR77-55-2-2 • WAR-81-2-1-1 • WAR81-2-12	• Abulai • Aninha • Atanham • Bandeira • Bêháma • Bentana • Berendugô • Bimbirim • Cataco • Catanha • Cáu • Caublac simples • Cablak • Caublac xau • Iácá pepel • Iácá tomáso • Iácá pami • Lóbsim • Mafanhi • Malmála • Malmom (N'conton) • Malu-malu	• Malu-raça • Mamussu • Murungo • N'conto • Nhiue • Nhoquê • N'thanthé • N'uérique • Péra n'djubi • Kissidugo • Quissampena/Sampena • Rd15 • Rok5 • Santi • Silá • Sili • Socubá • Some/Thom • Spínola • Thom-dam • Thom-som • Thorno • Yaca-keba • Yacuncola • Yaka	• Alaia • Aninha • Arica 06 • Arica 07 • Atanha • Baga-male • Bakungabu • Balenabu • Bamakabu • Barnonte • Batumpaiabo • Brasil • Bucar/Buré • Cablak/Caubla • Cataco • Catio • Djambaram/Jambaran • Djelele • Dus-cascas/4 cascas/Aferenqué • Edjur • Etelé • Iacai Adi • Iacai branco • Iacai Tomor	• Iacai vermelho • Kataco • Loque • Malan-dan • Malmon • Malubrasa • Malu-dingo • Malu-N'daure • Malu-sauho • Mamusso • N'conto • N'conto branco • N'conto preto • N'dolo-cpoc • N'gel • Nerica • N'thanthé • RD15 • Rok25 • Rok5 • Sampena/Quissampena • Seli/Sili • Thom • Yaca • Yaca branco • Yaca-saw / Xau
References	(Castro, 1950; Espírito-Santo, 1948; J. Espírito-Santo, 1949; Ferreira, 1968; Linares, 2002)	(Adesina and Seidi, 1995; Koehring, 1980; Miranda, 1993; Penot, 1995; Seidi, 1998; Temudo, 2011)	(Cormier-Salem, 1999; W Hawthorne, 2001; Penot, 1998, 1992; Temudo, 2011, 1998)	(Cossa, 2023; Teeken et al., 2012; Temudo, 2011; Tesio et al., 2021)	

The rice varieties may be classified based on the crop cycle duration: short-cycle varieties (> 90 days after sowing (das)), medium-cycle varieties (115 – 125 das), and long-cycle varieties (>135 das) (Cormier-Salem, 1999; Linares, 2002; Miranda, 1993; Penot, 1992; Teeken et al., 2012; Temudo, 2011; Tesio et al., 2021). This depends primarily on the rice species as *O. glaberrima* varieties tend to have a shorter growth cycle compared to O. *sativa* varieties (Adesina and Seidi, 1995; Dossou-Yovo et al., 2022; W Hawthorne, 2001). Nevertheless, comprehensive data on phenological stages, the temporal intervals between these stages, the quantification of phenological stages based on cumulative growing degree-days, and other pertinent factors are still missing. Understanding the phenological stages of these rice varieties and growth cycles is crucial for developing more precise agronomic recommendations. Therefore, rice varieties in GB lack comprehensive life cycle characterization. Particularly because there is limited evidence for defined phenological stages and growth durations.

As shown in the analysis above, rice varieties cultivated in GB have significant genetic variability. Therefore, both genetic and agronomic studies are essential to identify and fully characterize the local varieties specifically used in the MSRP agroecosystem. This information will support adequate agronomic recommendations in times of socio-environmental changes, particularly in terms of water scarcity and salinity issues.

4. Salinity and salt management in the MSRPS in GB

4.1. Base concepts

Soil salinity is an excessive accumulation of soluble salts (K^+, Ca^{2+}, Mg^{2+}, Cl^- and SO_4^{2-}) and/or exchangeable sodium (Na^+) in the rhizosphere or root zone (McGeorge, 1954). Salinity in agricultural waters and soils is ascribed to both hydro-geological and anthropogenic mechanisms. Soil salinity problems occur in a variety of climatic conditions but are most evident in arid and semi-arid climates where rainfall is insufficient to leach accumulated salts in the root zone of crops (Hopmans et al., 2021).

Secondary salinity became an adjunct of irrigated agriculture since it charted almost similar path with the commissioning of several irrigation schemes (Ghassemi 1940- et al., 1995; Hopmans et al., 2021). Major types of soil salinization include shallow groundwater associated salinity, transient dryland salinity, irrigation-induced salinity (Hopmans et al., 2021; Rengasamy, 2016), and the intrusion of saltwater from the sea (Hopmans et al., 2021).

High levels of soluble salts in the soil affect its physico-chemical properties, causes osmotic changes in soil water, namely increasing the osmotic potential, which leads to the reduction of plants water uptake, directly decreasing the plant growth rate, and consequently leading to a decrease in crop production (Ayers and Westcot, 1985a; Hoffman and Shannon, 2007; Hopmans et al., 2021; Minhas et al., 2020, 2019; Rengasamy, 2016; Rhoades et al., 1992). High sodium or low calcium levels in the soil or water affects the soil permeability and may cause crusting hazards. This reduces the rate of water infiltration into the soil to such an extent that not enough water is able to infiltrate and to refill the rootzone, thereby failing to provide the plant adequate water supply (Ayers and Westcot, 1985a; Minhas et al., 2020, 2019; Rhoades et al., 1992).

In sodic soils clay dispersion occurs when the electrolyte concentration falls below the clay flocculation value. Sodium-affected soils, that have low salinity have low structural stability, low hydraulic conductivities, and infiltration rates. These poor physical properties result in reduced crop yield caused by the combined effect of poor aeration and reduced water supply. Low infiltration rates can also lead to severe soil erosion particularly under heavy rain conditions (Sparks, 2003a).

The accumulation of salts in the soil leads to chemical imbalances within the soil matrix, subsequently giving rise to nutritional deficiencies in plants (Van de Craats et al., 2020). When the concentration of salts in the soil solution reaches a critical salinity level, called threshold salinity (Maas and Hoffman, 1977), it causes severe water deficits in plants, restricts plant growth, and can result in plant death (Machado and Serralheiro, 2017). Specific toxicity effects may occur in plants, mainly in woody perennials, in the presence of certain levels of chloride, sodium, and boron (Ayers and Westcot, 1985a; Hoffman and Shannon, 2007; Hopmans et al., 2021; Rhoades et al., 1992).

In saline soils, pH and acidity can also adversely affect plant growth. Soil acidity is primarily caused by an increase in the concentration of H^+ ions (Agegnehu et al., 2021; Sparks, 2003a). In tropical soils, the primary cause of acidity is the hydrolysis of Al^{+3}, whereas in soils with anoxic conditions and high organic matter content, acidity is directly caused by the release of H^+ (Agegnehu et al., 2021; Giri et al., 2022). In general, saline soils tend to have alkaline pH values (pH > 7), this may lead to issues with nutrient solubility in soil solution. However, this condition can change if other chemical compounds are present that can significantly reduce the pH, such as sulfates (Sylla, 1994). Extremes in soil pH (whether high or low) directly impact nutrients solubility, consequently diminishing essential nutrients uptake by plants (Fernández and Hoeft,

2021). Both conditions exist in mangrove soils, mainly in soil with good oxygenation and active redox changes (*Bolanha novo*). All these issues impact rice growth and yield.

The salinity quantification in the soil solution is easily determined by the electrical conductivity (EC) measurements evaluated in 1:2 (soil:water extract) or 1:5, and in soil saturated paste extract. The soil sodicity is based on the determinations of the Exchangeable Sodium Percentage (ESP) or the Sodium Adsorption Ratio (SAR) (Kargas et al., 2020; Machado and Serralheiro, 2017).

Salinity affected soils are classified into saline, alkali and saline alkali based on ESP and EC (McGeorge, 1954). Saline soils are those having an EC in saturated paste extract above 4 dS m^{-1} and an ESP < 5% (Kargas et al., 2020; Strawn et al., 2015). Sodic soils, present a high concentration of sodium, as indicated by an ESP > 15% and EC < 4 dS m^{-1}. The saline-sodic soils, which exhibit both high EPS (> 15%) and high EC (> 4 dS m^{-1}) (Sparks, 2003b; Strawn et al., 2015). If the system has high sodium concentration (ESP > 15%) and low EC (< 4 dS m^{-1}), there is a high probability of soil structure loss due to clay particle dispersion (Van de Craats et al., 2020).

Salinity management strategies usually aim to prevent salts accumulation in the root zone to levels that limit root water uptake, controlling salt balances in the soil–water system by preventing continuous accumulation in the root zone, and minimizing the hazardous effects of salinity on crop transpiration and consequently on crop growth and yield. Under saline conditions, irrigation should aim at maintenance of sufficiently high soil water potential and cause salt leaching in the soil profile (Maas and Hoffman, 1977; Minhas et al., 2020). However, under rainfed conditions, salt leaching occurs through precipitation, the timing of which may limit the suitability of the soil for crop production and/or sowing timing(Minhas et al., 2020).

Nowadays, remote sensing instruments and aerial photography are used to map salinity because it is impractical to directly measure root zone EC over large areas. The FAO has provided a world map of soil salinization, the GSASmap, derived from a harmonized world soil database (FAO., 2021). Unfortunately, this information is not available for GB, as no studies have been conducted in the country that could provide such information and is therefore a research gap that needs to be closed.

4.2. Salinity in the bolanhas of MSRPS

The impact of salinity represents one of the challenges in MSRP across West Africa. Some studies have indicated that drought (33%), iron toxicity (12%), cold (7%) and salinity/sodicity (2%) are the most prevalent and significant stresses affecting rice crops in Africa (Africa Rice., 2011; Balasubramanian et al., 2007; Dossou-Yovo et al., 2022). Plants exhibit a significant adaptive response to cope with water loss by enhancing stomatal closure, thereby reducing CO_2 exchange, impeding photosynthesis and, thus reducing yield (Agurla et al., 2018; Bazrafshan et al., 2020). Furthermore, evapotranspiration exacerbates the salinity effect, because water can mobilize cations from deeper soil layers into the upper layer near the rhizosphere.

Abiotic stress caused by salinity inhibits rice growth. The soil where MSR is cultivated are alluvial, formed by the deposition of sediments by seawater flows that naturally introduce salts into the system (Teixeira, 1962; Ukpong, 1997, 1995). These areas are highly saline and support rice growth only during the rainy season when a period of lower toxicity occurs (Chauhan et al., 2017). Maximum concentrations in some plots in GB were found to be between 195.8 and 5599 cmol(+) Na per kg soil and an electrical conductivity (EC) of 53.75 mS cm^{-1} (D'Amico et al., 2023). During the rainy season, salt concentration can drop to levels below 5 mS cm^{-1}, allowing weeds and rice to grow

(Écoutin et al., 1999; Penot, 1994). This period represents a strategic phase for farmers, to take advantage on these specific moments to grow rice. During the dry season, certain plots adjacent to mangroves and saltwater are used for extracting salt, especially intended for culinary purposes.

Due to the specificity of the MSRPS conditions a different classification for soils affected by salinity was proposed by (Sylla et al., 1995); the classification is based on EC (measured in 1:5 soil water suspension) and on the suitability of the soil for rice production as depicted in Figure 2.6. These systems are defined by their status at the end of the dry season, particularly at the beginning of the rainy season (Sylla et al., 1995). It has been found that rice cultivation can thrive in Class 1 (non-saline) and Class 4 (very saline) soils. This can be achieved by using salt-tolerant rice varieties and ensuring adequate rainfall to facilitate leaching and reduce soil cation levels.

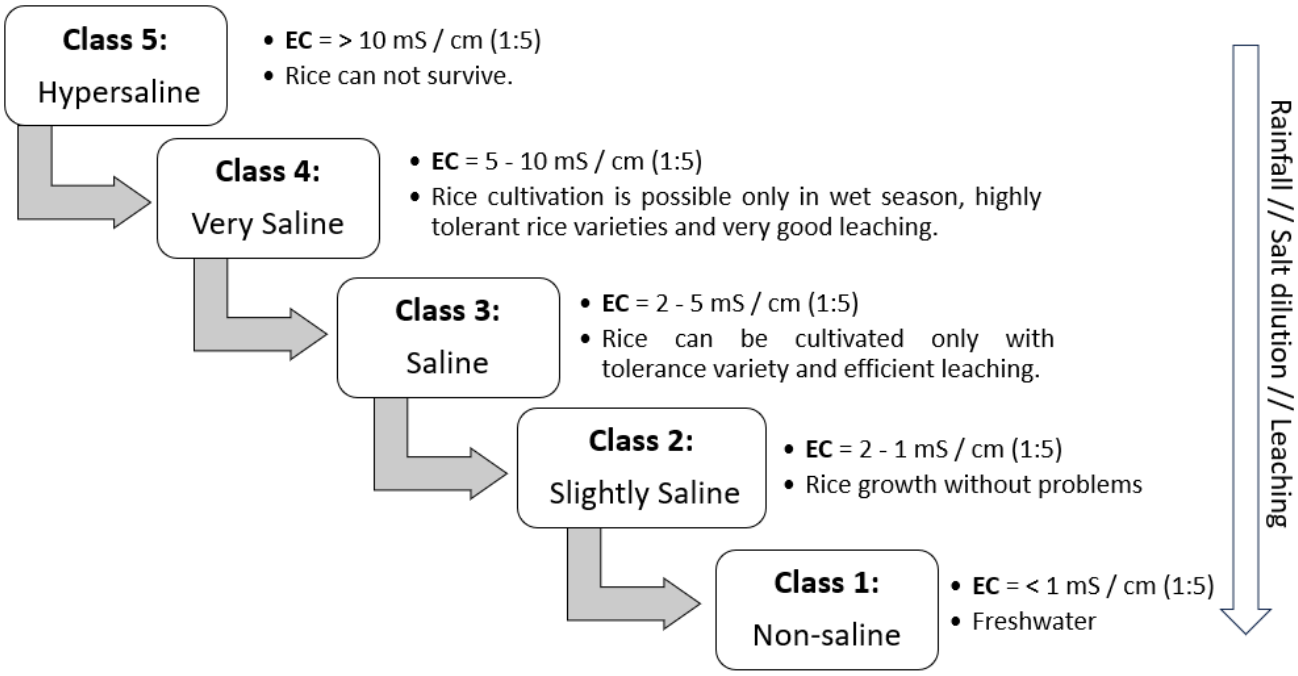

Figure 2.6. Salinity classes according to electrical conductivity (EC) in water suspension (1:5) for final dry condition (before the beginning of the rainfall season) based on the salinity tolerance of rice. Downward arrow illustrated decrease in class as a result of rainfall, salt dilution or leaching. (Adapted from (Sylla et al., 1995))

As previously stated, the MSRP in GB is determined by initial and final conditions regarding soil salinity concentrations. Due to the different initial salt concentrations in different plots, these conditions are not uniform everywhere (D'Amico et al., 2023; Guei et al., 1997), and depend on the amount of retained freshwater, resulting in additional dilution of salts as the MSRPS typically lacks proper drainage. Some reports have found that in mangrove systems in Nigeria, the spatial distribution of salinity is related to nutrient relationships and textural gradients (Ukpong, 1997). The initial rainfall, depending on the amount of water, may also favor the leaching of some salts to deeper horizons, possibly leading to their accumulation in the groundwater. The assessment of the initial salt concentration is performed by farmers when they start planting the rice. Due to the lack of appropriate tools farmers use biological (such as the presence of certain

weeds), and physical (such water temperature and the taste of the water) indicators. Comparable indicators have been documented in rice production in India (Padhy et al., 2022).

The final state of the rainy season has a direct impact on crop yield since salinity can influence the critical phenological stages of rice plants. The final phenological stages of rice (R5-R7) are crucial for productivity, as stress during this period can directly affect the yield (Sylla, 1994; The Republic of Guinea-Bissau., 2018; Thiam et al., 2019; van Oort, 2018). This happens every year when the plots revert to their original conditions. This typically occurs between two months after the last rainfall. At this time, water evaporation and crop transpiration increase the salt concentration in the plot, resulting in stress for non-tolerant rice varieties (Chauhan et al., 2017; Marius and Lucas, 1982; Wolanski and Cassagne, 2000). Some authors report that salinity is the most limiting factor in rice production in GB (Van Ghent and Ukkerman, 1993). For this reason, farmers in the northern region of the country strive to store and maintain the maximum amount of water in the plots. There are currently no regional studies on water-salt balance, osmotic effect on rice plants, and evapotranspiration corresponding to the varieties of MSRP found in GB. For this reason, some authors recommend conducting regional studies on soil salinity in MSRPS (Sylla et al., 1995; Thiam et al., 2019).

Only a few studies report on soil water balance and salt movement (Sylla et al., 1995; Thiam et al., 2019) and only one focuses on GB (Sylla et al., 1995; Thiam et al., 2019). Therefore, there is a research gap regarding the adequate characterization of the MSRPS in terms of the dynamics of salts during both the rice season and the offseason, which is essential for establishing an appropriate schedule for the timely commencement of rice production in each region/type of field.

4.3. Salinity and water productivity in the MSRPS

According to the recent review by Minhas et al. (Minhas et al., 2020) the relationship between plant growth and heterogeneous salinity in the root-zone is complex. Thus, plant growth responds to the weighted-mean salinity of the root-zone, as well as to the site-specific response of the roots and their ability to uptake water from the soil. Plants expend more energy to extract water from saline soil due to the high affinity of salts for water and therefore growth and yield are reduced.

Several studies have shown that crop yield and transpiration are less sensitive to low osmotic potential than to low matric potential (e.g., (Allen et al., 1998)). Under saline conditions, many plants can partially compensate for the low osmotic potential of soil water by building up higher levels of internal solute. This occurs through the absorption of ions from the soil solution and through the synthesis of organic osmolytes. However, the synthesis of organic osmolytes requires the expenditure of metabolic energy which will affect plant growth by reducing it under saline conditions. Reduced plant growth affects transpiration through the reduction of ground cover.

Aiming at assessing the reduction impacts of both soil and water salinity in crop evapotranspiration and yield, empirical crop salt tolerance response functions have been developed for several crops, namely rice (Maas and Hoffman, 1977). These functions allow defining yield reduction as a function of total soil solution salinity based on EC. The derived functions by combining yield-salinity equations (Ayers and Westcot, 1985b) with yield-ET equations (Doorenbos and Kassam, 1979). The resulting equation provides a first approximation of the reduction in evapotranspiration expected under various salinity conditions and has been widely used in field conditions (e.g. (Liu et al., 2022a, 2022b; Rosa et al., 2016)). Crop yields remain at potential levels until a specific threshold

of electrical conductivity of the saturation soil water extract ($EC_{e\ threshold}$) is reached (Allen et al., 1998; Maas and Hoffman, 1977). Once the average EC_e of the root zone exceeds this critical threshold, yield is assumed to decrease linearly in proportion to the increase in salinity (Allen et al., 1998; Pereira et al., 2007).

The rate of yield decline with increasing salinity is usually expressed as a slope, b, with units of % yield decrease per dS m^{-1} increase in EC_e. This is because not all plants respond similarly to salinity, as some crops are better able to make the necessary osmotic adjustments that allow them to extract water from a saline soil, or because they may be more tolerant to some of the toxic effects of salinity. According to the salt tolerance scale, rice is a sensitive plant and therefore does not tolerate high EC_e. The $EC_{e\ (threshold),}$ for rice is 3 dS m^{-1} (Allen et al., 1998; Maas and Hoffman, 1977). As discussed by (Grieve et al., 2012), this $EC_{e\ threshold}$ presents errors and further research is needed to reduce the uncertainty, particularly when using salt-tolerant varieties. In addition to this piecewise linear function, various non-linear models have been proposed to relate crop yield to salinity (Genuchten and Hoffman, 1984). Several authors (e.g. (Allen et al., 1998; Pereira et al., 2007)) have stated that the effects of soil salinity and water stress are generally additive in their impacts on crop evapotranspiration and therefore in terms of crop growth and yield.

On the one hand there are the steady-state models which assume that salt concentrations in soil water are almost constant for a given location and time period, allowing a simple representation of soil salinity and plant growth conditions. For example, the SIMDualKc model, which applies the FAO dual-crop coefficient approach to partition crop evapotranspiration into crop transpiration and soil evaporation, uses a steady-state salinity approach and computes the soil water balance daily using transient information (Pereira et al., 2007; Rosa et al., 2016, 2012), allowing appropriate water management and irrigation in saline/sodic environments. SALTMED model (Ragab,

2002) constitutes another example of models using this precise approach (Maas and Hoffman, 1977) for computing the soil water balance under salinity conditions.

On the other hand, there are the transient state models that simulate changes in soil–water content and salinity in the root zone caused by irrigation, rainfall, soil heterogeneity and management options. These changes may refer to timing and amount of irrigation, variable soil salinity conditions, variable crops and crop salinity tolerances, and variable irrigation water quality including rainfall. This group of models include, among others, UNSATCHEM (Šimůnek and Suarez, 1994), SWIM (Verburg, 1996), SALTMOD (Oosterbaan, 2000), SALTMED (Ragab, 2002), SWAP (Kroes et al., 2017; Van Dam et al., 2008), and HYDRUS (Šimůnek et al., 2016). Unfortunately, we have not found any salt modelling study related to rainfed rice, mangrove swamp rice or any rice-salt-modelling studies for GB or on the African continent.

As previously discussed, the MSRPS system in GB has a high concentration of soluble salts in the soil. In addition, there are no irrigation systems or others freshwater sources available (The Republic of Guinea-Bissau., 2018). Therefore, rice production is limited by the amount of rainfall, which is responsible for leaching salts to deeper layers (Cornelissen et al., 2020). Effective freshwater collection and management ensure rice production and, consequently, high-water productivity of collected rainwater. However, there is no information about the water and salt balance in the system to improve farmers' harvesting schedules. Therefore, such information is required to adequately design strategies and practices that enable better control of salinity and thus improve farmers' livelihoods.

To evaluate the performance of different rice farming systems, such as MSRPS, and develop practices that result in higher yields and/or water savings, it is important to use

indicators such as water productivity. This type of indicator allows comparing different cropping systems. The physical water productivity (WP, kg m^{-3}) is defined as the ratio of crop yield to the total water use (TWU) required to achieve the harvestable yield, expressed as kg m^{-3} (Ferreira et al., 2023; Pereira et al., 2012; Rodrigues and Pereira, 2009). The TWU is specified by the sum of four factors that quantify an approach of water consumed; thus, water productivity is computed as;

$$WP = \frac{\gamma_a}{P + \Delta SW + CR + I} \quad \text{(Eq 2.1)}$$

where:

γ_a*: total harvested grain (kg)*
P: seasonal rainfall amount (m^3)
ΔSW*: variation in soil water storage in the root zone from planting to harvest (m^3)*
CR*: capillary rise or groundwater contribution from a shallow water table (m^3)*
I*: total seasonal irrigation amount (m^3)*

As already mentioned, in saline soils, despite good agronomic management, the potential crop yield is not achieved and therefore the WP is reduced. Frequently, the WP denominator (Eq. 2.1) in MSRP does not take irrigation into account because it is not used. The reduction in water input is expected to be less than the reduction in yield, resulting in low WP (Bouman et al., 2007).

Under salinity conditions, an additional fraction of water is required to make the soil productive. Normally, irrigation water is increased by the leaching fraction (Maas and Hoffman, 1977; Minhas et al., 2020). Thus, the term TWU in Eq. 2.1 quantifies additional terms associated with salinity-induced stress on the crop (Pereira et al., 2012; Rodrigues and Pereira, 2009). First, $ET_{c\ act}$ is the seasonal actual evapotranspiration

(when cropped under salinity and other stresses such as water). Second, LF quantifies the volume of water used to leach the salts from the rhizosphere. Third, $N - BWU$ is the water not beneficial for the crop, meaning the excess water that flows beyond the rootzone (deep percolation or drainage), runoff from fields, water losses due to evaporation, and wind drift in sprinkling in irrigated systems. Therefore, WP quantifies the total production achieved based on the sum of three main factors as follows:

$$WPs = \frac{\gamma_a}{ET_{c\ act} + LF + N - BWU} \quad \text{(Eq 2.2)}$$

where:

WP_{salt}: water productivity in saline sites (kg m-3)
γ_a: total harvested grain (kg)
$ET_{c\ act}$: seasonal actual crop evapotranspiration (m3)
LF: water used for leaching salts from the rootzone (m3)
$N - BWU$: non-beneficial water use (m3)

In GB this WP_{salt} concept is most applicable to the MSRPS due to the presence of salt. However, no information is available to account for the losses in non-beneficial water use (N-BWU); these are mainly due to evaporation of paddies water, and in very few cases due to system drainage (Bouman et al., 2007). Runoff is commonly null unless precipitation events are high and in extreme cases may lead to the destruction of the dikes. Rice yield under salinity conditions may be improved through the implementation of breeding strategies which will increase WP_{salt}.

As discussed by Zwart (Zwart, 2013) comparing different rainfed cropping systems based on water productivity indicators must be performed with caution and non-manageable factors should be excluded. High WP values obtained under non-saline soils

or saline shallow water-table cannot be set as a benchmark value for a rainfed rice system; this means that regional or local optimized WP values should be used.

Essentially, constraints on rice yield within the MSRPS, and consequently on rice WP, are mainly related to challenges in efficient water management practices that enable soil salinity control. Every farmer must work closely with his neighbors to produce rice and gain a good understanding of water dynamics (through endogenous knowledge and informal networks of kin and kith) to ensure a successful rice harvest every year (Caeiro, 2019).

Due to the lack of information regarding local mangrove swamp rice yield, salt balance, and rice seasonal rainfall amounts there are, to our knowledge, no studies available about WP estimates in GB. Furthermore, we did not find any study on water productivity associated with mangrove swamp rice affected by salinity on the African continent.

5. General soil properties, taxonomy, and topography in MSR fields

MSR fields have different physicochemical soil properties and levels of anoxia compared to former mangrove soils. The latter are considered to be high-sulfur environments with a notable presence of clays and salts (Sylla, 1994). However, despite having the same pedogenic formation, *bolanhas'* soils are distinguished by high oxidation levels that allow the growth of plants susceptible to salinity (D'Amico et al., 2023). This allows the development of new soil horizons characterized by different chronologically deposited materials (Andriesse and Fresco, 1991).

5.1. Soil taxonomy in associated - tidal mangrove fields and tidal mangrove terrace

In general, GB presents three main soil categories in terms of soil physicochemical properties. The ferrallitic and ferruginous (non-hydromorphic) soils, in which a high concentration of iron predominates, are red in color and occur in upland areas. The hydromorphic soils, which include both marine alluvial (Halo-hydromorphic, as the ones of *bolanhas salgadas*) and continental (Grey, alluvial and terrace, Gley, Humic-gley) soils, characterized by long periods of anoxia and the presence of gley horizons (Oosterbaan and Vos, 1980; Teixeira, 1962; Ukpong, 1997). Finally, the lithic soils are characterized by the presence of rocks and consolidated materials in their horizons (Teixeira, 1962). A clear topo-sequence is observed in many villages (Table 2.4) with hydromorphic soils (*Bolanhas'* soils) occurring alongside ferrallitic soils (villages' upland soils). These ferrallitic soils are used for growing cash crops such as cashew, vegetables, and for rice nurseries.

Gleization soil conditions are prevalent in mangroves and plots soils, along with high concentration of sulphites and sulphates and a significant variability in soil organic carbon (SOC) concentration. Reduction conditions are commonly observed in mangrove soils (Teixeira, 1962). This extends across the entire soil profile, particularly within the first 150 cm of soil depth. In contrast, *Bolanhas'* soils are predominantly characterized by annual fluctuation in groundwater, with depths ranging from 30 to 150 cm below the soil surface (D'Amico et al., 2023). Soil taxonomic classifications reported for mangroves' and *Bolanhas'* soils are categorized based on the presence of sulphates and sulphites, horizon development, and organic matter content (Table 2.4). Thus, this variation is observed across the entire toposequence (tidal mangroves, associated mangroves, and old *Bolanha* fields), including mangrove areas and villages. In addition,

certain locations have been reported to have low concentrations of SOC derived from marine carbon (Andreetta et al., 2016). In this context, the deserted plots showed a significant decline across the soil profile compared to mangrove soils and new plots (Andreetta et al., 2016; D'Amico et al., 2023; Marius and Lucas, 1982).

The design of Guinea-Bissau's MSR plots varies depending on agroecologies' differences and the cultural practices of each ethnic group for water management, resulting in changes in the physicochemical properties of the soils. Different plot designs exist between the southern and northern regions of the country, with ethnic groups determining the size of plots based on the amount of stored fresh water they want to harvest (Figure 2.7). In the southern and central parts of GB, farmers construct dikes with significantly larger dimensions than those in the north. The probability arises from the soil texture, potentially facilitating the construction of larger dikes and deeper primary drainage channels (Figure 2.7, A.3), attributed to the clay deposit from alluvial sediments into the soil profile (D'Amico et al., 2023; Teixeira, 1962). In addition, the high rainfall levels lead farmers to modify internal drainage systems at the plot level to remove salts and increase leaching during the first rains (Cooper and McConkey, 2005; Espírito-Santo, 1949). For example, southern farmers design internal drainage systems (without outlets) within plots, while farmers in the north do not implement drainage systems to maintain a consistent water level within the plot (Oosterbaan and Vos, 1980). This has a significant impact on the salt concentration in the plots as farmers in the south manage to flush out the salt present in the upper soil layers with the first rainfall. Through the dilution of salts and their transport to the small drainage systems without outlets (Figure 2.7, A.5), farmers have a convenient method to open the plot and discharge the saline solution before soil tillage.

Table 2.4. Soil taxonomy and physicochemical characteristics in mangrove terrace, tidal mangrove and associated mangrove fields in Guinea-Bissau.

Characteristics	Tidal mangroves terrace	Tidal mangrove fields	Associated mangrove
Soil taxonomy (USDA)	Haplic sulfaquents, Typic sulfaquents, Sulfic Fluvaquents, Sulfic, Hydraquents, Sulfohimists, Hemists, Fibrists.	Histic Sulfaquents, Hapic sulfaquents, Typic Sulfaquept, Sulfic hydraqiuentsm, Tropofibrits Psammaquents, Sulfic tropaquepts, Typic tropaquepts, Aeric tropaquepts, Psammaquents.	Pisoplinthic, Hypothionic, Tidalic, Oxygleyic, Tropoquepts, Endoaquents.
Soil taxonomy (WRB-FAO)	Tidalic, Oxygleyic, Gleysol (clayic, hyposulfidic).	Hypothionic, Pisoplintic, Oxygleyic, Tidalic, Gleysol (vertic, drainic, salic, clayic).	Pisoplintic, Hypothionic, Gleysol (abruptic, loamy, drainic, salic, clayic, vertic).
Geochemical conditions	Anoxic	Sub-oxidation	Oxidation
Solubility of sulphates and sulphites	High	High – Medium	Low
Al - Fe^{+2} toxicity	High	High – Medium	Medium - Low
Na^{+}	High	High	Medium - Low
Soil organic carbon	High	High – Medium	Low
Possible chemical formations	Reduced iron (Fe^{2+}) Iron monosulfide (FeS) Iron disulfide (FeS_2)	Iron monosulfide (FeS) Pyrite ($2FeS_2$) Reduced iron (Fe^{2+}) Oxidized iron (Fe^{+3}) Hydrogen (H^{+}) Hydrogen sulfite (H_2S) Aluminum (Al^{+2}) Sulphate (SO_4^{2-}) Sulphites (SO_3^{2-})	Pyrite ($2FeS_2$) Hydrogen (H^{+}) Aluminum (Al^{+3}) Oxidized iron (Fe^{+3}) Sodium (Na^{+}) Sulphate (SO_4^{2-})
References	(Andreetta et al., 2016; D'Amico et al., 2023; Marius and Lucas, 1982; Teixeira, 1962)		

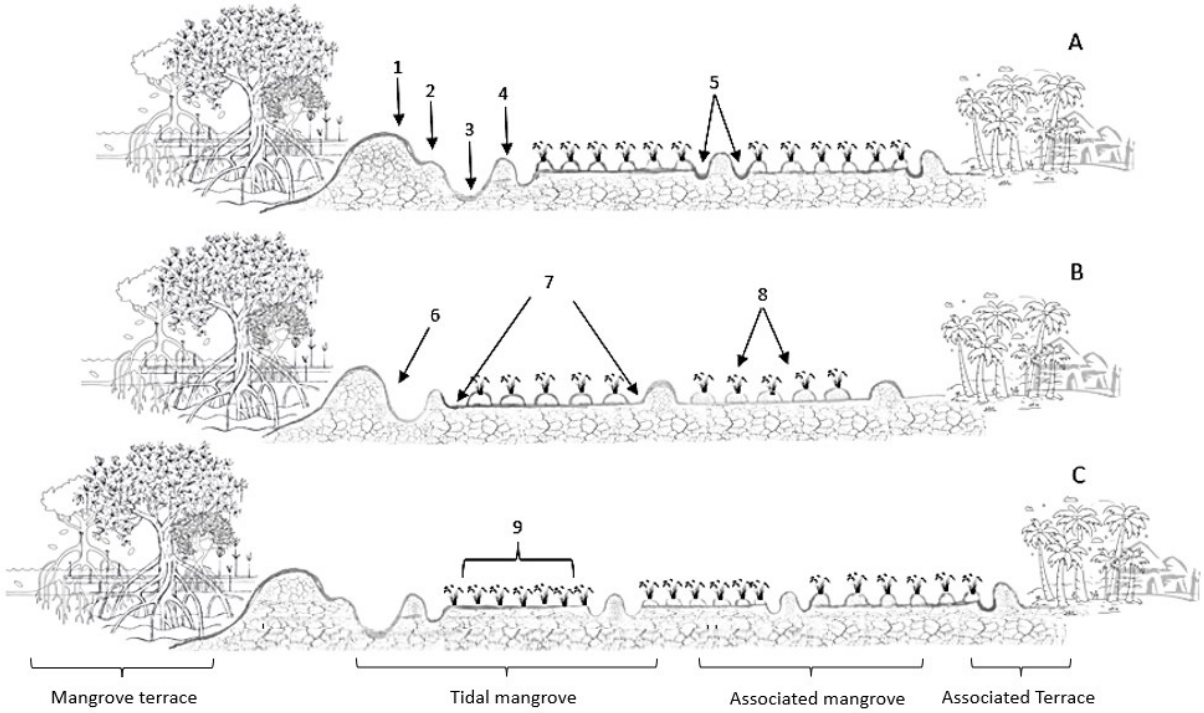

Figure 2.7. Characteristic of southern Balanta (A), northern Felupe and Baiote (B) and an example of new *bolanhas* (C) in Guinea-Bissau. 1 = Main dike in the South (*Orike grande*); 2 = Verandah (*Varanda*); 3= Main drainage (*Valeta*); 4 = Plots bunds (*Orike pekno*); 5 = Small drainage without outlets in the South (*Valeta do prike*); 6 = Main dike without verandah in the North (*Orike grande*); 7 = Plot without internal drainage in the North (*Prike*); 8 = Ridges (*Réguas*); 9 = New plot without ridges (*Bolanha novo*). Adapted from (Cooper and McConkey, 2005; Cormier-Salem, 1999; Merkohasanaj et al., 2022)

Soil fertility is significantly influenced by proximity to tidal mangrove areas, as these soils have higher accumulation of SOC. This is related to the quantity of organic materials present, which mineralize over time and release a significant amount of nutrients that benefit the crop (Merkohasanaj et al., 2022). Due to the decline in SOC occurring in old plots (Andreetta et al., 2016; D'Amico et al., 2023), farmers in GB frequently tend to develop new mangrove swamp fields (Figure 2.7, C.9), with the aim of finding more fertile and highly productive areas for growing rice. However, as previously mentioned the new plots (*bolanha novo*) are the only areas with a high concentration of

salts and sulfuric acids in the first surface layers of the soil. Due to their active oxidation state, this can potentially cause serious problems with rice growth. This is different from *bolanha de tarrafe* and *bolanha de metade* fields (plots located in the middle part of the paddies far from the mangroves), as these have undergone prolonged oxidation. Many of these salts, sulfites and sulfates, were leached by rainfall and settled in deeper horizons, where they do not affect rice growth (D'Amico et al., 2023).

5.2. Acidity formation in tidal mangrove soils.

Sulfuric acids in the soils of MSR fields start affecting the crop in the early stages of the new plots (first 3-5 years). New plots are the most vulnerable sites because they initiate the desalination process and exhibit active pedochemical acidification (Table 2.4, Figure 2.8). These chemical processes depend on the amount of rainfall in the system as fresh water catalyze chemical processes and leach toxic compounds such as sulfuric acid ($2SO_4^{2-}$), hydrogen sulfite (H_2S), pyrite ($2FeS_2$), reduced iron (Fe^{2+}) and iron monosulfite (FeS) into deeper soil layers (Sylla, 1994; Van Ghent and Ukkerman, 1993; van Oort, 2018). Within the dynamic systems of oxidation and reduction, pyrite and sulfuric acid are formed, and organic materials decompose (Figure 2.8). These processes can increase soil acidity, resulting in extremely low pH values (< 3.5), reducing the availability of various nutrients to plants (N, K, Ca, Mg, P, Zn) and causing toxicity (Al^{3+}, Fe^{2+}) in the soil (Dossou-Yovo et al., 2022; Sylla, 1994). However, in some tidal mangroves (*bolanha de Tarrafe*) and associated mangroves (*bolanha Metadi*) these processes only occur at deeper horizons where they do not affect the plant's root system (Andreetta et al., 2016; D'Amico et al., 2023; Sylla et al., 1995; Teixeira, 1962). In summary, villages in the northern and southern regions face problems of sulfuric acid toxicity especially in "*bolanha novo*", with some "*bolanha de Tarrafe"* occasionally affected by a strong influence of groundwater levels and tides (Marius and Lucas, 1982).

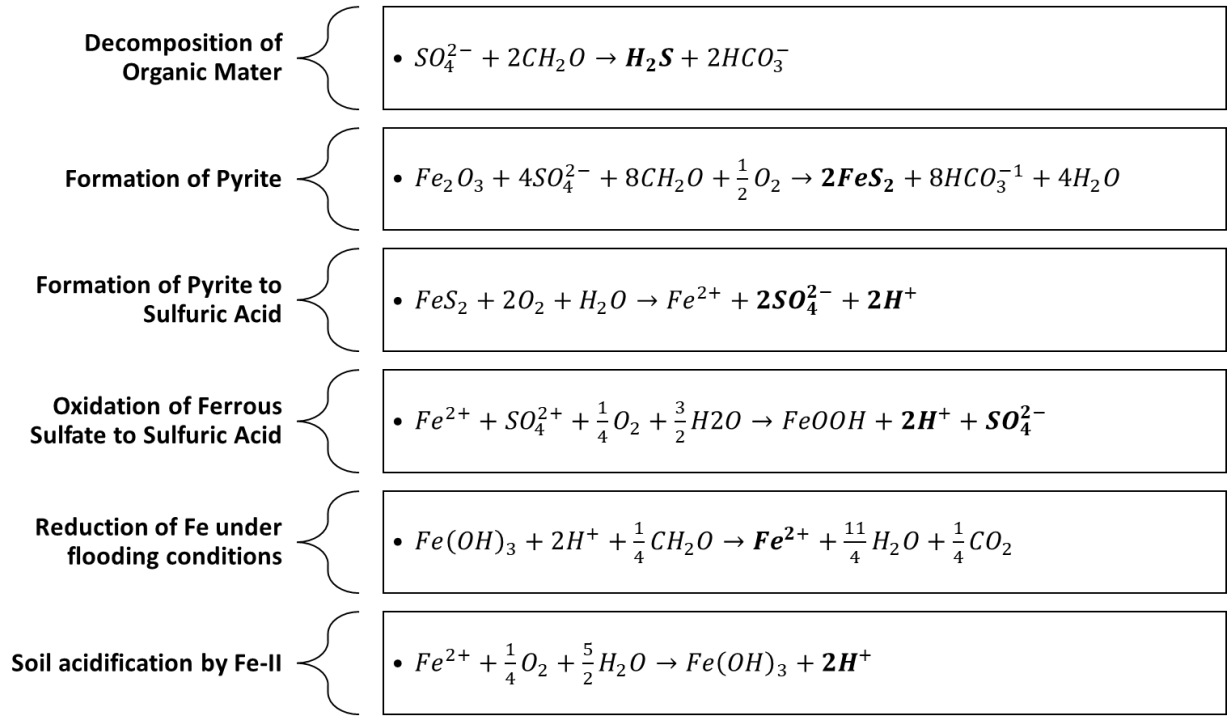

Figure 2.8. Chemical process in acid sulphate soils under Mangrove swamp rice production systems. Adapted from of (Sylla, 1994; Teixeira, 1962).

6. Rainfall patterns and farmers' agronomic practices related to water management in the MSRPS

The rice production cycle in GB is constrained by the rainy season (onset and duration and length of dry spells) and the accumulated rainfall. Fresh water availability is the limiting factor for rice production across the country, especially in the MSRPS. The system relies on salt leaching and substantial water accumulation to ensure a complete crop cycle. Recent rainfall reports have shown that rainfall patterns are heterogeneous (Mendes and Fragoso, 2023; Njipouakouyou et al., 2019). In the period from 1961 to 1985, there was a significant decrease in rainfall in the country (Figure 2.9). However, it is estimated that there has been a slight increase in annual rainfall of around 350 mm over the last 40 years (Figure 2.9). It is evident that the Bolama region consistently receives higher rainfall (1953 mm) than the Bafata (1276 mm) and Bissau (1524 mm) regions (Figure 2.9). For the other MSRPS regions, Tombali, Oio and Cacheu, there is currently

a lack of meteorological data. Some reports in the 1980s from the Casamance/Senegal, which lie close to Cacheu Region, estimated that the average annual rainfall ranged from 1200 and 5000 mm (Linares, 1981), which is sufficient to support MSR growth.

Although most regions of the country receive sufficient rainfall for rice production, the main challenge lies in the uneven distribution of rainfall, that occurs within a relatively short timeframe (Mendes and Fragoso, 2023). This condition has a significant impact on rice growth. Rainfall is the most important factor in soil management, agronomic practices for rice cultivation, and the overall sustainability of the MSRPS. This creates significant challenges in managing the water and salt balance in rice production (Luning, 1984).

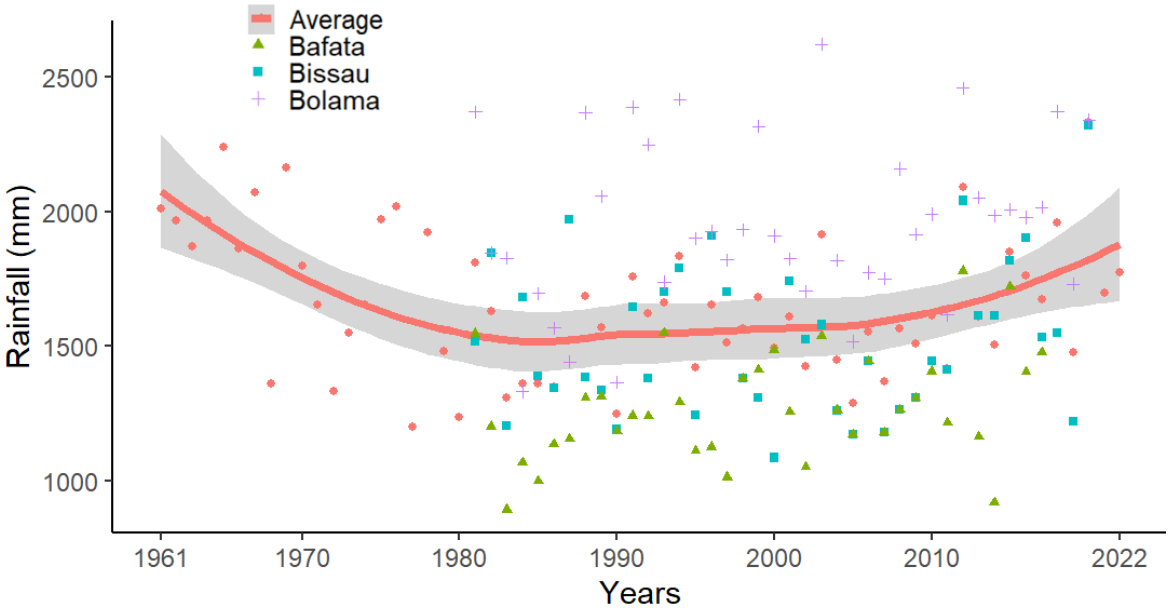

Figure 2.9. Smoothed conditional means plots of rainfall (mm) in Bolama, Bafata and Bissau, Guinea-Bissau, for the period 1961-2022. Data source: World Bank information (The World Bank, 2023) and National Institute of Meteorology of Guinea-Bissau.

The manual preparation of the plots' ridges, depends on ensuring adequate soil moisture for tillage, and therefore on the beginning of the rainy season (W Hawthorne,

2001; Van Ghent and Ukkerman, 1993). Nevertheless, sufficient soil moisture is required to avoid problems with soil plasticity during plowing. There is no information available on the plasticity limits associated with soil tillage, although there are old reports of the use of mechanization for soil tillage in GB (Cabral, 1954b). However, not all farmers have the necessary resources for mechanized operations, further exacerbated by limited access to large machinery on the plots (Cabral, 1954a). Furthermore, heavy machines can not only compact the clay soils, but also create/increase weed infestations. On the contrary, the manual plow is an affordable and sustainable tool that is accessible to all farmers in the villages (Bivar and Temudo, 2014; Martiarena and Temudo, 2023; Temudo, 1998), with which they can better control soil and weed conditions.

After soil tillage, farmers use two rice planting techniques: transplanting and direct seeding (Cossa, 2023; Temudo, 1998). Transplanting is the most used technique as it ensures more uniform distribution of the plants and usually a higher productivity (Nuijten et al., 2009). There is no exact date for planting in nursery, but generally it depends on the first rains, individual farmer's experience, soil moisture, and salinity levels at the sites. Direct seeding is most frequently used in *bolanha de Tarrafe*, where the farmer identifies sites with good fertility and low salinity (Röhrig et al., 2021; Temudo, 1998; Van Ghent and Ukkerman, 1993). In this technique, some sites are plowed while others simply planted or broadcasted with pre-germinated rice seeds (Cossa, 2023; Temudo, 1998).

The rice harvest usually begins in November and lasts through January but depends mainly on the schedule set by farmers, which mainly depends on each year rainfall distribution pattern in each village. There are agronomic and social problems in the villages preventing them from using short cycle varieties. When rice is mature in only few plots of a *bolanha*, it is very likely that the birds will concentrate their feeding destroying completely the potential harvest (Linares, 2002; Teeken and Temudo, 2021).

However, if all farmers harvest their rice at the same time, this problem is distributed among all plots (Temudo, 1998). Additionally, farmers must plan their harvests based on the water availability and salinity levels associated with their plots (W Hawthorne, 2001; Marzouk, 1991). At the end of the crop cycle, the dilution of salts has a reverse effect (decreases again due to the end of the rains), leading to water and salt stress in rice plants (Dossou-Yovo et al., 2022; Van Ghent and Ukkerman, 1993). In addition, evapotranspiration increases the salt concentration in the plots, leading to productivity problems (Abreu and Correia, 1993; Padhy et al., 2022).

6.1. The use of dikes, bunds and rigdes for water management in the paddies

The main dikes are structures used to prevent tidal water from entering the paddies (Figure 2.10), while the bunds are used by farmers to collect and store fresh water inside the plots. At the topographic scale of the system, the slopes toward the mangroves are in general minimal and serve only to channel water from one plot to another. In addition, soil texture, the level of the groundwater and the location of the plots within the paddies can either favor or hamper a rapid accumulation of fresh water in the plots. Consequently, dikes play a central role in rice cultivation due to their control over leaching, oxygenation, and water storage in the plot, distinguishing them from the mangrove forests' soils (The Republic of Guinea-Bissau., 2018).

Bunds or secondary dikes surrounding the plots are the primary structure responsible for managing water levels in the MSRPS (Figure 2.7, A.4). These play an important role in ensuring the appropriate water depth during rice growth. However, when heavy rainfalls occur during several consecutive days simultaneously with spring tides, farmers may be unable to divert the excess water to other plots and then to the sea branch. This kind of situation led to the loss of a significant portion of rice nurseries in mangrove

fields during 2022. There is no information about the distribution, quantity, and potential cumulative water content within the plots according to rain distribution, especially in relation to high tides (when it becomes impossible to drain excess freshwater through the drainage pipes to the river or sea branch).

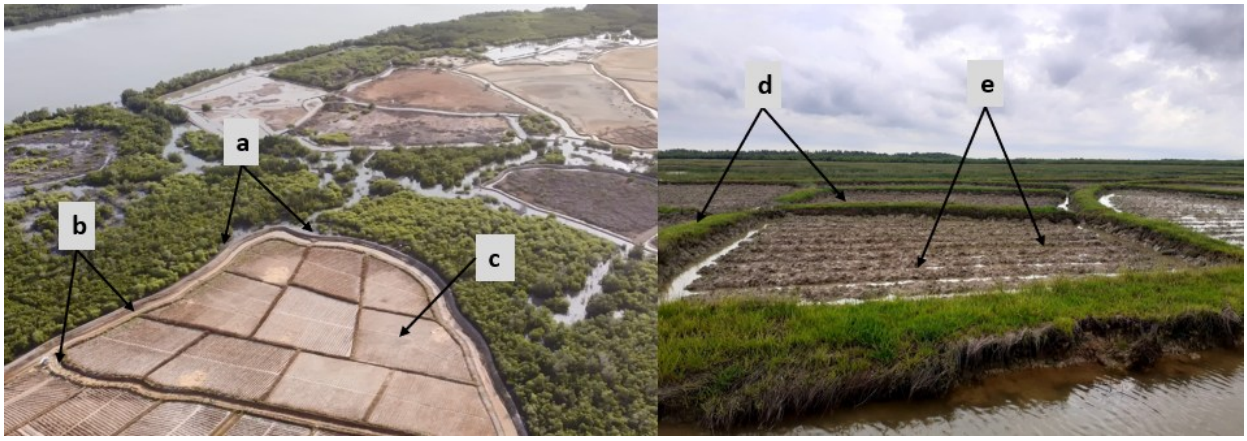

Figure 2.10. Plots of rice production system in mangrove of Elalab, Guinea-Bissau. Identification of (a) dikes, (b) drainage channels, (c) plots, (d) bunds, and (e) ridges.

Ridges play a critical role in the MSRPS by increasing soil fertility and reducing soil resistance to roots penetration. Soil tillage in MSR plots promotes the incorporation of existing weeds, increasing the amount of SOC and triggering the mineralization process. Mineralization gradually releases nutrients, promoting the growth of rice plants and generating satisfactory yields. Additionally, ridges facilitate better rice transplanting by reducing soil compaction. Some studies have shown that ridges also promote the leaching of salts and toxic concentrations of soil acids (J Espírito-Santo, 1949; The Republic of Guinea-Bissau., 2018). The use of ridges is specifically aimed at improving the management of the soil physicochemical properties in rice production systems. Only in a few cases, such as new plots, farmers do not use ridges (Figure 2.7, C.9), because the

soil is already high in fertility and lacks compaction (The Republic of Guinea-Bissau., 2018). They usually use these plots for rice nurseries or direct planting without tillage.

The bunds (Figure 2.10.d) are the main infrastructure for rice harvesting, agronomic management, and water conservation in the plots. Proper management of freshwater in plots can ensure good harvests (J. Espírito-Santo, 1949; W Hawthorne, 2001), effective pest control, and prevent salinization problems at critical phenological stages (R3-R6).

The potential of the plots for storing fresh water is determined by the height of the bunds and the topography of the plot floor. After rice transplantation, farmers control the level of stored fresh water according to the plant height. They open the bunds to ensure that the water level does not submerge the seedlings, which could lead to their death. When the rice plants reach a size beyond the limit of the bund, this is closed completely to maximize water storage. Since fresh water is present within the bund, only rice and other *Poaceae* species with aerenchyma tissue can thrive in waterlogging conditions. This prevents the growth of weeds that could affect rice cultivation. The ruptures in the main dikes are related to maintenance work, heavy rainfall, soil texture, and high tides. Soils with a high clay content offer increased rigidity to the dikes, enhancing their stability. Conversely, in regions characterized by sandy soils, dike maintenance requires substantial manual labor and constant attention (Bivar and Temudo, 2014; Temudo, 1998). In northern GB, there have been reports of dike maintenance problems due to labor shortage, resulting in saltwater intrusion into the polders and complete losses of rice production areas (Temudo et al., 2022; Temudo and Cabral, 2023). Dike maintenance is a collaborative task that requires strong cooperation and communication among farmers to prevent ruptures and facilitate a quick repair during the rainy season.

In 2020, high rainfall over a short period combined with high and strong tides, resulted in significant damage to many main dikes in several villages of GB (Mendes and Fragoso, 2023). This damage led to the intrusion of saltwater into the paddies, causing significant problems in rice production as farmers lost their harvests and substantial areas of rice fields and crops. Nevertheless, there is evidence from other countries that saline water intrusion can help eliminate weeds and increase soil fertility (Wolanski and Cassagne, 2000); this practice was also used by GB farmers during colonial times. However, allowing the invasion of the brackish water during the dry season requires high rainfalls for salt leaching, as it could lead to hypersaline problems at planting sites (Chauhan et al., 2017; J Espírito-Santo, 1949; The Republic of Guinea-Bissau., 2018; Wolanski and Cassagne, 2000).

7. Key issues overview and future research

With this review article, we aimed to characterize the mangrove swamp rice production system of Guinea-Bissau in relation to soil salinity, water use and water productivity.

The biophysical description serves as the initial approach to comprehending the intricate dynamics of MSRP in GB. These dynamics are based on over 2000 years of agricultural experience and acclimatization, during which farmers have learned to manage this complex system to render it productive for growing rice. Through observations and experimentations over time, farmers have learned to manage the physicochemical characteristics of sites, by using efficient water harvesting techniques and selecting appropriate rice varieties. This has enabled them to create specific swamp rice production areas (named *Bolanhas* in Kriol), where they conceptualize the working methods, suitable varieties for growth and the agronomic care required for each location

(“*Bolanha Belju”, “B. metadi”, “B. tarrafe”, “B. nobu” and “Nhatabas – Tarrafe novo*”).

This information is characteristic for each village, as each region presents vastly different and highly complex biosystems in terms of climatic conditions, soils, and crop management needs. Several questions remain to be answered such as: Why do farmers use drains on the swamp fields in the south, while these are not present in the north? Does salinity decrease if drains are used within the swamp fields? Can these drains help store a greater amount of freshwater? How are the initial salt conditions distributed in a MSRP field? When is the appropriate time for plants to grow without salt affecting their growth and productivity? There is a need to perform a biophysical characterization of the plots and create maps of certain physico-chemical soil properties. Due to the specificity of the system at each location there is therefore a research gap that needs to be overcome. With this in mind, studies were developed in Cafine-Cafal in the south and Elalab in the north of GB and presented in the companion article Garbanzo et al., (2024) (Chapter 3).

The agronomic practices developed in the MSRPS in GB are tailored exclusively for rice cultivation, aiming for optimizing rice yield and water conservation in the “*bolanhas*”. A greater availability of freshwater in the plots would ensure rice production in the villages, as the crop does not face issues of water-saline stress within the system. These practices have been refined through generations of farmers, benefiting from their specialized experiences. However, under the current and future climate change scenario, particularly in terms of variability and reduced rainfall, these already vulnerable systems will become more fragile. This fragility results mainly from the increase in soil salinity due to reduced salt leaching by rainfall. It is fundamental to adapt crop management to the variable rainfall calendar, labor efficiency and the soil hydro-salt dynamics. This set of constraints affects rice production, exposing communities in the villages to food

insecurity and malnutrition. Therefore, further information to characterize the biosystems and rice varieties is essential to develop tailored practices that meet the specific needs of each village. This information is crucial for supporting decision making when planning sustainable management of grain production in the near future.

The main constraints to agricultural performance and rice productivity in GB have been identified and are related to insufficient and irregular distribution of rainfall, declining soil fertility, and poor water management. The information collected indicated that there is:

- ✓ A wide range of rice varieties with different names is found in the MSRPS. Understanding their characteristics of each variety, particularly in terms of salt tolerance, could improve agronomic recommendations at the national level.

- ✓ A lack of understanding of water dynamics in MSRPS. This knowledge, obtained from field measurements and modelling, could facilitate the efficient planning of rice production cycles while minimizing problems related to toxicity and salinity.

- ✓ A lack of knowledge about the salt balance, especially regarding the initial and final salinity conditions in different contexts. The development of a tool that allows to assess the hydro-saline balance performance in the MSRP is crucial to optimize the cultivation calendar for the timely start of each rice production season.

- ✓ Limited information on soil fertility, nutrient dynamics, and their relationship to MSRPS productivity. Comprehensive soil chemical characterization and understanding of nutrient dynamics could improve on-site nutrient management.

- ✓ No information regarding the spatialization of physicochemical properties in swamp fields (“*bolanhas*"). Spatial mapping of soil properties could help identify areas with higher fertility, salinity, and the potential for improving rice productivity.

- ✓ Insufficient studies on plasticity related to adequate soil moisture at the beginning of farming operations. Generating maps in this regard could provide farmers with valuable tools, allowing them to prioritize sites with optimal conditions for soil tillage. The companion article by Garbanzo et al. (Garbanzo et al., 2024) developed soil consistency maps with the aim of supporting farmers in decision making.

- ✓ A lack of studies on tidal dynamics for the creation of an early warning system and on main dike management. Providing information about extreme climatic events, monitoring and identifying vulnerable zones and help in the dissemination of recent endogenous innovations on dike building and maintenance could help prevent saltwater intrusion and minimize losses in rice production.

- ✓ A lack of continuous regional climate monitoring programs. Characterization of regional climatic variables could assist in agronomic calculation of rice water requirements in the MSRPS of GB. This would enable the development of early warning systems to support decision-making in rice production.

- ✓ Local constraints to balance ecosystem sustainability with the food needs of coastal people, who feel urged to clear new mangrove areas to create rice fields even when there was a need to restore deforested areas to prevent dike ruptures and harvest failures. This implies that compensation mechanisms for poor coastal inhabitants must be created to protect ecosystem services in GB blue carbon environments.

- ✓ External interventions or development projects do not usually align with the local realities and the needs of farmers' leading to challenges in implementing sustainable practices.

- ✓ Limited programs to restore desertified swamp fields. Initiating restoration efforts for these plots could include planting trees through the introduction of agroforestry practices and/or improving the conditions for reviving rice cultivation.

Overall, there is still a lot of progress to be made in terms of research relative to MSRPS conservation and management.

Chapter 3

Moving toward the Biophysical Characterization of the Mangrove Swamp Rice Production System in Guinea Bissau: Exploring Tools to Improve Soil- and Water-Use Efficiencies

This chapter was published in *Agronomy*.

Garbanzo, G., Céspedes, J., Sandoval, J., Temudo, M., Paredes, P., Cameira, M. do R., 2024. Moving toward the Biophysical Characterization of the Mangrove Swamp Rice Production System in Guinea Bissau: Exploring Tools to Improve Soil- and Water-Use Efficiencies. Agronomy 14, 335. https://doi.org/10.3390/agronomy14020335

Keywords: Water Management; Water Harvesting; Soil Consistency; Soil Salinity; Soil Tillage; West Africa.

1. Abstract

The mangrove swamp rice production system (MSRPS) in West Africa faces significant challenges in soil, water, and salinity management, making rice production highly vulnerable to variations in the spatio-temporal distribution patterns of rainfall, which are exacerbated by climate change. This study's results can provide the initial basis for co-developing strategies with farmers aiming to contribute to the biophysical characterization of the MSRPS, in particular: (i) estimate the water-harvesting efficiency (WL_{ef}) of the plots in the north and south of Guinea-Bissau (GB); (ii) characterize the unevenness of the bottom of the plots, which leads to salinization spots; and (iii) create soil consistency maps to provide farmers with a tool to prioritize sites with optimal conditions for tillage. The research was conducted between 2021 and 2023 in the study site of Cafine-Cafal in the south and Elalab in the north of GB. Systematic soil sampling in a grid was designed to quantify the soil consistency and plot/ridge areas were determined. Linear models were developed to predict biophysical parameters (e.g., effective planting areas and water-logging depths) and geostatistics were used to create soil consistency maps for each study site. The results show precipitation water-harvesting efficiencies of 15% and 16% for the southern and northern regions, respectively. Furthermore, the plasticity limits of 18.6% for Elalab and 35.5% for Cafine-Cafal show the most appropriate times to start tillage in specific areas of the paddies. This study provides information on the efficient management of tillage and freshwater conservation, providing MSRPS farmers with useful tools to counteract the effects caused by salinity and rainfall variability.

2. Introduction

Rice is one of the main cereals in the diet of tropical countries worldwide. According to estimates by the Food and Agriculture Organization, its production has increased from 426 to 510 million tons over the last 10 years (Chauhan et al., 2017; Food and Agriculture Organization of the United Nations., 2018; Kraehmer et al., 2017).

In the tropical region of northwest Africa, rice is the most consumed cereal at a regional level, particularly in countries such as Senegal, Guinea-Bissau, Guinea Conakry, and The Gambia (Kyle, 2015). These countries have a specific rice production system linked to the mangrove forests of the coastal areas, designated as mangrove swamp rice production systems (MSRPSs).

An MSRPS results from the slashing of the mangrove trees and the construction of dikes for the creation of paddies (Ukpong, 1995). Thus, MSRPSs have been pointed out as the main cause of mangrove deforestation in Guinea-Bissau (García del Toro and Más-López, 2019; Temudo and Cabral, 2017). Among the West African countries practicing mangrove swamp rice cultivation, Guinea-Bissau has the largest area occupied by this farming system (Hawthorne, 2001; Temudo, 2011; Temudo and Cabral, 2017) and the highest total production. This distinctive agro-fishing livestock farming system is based on the development of expertise (for dike and dam construction and maintenance, water management, control of soil fertility and toxicity, and selection of rice varieties) and the intensive mobilization of labor (e.g., for land clearing of mangroves, the construction of dikes and canals, soil desalination, and plowing) at certain periods of the crop cycle (Hawthorne, 2001; Linares, 1981; Martiarena and Temudo, 2023; Temudo, 2018; Van Ghent and Ukkerman, 1993). Both the construction of dikes and bunds that delimit the plot and soil tillage are undertaken manually using a long iron-tipped wooden plow.

Rainfall is the only source of water to meet crop water needs and to flush salt from the soil profile (Écoutin et al., 1999; Espírito-Santo, 1949; Schwarz, 1993; Temudo, 2011). Therefore, rice is grown during the rainy season (July to November) when the planting sites become suitable for the rice plant, namely, the salinity has reduced to tolerable levels for rice varieties (Écoutin et al., 1999; Tesio et al., 2021). This makes plant growth difficult (Baggie et al., 2018; Ukpong, 1995; van Oort, 2018) and leads to a large variability in rice productivity across the country. However, the rainfall impact depends on both its annual value and its distribution (Davidson, 2009; Mendes and Fragoso, 2023). Climate change and poor water management have led to desertification and the abandonment of many fields, which have become infertile and have high salt concentrations (Andrieu, 2018; Raimundo Lopes et al., 2022; Temudo and Cabral, 2023).

Very few field studies on soil characterization and water management have been carried out on the MSRPS (Dossou-Yovo et al., 2022; Thiam et al., 2019). These soils have very particular physical and chemical properties because, as stated above, they were previously occupied by mangroves and flooded with brackish water. Furthermore, the water management of an MSRPS is mainly based on the accumulation of rainwater (Andreetta et al., 2016; van Oort, 2018).

The dimensions of plots are of great importance as they facilitate the harvesting of fresh water from rainfall, which is crucial for plowing, salt leaching, cation solubility, and optimal rice growth (Van Ghent and Ukkerman, 1993). The dimensions of the plots observed in one region should not be extrapolated to the national level, as there are different cultural practices and knowledge gaps regarding soil, water, and salt management. For example, in years and regions with limited rainfall (Mendes and Fragoso, 2023), farmers face the challenge of accumulating enough fresh water to manage their plots. Additionally, as farmers explore new cultivation areas, they change the size

of the plots, resulting in increased variability. Therefore, to ensure optimal soil and water management and effective salinity control, it is essential to have a detailed understanding of the plot dimensions at local and regional scales, rather than making generalized assumptions without empirical basis (Dexter and Bird, 2001). Although MSRPSs are dominant in coastal areas of Guinea-Bissau and Senegal (Casamance) (Linares, 1981; Penot, 1995), there is still a lack of comprehensive information on the specific regional dimensions of these structures.

The biophysical characterization of the MSRPS is an urgent need, with the aim to improve rice production, as suggested in the companion article Garbanzo et al. (Garbanzo et al., 2024). This involves studying its physical, biological, and chemical components to understand how they interact in a particular environment. Thus, this approach examines various elements, such as soil properties, climate, water availability, plant genetics, biodiversity, and land-management practices (Hongliang Fang et al., 2005; Martínez-López et al., 2021; Nambiar et al., 2001; Singh et al., 2008). The biophysical characterization of the MSRPS serves as a strategic approach to implementing development interventions from multiple perspectives with the goal of establishing a sustainable and productive system. The development of cropping diagnostic tools for efficient water and soil management represents the first step toward improving rice production (Bos et al., 2006; Ukpong, 1997). The national characterization of MSRPS in Guinea-Bissau can provide insights into the different ways in which they can become better adapted to local agroecological conditions in times of climate change (Merkohasanaj et al., 2022; Temudo et al., 2022). Additionally, the development of geospatial distribution maps (Fandé et al., 2022) for specific soil management variables could be helpful in scheduling manual soil preparation tasks. This could promote a more systematic approach to agriculture and rice production that is adapted to the micro-

climatic diversity of the country (Sylla et al., 1995). Therefore, characterizing parameters such as the techniques used in the construction of plots and dams and the soil physical parameters could provide an effective strategy for adapting to climate change by improving water harvesting, reducing rainfall needs, and mitigating desertification in the coastal villages of Guinea-Bissau.

Soil consistency limits play an important role in soil tillage, i.e., the preparation of the soil for growing crops. It determines the workability of the soil, and farmers' knowledge of it allows them to understand how easily the soil can be manipulated, shaped, and cultivated (Utomo and Dexter, 1981). It helps in deciding the right time to till the soil (Cresswell et al., 1991; Obour et al., 2017; Sharma and Bora, 2003). This can also prevent soil compaction, as working beyond the plastic limit can change the soil structure, making it more susceptible to compaction, and reducing the porosity, which has a negative impact on root growth and water infiltration (Arvidsson and Bölenius, 2006; Boekel and Peerlkamp, 1956; Keller et al., 2007; Keller and Dexter, 2012). Proper understanding and management of soil consistency limits contribute to the creation of an ideal seedbed. This facilitates seed germination, root growth, and overall plant development. Essentially, knowledge of soil consistency limits enables more informed decisions regarding the timing, depth, and intensity of tillage operations, ultimately contributing to improved soil quality and better crop yields. Soil consistency limits refer to the different moisture contents at which the soil behaves differently (Haigh et al., 2013).

Based on the relationships described above and the research gaps identified in the literature (e.g., Garbanzo et al., (2024) (Chapter 2); Martiarena and Temudo, (2023)), the present study aimed to contribute to the biophysical characterization of the MSRPS in the north and south of Guinea-Bissau in order to improve the understanding of the soil–water–

salinity relationship for optimized plot management. Specifically, our aim was to (i) estimate the water harvesting efficiency of the plots in the north and south of Guinea-Bissau; (ii) characterize the unevenness of the bottom of the plots, which leads to salinization spots; and (iii) create soil consistency maps to provide farmers with a tool to prioritize sites with optimal conditions for tillage.

3. Materials and Methods

3.1. Location and Main Characteristics of the Study Sites

The research presented in this paper was conducted between 2021 and 2023 in two regions of Guinea-Bissau (GB). Located in West Africa, GB covers an area of approximately 36,125 km^2 and is bordered by Senegal to the north, and Guinea Conakry to the east and south (Figure 3.1). Two case studies were selected, one in each region. The Elalab case study was located at 12°14′48.5″ N, 16°26′30.3″ W in the S. Domingos administrative sub-region of Cacheu, which is representative of the "Diola" and "Baiote" ethnic groups' techniques. The Cafine-Cafal case study was located at 11°12′40.4″ N, 15°10′26.7″ W in the Tombali region, which is representative of the "Balanta" ethnic group techniques (Figure 3.1). Both sites present elevations from zero to two meters above sea level.

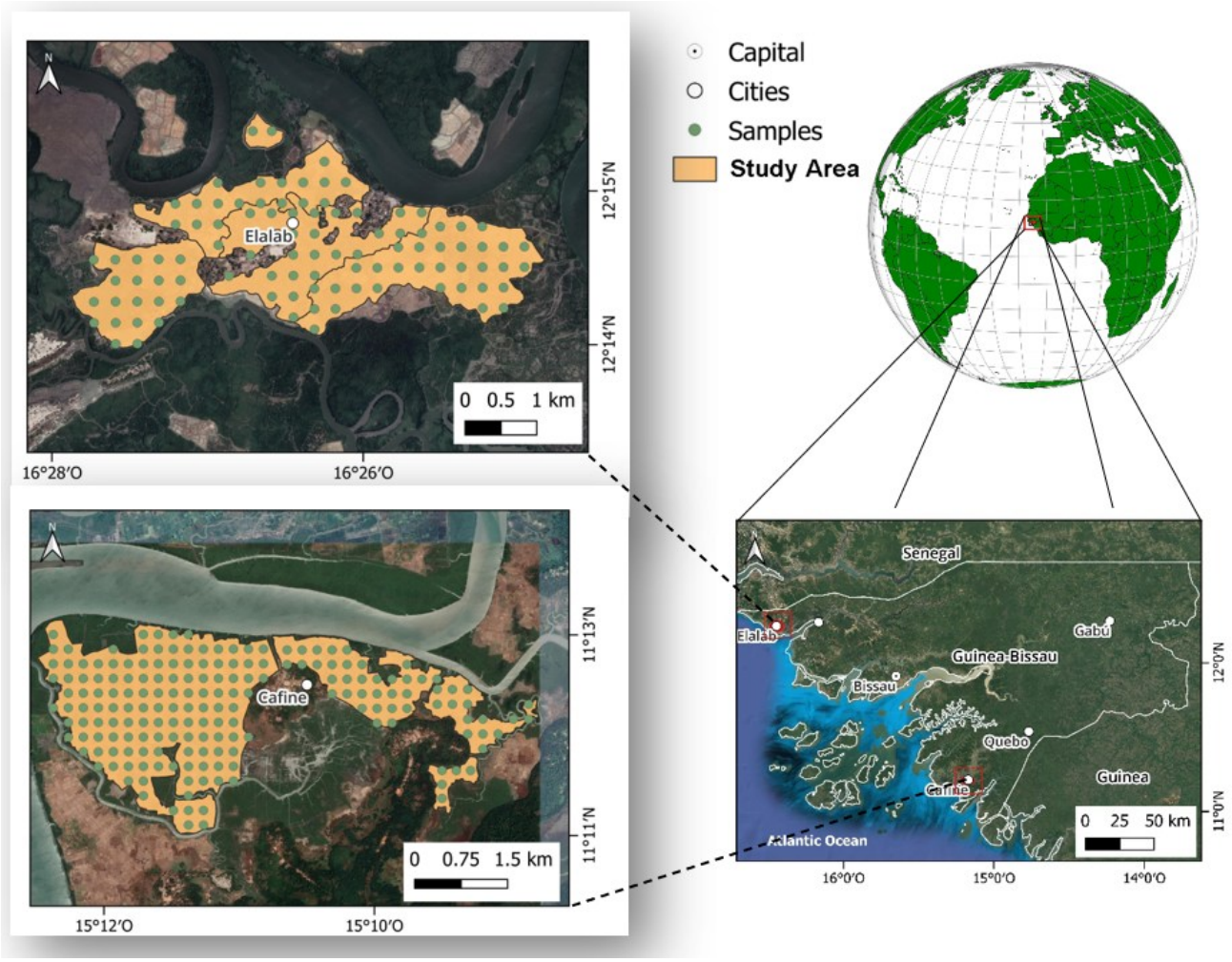

Figure 3.1. Locations of Guinea-Bissau and the study sites Elalab and Cafine-Cafal in the north (S. Domingos, Cacheu) and south (Tombali) of the country, respectively. The maps show points representing the locations where soil samples were taken for physical and chemical analysis.

According to the Koppen climate classification (Beck et al., 2018), the climate in these regions is AW, which is a tropical monsoon climate with heavy rainfall during the wet season, which usually lasts from June to October. The coastal zone presents an average annual rainfall between 1500 and 2500 mm (Mendes and Fragoso, 2023) and annual average temperatures range from 24 °C to 27 °C (Sambú, 2003). The temperature regime is characterized by a low annual variation, with May being the hottest month (29 °C) and January the coldest one (25 °C) (Mendes and Fragoso, 2023).

The agroecosystem has been classified as a rainfed wetland rice ecosystem, particularly within the sub-ecosystems prone to drought and flooding (Balasubramanian et al., 2007). These are characterized by high salt concentrations, which limits rice cultivation to periods when freshwater storage conditions allow for plant growth. In our case studies, samples were collected and observations were made on the entire mangrove swamp rice area (paddies), particularly the associated mangroves ("bolanha doce") and tidal mangroves ("bolanha salgada"). There are two traditional systems of rice swamp cultivation in GB the inland freshwater swamp fields ("bolanha doce") and mangrove swamp ("bolanha salgada"). Both systems refer to rainfed rice cultivated with a permanent depth of water (permanently flooded paddies) until or almost until the end of the rice cycle. The freshwater swamps ("bolanha doce") where rice is cultivated are located in inland valleys where there is a shallow water table or an impermeable soil layer that allows for water storage, and thus, assures fresh-water harvest. Differently, mangrove swamp rice ("bolanha salgada") is characterized by the former presence of mangrove forests invaded by the tides over the years in a fraction of or the whole area of the rice fields, thus leading to a high concentration of salts in the soils, as described in the companion paper Garbanzo et al. (Garbanzo et al., 2024).

The soils in the MSRPS areas were included in the orders of the Inceptisols and Entisols according to the Soil Taxonomy–USDA (Teixeira, 1962). These soils were formed by alluvial fans that resulted from tidal sedimentations (Marius and Lucas, 1991; Schoeneberger et al., 2012; Soil Survey Staff., 2022a; Sylla, 1994). They present a Ustic moisture regime, as they are dry for at least 90 cumulative days in a normal year (Soil Survey Staff., 2022a). Originally, they were mangrove soils that were converted into rice production fields through anthropogenic activities after three to five years of preventing seawater intrusion by building dikes around the planting sites.

3.2. Experimental Observations and Data Collection

Using geographical information system software (QGIS), polygons were generated to define the rice production areas in Cafine-Cafal and Elalab. Transects were used to assess plots and to delimit the main dikes of the paddies. Once the geographic coordinates of the site were determined, polygons were generated for delimiting the paddies ("Bolanhas") used for cultivation. Landsat satellite images were used to identify plots and accurately delineate the bunds, enabling the determination of their respective areas. These images were chosen randomly to provide comprehensive coverage of different paddy sites, with a meticulous recording of 100 observations (images) for each study site. Figure 3.2 shows an image obtained by a drone, illustrating the identification of plots within specific paddy sites, along with the delineation of ridges, furrows, and bunds utilized for rice production.

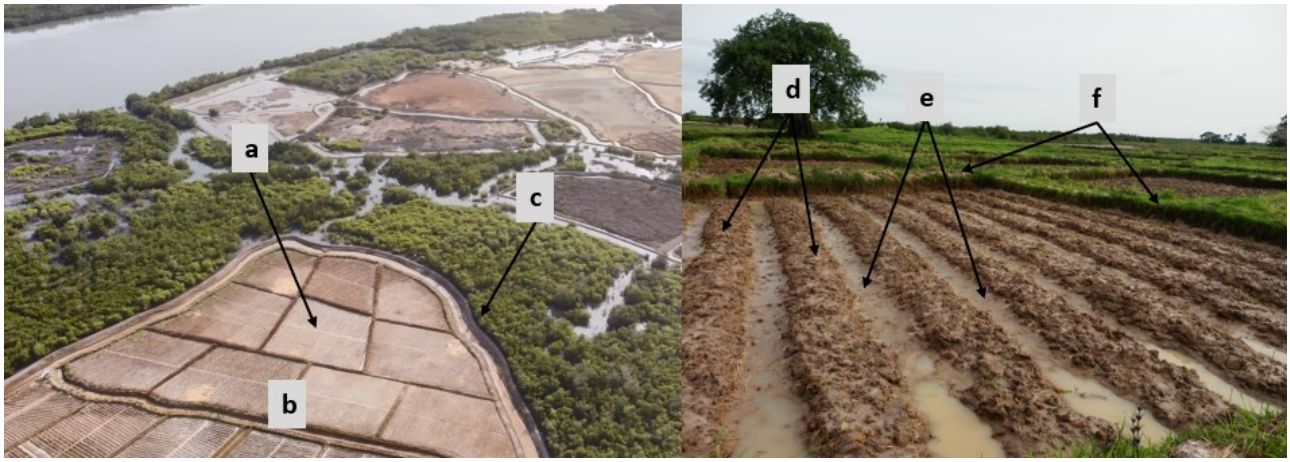

Figure 3.2. Plots in Mangrove swamp rice in Elalab, Guinea-Bissau. Identification of (a) plots, (b) paddies or "Bolanhas", (c) main dikes, (d) ridges, (e) furrows, and (f) bunds.

In order to generate a systematic sampling within a combined area of 1435 ha, a grid of 183 sampling points in Cafine-Cafal and 99 sampling points in Elalab was added to the maps of the rice production areas (Figure 3.1). The "Cartodroit" application (version V0.61.2_10166) created by the "Instituto Técnico Agrario de Castilla de León" was used for this purpose, as it works in areas without an internet connection. Vector

raster layers were generated in Sqlite format to locate the points within the rice production zones. The sampling points were uploaded to a GPS-equipped Android smartphone to precisely identify and locate points within the fields.

Soil samples (282) were collected at each grid point using an auger and shovel at a depth of 0 to 25 cm. The samples were placed in plastic bags and labeled for identification for further processing at the Soil and Water Laboratory of the Ministry of Agriculture and Rural Development of Guinea-Bissau. The soil consistency analyses were conducted in Guinea-Bissau, whereas the soil chemical analyses (Na, Ca, Mg, K, Al, Fe, pH, electrical conductivity (EC), and exchangeable acidity) were performed at the Soil and Foliar Laboratory of the Agronomic Research Center, University of Costa Rica.

Several measurements were taken in 60 randomly selected plots at each study site during the soil preparation phase (July and August) in order to characterize: (i) the area of the plots, (ii) the area exposed for rice cultivation (ridges), and (iii) the topography of the bottom of the plots.

The sizes of the ridges and the areas of the plots were evaluated in both study sites. The perimeters of the plots were measured with a scale-meter and the areas were quantified. Additionally, the dimensions of three ridges within each plot were measured to quantify the area exposed for rice planting.

The uniformity of plot depths was assessed during the months with the highest rainfall (August to September). The depths were determined by measuring the depth of water inside the plot (waterlogging height) at different points (Figure 3.3) using a vertical scale meter, yielding 180 measurements for each study site.

Meteorological data was collected during the experimental years in two automatics meteorological stations (ATMOS-41 and ZL6 datalogger): one in the Cafine-Cafal study site (11°13′0.588″ N, 15°10′32.358″ W) and the other in Elalab (12°14′47.54″ N, 16°26′36.424″ W). Data included precipitation, maximum, and minimum temperature.

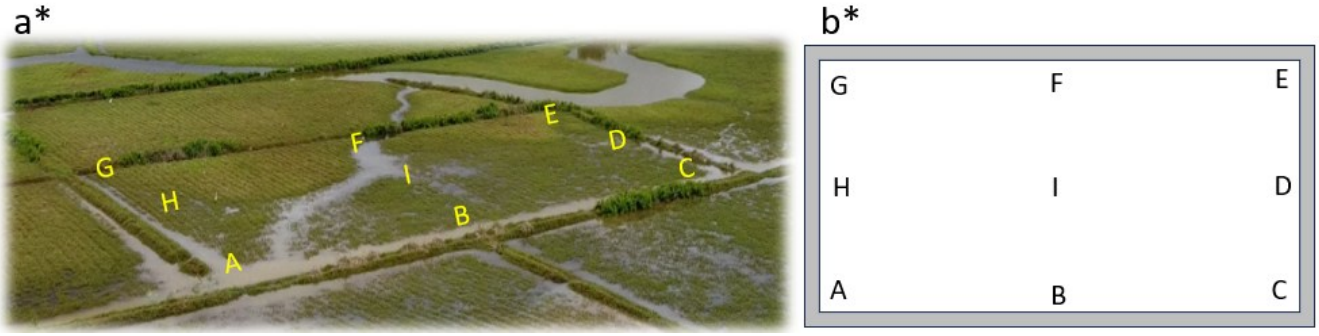

Figure 3.3. Designated location for measuring the water depth within the plot. (**a***) Drone photo of a plot in Cafine-Cafal and plot-measuring position. (**b***) Conceptual diagram of measuring position.

3.3. Data Treatment

3.3.1. Water Harvesting Efficiency

The water-harvesting efficiency (WL_{ef}) was calculated (Equation 3.1) based on the total rainfall recorded during the 2021 and 2022 rainy seasons, as well as the plot dimensions.

$$WL_{ef} = \frac{pa \times pn \times tr}{wl \times pa \times pn} \times 100 \quad \text{(Eq. 3.1)}$$

where WL_{ef} is the water harvesting efficiency of the plot (%), pa is the plot area (m^2), pn is the number of "plots numbers per ha" (n), tr is the annual rainfall ($m\ m^{-2}\ year^{-1}$), and wl is the waterlogging height (m).

3.3.2. Soil Consistency and Chemical Analysis

The soil consistency was evaluated using the commonly known methodologies for identifying the Atterberg limits (ASTM Committee D4318-17 on Soil and R Rock, 2010; Casagrande, 1958; Keller and Dexter, 2012; Sowers, 1965). For soil consistency determinations, soil samples were air-dried for one month, and sub-samples of 150 g were prepared to determine three consistency limits: the liquid limit (LL), which is the moisture content at which soil transitions from a plastic state to a liquid state (becomes semifluid); the sticky limit (SL), which represents the soil moisture at which the soil no longer adheres to a steel spatula; and the plastic limit (PL), which is the minimum moisture content at which soil remains moldable.

In order to quantify the soil consistency limits, each sample was individually processed as follows: first, the plastic limit (PL) was estimated using the "thread rolling test" in which a square ceramic plate was used to form a 3 mm thread. Second, 50 g of soil was mixed with water until a paste was formed, and then the adhesion was tested with a spatula in order to obtain the sticky limit (SL) (Haigh et al., 2013). The liquid limit (LL) was then determined using the long-validated methodology developed by Cassagrande (ASTM Committee D4318-17 on Soil and R Rock, 2010; Casagrande, 1958; Keller and Dexter, 2012; O'Kelly et al., 2018; Sharma and Bora, 2003; Sivakumar et al., 2015; Sowers, 1965). Finally, the gravimetric moisture content was determined in subsamples collected for each consistency limit.

Soil chemical analysis was carried out using extractions with ammonium acetate for Na, Ca, Mg, and K and with ammonium oxalate for Al and Fe. The extractions were analyzed using inductively coupled plasma mass spectrometry to quantify the concentration of elements in each soil sample. In addition, the pH (water), the EC (1:2),

and the soil exchangeable acidity were determined. Each soil analysis was conducted in accordance with the Soil Survey Staff methodology (Soil Survey Staff., 2022b).

3.3.3. Statistical Data Analysis

The data collected were analyzed separately for each study site. Linear regression analysis (Equation 3.2) was used to analyze the correlations between the variables total plot area, rice planting areas on ridges, number of rice production plots, and paddies area. A box plot was also created to analyze the soil consistency results. In addition, analysis of variance and multiple comparisons using Tukey's test ($\alpha = 0.05$) were performed to determine statistical differences between soil consistency results. To perform the above procedures, the RStudio Sofware version 1.4.1103, 2021 (Posit team, 2023), was used.

$$yi = \beta 0 + \beta 1 \chi i + ei \qquad \text{(Eq. 3.2)}$$

where yi is the estimated response (rice planting area on ridges (m^2), number of rice production plots (n)), $\beta 0$ is the estimated intercept in the regression, $\beta 1$ is the estimated slope in the regression, χi is the independent variable (total plot area (m^2), area (ha)), and ei represents the residual error.

A geostatistical analysis was performed using the Geostatistics for Environmental Science (GS+) program. First, the semi-variograms of the soil consistency distributions were analyzed, and the best-fitting model was estimated (Table 3.2). Second, the best-fitting models for the Z variables (soil consistency parameters) were created, which were then interpolated using the ordinary Kriging method. Third, the geostatistical analysis tool was used to perform cross-validation through resampling methods (leave-one-out cross-validation "LOOCV") on the previously interpolated information. Fourth, residual

errors "e_i" calculated for each observation point were extracted and subtracted from the original value of each observation point to obtain the predictive capacity of each process. Fifth, another geostatistical cross-validation (holdout method "HM") was carried out using 80% of the data to calibrate the models and the other 20% of the data to validate the model as an interpolation result.

This process involved removing one data point from the original group and predicting the value of the variable at the location of the removed data point. Subsequently, the root-mean-square error (RMSE), mean absolute error (MAE), and Pearson's correlation coefficient (ρ) were computed to validate the models according to the recommended methodology (Adhikari et al., 2013; Garbanzo-León et al., 2017; Mosleh et al., 2016; Poggio and Gimona, 2017; Zeraatpisheh et al., 2021). Finally, the calculated parameters were evaluated using spatial autocorrelation, which was determined using the "Global Mogan's I" statistic, the Z-score, and P-value calculations for each soil consistency parameter (Table 3.1). The interpolation procedures were performed using the ArcMap 10.8.2 Geostatistical Software and RStudio version 2023.09.1 Build 494 (Posit team, 2023).

Table 3.1. Geostatistical parameters used to calculate the interpolation of soil consistency limits in Cafine-Cafal and Elalab study regions in Guinea-Bissau.

Samples	Model	Nugget	Sill	Range
Cafine-Cafal map interpolation			(m)	
SL *	Exponential	22.1	44.2	3192
LL	Exponential	78.0	156.1	1515
PL	Spheric	27.7	73.7	8110
Elalab map interpolation			(m)	
SL	Linear	158.7	158.7	1470.7
LL	Linear	466.9	466.9	1470.7
PL	Linear	47.72	47.72	1470.7

* SL—sticky limit; LL—liquid limit; PL—plastic limit.

4. Results

4.1. Precipitation and Temperature

Figure 3.4 shows the meteorological data collected from both study sites from 2021 to 2023. Less rainfall was reported at the Elalab study site compared with the Cafine-Cafal site. The sites presented annual rainfalls of 1119–1749 mm and 2476–2679 mm, respectively. The months with the highest rainfall in both years were July, August, and September. The temperature ranged from 22 to 32 °C for both sites. In March and April, there were greater fluctuations between the maximum and minimum temperatures at both sites.

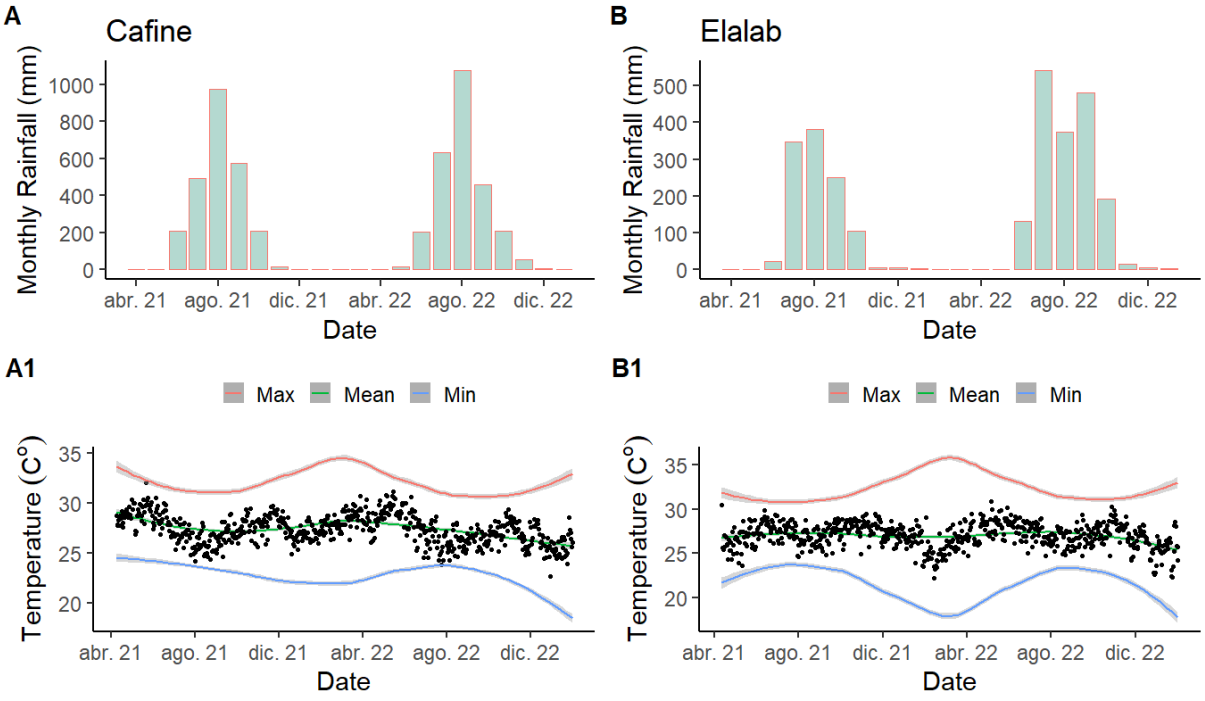

Figure 3.4. Rainfall and temperatures for Cafine-Cafal (**A**, **A1**) and Elalab (**B**, **B1**) case study sites from April 2021 to January 2023. The black dots represent the daily average temperature, while the lines illustrate the smoothed curve for maximum, minimum, and average temperatures.

4.2. *Soil Chemical Properties*

The chemical concentration of nutrients in the areas showed considerable variability (Table 3.2). The coefficient of variation ranged from 47% to 200% for the Ca, Mg, K, Na, Al, and Fe concentrations. The soils exhibited a pH above 4.4. The Cafine-Cafal soils may present problems associated with exchangeable acidity (>0.5 cmol(+) kg^{-1}), which can affect nutrient availability, hinder root growth, and impact the overall health of crops (Espinosa and Molina, 1999; Kunhikrishnan et al., 2016). Furthermore, the average cation-exchange capacity (CEC) was 8.98 cmol(+) kg^{-1} in Elalab and 24.88 cmol(+) kg^{-1} in Cafine-Cafal, with values of Na between 0.11 and 234.96 cmol(+) kg^{-1}. The latter is a substantial amount of sodium, potentially indicating the need for soil amendments or management practices to ensure good conditions for plant growth (Kirkby et al., 2023; Espinosa and Molina, 1999; Grattan and Grieve, 1992). The notable percentage of saturation bases (SB) indicates high cation concentrations (>175.7 %), which may be due to a high sodium concentration in some sites and a low CEC.

Table 3.2. Soil chemical analysis results for the Elalab and Cafine-Cafal study sites, as measured from samples collected at the beginning of the rainy season between May and June 2021 and 2022.

Site	Statistic	pH	Exchangeable Acidity	Ca	Mg	K	Na	CEC *	SB *	Al	Fe
		H_2O	(KCl 1M)	Extractable NH_4OAC (pH 7.0)						$(NH_4)_2C_2O_4$	
				cmol(+) kg^{-1}						%	
Elalab n = 99	Mean	5.9	0.18	3.68	13.66	2.49	75.72	8.98	100	0.04	0.22
	Median	6.0	0.10	2.89	10.77	1.96	59.10	7.02	100	0.03	0.16
	Min	3.7	0.07	0.50	0.17	0.02	0.11	0.510	54.1	0.008	0.02
	Max	7.8	2.50	16.89	16.89	9.84	429.00	31.72	100	0.12	1.10
	Std. dev	1.13	0.28	3.29	11.89	2.38	79.32	7.58	100	0.027	0.22
	Coef. var	0.19	1.59	0.89	0.87	0.96	0.99	0.84	1.4	0.77	1.00
Cafine-Cafal n = 183	Mean	4.4	1.12	3.51	12.99	1.95	25.75	24.88	100	0.31	0.86
	Median	4.2	0.62	3.19	12.47	1.58	16.49	25.46	100	0.11	0.74
	Min	3.2	0.07	0.45	0.09	0.04	0.10	9.25	3.7	0.04	0.13
	Max	7.7	10.90	11.43	33.57	52.96	234.96	42.07	100	5.65	14.71
	Std. dev	0.60	1.38	1.72	6.05	3.92	31.8	4.14	100	0.65	1.09
	Coef. var	0.14	1.24	0.49	0.47	2.00	1.24	0.17	0.9	2.13	1.26

* CEC = cation exchange capacity; SB = percent base saturation ({[Ca + Mg + K + Na] / CEC} × 100).

4.3. Effective Planting Areas and Number of Plots

Figure 3.5 shows the effective planting area (planting area of the ridges) as a function of the plot areas. The total ridge area was 9.5% greater in the northern study sites (Elalab study site) compared with the southern ones (Cafine-Cafal study site) in Guinea-Bissau. In Cafine-Cafal (Figure 3.5A), the planting area was 42.3%, while in Elalab (Figure 5B), it was 51.8% ($r^2 > 0.9$, $p < 0.001$). The furrow area (Figure 3.2) varied between 48.2% and 57.7% between the two study sites when comparing the plots' area with the ridges' rice planting area.

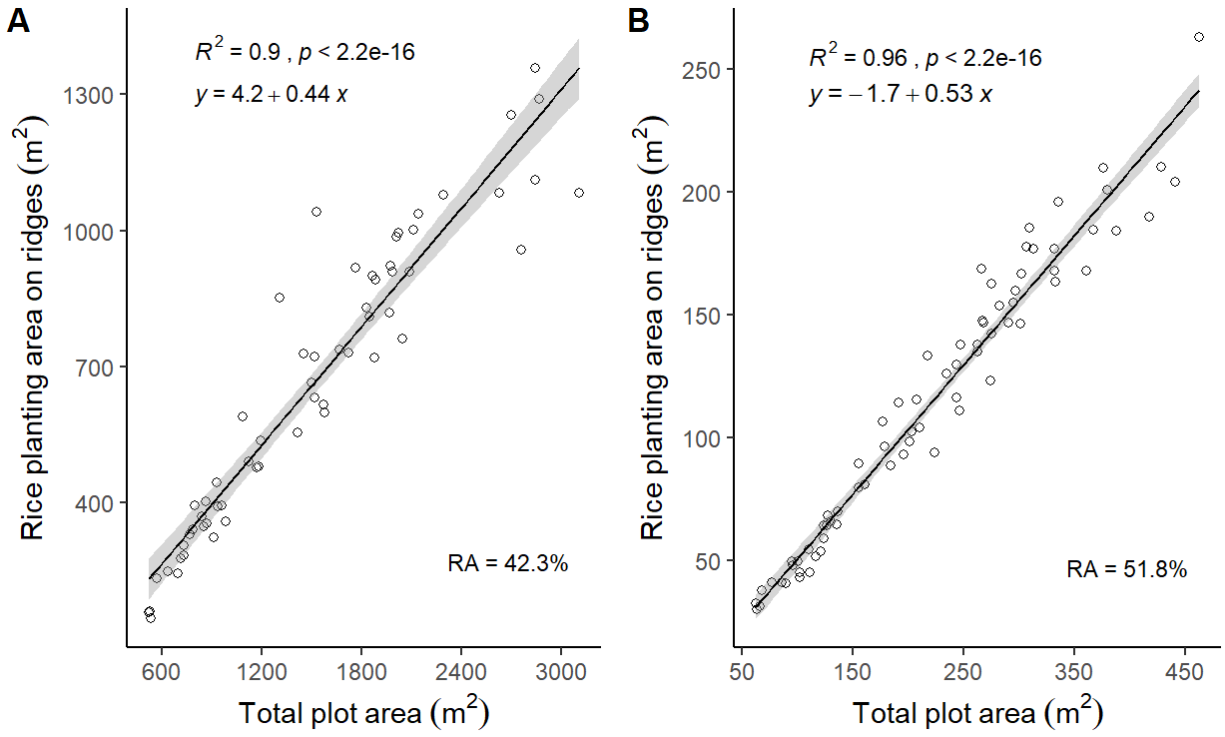

Figure 3.5. Effective rice-planting area on ridges (RA) evaluated in MSRPS plots in (**A**) Cafine-Cafal and (**B**) Elalab case study regions.

The number of rice production plots per hectare was seven times higher in the north than in the south of Guinea-Bissau (Figure 3.6). The results showed that Elalab had approximately 53 plots per ha (10,000 m^2), while Cafine-Cafal had only about 7 plots per

ha. When examining larger areas (>1 ha), there was high variability in the plots, as shown by the linear regressions (r^2 = 0.72–0.75, $p < 0.001$).

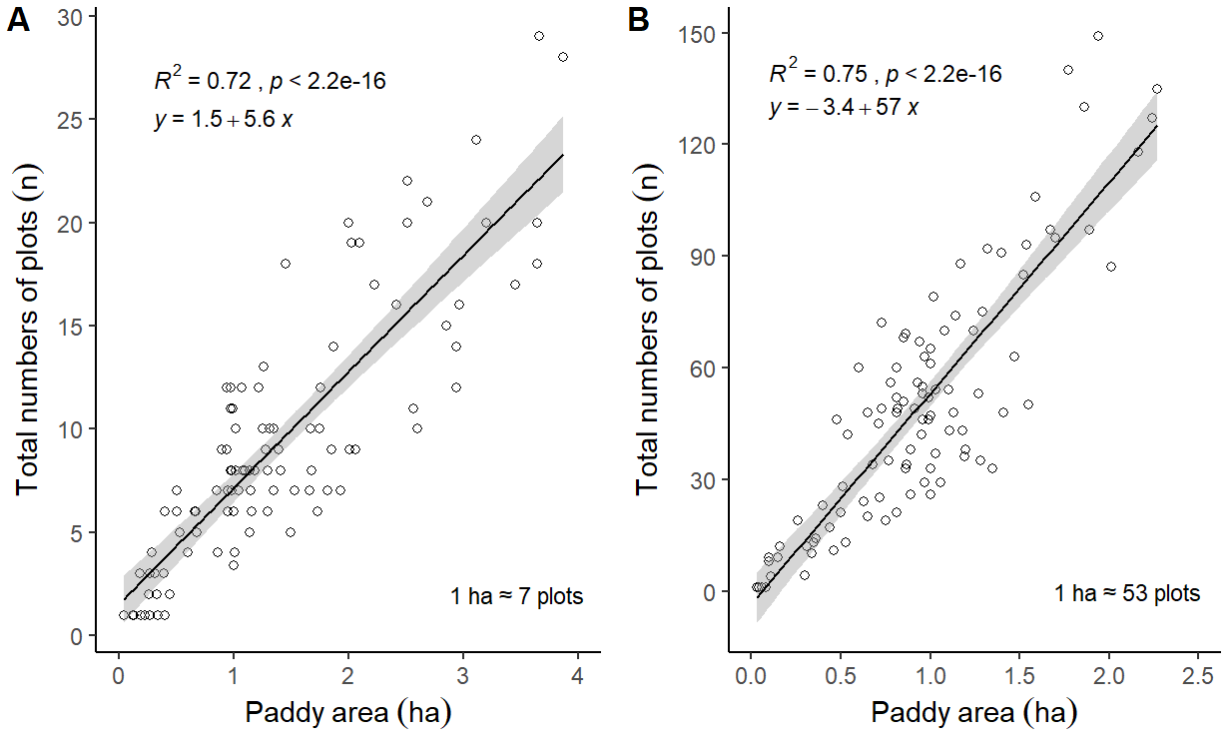

Figure 3.6. Estimation of the total numbers of plots per hectare in the MSRPSs of (**A**) Cafine-Cafal and (**B**) Elalab in Guinea Bissau.

4.4. Water-Harvesting Efficiency

As described in Section 2.2 (Experimental Observation and Data Collection), water depths were measured for nine points, as shown in Figure 3.3. Cafine-Cafal exhibited greater variation in waterlogging depths compared with Elalab (Figure 3.7), but the water depths in Elalab plots showed greater homogeneity. On average, a waterlogging depth of 37 cm was observed in Cafine-Cafal, while Elalab had a depth of 23 cm. The water-harvesting efficiencies (WL_{ef}) were 15 and 16% in Cafine-Cafal and Elalab. This approach quantified the hydrological effectiveness of a system by evaluating its water harvesting capacity relative to annual rainfall within the defined planting area of the plots. It is noteworthy that the recorded rainfall in the southern region during the 2021–2022 period

amounted to 1411 mm in Elalab and 2426 mm in Cafine-Cafal (Figure 3.4). Thus, the water-harvesting efficiency was found to be similar due to the considerable number of plots in Elalab within one hectare.

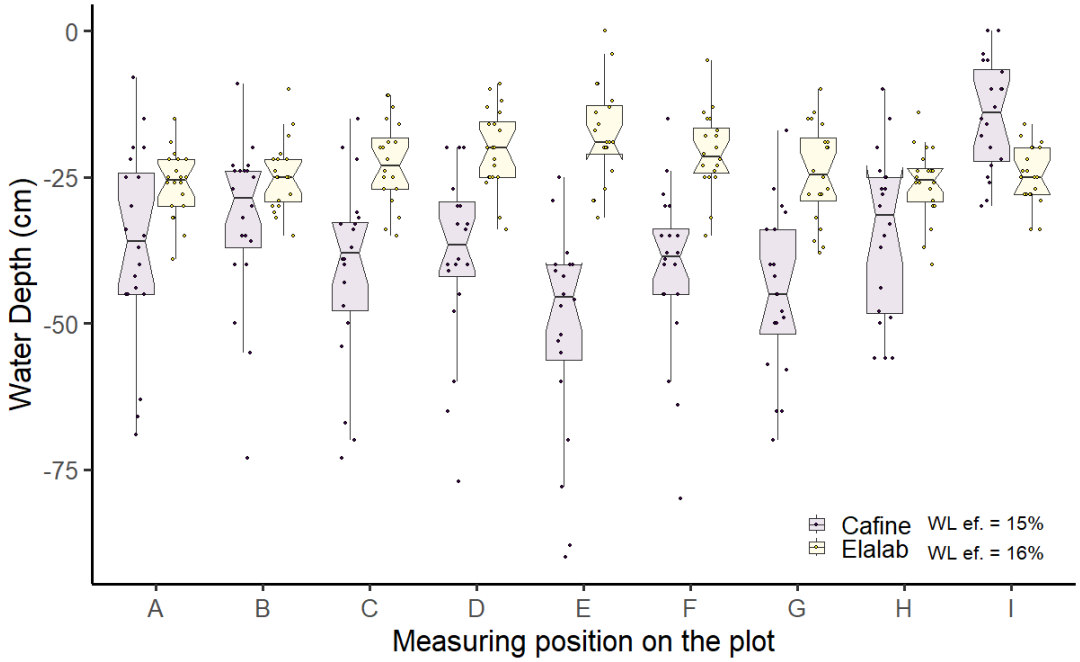

Figure 3.7. Variations in the waterlogging depth (August–September, peak rainfall) and water harvesting efficiency based on the total rainfall (WL_{ef}) in the 2021 and 2022 rainy seasons.

The water depth is a proxy for the topography of the plot floor. The bottom of the plots was more heterogeneous in the south of the country. Spatial analysis of the water levels in the southern plots revealed that the center had a shallower water depth (14.4 cm), while the edges (near the boundary) had greater depths and water accumulations (<50.95 cm) (Figure 3.8A). Furthermore, water runoff showed a lateral distribution, with greater intensity in the corners of the plots. In contrast, in the Elalab study site, a more homogeneous distribution was found in the water level variation across the plots (Figure 3.8B). Thus, the water depth ranged between 17.6 cm and 26.6 cm and had a slope gradient directed toward one side of the plots.

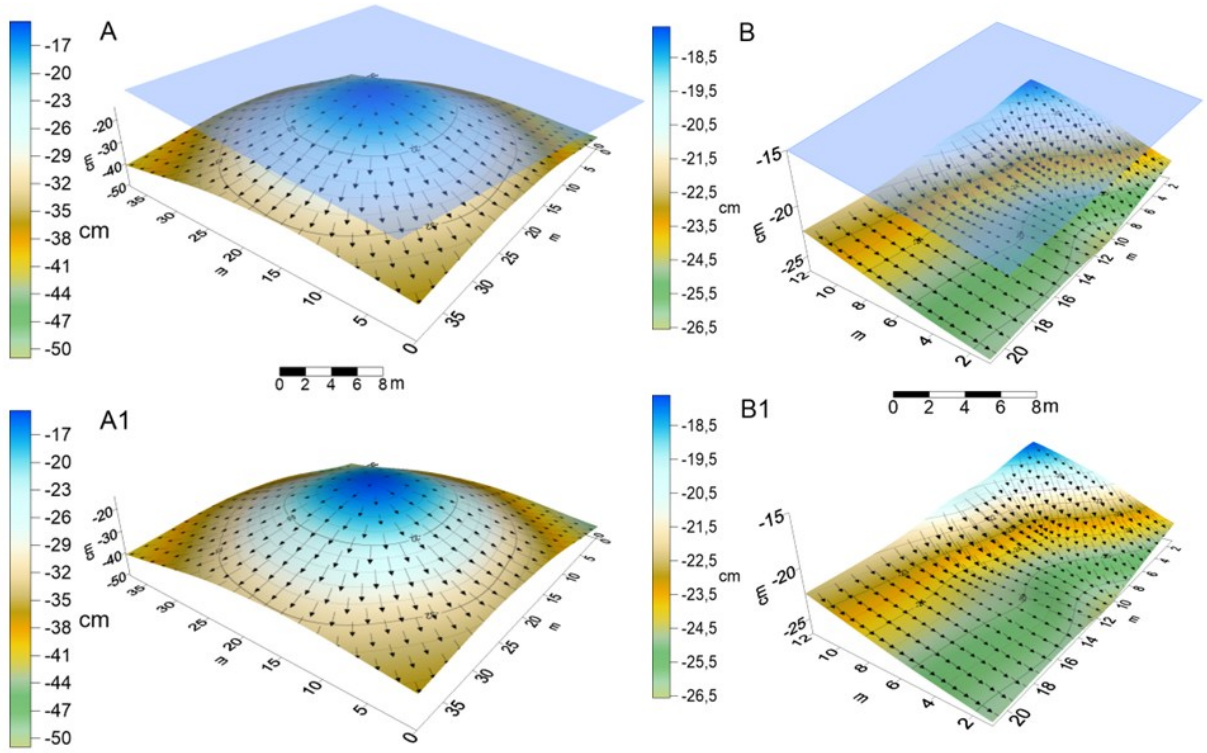

Figure 3.8. Radial basis function model used to estimate water level variation and water movement directions in the MSRPS plots in Guinea-Bissau. Depth of the water (**A**) and slope gradient (**A1**) in Cafine-Cafal. Depth of the water (**B**) and slope gradient (**B1**) in Elalab.

4.5. Soil Consistency Limits

The soil consistency analysis shows that the plastic limit (PL) was higher for the southern study site than in the north. In Cafine-Cafal, PL corresponded to a gravimetric moisture content (θ_g) of 35.5% (Figure 3.9), which was statistically different ($p < 0.01$) from both the liquid limit (LL) (θ_g = 65.4%) and the sticky limit (SL) (θ_g = 29.8%). In Elalab, the PL was reached with a θ_g of 18.6%, and there was no statistical difference from the SL (θ_g = 16.7%). However, the LL showed a significant difference ($p < 0.01$) compared with the other limits (θ_g = 33.5%). The effort required for soil tillage in northern soils was likely significantly lower under conditions exhibiting less plasticity, as opposed to the plasticity condition observed in Cafine-Cafal.

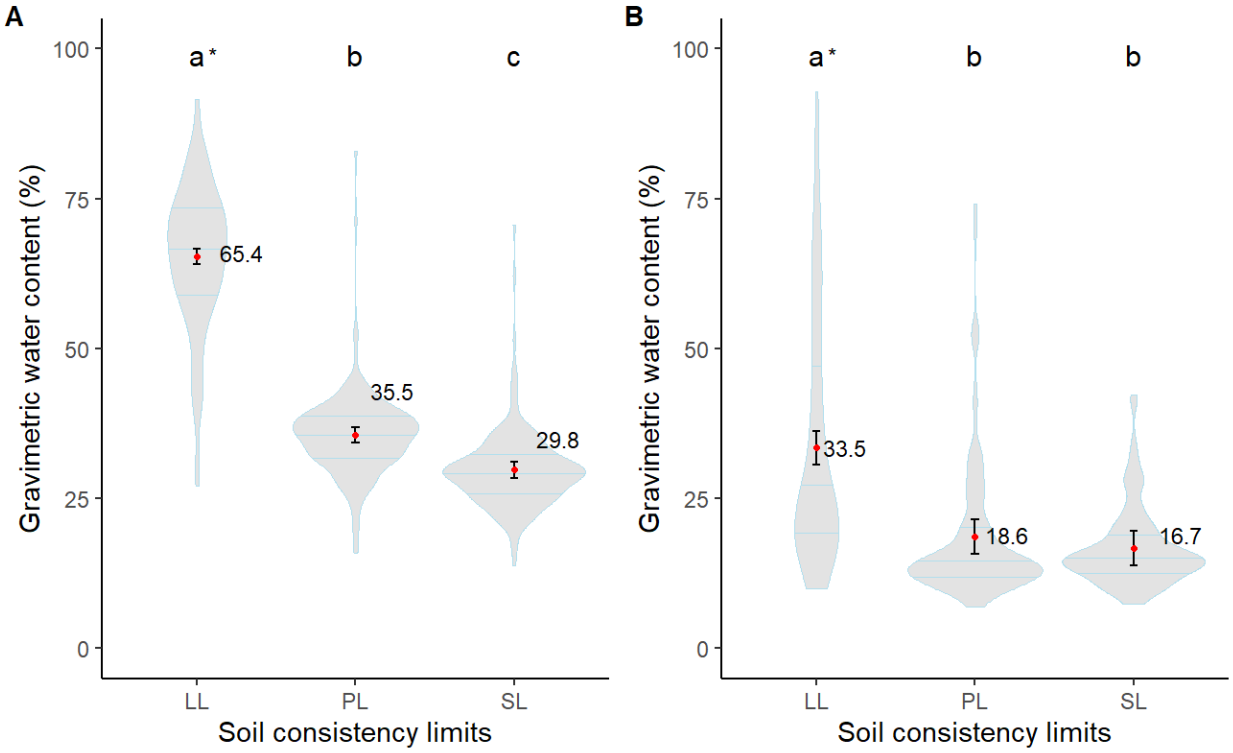

Figure 3.9. Soil consistency limits (including sticky limit [SL], plastic limit [PL], and liquid limit [LL]) in rice paddies for (**A**) Cafine-Cafal and (**B**) Elalab study sites in Guinea-Bissau. * Mean values with the same letter did not differ significantly according to Tukey's test (α = 0.05).

Within the context of the spatial analysis, the consistency limits were found to be a regionalized variable, that is, they showed a pattern across a geographic area. This is shown by the geo-statistical interpolation parameters presented in Table 3.3. The geospatial correlation analysis demonstrated a global Moran's I index < 0, indicating spatial autocorrelation due to the high similarity of nearby points (Chen, 2013). The variance in the consistency parameters was found to have a mean value of 0.002 in both study sites. The variance in Elalab showed a mean value ranging from 0.001 to 0.01. The clustering patterns were observed to be random (p = 0.01–<0.001). Therefore, interpolation indicates that they were related to spatial autocorrelation, which means they were random.

Table 3.3. "Global Moran's I" evaluation and cross-validations calculated for soil consistency limits interpolation in Cafine-Cafal and Elalab in Guinea-Bissau.

Samples	Global Moran's I	Variance	Z Punctuation	*p*-Value *	MAE	RMSE	P	MAE	RMSE	P	MAE	RMSE	P
	Cafine-Cafal Maps Interpolation					**LOOCV**		**LOOCV—e_i**			**HM—e_i**		
SL	0.182	0.002	3.964	<0.001	0.007	0.03	0.93	0.004	0.005	0.99	0.02	0.06	0.78
LL	0.159	0.0006	3.422	<0.001	0.02	0.04	0.94	0.01	0.02	0.99	0.05	0.08	0.76
PL	0.149	0.002	3.282	<0.001	0.02	0.04	0.90	0.01	0.02	0.98	0.04	0.07	0.73
	Elalab Maps Interpolation												
SL	0.22	0.002	4.502	<0.001	0.05	0.09	0.66	0.06	0.09	0.72	0.05	0.07	0.70
LL	0.115	0.003	2.333	0.01	0.10	0.14	0.75	0.09	0.13	0.80	0.10	0.13	0.79
PL	0.123	0.002	2.516	0.01	0.03	0.05	0.65	0.03	0.05	0.71	0.02	0.03	0.68

SL—sticky limit, LL—liquid limit, and PL—plastic limit. * A probability of less than 2% that the clustered pattern could be the result of a random likelihood. LOOCV—leave-one-out cross-validation. HM—holdout method (cross-validation). e_i—residual errors. RMSE—root-mean-square error. MAE—mean absolute error. P—Pearson's correlation coefficient.

The predictive ability of the interpolation was improved by subtracting residual errors "e_i" associated with previously interpolated values for each observation. It was found that after subtracting the residual errors, the LOOVC showed better parameter prediction (MAE and RMSE > 0.13) for each study site compared with the HM (Table 3.3). However, Elalab showed less accurate consistency limits prediction compared with Cafine-Cafal using the best predictive model. The average correlation between the observed and interpolated values showed that Cafine-Cafal had a rho (P) ranging from 98–99%, while Elalab showed a P between 71 and 80%. Therefore, a prediction model employed for the construction of a soil consistency map used LOOCV—e_i. This model could efficiently predict the specific locations or plots where farmers could identify the site for first plowing activities.

The geospatial distribution of soil consistency limits showed the sites with the highest plastic limit (PL) in the rice fields of Cafine-Cafal and Elalab (Figure 3.10). Paddies (Figure 3.2) exhibited a heterogeneous distribution in soil moisture contents, with a significantly lower PL found in the associated mangrove fields. The maximum PL was 57% in Cafine-Cafal and 28% in Elalab, suggesting that higher values of gravimetric moisture are suitable for manual soil preparation. The liquid limit (LL) range determined in Cafine-Cafal was between 35% and 86%, while in Elalab, these values ranged between 19% and 62%. The distribution of gravimetric moisture corresponding to each consistency limit on the maps shows the locations where the soil moisture suitable for plowing was reached more quickly.

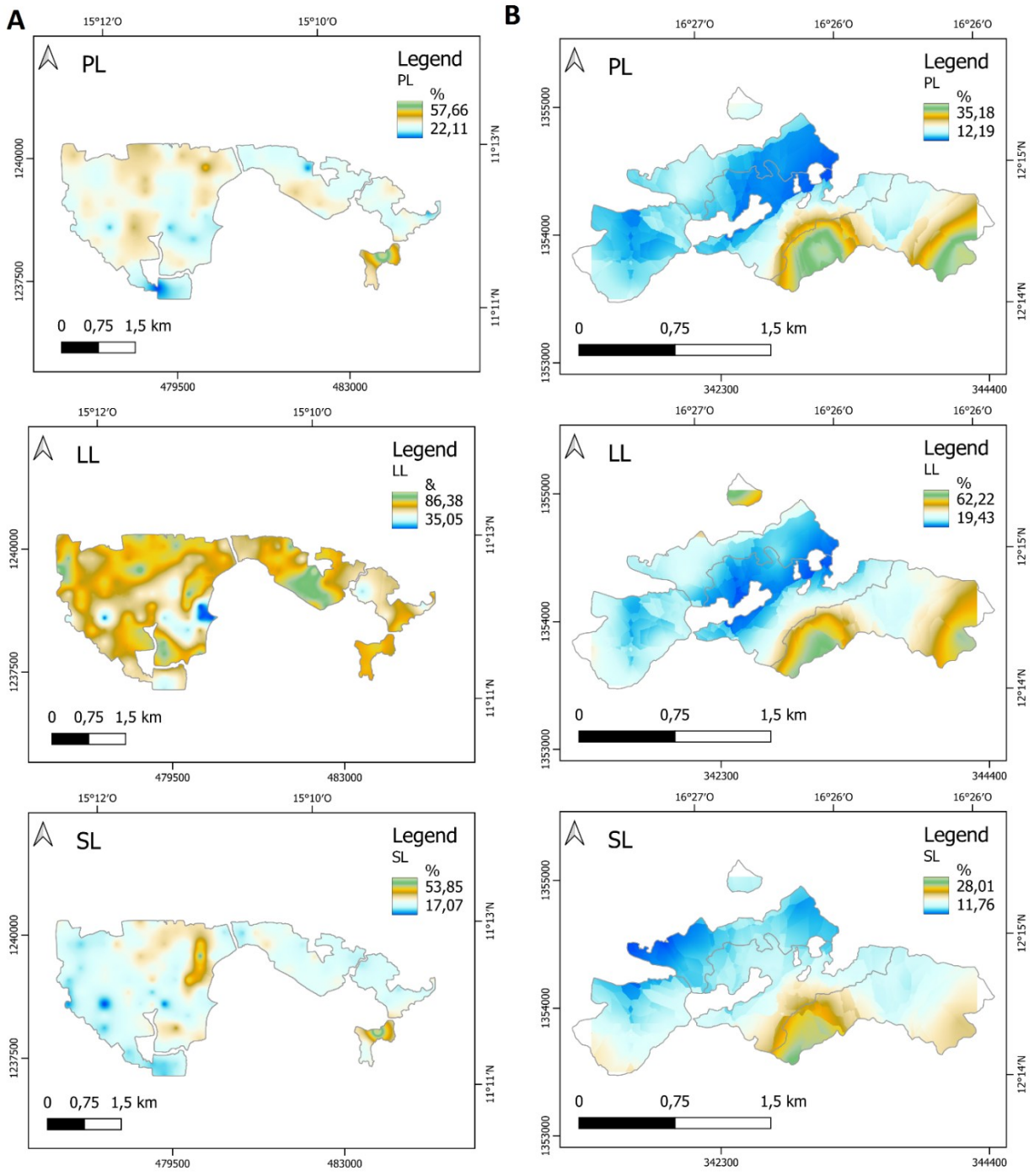

Figure 3.10. Interpolation of soil consistency limits, including the sticky limit (SL), plastic limit (PL), and liquid limit (LL), in MSRPSs of Cafine-Cafal (**A**) and Elalab (**B**), Guinea-Bissau.

5. Discussion

The highly spatio-temporal variation in rainfall distribution (Figure 3.4) has a major impact on the MSRPS soil tillage calendar. While the total amount of rainfall (mm) has increased during recent decades, the rainy season often starts later and ends earlier, and there are many long dry spells. At the same time, rainfall is concentrated in fewer days, and heavy precipitations may occur, which can lead to flooding, dike breaches, brackish water entering the plots, and frequent harvest failures (Mendes and Fragoso, 2023). Thus, a high annual rainfall no longer guarantees a correspondingly high rice productivity. Until three decades ago, farmers used to sow the first nurseries between May and June, but today they have to wait until July or even August (Figure 3.4), depending on the location (Dossou-Yovo et al., 2022). Then, the MSRPS depends on the amount of accumulated rainfall in the paddies and good water management (Fandé et al., 2022; Santos and Mourato, 2022). Normally, soil tillage cannot begin until the paddies are sufficiently filled with rainwater (Figure 3.10) to leach or dissolve the salt, but according to soil consistency (Figure 3.9), it may not be necessary to wait until the plot is full of water. However, farmers drain the water (southern study site) in order to work the soil more easily and with less physical effort. However, the paddies must be filled with fresh water again so that rice can be transplanted or directly sown.

Rice production requires greater adaptability due to rainfall patterns in GB, and agricultural practices in the MSRPS need to be adapted to biophysical characteristics (Figure 3.10). Farmers usually start their cultivation on the plots given to them by their families (grandparents or parents) for soil preparation and have significant practical knowledge of MSRPSs (Temudo, 1998). Many of these plots in both study sites (Figure 3.1) were located near the mangrove boundaries (tidal mangroves), where they require higher soil moisture due to a high Na^+ concentration (Table 3.2). Likewise, in many cases,

these sites had a clay texture and required higher rainfall in order to overcome the plasticity limit, and thus, facilitate soil tillage. With changing rainfall patterns and a short rainy season window, farmers need to adapt and start tilling on plots that require less rainfall or soil moisture, such as plots with a loam or sand texture (Unger, 1984). In this way, they can use these plots to plant nurseries and initiate the rice growth cycle since the species *Oryza glaberrima* and *O. sativa* require approximately 90 to 135 days from sowing to harvest (Linares, 2002; Miranda, 1993; Penot, 1992; Temudo, 2011; Tesio et al., 2021). This paper proposes an adaptation strategy that allows farmers to identify the sites where it is appropriate to initiate soil tillage (Figure 3.10). This will enable them to promote agriculture that is better adapted to rainfall patterns, which are likely to be more variable in the medium and long term. This is important for sustainable agriculture in GB given the climate variability (Temudo, 2011).

The water management techniques used in Cafine-Cafal and Elalab differed (Figure 3.5), but both had similar water-harvesting efficiencies (Figure 3.7). When analyzing the Elalab study site ("Diola" and "Baiote" systems), it was clear that there was a much higher concentration of plots in a single hectare than in the southern study site of Cafine-Cafal ("Balanta") (Figure 3.6). The smaller paddies in the northern region (Elalab study site) allowed for better management of the scarce water supply. For example, the average rainfall in the 2021 and 2022 rainy seasons was 1454 mm in the Elalab study site and 2578 mm in Cafine-Cafal (Figure 3.4). These results are consistent with those of other researchers (Mendes and Fragoso, 2023). Although the plots may be larger in newly opened paddies, when Elalab farmers observed water accumulation in some areas, they divided them into two or more smaller plots (Figure 3.5). Smaller plots allowed for a more even distribution of water logging across the soil surface, both at the beginning and end of the rainy season (Figures 3.7 and 3.8). This meant that the desalinization of the paddies occurred more

evenly and the amounts of water within the plots could be controlled more efficiently (Baggie et al., 2018; Dossou-Yovo et al., 2022; van Oort, 2018). In contrast, Cafine-Cafal case study plots were seven times larger, and water management was less efficient despite the higher rainfall rates in the south of the country (Figure 3.6). This could lead to more heterogeneous runoff within plots, resulting in hot spots of salinization in the center of the paddies (Figure 3.8).

The efficiency in the use of production space was also higher in the north of Guinea-Bissau than in the south. The Elalab case study achieved greater homogeneity of their ridges and furrows by using smaller plots (Figure 3.5) because the length of the ridges was shorter compared with those in the south ("Balantas"). On small plots, ridge dimensions can be better controlled when farmers till the soil. Since the ridges cover a larger area, farmers in the north could use four planting holes per row, while in the south, they used three holes in a triangle. This meant that northern farmers ("Diolas" and "Baiotes") were making better use of the area. In summary, the Elalab case study showed that the system had more efficient water management and labor use and was better adapted to water stress conditions. In the future, there is a possibility that the strategies implemented in the northern study sites will be effectively expanded to the southern regions and serve as an adaptive response to decreasing rainfall conditions.

Plastic limits (PLs) determine the time at which tillage can begin in the MSRPS fields (Figure 3.9). Currently, the agricultural calendar has a shorter time window, and gravimetric soil moisture (θ_g) is a tool that can be used to help define the appropriate moment and plots to start soil tillage each year. For this purpose, maps were modeled to determine the paddy areas where producers could start soil preparation (Table 3.3) to take advantage of the longest period of favorable conditions (high salt solubility) in the plots (Figure 3.10). It was found that the Cafine-Cafal farmers could start soil preparation with

a θ_g = 36%, while in Elalab, approximately θ_g = 20% was required (Figure 3.9). These delineations provide farmers with valuable insights into the strategic management of soil friability and ensure avoiding soil sticking to the manual plows that are commonly used in MSRPS practices (Temudo, 2018, 2011; Tesio et al., 2021). This is consistent with previous studies on soil workability and friability for agricultural production, which aim to help farmers make decisions on tillage operations (Arvidsson and Bölenius, 2006; Keller et al., 2007; Keller and Dexter, 2012; Obour et al., 2017; Utomo and Dexter, 1981). Therefore, soil consistency is a tool to make soil management more efficient and achieve better water efficiency. However, it is the soil salinity that determines if it is possible to start planting or direct sowing immediately after plowing (Baggie et al., 2018; Bos et al., 2006; Dossou-Yovo et al., 2022; Sylla et al., 1995).

MSRPS infrastructures (bunds and dikes) are primarily designed for freshwater accumulation rather than salt removal or drainage. The vast majority of farmers only drain the water from the plots when they need to maintain a desired level of waterlogging according to the height of the rice plants. Nevertheless, farmers in the Elalab case study ("Diolas and Baiote") prioritized plowing the soil under waterlogging conditions to conserve the limited water availability (Figure 3.7). In addition to the additional physical effort required for soil preparation, this practice allowed the dissolved salts to remain in the water. This is in stark contrast with conventional irrigation systems, where many water management calculations are designed to facilitate salt leaching and removal, particularly in systems characterized by low rainfall but with greater availability of freshwater from wells or rivers. Therefore, MSRPS cultivation in both the northern and southern regions of Guinea-Bissau presents complex variability in the biophysical characteristics of rice production areas, which pose major challenges.

6. Conclusions

Rice production requires greater adaptability due to rainfall patterns in GB, and agricultural practices in the MSRPS need to be adapted to biophysical characteristics. The highly spatio-temporal variation in rainfall distribution has a major impact on the MSRPS soil tillage calendar. This paper proposes an adaptation strategy that allows farmers to identify the sites where they can initiate soil tillage. This will enable them to promote agriculture that is better adapted to rainfall patterns, which are likely to be more variable in the medium and long term. This is important for sustainable agriculture in GB given climate variability.

It could be concluded that the water management techniques used in the north and the south of the country differed, but both had similar water-harvesting efficiencies. The smaller paddies in the northern region (Elalab study site) allow for better management of the scarce water supply. Smaller plots allow for a more even distribution of water depths across the soil surface, both at the beginning and end of the rainy season. This means that the desalinization of the paddies occurred more evenly and the amounts of water within the plots can be controlled more efficiently. In contrast, in the south, plots were seven times larger, and water management was less efficient despite the higher rainfall rates, which could lead to more heterogeneous runoff within plots, resulting in hot spots of salinization in the center of the paddies.

Currently, the agricultural calendar has a shorter time window and gravimetric soil moisture (θ_g) is proposed as a tool to help determine the appropriate time and sites to start tillage each year. Soil consistency maps were modeled to determine the plots where producers could begin soil preparation to take advantage of the longest period of favorable conditions (high salt solubility) in the plots. These delineations provide farmers with

valuable insights into the strategic management of soil friability and ensure avoiding soil sticking to the plows that are commonly used in MSRPS practices.

The comparative study of some biophysical properties between study sites facilitated the identification of specific constraints hindering rice growth and productivity due to salinity and water management. The key limitations identified that will guide our future research were as follows: **(i)** The lack of an effective drainage system in the plots resulted in the productivity of the plots relying solely on leaching and salt dissolution. **(ii)** Irregularities in the topography of the plots could lead to a heterogeneous accumulation of salts, leading to significant variability in rice production. **(iii)** Inadequate knowledge of the chemical composition of salts and the physical properties of soil hindered the ability to effectively address challenges related to managing soil alkalinity, toxicity, and acidity. The MSRPS lacked maps that provide information on initial salinity conditions, and the development of such resources could greatly improve decision-making processes, particularly during periods of low rainfall. **(iv)** The MSRPS did not have a water–salt balance that allowed for determining the optimal conditions for rice growth in both the initial and final growth stages.

Chapter 4

Advances in soil salinity diagnosis for mangrove swamp rice production in Guinea Bissau, West Africa

This chapter was published in *Science of Remote Sensing*.

Garbanzo, G., Céspedes, J., Temudo, M., Cameira, M. do R., Paredes, P., Ramos T. 2024. Advances in soil salinity diagnosis for mangrove swamp rice production in Guinea Bissau, West Africa. Science of Remote Sensing, 11, 100231. https://doi.org/10.1016/j.srs.2025.100231

Keywords:

Soil texture, Electric Conductivity, Machine Learning, Remote Sensing Technology, Agricultural Management, Planet Scope Project.

1. Abstract

Rice is one of the most important crops in many West African countries and has a direct impact on food security. Mangrove swamp cultivation is the most productive rice system in this area but is highly vulnerable to changes in rainfall patterns due to soil salinity. Diagnosing and identifying areas of high salinity concentration are essential strategies for adapting to climate change and mitigating its impacts. The aim of this study is to provide a methodological approach to identify the causes of soil salinity and map the spatial distribution of hypersaline areas, focusing on three case studies in Guinea-Bissau. At three study sites in the north, center, and south of the country, 382 soil samples were collected under initial conditions before rice cultivation. Indices derived from spectral bands and soil texture raster of the Planet Scope project were used to calibrate the three-machine learning based models: Random Forest (RF), Support Vector Machine, and Convolutional Neural Networks. Chemical analysis of the soil revealed that Mg^{2+} and Na^{+} were the extractable cations with the highest concentration in all three study sites. The RF showed the highest accuracy for salinity prediction (R^2 = 0.84, MAE = 13.35 dS m^{-1}, RMSE = 20.89 dS m^{-1}, NRMSE = 2 %, BIAS = 0.45, PBIAS = 0.04 %), with normalized difference salinity index (RNDSI, calculated with red edge). Silt raster, normalized salinity index (NDSI), and normalized difference water index (NDWI) were the main contributors in the predicted data for soil electrical conductivity of the saturation paste extract (EC_e, (dS m^{-1}). This approach produced a reliable approximation during validation for the three study sites (R^2 = 0.71 to 0.81, MAE = 10.81 dS m^{-1} to 19.68 dS m^{-1}, RMSE = 15.59 dS m^{-1} to 29.23 dS m^{-1}, NRMSE = 36% to 51%, BIAS = -2.25 to 1.79, PBIAS = -5.73% to 5.81%), each exhibiting unique edaphoclimatic characteristics. This study highlights the critical importance of diagnosing hypersaline sites to improve agronomic management practices by introducing improved water management infrastructures, conserving mangrove forests, and promoting regional ecological resilience.

2. Introduction

Rice (*Oryza sativa* L. and *Oryza glaberrima* Steud.) is one of the most important staple foods in West Africa and plays a crucial role in the daily diet. In rural areas, it is mainly grown by smallholders (FAO, 2018). Rice production in West Africa occurs in four major agroecosystems (Balasubramanian et al., 2007) defined by their surface water regimes such as dryland ecosystems (after slash-and-burn of forests or woodlands), rainfed wetlands, deepwater, and mangrove swamps (after slashing the mangrove trees and dike building).

In Guinea-Bissau (GB), the mangrove swamp rice production system (MSRP) accounts for about 49% of the crop production area (The Republic of Guinea-Bissau, 2018). This system shows evidence of salinity as the land was formerly occupied by mangrove forests and is vulnerable to saline seawater intrusion (Linares, 1981; Ukpong, 1997). Increased concentrations of soluble salts in the soil alter its physicochemical properties and increase the osmotic potential. Therefore, the ability of rice plants to absorb water is reduced, which in turn reduces the growth rate and ultimately leads to lower crop yields (Garbanzo et al., 2024a). Because rice is sensitive to salinity stress (Ayers and Westcot, 1985; Minhas et al., 2020), farmers rely on rainwater harvesting to dissolve and leach salts accumulated in the paddies to make the site productive (Dossou-Yovo et al., 2022; Marius and Lucas, 1991). Recently, desalination of paddy fields has become increasingly difficult due to rainfall patterns affecting rice production (Mendes and Fragoso, 2024; Temudo et al., 2022). In Guinea-Bissau, salinity problems are mainly related to the hydro-saline balance, as salinity can affect both the beginning and the end of the rice growing season (D'Amico et al., 2024; Garbanzo et al., 2024b; Van Ghent and Ukkerman, 1993). However, salinity is not present in all plots and occurs mainly in the

plots near the mangroves (Garbanzo et al., 2024a), where poor drainage affects salt leaching.

Poor diagnosis of saline sites hampers the development of agronomic management plans, which are essential to ensure rice production and avoid yield losses (Wolanski and Cassagne, 2000; Zenna et al., 2017). However, in GB, this diagnosis relies solely on farmers' local knowledge and practices, some of which are poorly adapted to socio-environmental changes (Martiarena and Temudo, 2023). Furthermore, few studies have been conducted to identify, characterize, and manage soil salinity in the MSRP, hindering the development of alternative management solutions namely under climate variability and climate change. For this reason, it is essential to develop tools tailored to the specific characteristics of MSRP fields to improve the diagnosis and management of salinity in this production system.

Tools for managing salinity in agricultural systems can use different types of models, such as statistical and deterministic. Deterministic models provide precise and predictable insights, as reported by Ramos et al. (2024), Stulina et al. (2005), and Van Dam et al., (2008). However, their complexity and high data input requirements make them more suitable for research rather than practical management in regions with limited data and technical expertise.

In contrast, machine learning-based statistical models show significant promise for diagnosing and managing salinity in mangrove rice fields (Sarkar et al., 2023; Xiong et al., 2024). These models handle complex relationships and large datasets, and provide accurate and adaptable predictions. Nevertheless, they face challenges related to data requirements, interpretability, and technical demands. Combining these models with local

knowledge and practices, as well as ensuring transparency and stakeholder engagement can enhance their effectiveness in salinity management.

Using remote sensing images to feed machine-learning models for salinity management in the MSRP areas provides significant advantages in large-scale, high-resolution monitoring and cost-effectiveness. Satellite platforms such as Sentinel (European Space Agency, European Union), Landsat (National Aeronautics and Space Administration Agency, USA), MODIS (National Aeronautics and Space Administration Agency, USA), PlanetScope (Planet, USA), and SAOCOM (National Commission for Space Activities, Argentina) capture multispectral reflected energy and enable diagnosis of surface properties, including vegetation changes, climatic variability, and soil composition (Wulder et al., 2022). These images enable non-intrusive observation of vast or inaccessible areas (Cawse-Nicholson et al., 2021; Salem et al., 2023). Calibration of spectral reflectance creates robust diagnostic tools for analyzing spectral patterns and changes over time (Martins et al., 2022; Pettorelli et al., 2005), crucial for informed agricultural decision-making and understanding of site-specific characteristics affecting crop production (Roy et al., 2019; Valman et al., 2024).

Spectral reflectance has been extensively studied and calibrated to diagnose soil salinity in different agroecosystems using various algorithms (Hopmans et al., 2021; Ivushkin et al., 2019; Metternicht and Zinck, 2003). Commonly used satellite indices are the Normalized Difference Vegetation Index (NDVI), the Normalized Difference Salinity Index (NDSI), the Intensity Index (Int), the Salinity Index on Spectral Angle Mapper (SAM), and the Salinity and Water Stress Index (SWSI), all of which are directly related to soil or vegetation (Lopes et al., 2020; Tan et al., 2023). These indices must be calibrated and validated with ground-truth salinity data to account for spatial variability and atmospheric disturbances (Hadjimitsis et al., 2010; Pettorelli et al., 2005), ensuring

accurate predictions (Liu et al., 2025; Ramos et al., 2020; Scudiero et al., 2015; Timm and McGarigal, 2012). Proper calibration enhances the assessment of spatial variations in soil salinity, which is crucial for effective management of agricultural systems (Bell et al., 2001; Ivushkin et al., 2019).

Several machine-learning algorithms are nowadays available for calibrating indices with ground truth data to generate predictive models (He et al., 2023; Mondal et al., 2019; Naimi et al., 2021). Among the most popular are: (i) Random Forest (RF), an ensemble learning method that uses statistical classification and regression techniques and creates multiple decision trees with random variations to arrive at a single result (Breiman, 2001; Latifi et al., 2012; Liu et al., 2012); (ii) Support Vector Machine (SVM), also a supervised learning algorithm that uses regression and classification methods to try to find the most accurate hyperplane to classify various features (Cortes and Vapnik, 1995; Decoste and Schölkopf, 2002; Huan et al., 2009); and (iii) Neural Networks (NNs), which are more complex models inspired by the brain's neurons and composed of layers with interconnected nodes, including an input layer, several hidden layers, and an output layer (Haykin, 1999; Rosenblatt, 1967). NNs establish an associated index or weight to form a classification, relying on training data to improve predictions through self-learning (Bishop, 1995; Farifteh et al., 2007). These algorithms enable the correlation of site variables with different spectral indices to determine a spatial prediction model that best fits the natural behavior of the data.

Diagnosis of soil salinity using indices calculated from satellite imagery and environmental covariates has shown promising results through various supervised learning algorithms. These include attempts to use SVM to calibrate the indices using ground-truth soil salinity data (Abd El-Hamid et al., 2023; Liu et al., 2023; Yang et al., 2023), RF (Kaplan et al., 2023; Yang et al., 2023; Zhao et al., 2023), and NNs (Pouladi

et al., 2019; Zhang et al., 2023). Other approaches included soil physical parameters such as soil moisture (Avdan et al., 2022), groundwater salinity (Chaaou et al., 2022), soil texture (Golabkesh et al., 2021; Hossain et al., 2020; Liu et al., 2023; Shi et al., 2022; Sun et al., 2022), and organic matter content (Shrestha et al., 2021) as variables; most of these models were developed for regions in Asia and the Middle East. However, no predictive model has been developed for the diagnosis of salt-affected soil in the tropical zones of West Africa (Mondal et al., 2019). Developing a model to diagnose soil salinity is essential to optimizing agricultural rice productivity, enabling precise resource management, and supporting sustainable land use. This will help ensure food security and environmental resilience to climate variability and change.

The aim of the study is to characterize the cations that contribute to soil salinity, develop a predictive model to assess spatial distribution and provide recommendations for soil salinity management in mangrove swamp rice cultivation in Guinea-Bissau. This article describes the development of a tool leveraging a supervised machine learning algorithm, that integrates satellite imagery with ground truth data. This tool can be used with the same aim in other rice-producing areas with salinity problems and ultimately be adapted to help select sites for mangroves restoration activities.

3. Materials and methods

3.1. Location and main characteristics of the study sites

The research was conducted between 2021 and 2023 at the study sites of Elalab (12°14'48.5" N, 16°26'30.3"W), Enchugal (12°02'52.0" N, 15°26'06.9" W), and Cafine-Cafal (11°12'40.4" N, 15°10'26.7" W) in Guinea-Bissau (GB), West Africa (Figure 4.1). The study sites are located in the coastal regions of Cacheu, Oio, and Tombali, where MSRP is practiced. Historically, farmers in the upper part of the catena began growing rice and gradually opened up new fields by clearing mangrove forests and building dikes and ducts. In the specialized literature (Van Ghent and Ukkerman, 1993), the agroecology of the upper fields is called associated mangroves (AM), and that of the fields closer to the brackish water is called tidal mangroves (TM) (Garbanzo et al., 2024a).

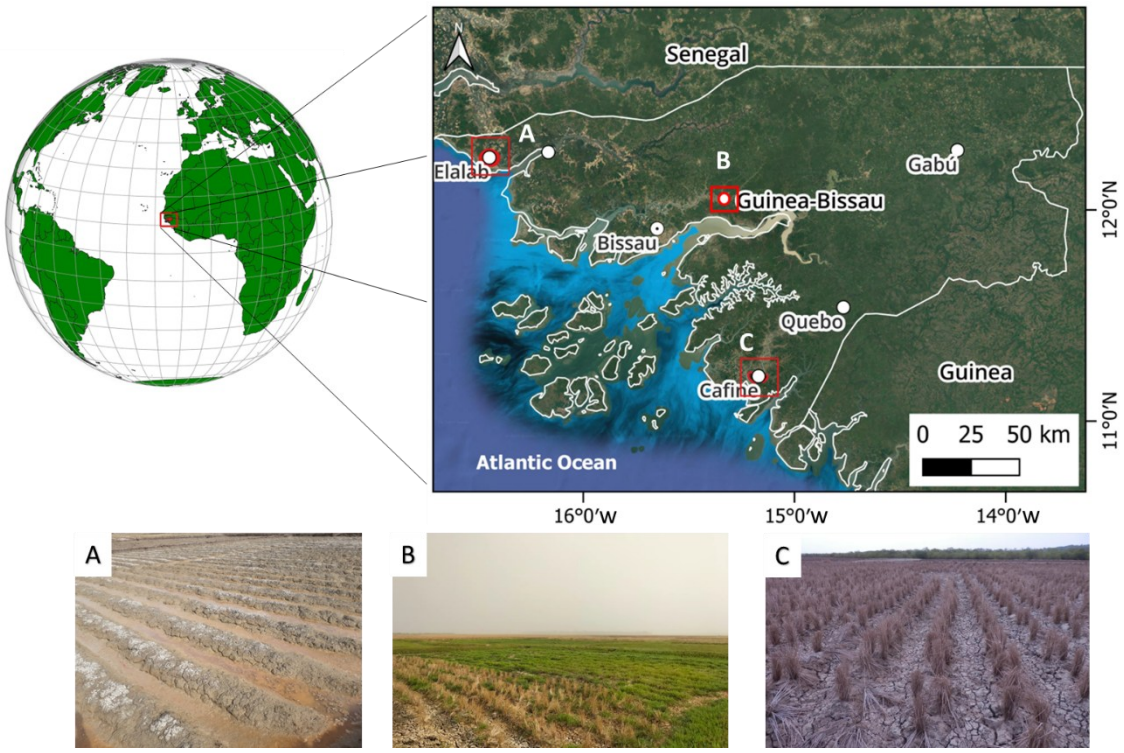

Figure 4.1. Location and perspective of soil salinity problems in (A) Elalab in the north, (B) Enchugal in the central region, and (C) Cafine in the south of Guinea-Bissau, West Africa.

According to the Köppen – Geiger classification, the climate is tropical monsoon (AW), which indicates heavy rainfall during the rainy season (Beck et al., 2018). In addition, the Holdridge Classification (Harris, 2014; Holdridge, 1947) identifies two life zones: the southern part (Cafine-Cafal) is classified as tropical moist forest, while the central (Enchugal) and northern (Elalab) regions are tropical dry forests. Currently, rainfall usually begins in June and ends by late September or October, with average annual ranging between 1500 mm (North) and 2500 mm (South) (Mendes and Fragoso, 2024). Average annual temperatures vary between 24 °C and 27 °C, with temperature patterns showing minimal annual fluctuations (Garbanzo et al., 2024b).

Soil consists primarily of alluvial deposits resulting from sedimentation caused by tidal channels extending into the continent. Their dynamics are influenced by active oxidation-reduction processes, mainly caused by tidal effects, particularly in mangrove areas, combined with the accumulation of freshwater during the rainy season. These soils have an ustic moisture regime, characterized by over 90 consecutive dry days in typical years (Soil Survey Staff., 2022).

The MSRP agroecosystem is a type of rainfed wetland rice ecosystem that is particularly vulnerable to both drought and flooding (Balasubramanian et al., 2007). Soil salinity limits rice production because optimal plant development only occurs under conditions of sufficient freshwater storage and minimal salt concentration within the plots. Originally, the soils were tidal terraces with mangrove forests, which were converted into rice fields by anthropogenic activities. Farmers adopt strategies to prevent saltwater intrusion by building a primary dike, followed by bunds to retain freshwater, thus facilitating desalination of the plots (Garbanzo et al., 2024b; Linares, 1981). Over a period of two to five years, these areas are desalinated and become productive for rice cultivation. However, tidal influence affects drainage conditions and salt accumulation in

the lower plots. In addition, farmers used to allow brackish water to enter the TM fields during the dry season to increase soil fertility, reduce the development of soil toxicity, and control weeds' infestation and pests' attacks. Currently, this practice is seldom used due to the extreme irregularity of the rainfall regime, which no longer allows the dissolution and drainage of saltwater before rice cultivation. Furthermore, extreme rainfall events and strong tides coupled with sea-level rise result in dike breaches and brackish water intrusion into fields (Mendes and Fragoso, 2023).

3.2. Field data collection and analysis

Due to logistical challenges posed by the distances between villages and the time required to collect soil samples in rice fields, soil sampling was conducted in different years. Therefore, sampling was carried out in Cafine-Cafal and Elalab in 2022 and in Enchugal in 2023. Soil samples (n = 382) were collected using an auger at depths of 0–25 cm within the paddy fields (Figure 4.A1), corresponding to a sampling area of 1820 ha (Garbanzo et al., 2024b). The sampling was carried out before the start of the rainy season (May-June), to quantify the initial salinity conditions before the start of rice production activities. The soil particle size distribution was determined using the hydrometer method (Bouyoucos, 1926; Day, 2015; Soil Survey Staff, 2022) according to USDA particle size limits. Soil pH (H_2O) and electrical conductivity (EC) were measured on a suspension of soil and distilled water (1:2.5 w/v soil/solution) using the potentiometric method (Rhoades, 1996; Thomas, 1996). In addition, the Mehlich-3 method (Zhang et al., 2014) was used to quantify the extractable concentrations of Ca^{2+}, Mg^{2+}, Na^{+} (cmol(+) L^{-1}). Cation concentrations were measured using inductively coupled plasma mass spectrometry (Wilschefski and Baxter, 2019).

The EC was the converted from the laboratory-estimated solution ($EC_{1:2.5}$, dS m^{-1}) to the saturated soil paste extract (EC_e, dS m^{-1}). This conversion was necessary because EC_e serves as a standard indicator for assessing soil salinity and provides a consistent interpretation over time and space (U.S. Salinity Laboratory Staff, 1954). The following equation was used (Sonmez et al., 2008):

Fine textures	$EC_e = 3.68\, EC_{1:2.5} + 0.22$	Eq. 4.1.1
Coarse textures	$EC_e = 4.34\, EC_{1:2.5} + 0.17$	Eq. 4.1.2
Medium textures	$EC_e = 3.84\, EC_{1:2.5} + 0.35$	Eq. 4.1.3

3.3. Compilation of remote sensing data

The satellite imagery data used in this study was downloaded from the Planet Scope Project (Planet Labs PBC, 2024) with atmospheric corrections already applied to surface reflectance. The sensor operates with a spatial resolution of 3 m x 3 m, daily temporal data and captures spectral information across bands from B1 to B8. Images taken between May 10th and 25th, 2022, were selected for the Elalab and Cafine-Cafal sites. For the Enchugal site, images between May 10th and 25th, 2023 were selected. The selection process focused on identifying images without cloud cover or traces of Sahara Desert particles. These images were viewed on the PlanetScope platform website. One image per study site was downloaded to cover the entire study area. These images represent the initial state of soil salinity before the onset of rainfall and rice production in GB. The images were then stored in a designated asset repository on the "Google Earth Engine" platform and subsequently accessed in the "Google Collaboratory" environment via the "Geemap" library. The Python programming language version 3.11 (Van Rossum and

Drake, 2009) was used via the “Google Collaboratory” interface for image processing, spectral band extraction, and algorithm training.

4. Theory and Calculation

Figure 4.2 describes the modeling approach used in this study, which involves identifying vegetation indices and particle size classes that best correlate with the EC_e ground truth data, as well as generating machine learning models using three different algorithms (Random Forest, RF; Support Vector Machine, SVM; and Convolutional Neural Network, CNN), and the validation of modeling results for soil salinity assessment in Elalab, Enchugal and Cafine-Cafal using different goodness-of-fit indicators. The following sections describe the procedures in detail.

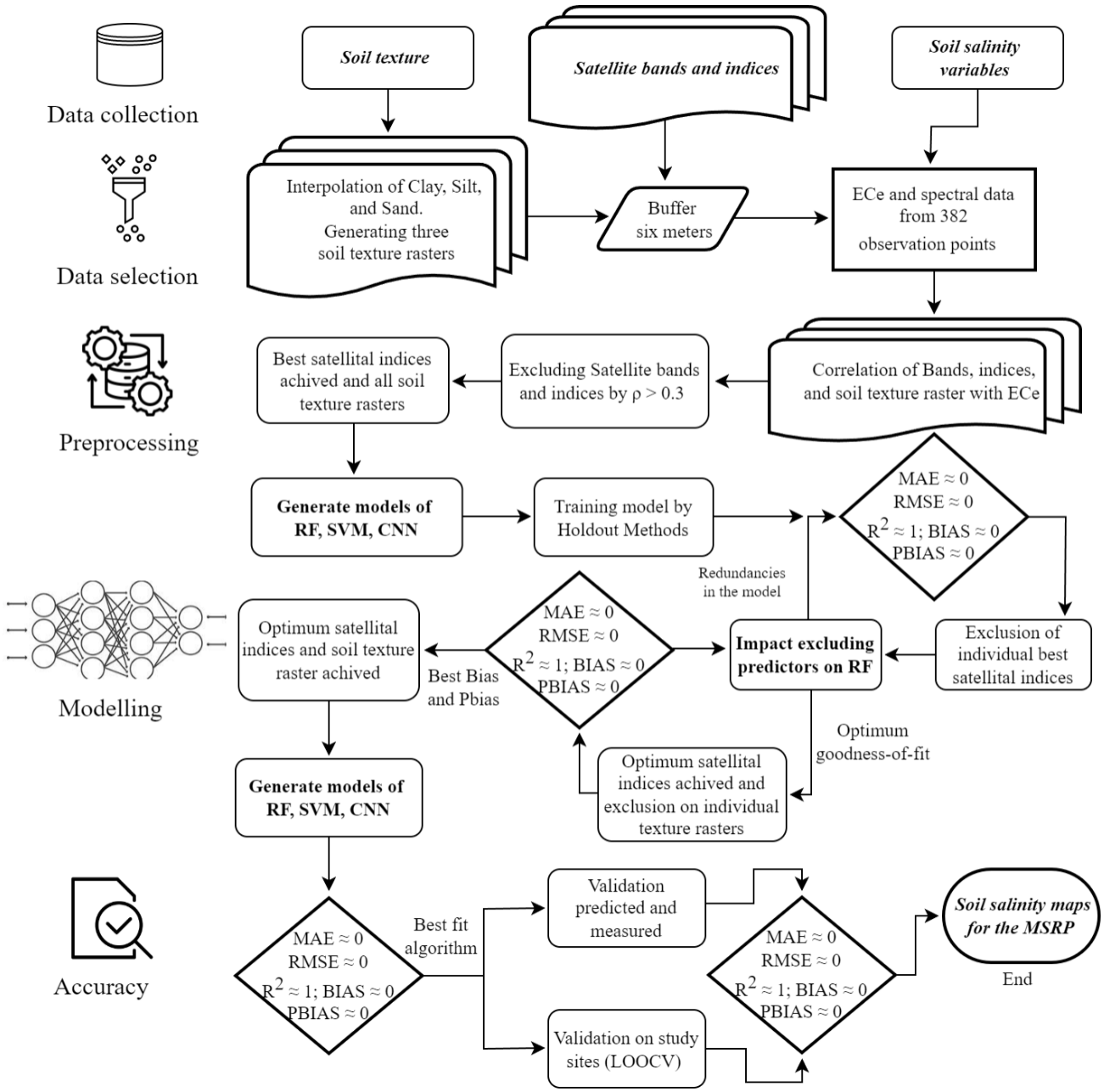

Figure 4.2. Generalized flowchart describing the computational procedures for developing predictive models (Random Forest, RF; Support Vector Machine, SVM; and Convolutional Neural Network, CNN) and diagnosing soil salinity in relation to soil texture within the MSRP in GB (EC_e = electrical conductivity of saturation paste extract in dS m^{-1}; MAE = mean absolute error; RMSE = root mean square error; ρ = Pearson's correlation coefficient; R^2 = coefficient of determination; BIAS; PBIAS = percentage BIAS; LOOCV = Leave-One-Out Cross Validation).

4.1. Data preparation and models training

4.1.1. Interpolation of textures and raster generation

The Geoestatistics for Environmental Science (GS+) software was used to map the soil texture in the study areas. The semivariograms were fitted to the measured proportions of sand, silt, and clay to determine the spatial correlation between the sampled points and to obtain the parameters necessary to predict soil texture at unsampled sites (Table 4.A1). Subsequently, the ordinary Kriging method (Ahmed and De Marsily, 1987) was used for the interpolation process. Spatial autocorrelation analysis was then applied using the "Global Moran´s Index" statistic. Z-score calculations and derived p-values for each soil texture class were performed to determine statistical significance.

Geostatistical analysis tools were used to validate soil texture maps using resampling techniques, particularly Leave-One-Out cross-validation (LOOCV). The root mean square error (RMSE), the mean absolute error (MAE), and the Pearson´s correlation coefficient (ρ) were calculated to validate all interpolated maps according to the recommended methodology (Chuvieco, 2020). The resulting interpolation (raster) was integrated into the machine learning models as a predictor (Figure 4.2). Four raster of soil texture analyses were performed using the geostatistical module in ArcMap 10.8.2.

4.1.2. Use of buffering

Buffers were used to standardize the areas of analysis, and average values were extracted from each buffer area. This method captures spatial variability more effectively because a single pixel (3 m x 3 m) may not accurately represent the existing spatial variability in a paddy field. To this end, data on field dimensions derived from the biophysical characterization of the MSRP (Garbanzo et al., 2024b) was used to determine an approximate radius for all sites. The buffer size for the MSRP analysis was based on

the dimensions of the smallest plot within the rice fields, which was approximately 6 m long. This approach follows the methodology used in soil salinity diagnosis (Wu et al., 2018). To cover an area of approximately 111.26 m^2, a circular buffer with a radius of 6 m, divided into five segments, was used. This data homogenization method effectively approximates the information derived from multiple pixels within an image. The buffer, which covers a larger area and represents approximately 13 pixels, provides a more comprehensive representation of spatial data. As a result, the information within the analysis domain was standardized using ground truth data, with averages extracted from each band or rasters layer used.

4.1.3. Band and index selection

The selected bands and indices were based on various studies developed worldwide (Abd El-Hamid et al., 2023; Aksoy et al., 2022; Barreto et al., 2023; Bouaziz et al., 2018; Chaaou et al., 2022; Dakak et al., 2023; Golabkesh et al., 2021; Li et al., 2022; Mzid et al., 2023; Shi et al., 2022; Tan et al., 2023; Triki Fourati et al., 2017; H. Zhang et al., 2023; Zhou et al., 2022), and are defined in Appendix Table 4.B2. The formulas of the various indices were programmed directly into the "Google Collaboratory" platform, which provides access to the "Jupyter Notebook Environment". Google Collaboratory was used to access GPU and TPU servers, providing greater analytical power for the machine learning models.

The satellite bands extracted by the Planet Scope sensor, namely B1 (Coastal Blue; 431 – 452 nm), B2 (Blue; 465 – 515 nm), B3 (Green I; 513 – 549 nm), B4 (Green; 547 – 583 nm), B5 (Yellow; 600 – 620 nm), B6 (Red; 650 – 680 nm), B7 (Red Edge; 697 – 713 nm), and B8 (Near-infrared; 845 – 885 nm), were also integrated as raster variables following the methodology described by Chuvieco (2020). This process was performed

using JavaScript and integrated into the Google Engine to generate an asset and standardize the file format (compatibility) for execution in the simulated model on Google Collaboratory.

Preliminary selection of spectral bands and indices was done using Pearson correlation, using a threshold ρ greater than 0.30. Bands and indices were tested against EC_e ground truth data. This process allowed the elimination of indices with limited significance for salinity diagnosis and the avoidance of overfitting. Filtering involved selecting the best correlated indices with a significant relationship to EC_e (in Appendix Table 4.C3 and Figure 4.D1).

4.1.4. Machine learning model selection and calibration

Soil salinity within the MSRP in GB was modeled using three algorithms: Random Forest (RF), Support Vector Machine (SVM), and Convolutional Neural Networks (CNN). The variables included were the bands, selected indices, and the soil texture raster. The data was split into a training set (80%) and a test set (20%) using the "train-test split" method. The dataset for this study totaled 5730 units (382 EC_e ground truth data multiplied by 15 variables representing satellite indices (11) and soil texture data (4) (in appendix Figure 4.E2). Predictors were scaled using "StandarScaler" to normalize training and testing values. This standardization is a requirement for machine learning algorithms (which assume zero mean and unit variance) because they may not perform optimally if the predictors are not approximately normally distributed (Geron, 2019; Kuhn and Johnson, 2013).

The RF model used the ensemble regression tree method developed by Breiman (2001), which is widely used in the literature to identify salt-affected areas (Cui et al., 2023; Li et al., 2022; Periasamy et al., 2022; Tan et al., 2023; Wang et al., 2021). Equation

4.2 was used to calculate the prediction y of RF for data point x; where B represents the total number of trees in the forest, and $T_b(x)$ is the prediction of the b-th tree for the input x.

$$y(x) = \frac{1}{B}\sum_{b=1}^{B} T_b(x)$$

Eq. 4.2

Each tree provides an independent prediction, and the final output is the average of these predictions, reducing variance and improving the accuracy of the models. Therefore, the number of trees and splits (ntree and mtry) required for training needs to be adjusted.

The model was programmed using standard tree generation, with interactions tested at 50-unit intervals ranging from 100 to 2000 trees. The optimal number of trees was determined using the "GridSearchCV" function (Siji and Sumathi, 2020) from the "Sklearn library". Since RF integrates regression from the decision trees created, it then provides an average of the value index in the most accurate output prediction. Based on the bootstrap theory, each output of decision trees randomly selects training samples during growth. This approach enables high-precision analysis by including many input samples without reducing dimensionality. Further details can be found in Breiman (2001). In the current study the RF regressor was calibrated with two splits, 100 trees, 27 random states, and root mean square error as the criterion calculated in each analysis run.

The SVM-supervised learning algorithm serves as a tool for predicting continuous output variables based on a comprehensive set of input data features (Boser et al., 1992; Cortes and Vapnik, 1995). The aim of this method is to identify a function that predicts a continuous variable within a defined margin of error, which is set to epsilon of 0.1 in the SVM model. This tool is adjusted based on training data to maximize the prediction

margin and minimize modeling errors (Decoste and Schölkopf, 2002; Huan et al., 2009). SVM was accessed using Equation 4.3, where α_i are the Lagrange multipliers, which are non-zero for support vectors; y_i are the labels of the training data; x_i are the support vectors (training data points that contribute to the model); $K(x_i, x)$ is the RBF kernel used to calculate the dot product in a higher-dimensional space (See Eq. 4.4); γ is a parameter that determines how quickly the value of kernel decreases with an increase in the distance between the support vector x_i and the input point x; and b is the BIAS term used in the function.

$$\mathrm{f(x)} = \sum_{i=1}^{n} \alpha_i y_i K(x_i, x) + b$$

Eq. 4.3

$$K(x_i, x) = (-\gamma\ (x_i - x)^2)$$

Eq. 4.4

SVM allows the nature of the input data to be mapped into a higher dimensional space, enabling the capture of complex patterns in the data. More details on solving optimization problems in soil salinity prediction can be found in the literature (Periasamy et al., 2022; Venugopal et al., 2023; Xiao et al., 2023). The SVM model was programmed in Python from the "Scikit-learn" library. It was initialized with a kernel radial basis function (rbk), a margin of tolerance where no penalty is given to errors of 0.1 (epsilon), parameter for the kernel function of 0.01 (coef), size of kernel cache of 200 (cache size), regularization parameter of 1.0, maximum number of interventions for optimization of -1 (no limit), and tolerance for the stopping criterion of 0.001.

CNN was used in the current study with the aim of improving the efficiency in effectively capturing local and spatial predictors, which is crucial for accurate regression tasks (Goodfellow et al., 2016; LeCun et al., 2015). CNNs use convolutional operations

to process spatial data that apply a pooling function to reduce dimensionality while preserving the most relevant predictor from the input data (Goodfellow et al., 2016). The convolutional operation applies a filter or kernel to the input to generate a predictor map that enables the detection of increasingly complex patterns across different network layers (Krizhevsky et al., 2017). This convolution is successively applied by the deep layer of the neural network, facilitating the transfer of learning from the initial layer to the output layer (Simonyan and Zisserman, 2014; Zeiler and Fergus, 2013). For regression purposes, CNN are particularly useful in mapping input data to continuous output values, where the translational invariance of predictors enables robust predictions (Pongrac and Gleich, 2021; Zhang et al., 2022). This approach significantly reduces the number of required parameters and increases the accuracy of continuous value prediction (Goodfellow et al., 2016; Simonyan and Zisserman, 2014).

In the current study, a one-dimensional CNN was used and programmed using the "PyTorch" library (Ansel et al., 2024; Howard and Gugger, 2020). Data frames were created with the selected indices and EC_e. The CNN architecture included a 1-D convolutional layer and eight fully connected layers, each with 78 neurons (See Appendix F). The first estimation of the hyperparameters was performed using the "GridSearchCV" function (Siji and Sumathi, 2020) from the "Sklearn library". The function optimizes the parameters of the estimator through a cross-validated grid search over a given parameter grid (Buitinck et al., 2013; Pedregosa et al., 2011). The model was then manually fitted by analyzing the loss function plot and calculating the selected goodness-of-fit indicators (Section 3.2) from the observed data compared with the predicted data to achieve a more accurate fit to the training data. In addition, it included 34 batch normalization layers and a dropout layer with a rate of 1.0×10^{-3} to prevent overfitting. Structural stabilization was achieved with a hidden size of 78 and 32 epochs. An "Adagrad" optimizer with a

learning rate of 2.37×10^{-2} and a regularization parameter of 1×10^{-2} was also used. The loss function was programmed using "SmoothL1Loss", which was carefully monitored during training.

4.1.5. Evaluation of the performance of the salinity prediction model

Several goodness-of-fit indicators were used to assess the performance of the model considering both the "testing data" and "all predicted data". These included the root mean square error (RMSE, dS m^{-1}), the root mean square error normalized by the mean of the observations (NRMSE, %), the mean absolute error (MAE, dS m^{-1}), the Pearson correlation coefficient (ρ), the coefficient of determination (R^2), the average direction and magnitude of the systematic error represented by the BIAS, and the percent bias (PBIAS, %) which measures the average tendency of the estimates to be larger or smaller than the corresponding ones observed (Hodson, 2022; Paredes et al., 2018; Plevris et al., 2022; Steurer et al., 2021). Additionally, the ratio of performance to interquartile error range (RPIQ) were used as a robust metric for evaluate model accuracy. RPIQ emphasizes the reliability of predictions withing the central 50% of observed data, following the methodology of Bellon-Maurel et al., (2010); Krause et al., (2005). These metrics were used to validate texture raster interpolation maps, to adjust hyperparameters in RF, SVM, and CNN, and evaluate model performance in predicting soil salinity in the study sites.

For the superior accuracy algorithm (RF in this study), the percentage importance of each variable was estimated (Figure 4.E2). The predictor importance was calculated by assessing how much each predictor contributed to reducing the mean squared error (MSE) in the predicted data (Breiman, 2001). This process, also referred to as impurity reduction, quantifies the importance of each predictor by assessing the reduction in impurities, particularly the reduction in MSE (Louppe et al., 2013). It occurs when a

predictor is used to split a node in the decision trees. The cumulative reduction in MSE for each predictor is then calculated for all trees and nodes in the RF. This value is normalized to obtain the predictor importance, which reflects how much each predictor contributes to reducing the overall prediction error in the RF model (Buitinck et al., 2013; Pedregosa et al., 2011).

Redundancies in the model were assessed manually for each predictor (in appendix Figure 4.D1). To achieve this, the RF model was re-run, excluding individual predictors (see appendix Figure 4.E2). Since each predictor contributed significantly to the model, its absence from the model inputs reduced the optimal goodness-of-fit indicators (highest R^2 values, and lowest values of MAE, RMSE, BIAS, and PBIAS) achieved in this study (Table 4.1). To identify statistical differences in Ca^+, Mg^{2+}, Na^+, and EC_e concentrations between study sites analysis of variance was also performed, followed by Tukey´s multiple comparison test (α= 0.05) (Tukey, 1949). Metrics were calculated at each programming step using Python, while additional statistical analyses were performed using R software version 2024.04.1 (R Core Team, 2024). Finally, soil salinity mapping was created using QGIS version 3.28 (QGIS Development Team, 2024).

5. Results

5.1. Soil salinity in the study sites

The village of Elalab exhibited significantly (α= 0.05) higher EC_e values than the other sites, averaging 82.1 dS m^{-1}, with a range from 0.4 to 228.7 dS m^{-1} (Figure 4.3). The lowest EC_e values were reported at Cafine-Cafal, averaging 30.8 dS m^{-1} and ranging from 0.5 to 150.9 dS m^{-1}. Sodium was found to be the main cation influencing soil salinity, with extractable concentrations ranging from 0.1 - 173 cmol(+) L^{-1} in Elalab, 0.2 - 122.4 cmol(+) L^{-1} in Enchugal, and 0.3 - 99.3 cmol(+) L^{-1} in Cafine-Cafal. Magnesium also displayed a pronounced distribution, particularly in the village of Elalab and the specific location of Enchugal, with the highest concentrations reaching 41 cmol(+) L^{-1}. This underscores the significant influence of Na^+ and Mg^{2+} on hypersaline zones in the MSRP of GB.

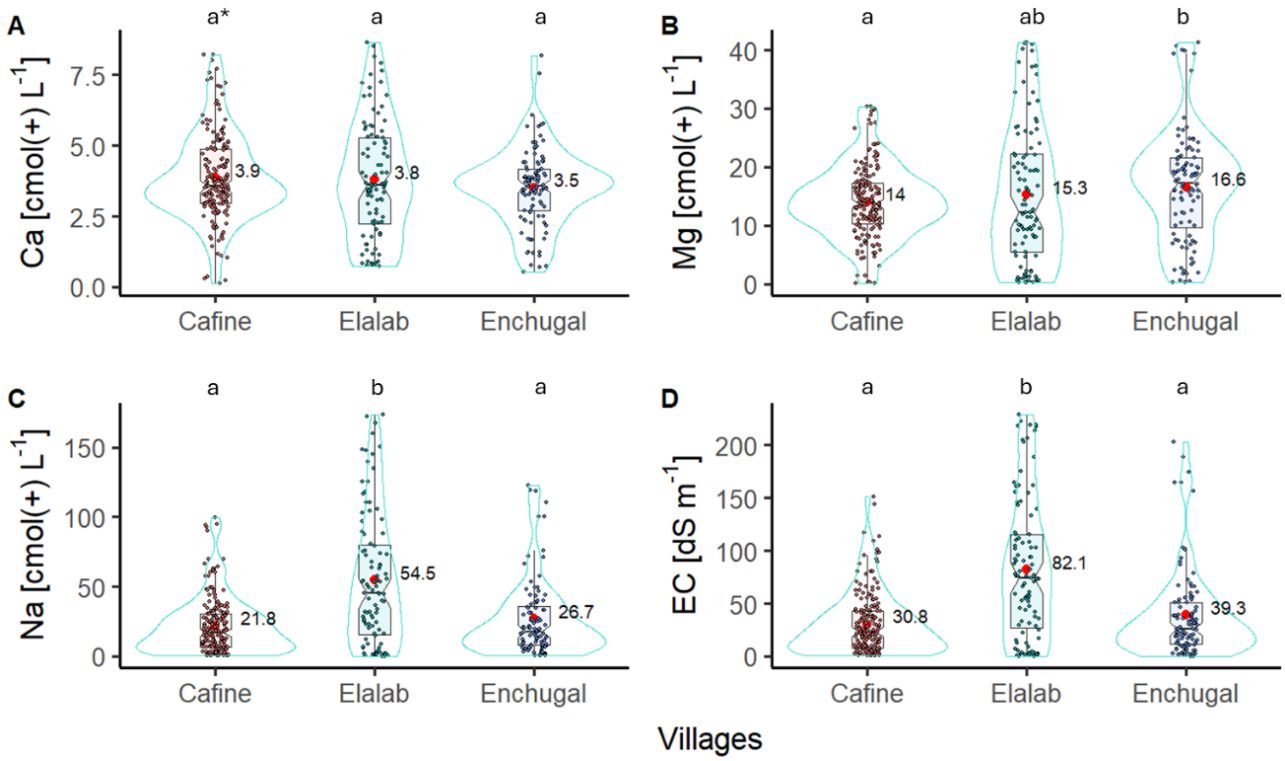

Figure 4.3. Concentration of extractable Ca^{+}, Mg^{2+}, and Na^{+}, and electrical conductivity of the saturation paste extract (EC_e) in the study sites of Elalab, Enchugal, and Cafine-Cafal, Guinea-Bissau. * Different letters indicate statistically significant differences (α= 0.05) according to Tukey´s test.

The data density, as assessed from the samples analyzed across the three study sites, exhibited considerable variability depending on the geographical location of the sampling sites (Figure 4.4). The Cafine-Cafal and Enchugal sites showed similar clay contents across all sampling locations. In contrast, Elalab was characterized by lower clay contents. In the Cafine-Cafal and Enchugal, silt showed notably higher data density between 20% and 60%. Thus, MSR fields exhibit similar distribution patterns for the diverse texture in Enchugal and Cafine-Cafal, while in Elalab fields a more homogeneous distribution of their physicochemical characteristics occurred (Figure 4.3).

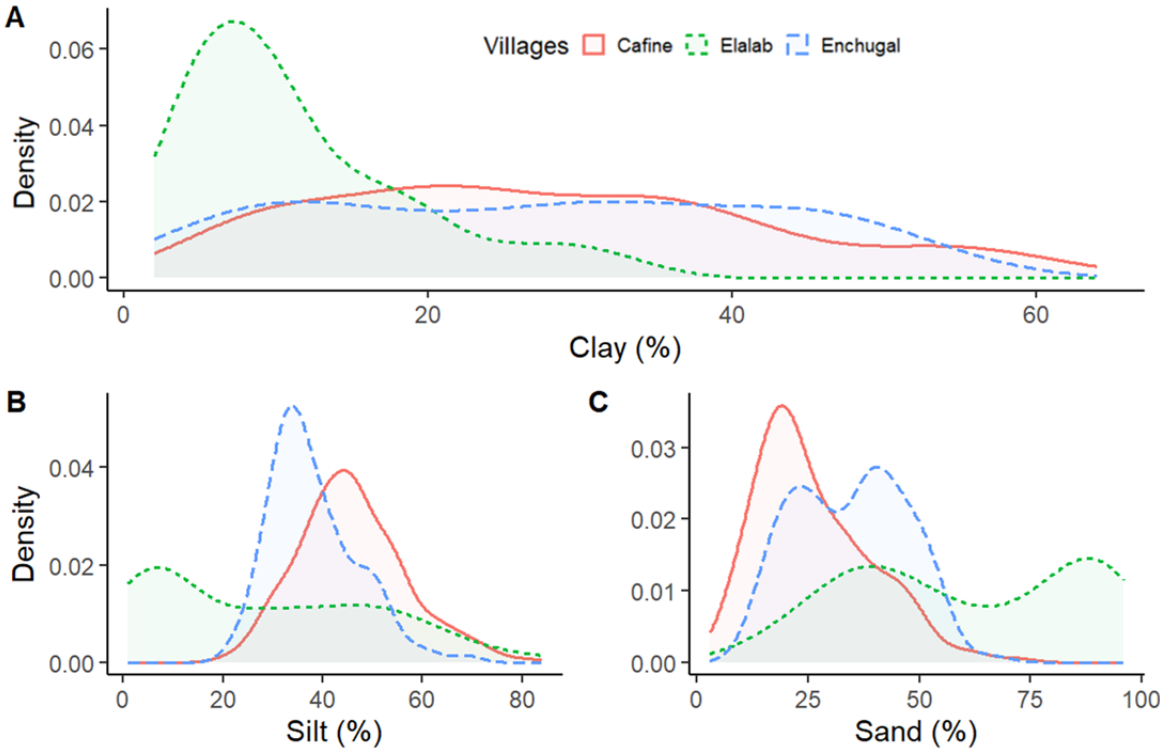

Figure 4.4. Kernel density estimation for data on clay (A), silt (B), and sand (C) percentage analyzed in the study sites of Cafine-Cafal, Elalab, and Enchugal in Guinea-Bissau.

Analysis of the MSRP soil textures at the study sites revealed that Elalab soils were characterized by a higher sand content than Enchugal and Cafine-Cafal, where medium, medium-fine and fine textures predominated (Figure 4.5). However, there were also many locations in Elalab with medium (loam) and medium fine textures (loam silt and silty loam). When the EC_e values are plotted into the texture diagram, it becomes clear that higher EC_e values are mainly found in medium fine texture soils.

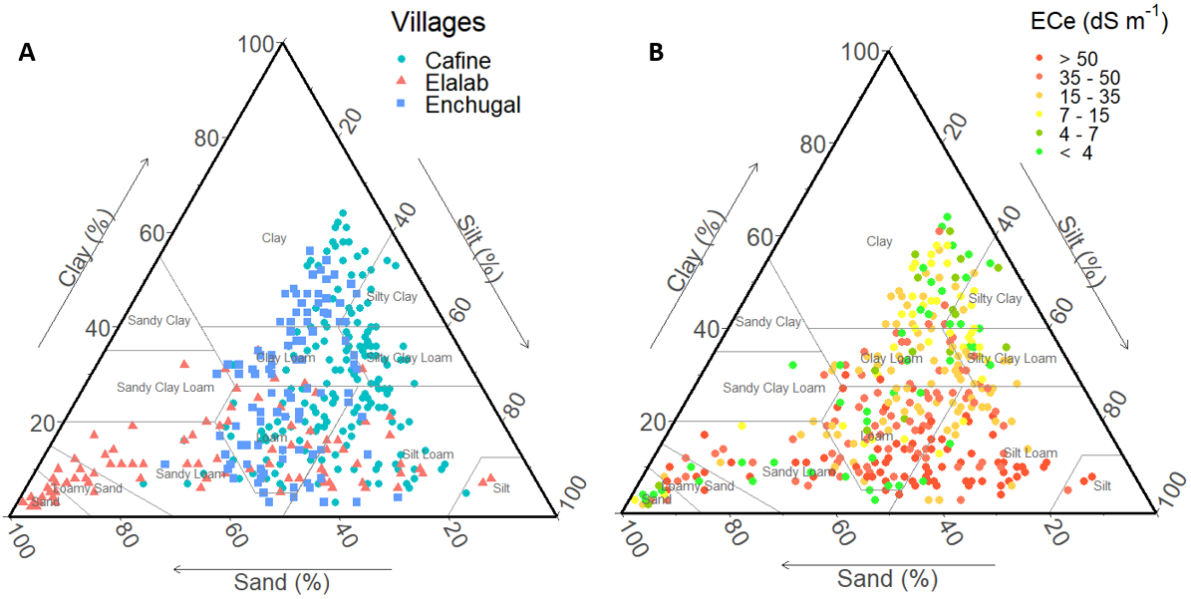

Figure 4.5. Soil particle (clay, silt, sand) (A) and EC_e (B) distribution in the texture triangle.

5.2. Selection of salinity predictors

Redundancies were identified when a large number of predictors were used in this study (Table 4.1). The exclusion analysis revealed that removing indices with lower correlation with EC_e had no impact on the maximum metrics achieved during model training. However, excluding indices with higher correlation with EC_e significantly changes all goodness-of-fit metrics (R^2= 0.26, MAE = 32.69 dS m^{-1}, RMSE = 45.44 dS m^{-1}, NRMSE = 102%, BIAS = -0.18, and PBIAS = -0.41%). This pattern was also observed when using all texture rasters. Combining of all soil texture raster with the best indices significantly improved the model metric (R^2= 0.59, MAE = 23.02 dS m^{-1}, RMSE = 33.89 dS m^{-1}, NRMSE = 76%, BIAS = -1.95, and PBIAS = -4.39%). However, some texture rasters exhibited similar behaviors, which led to redundancies in the predictions. This issue was particularly evident when the best indices and texture raster were modeled individually. While the use of silt and clay rasters showed sufficient precision (R^2= 0.58, MAE = 23.38 dS m^{-1}, RMSE = 34.01 dS m^{-1}, NRMSE = 77%, BIAS = -2.45, and PBIAS

= -5.53%), they tended to overestimate salinity by associating a high EC_e value to all sites with high clay content. This observation was confirmed through map interpolation using two texture rasters, which incorrectly identified high EC_e locations where such conditions did not exist. For this reason, the decision was made to use only one raster to enhance the accuracy of the salinity map predictions. Therefore, a combination of indices and texture rasters used in this study, which achieved optimal goodness-of-fit indicators in terms of BIAS and PBIAS was used in this study (R^2= 0.53, MAE = 26.79 dS m^{-1}, RMSE = 36.14 dS m^{-1}, NRMSE = 81%, BIAS = -0.26, and PBIAS = -0.59%). These predictors were selected because during the training phase showed the highest accuracy in the data set.

At the MSRP sites in GB, three satellite indices showed the highest correlation (0.34 – 0.51) with the ground-truth EC_e (Figure 4.6). These indices were the normalized difference salinity index (RNDSI) calculated with Red Edge (Band 4.7), normalized difference salinity index (NDSI), and normalized difference water index (NDWI). The respective formulas/definition and selection criteria can be found in the appendix (Table B2 and Table C3). The data showed positive correlations for RNDSI, NDSI, and NDWI. Furthermore, the silt raster showed a correlation with the ground-truth EC_e, with a correlation coefficient of 0.10. This indicates a low direct correlation with soil salinity, compared to the sand raster (0.23) and clay raster (-0.43).

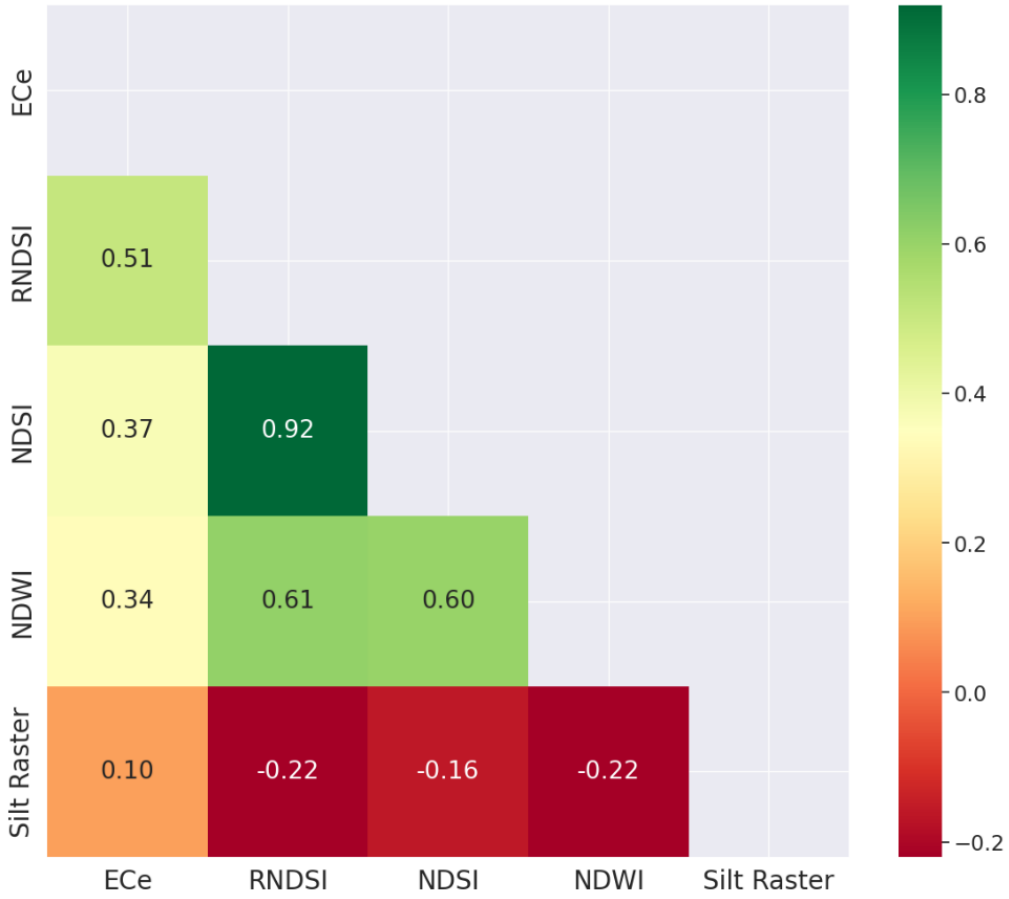

Figure 4.6. Pearson correlation coefficients between selected variables and ground-truth EC_e (dS m^{-1}).

Table 4.1. Impact of excluding predictors on RF model and optimum goodness-of-fit indicators achieved in the training data set.

Indices included in the model	Indices excluded from the model	R^2	MAE (dS m^{-1})	RMSE (dS m^{-1})	NRMSE (%)	BIAS	PBIAS (%)
Exclusion of individual indices							
All Indices	-	0.44	27.89	39.42	89	-0.29	-0.65
RNDSI, RNDVI, NDSI, NDWI, SAVI, YRNDSI, NDVI, YRNDVI, GRVI, GCVI	GNDVI	0.46	27.70	38.85	88	-0.13	-0.29
RNDSI, RNDVI, NDSI, NDWI, SAVI, YRNDSI, NDVI, YRNDVI, GRVI	GNDVI, GCVI	0.46	27.41	38.78	87	-0.38	-0.86
RNDSI, RNDVI, NDSI, NDWI, SAVI, YRNDSI, NDVI, YRNDVI	GNDVI, GCVI, GRVI	0.45	27.62	38.90	88	-0.30	-0.67
RNDSI, RNDVI, NDSI, NDWI, SAVI, YRNDSI, NDVI	GNDVI, GCVI, GRVI, YRNDVI	0.46	27.47	38.81	87	-0.67	-1.50
RNDSI, RNDVI, NDSI, NDWI, SAVI, YRNDSI	GNDVI, GCVI, GRVI, YRNDVI, NDVI	0.45	27.65	38.11	88	-0.69	-1.56
RNDSI, RNDVI, NDSI, NDWI, SAVI	GNDVI, GCVI, GRVI, YRNDVI, NDVI, YRNDSI	0.45	28.04	39.19	88	-0.35	-0.78
RNDSI, RNDVI, NDSI, NDWI	GNDVI, GCVI, GRVI, YRNDVI, NDVI, YRNDSI, SAVI	0.44	28.15	39.54	89	-0.27	-0.60
RNDSI, RNDVI, NDSI	GNDVI, GCVI, GRVI, YRNDVI, NDVI, YRNDSI, SAVI, NDWI	0.26	32.69	45.44	102	0.18	0.41
RNDSI, RNDVI, NDWI	GNDVI, GCVI, GRVI, YRNDVI, NDVI, YRNDSI, SAVI, NDSI	0.31	31.05	43.84	99	-0.72	-1.62
RNDSI, NDWI, NDSI	GNDVI, GCVI, GRVI, YRNDVI, NDVI, YRNDSI, SAVI, RNDVI	**0.45**	**27.98**	**39.18**	**88**	**-0.41**	**-0.92**
RNDSI, NDWI, NDSI, SAVI	GNDVI, GCVI, GRVI, YRNDVI, NDVI, YRNDSI, RNDVI	0.46	27.63	38.80	87	-0.53	-1.19
RNDSI, NDWI, NDSI, SAVI, NDVI	GNDVI, GRVI, GCVI, YRNDVI, YRNDSI, RNDVI	0.47	27.44	38.47	87	-0.64	-1.44
RNDSI, NDWI, NDSI, NDVI	GNDVI, GRVI, GCVI, YRNDVI, YRNDSI, RNDVI, SAVI	0.46	27.62	38.66	87	-0.52	-1.17
RNDSI, NDWI, NDSI, NDVI + **all soil texture raster**	GNDVI, GRVI, GCVI, YRNDVI, YRNDSI, RNDVI, SAVI	0.60	22.83	33.47	75	-1.82	-4.10
RNDSI, NDWI, NDSI + **all soil texture raster**	GNDVI, GRVI, GCVI, YRNDVI, YRNDSI, RNDVI, SAVI, NDVI	**0.59**	**23.02**	**33.89**	**76**	**-1.95**	**-4.39**
RNDSI, NDWI, NDSI, SAVI, NDVI + **all soil texture raster**	GNDVI, GRVI, GCVI, YRNDVI, YRNDSI, RNDVI	0.60	22.64	33.12	75	-1.96	-4.42

** Table is continuing in the next page.

Indices included in the model	Indices excluded from the model	R^2	MAE (dS m^{-1})	RMSE (dS m^{-1})	NRMSE (%)	BIAS	PBIAS (%)
Best indices achieved + exclusion of individual soil texture							
Indices + soil texture included	**Soil texture raster excluded**						
RNDSI, NDWI, NDSI, silt raster, Clay raster, Clay+Silt raster	Sand raster	0.59	22.87	33.72	76	-2.56	-5.77
RNDSI, NDWI, NDSI, silt raster, Clay raster	Sand raster, Clay + Silt raster	0.58	23.38	34.01	77	-2.45	-5.53
RNDSI, NDWI, NDSI, Silt raster	Sand raster, Clay + Silt raster, Clay raster	**0.53**	**26.79**	**36.14**	**81**	**-0.26**	**-0.59**
RNDSI, NDWI, NDSI, Clay raster	Sand raster, Clay + Silt raster, Silt raster	0.53	24.44	36.16	82	-3.19	-7.19
RNDSI, NDWI, NDSI, Clay + Silt raster	Sand raster, Silt raster, Clay raster	0.50	25.84	37.30	84	-1.12	-2.53

RMSE = root mean square error. NRMSE = Normalized root mean square error. MAE = mean absolute error in dS m-1. PBIAS = Percent Bias. p = Pearson's correlation coefficient. R^2 = coefficient of determination. Observations = 382. Samples used to train the model = 305. N. testing data = 77. Index and rasters used = 15. n. matrix = 5730. Red Number indicates lowest accuracy. Bold numbers indicate the best goodness-of-fit achieved.

5.3. Soil salinity models

The RF algorithm accurately predicted EC_e using three satellite indices (RNDSI, NDSI, NDWI) and a silt raster (Table 4.2). When analyzing the training data for the RF, SVM, and CNN models, all models achieved a Pearson correlation coefficient exceeding 0.67 (strong to high correlation (Taylor, 1990)). However for this study, the model with the highest R^2 (0.84), and ratio of performance to interquartile range (RPIQ = 2.53), lowest NRMSE (2 %), BIAS (0.45), and PBIAS (0.04%) (Table 4.1), was considered the best model. Therefore, the RF model has the highest precision and accuracy ($R^2 > 0.84$) in predicting EC_e (MAE = 13.35 dS m^{-1}, RMSE = 20.89 dS m^{-1}), with a Pearson correlation (ρ) of 0.91 and a high RPIQ of 2.53. Finally, the low positive BIAS in the RF resulted in slight overfitting, reflected in a PBIAS of 0.04% across the predicted data set. This indicates a systematically low percentage of overestimations in the prediction model results (Figure 4.7A).

Table 4.2. The accuracies of the models in RF, SVM, and CNN for Leave-One-Out Cross Validation were used to predict EC_e in Elalab, Enchugal, and Cafine-Cafal in Guinea-Bissau, West Africa.

Models	ρ	R^2	MAE (dS m^{-1})	RMSE (dS m^{-1})	NRMSE (%)	BIAS	PBIAS (%)	RPIQ
RF	0.73	0.53	26.79	36.14	81	-0.26	-0.59	1.43
SVM	0.67	0.16	32.63	48.19	109	-12.05	-27.17	1.07
CNN	0.70	0.43	25.87	39.93	90	-10.71	-24.15	1.27
RF	0.91	0.84	13.35	20.89	2	0.45	0.04	2.53
SVM	0.59	0.12	29.70	45.86	98	-13.47	-28.78	1.16
CNN	0.70	0.43	22.89	37.40	81	-10.37	-22.39	1.38

RMSE = root mean square error. NRMSE = Normalized root mean square error. MAE = mean absolute error. PBIAS = Percent Bias. ρ = Pearson's correlation coefficient. R^2 = coefficient of determination. RPIQ = ratio of performance to interquartile range. RN = Random Forest. SVM = Support Vector Machine. CNN = Convolutional Neural Networks. Observations = 382 soil samples. Samples used to train the model = 305. N. testing data = 77. Soil texture raster used = 1. Satellite indices used = 3. Total n. matrix = 1528.

Silt raster contributed significantly to the prediction of soil salinity in the three study areas (Figure 4.7B). When evaluating the importance of the indices' for predictions, RNDSI and Silt raster emerged as the primary contributors for model calibration, explaining 18.6% – 47.2%. In addition, NDSI and NDWI individually contributed 17.4% and 16.8% respectively. These findings underscore the potential of these indices as valuable tools for predicting soil salinity in the three GB regions within the MSRP.

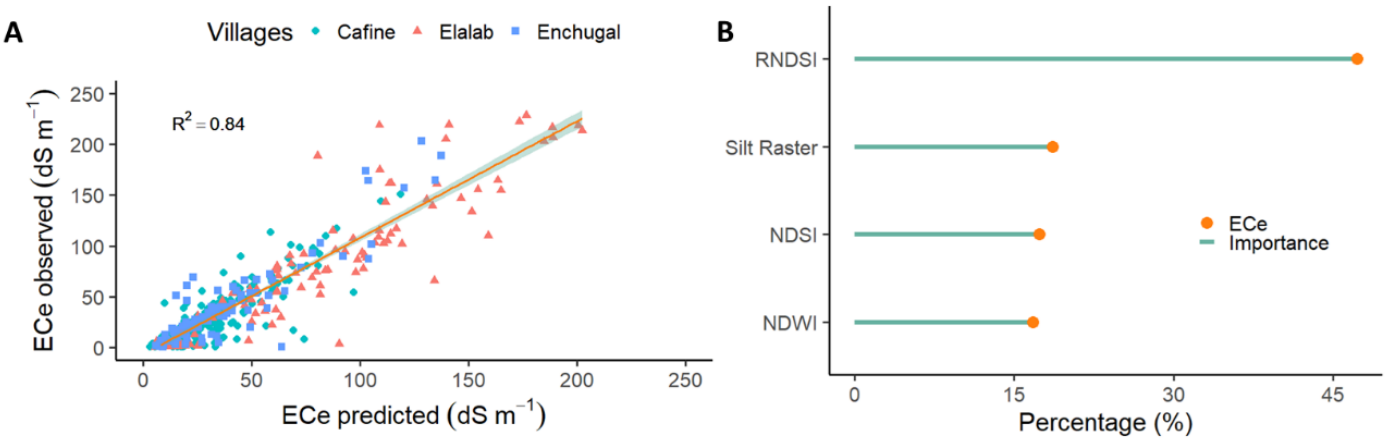

Figure 4.7. Scatterplot between observed and predicted values in EC_e and percentage of index importance in predictions generated by RF in the Elalab, Enchugal, and Cafine-Cafal study sites in GB. A) Scatterplot of predicted vs observed EC_e. B) Percentage of importance by index contribution in the model.

The salinity models effectively predicted the spatial distribution of EC_e in the country's MSRP, which was confirmed by cross-validation between the three study sites (Table 4.3). The RF model showed a maximum ρ value of 85%, while the R^2 values at the three sites ranged from 0.71 to 0.81. Notably, Cafine-Cafal achieved the most accurate predictions, with a MAE of 10.81 dS m^{-1}, and a RMSE of 15.59 dS m^{-1}. Based on the BIAS analysis, the modeled values of all three study sites were found to have low values (PBIAS ranged from -5.73% to 5.81%), indicating a systematic slight overestimation tendency in Cafine-Cafal and a slight underestimation tendency in Elalab and Enchugal. Then, the RPIQ values for the three sites were 3.01 (Elalab), 2.56 (Cafine - Cafal) and 2.07 (Enchugal), indicating strong prediction performance, particularly in Elalab village. Consequently, the RF model provides a robust validation for the diagnosis of soil salinity at the three sites in different regions (Tombali, Oio, Cacheu), each characterized by different edaphoclimatic conditions (Figure 4.8).

Table 4.3. Model accuracy in RF cross-validation between Elalab, Cafine-Cafal and Enchugal used to predict EC_e in Guinea-Bissau.

RF by study sites	ρ	R^2	MAE (dS m^{-1})	RMSE (dS m^{-1})	NRMSE (%)	BIAS	PBIAS (%)	RPIQ
Elalab	0.90	0.81	19.68	29.23	36	-0.97	-1.19	3.01
Cafine-Cafal	0.85	0.71	10.81	15.59	51	1.79	5.81	2.26
Enchugal	0.91	0.80	11.71	19.39	49	-2.25	-5.73	2.07

RMSE = root means square error. NRMSE = Normalized root means square error. MAE = mean absolute error. PBIAS = Percent Bias. p = Pearson's correlation coefficient. R^2 = associated with Linear model. RPIQ = ratio of performance to interquartile range. RN= Random Forest.

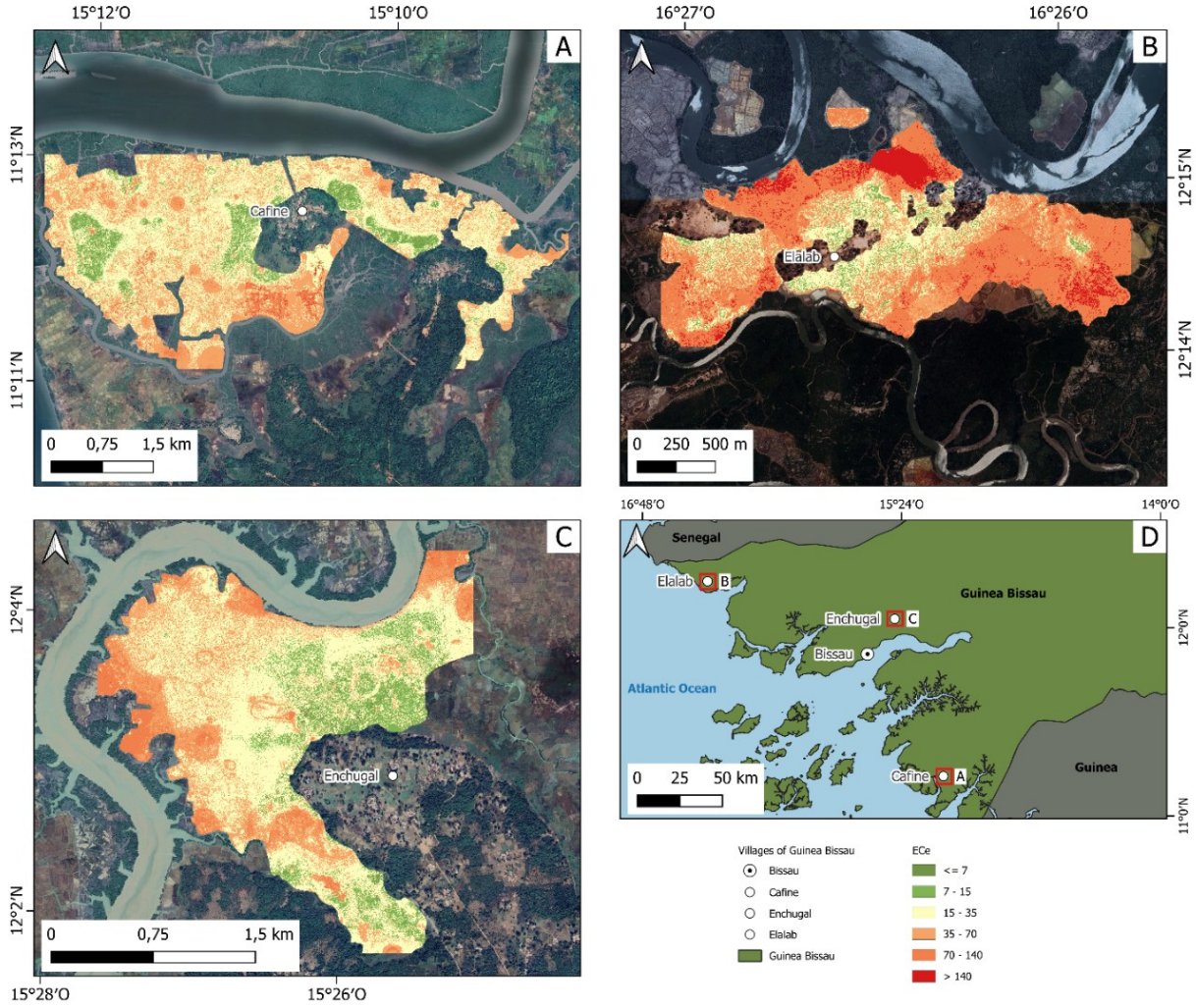

Figure 4.8. Soil salinity map located in the Cafine-Cafal (A), Elalab (B), and Enchugal (C) of Guinea-Bissau (D), West Africa. Soil salinity scale for the mangrove rice agroecosystem according to Sylla et al., (1995) adapted to EC_e (dS m^{-1}) (Sonmez et al., 2008).

6. Discussion

6.1. Soil salinity and texture in MSRP

The variability of EC_e across the three study sites in GB ranged from 0.5 dS m^{-1} to 353.7 dS m^{-1}, with higher conductivity values observed near creeks/sea branches, and lower values in the middled rice fields (Figure 4.8). This pattern is likely due to the recent conversion of these areas to rice cultivation, as they are still influenced by tidal effects (Garbanzo et al., 2024a). Among the three study sites, the northern region exhibited higher EC_e levels, likely resulting from a combination of lower rainfall distribution and agricultural management practices that promote salt accumulation in certain zones of the MSR fields. At the onset of the rainy season, rice cultivation in these areas is only possible if rainfall is sufficient to leach out salts from the rootzone, and if salt dissolution does not significantly hinder osmotic water uptake by rice varieties grown (see also, Muchate et al., 2016; Rodríguez Coca et al., 2023). A detailed discussion of rice production in these area and the key factors influencing soil salinity is available in (Garbanzo et al., 2025).

The extremely high EC_e values identified in this study are characteristic of hypersaline environments and are consistent with findings from other research conducted in mangrove rice fields in GB (Andreetta et al., 2016; Sylla et al., 1995), once the data are standardized to EC_e. D'Amico et al., (2024) even reports higher, potentially unrealistic values. Comparable salinity levels have also been documented in mangrove ecosystems (Ahmed et al., 2022) and other hypersaline regions globally, such as Australia (Parker, 2004), the USA (Scudiero et al., 2015; Timm and McGarigal, 2012), Mexico (Navarro-Noya et al., 2015), Iran (Golestani et al., 2023), or Spain (Herrero et al., 2015; Herrero and Castañeda, 2023). Nonetheless, the elevated EC_e values reported in this study should

be interpreted with caution, as no established conversion procedure currently exists for salinity levels this high.

Salinity in MSRP fields in GB depends on the concentration of Na^{+}, Mg^{2+}, and Ca^{+2} in the soil solution. These are the main cations that cause osmotic stress, and hinder water uptake by rice plants in some areas (Golabkesh et al., 2021). Particularly noted is the presence of high extractable Na^{+} concentrations (ranging from 50 to 173 cmol(+) L^{-1}), which largely contributed to soil salinity observed in these locations. These constitute 21% of the samples, all of which were previously mangrove forest soils (Andrieu et al., 2019; Naidoo, 2023; Temudo et al., 2015; Temudo and Cabral, 2017). The high Na^{+} concentration observed in this study is consistent with those recently reported by D'Amico et al., (2024) in GB (0.17 – 1763.8 cmol(+) kg^{-1} with ammonium acetate. The increased concentrations of these elements originate from the genesis of these soils resulting from the alluvial sedimentation of particles near saline water bodies and the sedimentary impacts induced by tidal dynamics (D'Amico et al., 2024; Sylla, 1994; Sylla et al., 1995). The concentration of extractable Ca and Mg exceeded the critical levels for plants (Ca = 5, and Mg = 0.7 cmol(+) L^{-1}), as reported by Cabalceta and Molina (2005).

Medium fine soil textures (silty textures) had the highest EC_e values determined in this study. These soils are characterized by poor structure and drainage conditions. The microporosity of the soil facilitates the upward movement of water and salts resulting from crop evapotranspiration. At the same time, low infiltration rates make the natural leaching process caused by rainfall challenging. Furthermore, loam soil textures have larger pores compared to fine texture classes, facilitating water movement through soil profiles (Ju et al., 2024; Lipiec et al., 2006). Infiltration rates are significantly higher in loamy and sand soil textures, facilitating the downward movement of solutes to deeper horizons, and thus leaching of salts (Allaire-Leung et al., 2000; Liu et al., 2023; Sun et

al., 2022). In contrast, clayed soil exhibit microporosity, resulting in greater tortuosity in the movement of water and solutes (Salmas et al., 2003; Singh, 2024). These soils tend to be well structured which can facilitate leaching. However, high sodium concentrations also disrupt soil structure, affecting pore continuity due to particle dispersion, and thereby destroying soil structure (Rengasamy and Olsson, 1991).

Further research on the hydrological and geochemical processes governing water and salt transport in MSR fields is essential. To ensure the sustainability of MSR, it is therefore imperative to educate farmers and decision makers about the complex dynamics of these processes (Bazrafshan et al., 2020; van de Craats et al., 2020). As discussed by others (Li et al., 2022), differences in agroclimatic and pedogenetic characteristics between sites likely result in divergent patterns in water and salt fluxes. Notably, the northern and central study sites experience less precipitation compared to their southern counterparts, resulting in less salt leaching (see Van der Zee et al., 2017). This suggests a possible correlation between fluctuations in the groundwater level and its proximity to the soil surface. Some studies suggest that leaching of salts due to high tides is related to the ease of water movement in loamy soils (White and Madsen, 2016). In all coastal regions of the country where MSR is produced, endopedons tend to be saline (Andreetta et al., 2016; D'Amico et al., 2024), resulting in high concentration of dissolved salts in the phreatic zone (Van de Craats et al., 2020, White and Madsen, 2016). It is possible that in regions with sandy and loamy textures (such as the Elalab village), increased salt concentration occurs in the upper horizons in combination with the pressure effects of tidal movements, high soil evaporation, and low annual rainfall. Thus, tidal influences can directly impact groundwater dynamics, facilitate salt migration toward surface horizons and interact with soil water evaporation during the peak of the annual rainy season.

This likely contributes to hypersalinity in certain MSRP areas, as also reported by Sylla (1994). Additionally, water management practices have a direct impact on cation leaching from plots. For example, farmers in the north (Elalab) no longer drain freshwater (rainwater) that accumulates before plowing. In contrast, farmers in the South (Cafine-Cafal) and certain areas of the Oio region (Enchugal) drain excess water before plowing. This practice promotes desalination of sites during high rainfall years. In Elalab village, progressive accumulation of salts occurs due to limited leaching, resulting in salts remaining in the system and exacerbating soil salinity.

6.2.Spatial distribution of hypersalinity in MSRP fields

The RNDSI index contributed the most to improving soil salinity predictions in the MSRP in GB (Figure 4.8). This is likely because they provide essential information about the reflectance of areas with diverse vegetation cover. These findings are consistent with those of other studies (e.g. Tan et al., 2023). The initial conditions of the paddies fields show large variations in various factors such as vegetation cover, dry and wet areas, in remnants of previous crops, and the occurrence of saline water intrusion. These likely provide information through reflectance in locations, such as energy transfer in soil or in various vegetation covers (Cui et al., 2023). Salinity index is widely used to monitor soil salinity and evaluate vegetation changes (Sirpa-Poma et al., 2023; Xiao et al., 2023; Zhang et al., 2022). In particular, the silt raster provides the model with a direct way to identify regions associated with high salt concentration, as discussed in Section 5.1. In addition, NDSI and NDWI also played an important role in the model (Figure 4.7.B). Manual exclusion of each index resulted in reduced prediction accuracy (Table 4.1), underscoring their common importance in predicting soil salinity. These results are consistent with other studies indicating that variations in salinity reflectance spectra are

not due to a single soil property (Csillag et al., 1993) but rather to a complex interplay of site-specific characteristics (Dehaan and Taylor, 2002; Kalambukattu et al., 2023; Pettorelli et al., 2005) the combined contribution of salinity indices (RNDSI, NDSI), soil texture and water index (NDWI) were important for training the RF model. These indices have shown good accuracy in other soil salinity studies, such as using RNDSI (Tan et al., 2023), NDSI (Venugopal et al., 2023), and NDWI (Lopes et al., 2020). Recently, Liu et al., (2023) successfully used SVM, RF regression, and multiple linear regression (MLR) to couple MODIS-NDVI, with electrical conductivity and soil texture to predict salinity conditions in Punjab, Pakistan.

The results show that the RF regression algorithm was effective in identifying hypersaline sites within the MSRP (Figure 4.8). The exclusion analysis (Table 4.1) revealed that several features were non-essential for predicting EC_e, although it is important to accurately assess the spatial distribution of salt concentrations in the MSRP, especially given the elevated EC_e values (> 15 dS m^{-1}). Similar results were reported by Sylla et al. (1995) on soil salinity in West Africa and supported by recent studies identifying high-risk hypersaline zones (D'Amico et al., 2024; Naimi et al., 2021; Yang et al., 2023), that are not easily detectable with remote sensing (Bannari et al., 2008). Such extreme site conditions could pose a challenge to rice production at the beginning and/or late phenological stages (e.g., flowering, grain filling), due to their high susceptibility to soil salinity (Minhas et al., 2020). While some studies used RF classification to predict salinity (Sirpa-Poma et al., 2023; Timm and McGarigal, 2012; Wang et al., 2021), these studies included sites with comparatively lower salinity (< 8 dS m^{-1}) than those used for MSRP in GB. Furthermore, in these previous studies, the method was often applied to crops with low salinity tolerance, as is the case of some rice varieties (Sirpa-Poma et al., 2023; Wang et al., 2021).

The mangrove swamp areas in GB have shown that rice production is feasible in hypersaline locations. Smallholders grew rice under these initial hypersaline conditions and were able to become self-sufficient in rice (Garbanzo et al., 2024a; Martiarena and Temudo, 2023). The key to rice production in these locations lies in the efficient management of rainwater collection (Singh, 2021), which helps to dissolve salts in the fields and use the fields for fresh-water storage (Dossou-Yovo et al., 2022; Garbanzo et al., 2024b). Periasamy et al., (2022) highlighted the challenges for agricultural production in such systems. Nevertheless, farmers in GB have identified and demonstrated effective strategies for cultivating rice in highly saline environments. Although farmers have been able to manage salinity with the variable rainfall, these hypersaline locations remain extremely vulnerable (Han et al., 2024), especially in the face of climate variability and change. This fact requires a detailed understanding of the dynamics of salt movements and the solubility of salt within the system to optimize agronomic management in rice production.

6.3. Consideration regarding the utilized model

In this study, the RF model showed the highest accuracy, i.e. the lowest MAE, RMSE, and BIAS values, in diagnosing soil hypersalinity in GB (Table 4.2). The metric showed that it was superior in predicting EC_e compared to SVM and CNN. As discussed by Breiman (2001), the RF model provides robustness to dimensional issues and data noise and enables efficient capture of complex patterns while controlling the inherent variance in model fitting (Liaw and Wiener, 2002; Liu et al., 2012; Siji and Sumathi, 2020). Compared to SVM and CNN, RF may face challenges with highly variable and linear regression as reported in several studies (Decoste and Schölkopf, 2002; Huan et al., 2009; Krizhevsky et al., 2017). However, CNN is more commonly used for image

prediction due to its ability to automatically learn hierarchical features (Bishop, 1995; Haykin, 1999; Krizhevsky et al., 2017), and has the advantage of detecting patterns in image data, as it requires large data-sets for training (Bishop, 1995). On the other hand, SVM can become inefficient as it allows manipulation of fewer hyperparameters compared to CNN and RF.

CNN and RF showed no significant differences ($p<0.05$) in data prediction during the training phase, conversely, they showed significant differences in prediction of all data-sets. These findings are consistent with those of Louppe et al., (2013). In the current study, all three models were tested because existing literature on soil salinity recommended their use (Cui et al., 2023; Naimi et al., 2021). Salinity in MSRP fields had high variability in EC_e, and no existing literature was found to recommend an optimal model for analyzing soil hypersalinity levels. Furthermore, some studies show that RF is an optimal model for soil salinity analysis, due to its high accuracy, robustness to overfitting, ability to provide insights into feature importance, and scalability for processing large data-sets (Kalambukattu et al., 2023; Xiao et al., 2023). Similar results have been reported for mapping mangrove systems in West Africa (Mondal et al., 2019).

Finally, the exclusion analysis using the RF model in this study revealed a high R^2 value using the Clay and Silt raster together. However, the generated interpolation maps did not agree with the field observations. The inclusion of the clay raster in the model leads to the incorrect classification of all sites with high clay content in the MSR fields as saline. This misclassification is due to the high clay content of most sites and can lead to systematic prediction errors in the model. Therefore, it is recommended to review the BIAS and PBIAS metrics to determine the most accurate soil texture raster that more accurately reflects actual field conditions.

7. Conclusions

Understanding MSR farming and water management practices, as well as the influence of Mg and Na on soil salinity is crucial for sustainable rice cultivation in GB. Soil salinity and its spatial distribution in MSRP areas showed significant correlations to silt raster, and different satellite indices (RNDSI, NDSI, NDWI). The use of algorithms such as RF proved to be an effective tool for understanding and improving the spatial distribution of EC_e in the MSRP system. This approach provides an accurate approximation when validated at three different study sites, each regionally separated and with unique edaphoclimatic characteristics. The methodology outlined in this article for analyzing the spatial distribution of soil salinity in village paddies will facilitate the accurate identification of areas vulnerable to salinity in the mangrove swamp rice agroecosystem. This precision is important for the collaborative development of effective strategies to mitigate soil salinity. However, given the extremely high salinity levels observed at the onset of the rainy season, prior to rice planting, it is important to further explore and refine EC_e conversion models for these upper salinity ranges. Enhancing these models would improve the accuracy of current monitoring approaches, most of which using more expedite extracts for soil analysis and characterization.

Furthermore, the study highlights the imperative need for targeted interventions to address excessive soil salinization to optimize rice cultivation and water management practices in the MSRP in GB. Research carried out in GB over the past few decades has shown that the most successful measures to improve agricultural productivity and control soil salinity have been oriented towards creating of a semi-automated water management system operating both at the level of the entire village rice field and at the level of individual plots (see www.universsel.org). The developed model can thus help to identify the hypersaline locations of the rice fields where the installation of drain valves can allow

rapid and efficient drainage of the salts after the first rains. Furthermore, given the poor results of mangrove plantation in the country, this methodology can be adapted to identify the locations where plantation/sowing is prone to failure and provide nature-based solutions for mangrove forests recovery and increasing blue carbon sequestration in coastal areas of Guinea-Bissau and West Africa. Such strategic actions are essential for promoting sustainable agricultural practices and ecological resilience in the region and will contribute to achieving the Sustainable Development Goals SDG1, SDG2, SDG12, SDG13, and SDG14 (United Nations, 2024).

This research represents one of the first attempts to map MSR areas in GB using machine learning techniques. While initial results are promising, additional validation and calibration of the prediction model across diverse geographic and climatic environments is necessary to ensure its robustness and applicability in West Africa. This is a key area for future work. Furthermore, there is a lack of comprehensive understanding of the specific roles and interactions of different cations in soil salinization, which could provide deeper insights into salinity dynamics. The lack of long-term monitoring studies limits the ability to assess the effectiveness of current salinity management practices and to refine the model over time, taking into account changing climatic conditions. Addressing these gaps will be crucial to advancing the scientific field and improving soil salinity management strategies.

8. Appendix

8.1. Appendix A. Sampling point map and geostatistical analysis and validation for soil texture raster.

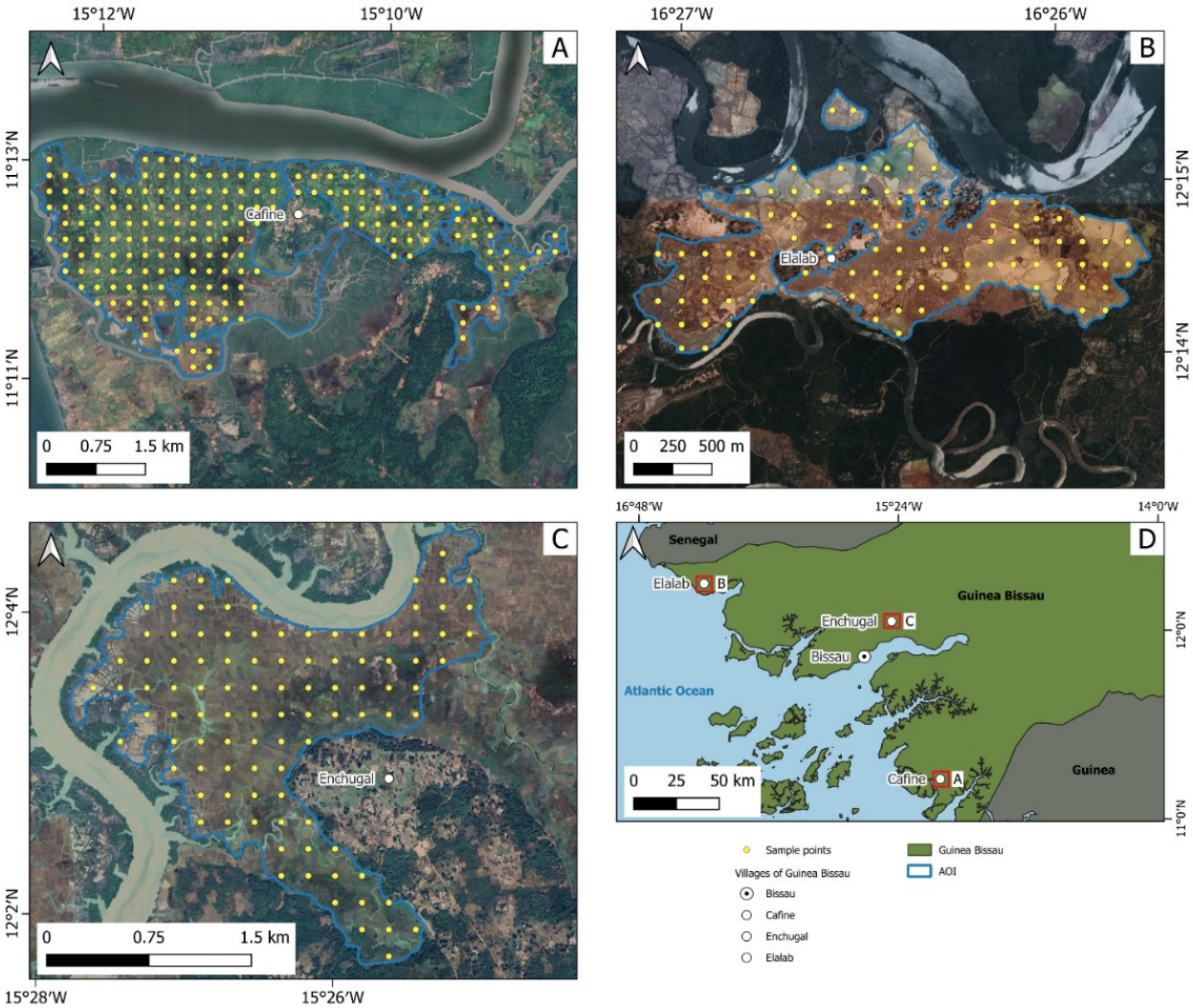

Figure 4.A1. Maps showing the specific points where soil samples were collected.

Table 4.A1. Geostatistical parameters and "Global Moran's Index" evaluation, along with cross validation, used to map soil texture in Cafine-Cafal, Enchugal, and Elalab in Guinea-Bissau.

Samples	Model	Nugget	Sill	Range	Global Moran's I	Variance	Z punctuation	p-value*	MAE	RMSE	ρ
		------ index ------		m	---------- Index ----------						
Cafine-Cafal maps interpolation (n = 183)											
Sand	Exponential	0.002150	0.0171	564	0.10	0.00373	1.755	<0.001	0.013	0.0172	0.99
Silt	Exponential	0.001420	0.01154	480	0.0997	0.00373	1.704	0.088	0.010	0.0134	0.99
Clay	Exponential	0.002410	0.02212	507	0.198	0.00375	3.334	<0.001	0.013	0.0164	0.99
Elalab maps interpolation (n = 99)											
Sand	Exponential	0.0466	0.1433	1579.93	0.381	0.005	5.463	<0.001	0.149	0.174	0.77
Silt	Gaussian	0.0331	0.1516	4520.65	0.348	0.005	5.010	<0.001	0.121	0.145	0.78
Clay	Linear	0.006823	0.00682	1470.36	-0.053	0.005	-0.612	0.54	0.053	0.067	0.56
Enchugal maps interpolation (n = 100)											
Sand	Spherical	0.00003	0.01516	471	0.0258	0.0034	4.601	<0.001	<0.001	0.001	0.99
Silt	Exponential	0.00054	0.00745	462	0.078	0.00334	1.53	0.12	0.006	0.008	0.99
Clay	Spherical	0.00029	0.02298	447	0.238	0.0034	4.257	<0.001	0.003	0.003	0.99

* a probability of less than 2% that the clustered pattern could result from a random likelihood. LOOCV = Leave-one-out cross-validation. RMSE = root mean square error. MAE = mean absolute error. ρ = Pearson's correlation coefficient.

8.2. Appendix B. Bands and indices used in soil salinity studies.

Table 4.B2. Definition of bands and index used to calibrate the models in MSRPS of Guinea-Bissau, West Africa.

Index	Definition	Index	Definition	Index	Definition	Index	Definition
B1	Costal Blue	S6_G1	(R × NIR) / G1	RSI1_G2	$(G2 \times Re)^{0.5}$	YRInt1_G2	(G2 + Y)/2
B2	Blue (B)	S6_G2	(R × NIR) / G2	RSI2_G1	$[(G1)^2+(Re)^2+(NIR)^2]^{0.5}$	YRInt2_G1	(G1 + Y + NIR)/2
B3	Green 1 (G1)	SI	$(B + R)^{0.5}$	RSI2_G2	$[(G2)^2+(Re)^2+(NIR)^2]^{0.5}$	YRInt2_G2	(G2 + Y + NIR)/2
B4	Green 2 (G2)	SI1_G1	$(G1 \times R)^{0.5}$	RSI3_G1	$[(G1)^2+(Re)^2]^{0.5}$	YRNDSI	(Y − NIR)/(Y + NIR)
B5	Yellow (Y)	SI1_G2	$(G2 \times R)^{0.5}$	RSI3_G2	$[(G2)^2+(Re)^2]^{0.5}$	YRNDVI	(NIR − Y)/(NIR + Y)
B6	Red (R)	SI2_G1	$(G1)^2 + (R)^2 + (NIR)^2]^{0.5}$	RInt1_G1	(G1 + Re)/2	YBS1	Y/R
B7	Red edge (Re)	SI2_G2	$(G2)^2 + (R)^2 + (NIR)^2]^{0.5}$	RInt1_G2	(G1 + Re)/2	YBS2	(Y − R)/(Y + R)
B8	Near-infrared (NIR)	SI3_G1	$((G1)^2 + (R)^2)^{0.5}$	RInt2_G1	(G1 + Re + NIR)/2	YBS4	(Y × R) 0.5
NDVI*	(NIR-R) / (NIR + R)	SI3_G2	$((G2)^2 + (R)^2)^{0.5}$	RInt2_G2	(G1 + Re + NIR)/2	YBS5_G1	(Y × R)/G1
NIR	B8	Int1_G1	(G1 + R) / 2	YRS1	B/Y	YBS5_G2	(Y × R)/G2
SR	NIR / R	Int1_G2	(G2 + R) / 2	YRS2	(B − Y)/(B + Y)	YBSI	(Y + R) 0.5
GCVI	(NIR / G) − 1	Int2_G1	(G1 + R + NIR) / 2	YRS3_G1	(G1 × Y)/B	YGS3	(Y × R)/B
NDWI	(G − NIR) / (G + NIR)	Int2_G2	(G2 + R + NIR) / 2	YRS3_G2	(G2 × Y)/B	YGSI1	(Y × R) 0.5
VARI	(G − R) / (G + R − B)	RS1	B/Re	YRS4	$(B \times Y)^{0.5}$	YGSI2	$[(Y)^2+(R)^2+(NIR)^2]^{0.5}$
GRVI	(NIR / G)	RS2	(B − Re)/ (B + Re)	YRS5_G1	(B × Y)/G1	YGSI3	$[(Y)^2+(R)^2]^{0.5}$
GNDVI	(NIR − G) / (NIR + G)	RS3_G1	(G1 × Re)/B	YRS5_G2	(B × Y)/G2	YGInt1	(Y + R)/2
NDSI	(R − NIR) / (R + NIR)	RS3_G2	(G2 × Re)/B	YRS6_G1	(Y × NIR)/G1	YGInt2	(Y + R + NIR)/2
SAVI	(NIR − R) / ((NIR + R + 0.5) × 1.5)	RS4	$(B \times Re)^{0.5}$	YRS6_G2	(Y × NIR)/G2	YNS6_G1	(R × Y)/G1
VSSI	2 × B3 – 5 (B4 + B5) / G × (B3)	RS5-G1	(B × Re)/G1	YRSI	(B + Y) 0.5	YNS6_G2	(R × Y)/G2
S1	B / R	RS5-G2	(B × Re)/G2	YRSI1_G1	(G1 × Y) 0.5	YNSI2_G1	$[(G1)^2+(R)^2+(Y)^2]^{0.5}$
S2	(B − R) / (B + R)	RS6_G1	(Re × NIR)/G1	YRSI1_G2	(G2 × Y) 0.5	YNSI2_G2	$[(G2)^2+(R)^2+(Y)^2]^{0.5}$
S3_G1	(G1 × R) / B	RS6_G2	(Re × NIR)/G2	YRSI2_G1	$[(G1)^2+(Y)^2+(NIR)^2]^{0.5}$	YNInt2_G1	G1 + R + Y)/2
S3_G2	(G2 × R) / B	**RNDSI**	(Re − NIR)/ (Re + NIR)	YRSI2_G2	$[(G2)^2+(Y)^2+(NIR)^2]^{0.5}$	YNInt2_G2	(G2 + R + Y)/2
S4	$(B \times R)^{0.5}$	RNDVI	(NIR − Re)/ (NIR + Re)	YRSI3_G1	$[(G1)^2+(Y)^2]^{0.5}$	YNNDSI	(R − Y)/(R + Y)
S5_G1	(B × R) / G1	RSI	$(B + Re)^{0.5}$	YRSI3_G2	$[(G2)^2+(Y)^2]^{0.5}$	YNNDVI	(Y − R)/(Y + R)
S5_G2	(B × R) / G2	RSI1_G1	$(G1 \times Re)^{0.5}$	YRInt1_G1	(G1 + Y)/2	-	-

* NDVI = Normalized Difference Vegetation Index. NDSI = Normalized difference vegetation index. SAVI = Soil adjusted vegetation index. VSSI = Vegetation soil salinity index. S1, SI, RS and YRS = Salinity index. Int = Intensity index. GCVI = Green chlorophyll vegetation index. VARI = Visible atmospherically resistant index. NDWI = Normalized difference water index. SR = simple ratio index. GRVI = Green Ratio Vegetation Index. GNDVI = Green light normalized difference vegetation index. Source: (Abd El-Hamid et al., 2023; Aksoy et al., 2022; Barreto et al., 2023; Bouaziz et al., 2018; Chaaou et al., 2022; Dakak et al., 2023; Golabkesh et al., 2021; Li et al., 2022; Mzid et al., 2023; Shi et al., 2022; Tan et al., 2023; Triki Fourati et al., 2017, 2015; H. Zhang et al., 2023; Zhou et al., 2022).

Appendix C. Correlation of EC_e data with salinity indices and bands.

Table 4.C3. Pearson correlation (ρ) between EC_e (dS m^{-1}) and Satellite indices evaluated in three study sites in Guinea-Bissau, West Africa.

Index	ρ	Index	Definition	Index	ρ	Index	ρ
RNDSI	0,51	YRS2	-0,17	SI1_G1	0,11	S5_G1	-0,08
RNDVI	-0,51	VSSI	0,16	YRSI2_G1	-0,11	YRS4	0,08
Clay Raster	-0,43	S3_G1	0,16	YNSI2_G1	0,11	S1	-0,07
YRNDSI	0,39	YGS3	0,16	YBS2	0,11	Int2_G1	-0,07
YRNDVI	-0,39	YRS3_G1	0,15	YNNDSI	-0,11	Int2_G2	-0,06
SAVI	-0,37	b4	0,15	YNNDVI	0,11	RSI	0,06
NDVI	-0,37	YRSI1_G2	0,15	YNSI2_G2	0,11	RS5_G1	-0,06
NDSI	0,37	YRInt1_G2	0,14	RSI3_G2	0,11	b6	0,06
NDWI	0,34	RS2	-0,14	YRSI2_G2	-0,11	RS5_G2	-0,06
GNDVI	-0,34	YRSI3_G2	0,14	RSI2_G1	-0,11	YGInt2	-0,06
GCVI	-0,31	RS1	-0,14	RSI2_G2	-0,11	RInt2_G1	-0,06
GRVI	-0,31	b3	0,14	Int1_G1	0,10	RInt2_G2	-0,05
YRS6_G2	-0,28	YRSI1_G1	0,14	SI1_G2	0,10	RS4	0,05
RS6_G2	-0,28	YRInt1_G1	0,14	YGSI2	-0,10	YRInt2_G2	-0,05
SR	-0,27	YRSI3_G1	0,13	Silt Raster	0,10	YRInt2_G1	-0,05
b8	-0,26	RSI1_G1	0,13	YBS4	0,10	YBS5_G2	0,04
pc2	-0,25	b5	0,13	YGSI1	0,10	YNS6_G2	0,04
YRS6_G1	-0,25	VARI	0,13	Int1_G2	0,10	SI	0,04
YRS3_G2	0,23	SI2_G1	-0,13	YGInt1	0,10	pc1	0,04
S6_G1	-0,23	pc3	0,13	YGSI3	0,10	S4	0,04
S6_G2	-0,23	RInt1_G1	0,12	SI3_G1	0,10	YBS5_G1	0,03
Sand Raster	0,23	SI2_G2	-0,12	SI3_G2	0,09	YNS6_G1	0,03
Clay+Silt Raster	-0,23	RSI1_G2	0,12	YBS1	0,09	YRS5_G1	-0,03
RS6_G1	-0,21	RInt1_G2	0,12	b7	0,09	b8_asm	0,03
RS3_G2	0,21	YNInt2_G1	0,12	YBSI	0,09	YRS5_G2	-0,02
RS3_G1	0,19	b1	0,12	YRSI	0,09	b2	0,01
YRS1	-0,18	RSI3_G1	0,11	S2	-0,08	EC_e	1,00
S3_G2	0,17	YNInt2_G2	0,11	S5_G2	-0,08	-	-

8.3. Appendix D. Confusion matrix of EC_e data with salinity indices and soil texture raster.

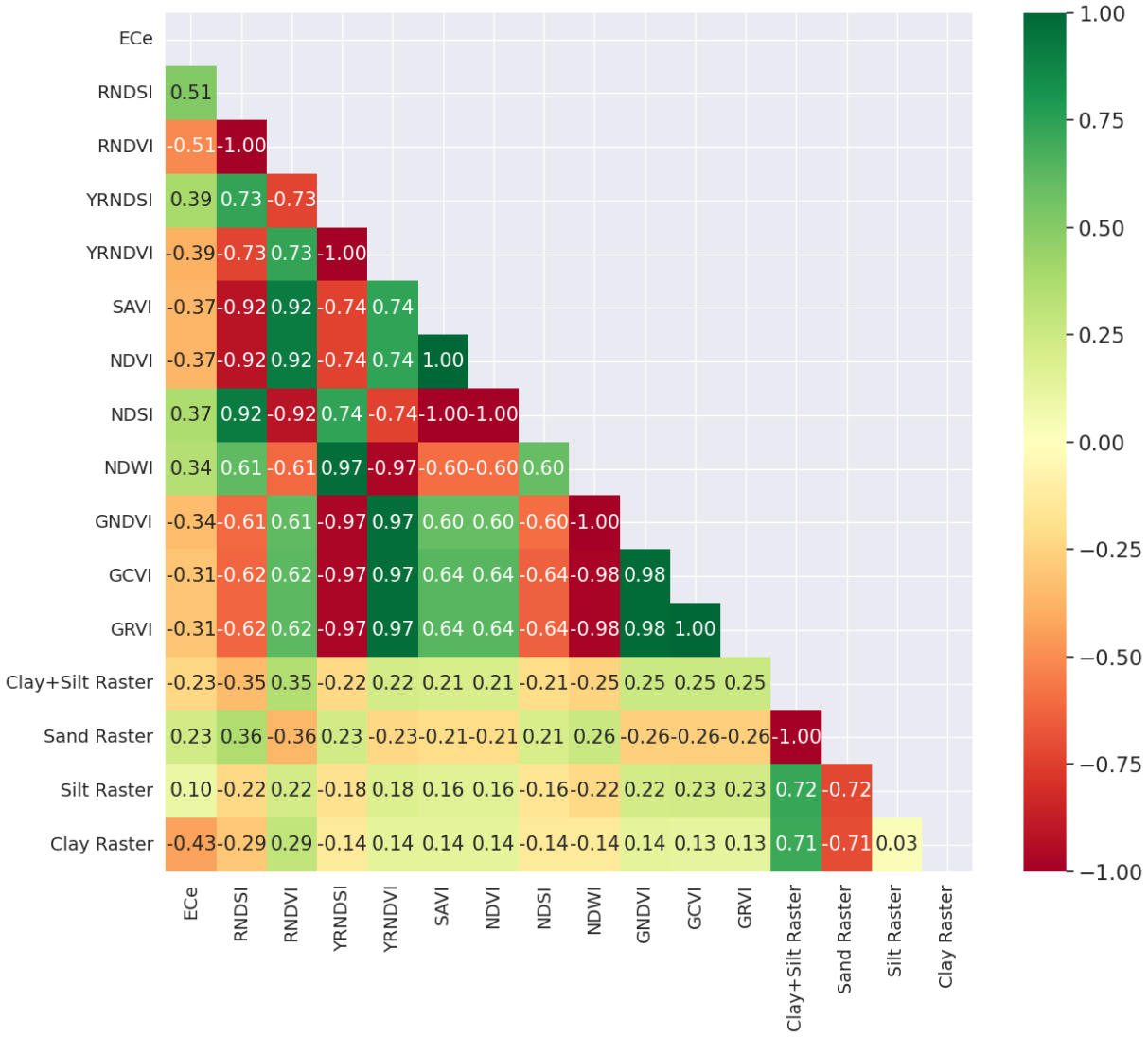

Figure 4.D1. Pearson correlation coefficients between selected satellite indices (above ρ > 0.30 and -0.30), soil texture raster, and ground-truth EC_e (dS m^{-1}).

8.4. Appendix E. Importance of features in modeling.

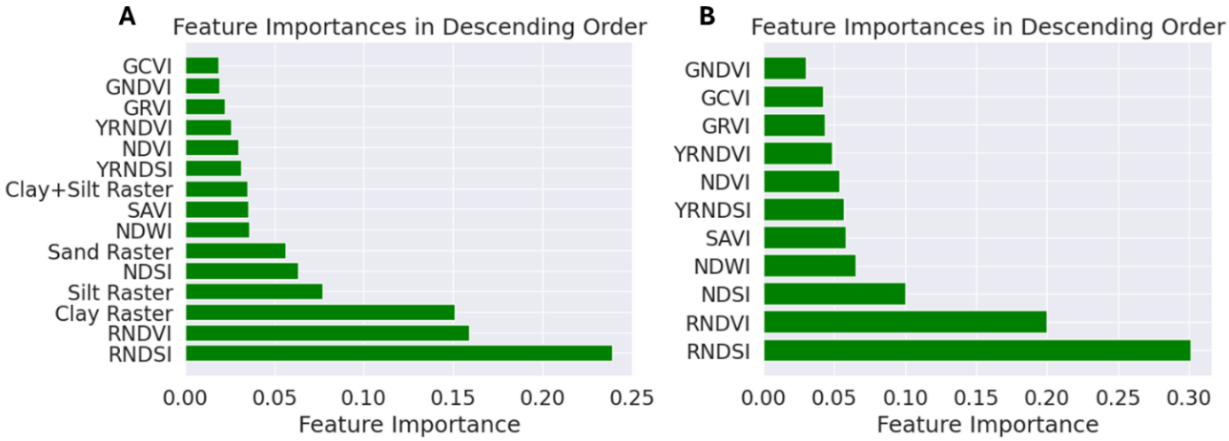

Figure 4.E2. Analysis of the best satellite indices and soil texture raster contributions within the RF model was conducted to select the most critical predictor for ground-truth EC_e (dS m^{-1}) estimation in the MSRP, West Africa.

8.5. Appendix F. General computational flow of the CNN.

A) Input to the model.

All input vectors represent the standardized features extracted from the data-set.

B) 1D convolutional layer.

$$a^l = f(W^l * x^{l-1} + b^l)$$

Eq. 4.1F

Where a^l is the activation layer at layer l, W^l, b^l, are the weights and biases of the convolutional layer; x^{l-1} is the input from the previous layer or the initial input; $*$ denotes the convolution operation; and f is a non-linear activation function.

C) Batch Normalization.

$$y^l = \gamma^l \left(\frac{a^l - \mu^l}{\sqrt{(\sigma^l)^2 + \epsilon}} \right) + \beta^l$$

Eq. 4.2F

Where y^l is the batch Normalization; μ^l and $(\sigma^l)^2$are the mean and variance calculated over the batch for the layer l; γ^l and β^l are parameters to be learned, and ϵ is small constant added for numerical stability.

D) Fully connected layers.

$$z^l = W^l a^{l-1} + b^l$$

Eq. 4.3F

$$a^l = f(z^l)$$

Eq. 4.4F

Where z^l is the input to the fully connected layers l, processed through one or more such layers; W^l and $b^l$are the weights and biases of the fully connected layer l; and f is the activation function.

E) Smoot L1 loss function.

$$\mathrm{L}(y, \hat{y}) = \begin{cases} 0.5(y - \hat{y})^2 \ \ if \ |y - \hat{y}| < 1 \\ |y - \hat{y}| - 0.5, \ \ otherwise \end{cases}$$

Eq. 4.5F

Where y is the actual target value and $\hat{y}$ is the predicted value from the network. CNN manages errors and learns from the input data to make accurate predictions, ultimately influencing the performance of the model and effectiveness in regression tasks.

Chapter 5

Addressing weather data gaps in reference crop evapotranspiration estimation: A case study in Guinea Bissau, West Africa

This chapter was published in *Hydrology*.

Garbanzo, G., Céspedes, J., Temudo, M., Tiago Ramos, Cameira, M. do R., Pereira, LS. Paredes, P. 2025. Addressing weather data scarcity in estimating reference crop evapotranspiration: A case study from Guinea Bissau, West Africa. Hydrology, 12(7), 161. https://doi.org/10.3390/hydrology12070161

Keywords:

ET_o in tropical climates, accuracy and quality assessment, L-BFGS-B method, Numerical method, aridity index, FAO-PMT, AgERA5, MERRA2.

1. Abstract

Crop water use (ET_c) is typically estimated as the product of crop evapotranspiration (ET_o) and a crop coefficient (K_c). However, the estimation of ET_o requires various meteorological data which are often unavailable or of poor quality, particularly in countries such as Guinea-Bissau where the maintenance of weather stations is frequently inadequate. The present study aimed to assess alternative approaches, as outlined in the revised FAO56 guidelines, for estimating ET_o when only temperature data is available. These included the use of various predictors for the missing climatic variables, referred to as the Penman-Monteith temperature (PMT) approach. New approaches were developed, with a particular focus on optimizing the predictors at the cluster level. Furthermore, different gridded weather datasets (AgERA5 and MERRA-2 reanalysis) were evaluated for ET_o estimation to overcome the lack of ground truth data and upscale ET_o estimates from point to regional and national levels, thereby supporting water management decision-making. The results demonstrate that the PMT is generally accurate, with RMSE not exceeding 26% of the average daily ET_o. With regard to shortwave radiation, using the temperature difference as a predictor in combination with cluster-focused multiple linear regression equations for estimating the radiation adjustment coefficient (kRs) yielded accurate results. ET_o estimates derived using raw (uncorrected) reanalysis data exhibit considerable bias and high RMSE (1.07-1.57 mm d^{-1}), indicating the need for bias correction. Various corrections methods were tested, with the simple bias correction delivering the best overall performance, reducing RMSE to 0.99 mm d^{-1} and 1.05 mm d^{-1} for AgERA5 and MERRA-2, respectively and achieving a normalized RMSE of about 22%. After implementing bias correction, the AgERA5 was found to be superior to the MERRA-2 for all the studied sites. Furthermore, the PMT out-performed the bias-corrected reanalysis in estimating ET_o. It was concluded that PMT-ET_o can be recommended for further application in countries with limited access to ground-truth meteorological data as it requires only basic technical skills. It can also be used alongside reanalysis data, which demands more advanced expertise, particularly for data retrieval and processing.

2. *Introduction*

An accurate estimation of the reference crop evapotranspiration (ET_o) is critical for agricultural water resources planning and management (Allen et al., 1998; Pereira et al., 2015, 2025). ET_o quantifies the natural loss of water to the atmosphere, incorporating an approximation that accounts for both evaporation and transpiration from a reference surface (Allen et al., 1998; Pereira et al., 2025). The FAO-PM ET_o was parametrized for a hypothetical reference crop with specific characteristics in terms of height (0.12 m), albedo that reflects 23% and absorbs 77% of the incoming radiation under standard conditions, and a fixed surface resistance of 70 s m^{-1} (Allen et al., 1998). ET_o is essential for estimating crop water use (ET_c) as it represents the climatic demand conditions. Crop ET is commonly estimated using the FAO approach , which involves multiplying ET_o by a crop coefficient (Kc). The latter considers the differences in characteristics of the crop under study relative to the reference crop. Therefore, it enables the quantification of water use by any agroecosystem, landscape, wetland, and riparian ecosystem (Pereira et al., 2024). Under water or salinity stress, crop ET decreases (Allen et al., 1998; Liu, Paredes, et al., 2022; Liu, Shi, et al., 2022; Rosa et al., 2016).

The FAO-PM ET_o requires data on several weather variables, including maximum and minimum temperature, shortwave or net radiation, relative humidity or dew point temperature, and wind speed. The FAO 56 guideline (Allen et al., 1998), which have recently been revised (Pereira et al., 2025), describes alternative approaches for estimating missing weather variables data, namely when using temperature data only (FAO-PMT), making these tools particularly valuable in regions with insufficient weather stations or low maintenance capabilities (Allen et al., 1998; Pereira et al., 2025). To improve the accuracy of the ET_o PMT estimates, the calibration of the predictors may be performed for local conditions (Almorox et al., 2018; Paredes, Fontes, et al., 2018;

Popova et al., 2006; Raziei & Pereira, 2013) or, alternatively, simplifications to the method can be adopted (Paredes et al., 2020; Pereira et al., 2025). The accuracy of the PMT approach has been demonstrated in several studies conducted across Africa (Djaman et al., 2016, 2017; Koudahe et al., 2018; Landeras et al., 2018; Yonaba et al., 2023), although in many of these cases, adequate observed weather datasets were not available for a consolidated assessment of alternative approaches. Another commonly used approach that uses temperature data only for ET_o estimation is the Hargreaves-Samani (HS) equation, earlier developed for the Senegal River Basin (Hargreaves et al., 1985) and later commonly used (Abdul-salam et al., 2023; Moratiel et al., 2020; Musa & Elagib, 2025; Paredes et al., 2020). The ET_o estimates with HS can also be used with the FAO K_c-ET_o approach despite the need for adjustments.

Various heuristic approaches have also been used to estimate ET_o with minimal data availability, with machine learning (ML) algorithms being among the most widely used. However, as discussed by Pereira et al. (Pereira et al., 2015), these approaches do not use the fundamental physics underlying the FAO-PM ET_o equation, which is considered relevant when selecting alternative approaches to calculate ET_o when weather datasets are incomplete. These algorithms leverage training data to model variables for specific regions or sites (Zhu et al., 2020). However, they have limited applicability as they are generally not transferable and are only effective for the sites for which they were developed. Examples of these approaches include support vector machines (SVMs) and random forest (RF), which are renowned for their accuracy in predictions using limited input data (Wu et al., 2019; Zereg & Belouz, 2023).

Alternative sources of weather data are those based on observational data with different spatial and temporal resolutions and different available weather variables. Examples include the Climate Research Unit Time Series (CRU) (Harris et al., 2020) and

WorldClim for the globe (Hijmans et al., 2005), E-OBS for Europe (Anwar et al., 2023), PRISM climate data for the USA (Daly et al., 2008), Iberia01 (Herrera et al., 2019) for the Iberian Peninsula, or those provided by (Xavier et al., 2022) for Brazil. For given weather variables, such as shortwave radiation, satellite data can be obtained, e.g. data provided by the geostationary Meteosat Second Generation (MSG) system, which includes the Satellite Application Facility for Land Surface Analysis (LSA-SAF) (Gebremedhin et al., 2022; Paredes et al., 2021; Trigo et al., 2018).

Other sources of weather data include reanalysis gridded data obtained by integrating observations from various sources, including ground-based weather stations, ocean buoys, ships, aircraft, and satellite sensors (Demchev et al., 2020; ECMWF, 2020). This integration is carried out by modelling and data assimilation systems, which provide accurate and continuous estimates of climate and meteorological variables (Dee et al., 2011; Toreti et al., 2019). Their temporal resolution can be hourly, daily, or monthly. The spatial resolution varies, depending on the data source. One of the most widely used sources is the ERA5 reanalysis, made available by the European Centre for Medium-Range Weather Forecasts (ECMWF) (Dee et al., 2011; Xue et al., 2019). The AgERA5 dataset, which focuses on agriculture, is derived from this data set. This dataset provides hourly data with a spatial resolution of 0.1° (Brown et al., 2023; Kruger et al., 2024). Another often used reanalysis dataset is MERRA-2 version 2, an atmospheric reanalysis developed by NASA (National Aeronautics and Space Administration). MERRA-2 provides a reanalysis of global climatic and weather information (Rienecker et al., 2011). Another reanalysis-based dataset is that provided by the National Centers for Environmental Prediction – National Center for Atmospheric Research (NCEP/NCAR) (Kistler et al., 2001). Reanalysis data have been used in several studies to estimate ET_o and assess its spatial distribution (Kruger et al., 2024; Martins et al., 2017; Nouri &

Homaee, 2022; Xi et al., 2023; Zhang et al., 2021). One of the key advantages of using reanalysis data is that they provides all the weather variables required to calculate ET_o without any gaps (Meng et al., 2022; Vicente-Serrano et al., 2023). However, many studies have found that these gridded datasets require bias corrections, such as additive bias correction (Paredes et al., 2021; Paredes, Martins, et al., 2018), simple regional bias correction (Gourgouletis et al., 2023; Pelosi et al., 2020) and Kalman filtering for temperature modelling (Pelosi et al., 2017), as well as adequate downscaling methods (Viggiano et al., 2019) to improve their quality.

The above-cited studies emphasize the critical importance of bias correction, particularly in regions lacking baseline meteorological information, such as many tropical areas (Dee et al., 2011), including part of Africa. This is the case of Guinea-Bissau (GB), located in West Africa, with an economy based primarily on agriculture. GB has limited economic resources, which has led to a decline in government investment in meteorological and agricultural information after independence. Although long term weather records exist at three sites in the country (Bissau, Bafata and Bolama), they are incomplete due to the loss of documents during the civil war (1998 - 1999), poor resources for digitizing the data and maintaining the weather stations, and a lack of financial resources for purchasing new sensors (Ferreira, 2004; Kovsted & Tarp, 1999). However, these sites only cover a small part of the country as they exclude the most important agricultural areas, regions in the north affected by drought, humid zones in the south, and the archipelago of Bijagós (Republic of Guinea Bissau, 2014, 2018; Samuel et al., 2019). This hinders the spatial quantification of ET_o across the country, particularly in agricultural water management studies (Garbanzo, Céspedes, et al., 2024; Garbanzo, do Rosário Cameira, et al., 2025), and highlights the need for easy-to-use approaches to cope with reduced weather datasets.

Therefore, the main objective of this study is to evaluate different approaches for estimating FAO-PM ET_o using only temperature data (PMT). In addition, the study aims to assess the accuracy of AgERA5 and MERRA-2 reanalysis weather datasets to support the scaling of ET_o estimates from field level to regional and national levels. This is the first study of its kind conducted in Guinea-Bissau, and its novelty lies in the combined use of ground-truth meteorological observations and reanalysis datasets. The methodologies developed will be made accessible to GB technical staff, who have diverse skills levels, namely relative to the use modeling tools aimed at improving water management in mangrove rice cultivation. Furthermore, the results of the current study are expected to enhance water resource management across different spatial scales and may contribute to improved water governance, particularly under conditions of climate variability and freshwater increasing scarcity.

3. Material and methods

3.1. Climate

The study was conducted in GB, West Africa (Figure 5.1). The study sites were located mainly in the coastal region (Figure 5.1), where, according to the Köppen–Geiger classification (Beck et al., 2018; Kottek et al., 2006) , the climate is of equatorial savannah with dry winter (Aw) but with different life zones as per the Holdridge classification (Harris, 2014; Holdridge, 1947). The aridity index (AI, Table 5.S2 in supplemental material), as defined by (UNEP, 1997), is the ratio of the long-term mean annual precipitation (P, mm) to the (Thornthwaite, 1948)) to the mean annual climatic evaporation index (CEI_{TH}, mm). The northern part of GB is classified as moist sub-humid ($AI \approx= 0.7$), while the south of the country has ($AI > 1.0$).

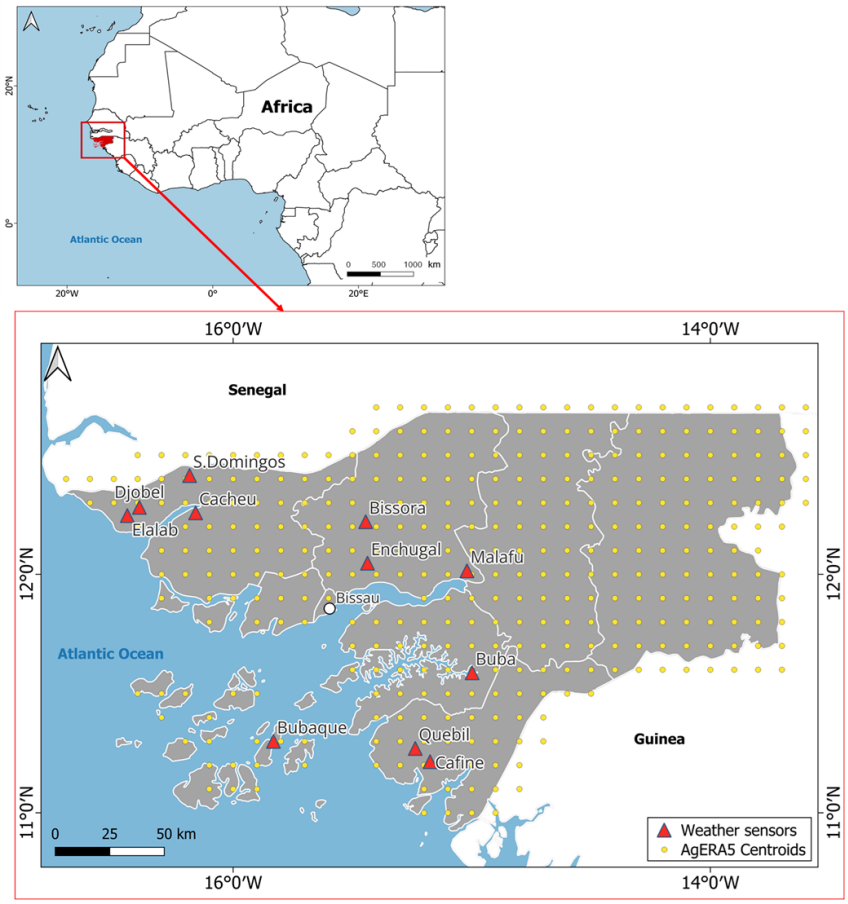

Figure 5.1. Location of Guinea-Bissau in West Africa (top), reanalysis grid points within the country, and distribution of weather stations (bottom).

3.2. Data

3.2.1. Ground truth weather data

Automatic weather stations were installed over well-watered grass at various locations across the country (Table 5.1, Figure 5.1), situated in open areas, away from trees and buildings. The ATMOS 41 weather stations (Meter Environment Products, USA) were mounted on metal poles at a height of two meters above ground level, oriented northward according to the installation guidelines. Data were recorded every 30 minutes using ZL6 data loggers (Meter Group, Pullman, WA, USA). The stations were regularly maintained to ensure data quality, including the removal of Saharan dirt and dust, inspection of battery levels and cleaning of the solar panels on the data loggers, typically every two

months or whenever malfunctions were detected. Detailed information on weather station locations (Figure 5.1) and data collection periods is provided in Table 5.1.

Table 5.1. Geographic coordinates, elevation, and data recording periods of the weather stations in Guinea-Bissau.

Region	Weather Station	Latitude (°N)	Longitude (°W)	Elevation (m)	Start of Data Collection	End of Data Collection	Number of 30 min Records
South	Cafine	11.214919	−15.174659	6.0	8 April 2021	1 June 2024	45,563
	Quebil	11.270221	−15.236727	8.4	10 March 2021	30 May 2024	16,378
	Buba	11.587290	−14.998417	10.9	22 August 2021	30 May 2024	45,193
Central	Malafu	12.014828	−15.020001	24.9	10 April 2021	30 May 2024	48,388
	Enchugal	12.046918	−15.436894	16.6	11 April 2021	29 May 2024	43,768
	Bissora	12.220728	−15.444387	15.1	11 January 2022	3 June 2024	41,951
	Cacheu	12.258014	−16.157159	21.2	12 January 2022	11 June 2024	42,280
North	S. Domingos	12.414232	−16.182400	12.5	12 April 2021	4 June 2024	45,132
	Djobel	12.280922	−16.392913	10.0	12 July 2022	5 June 2024	49,978
	Elalab	12.246547	−16.443420	10.8	12 April 2021	4 June 2024	45,176
Island	Bubaque	11.299951	−15.831088	29.8	9 January 2022	31 December 2023	34,634

This study was carried out using the daily weather data recorded at each weather station. Thirty-minute measurements were processed to obtain daily values of maximum and minimum temperature (T_{max}, T_{min}, ºC), maximum and minimum relative humidity (RH_{max}, RH_{min}, %), wind speed at 2 m height (u_2, m s^{-1}), and short wave solar radiation (R_s, MJ m^{-1}). In line with common practices in several meteorological services, the RH measured at 9 a.m. (RH_9) was taken to represent the mean daily conditions (RH_{mean}). Rainfall (mm) data at 30 min intervals (mm) were also available from all weather stations.

3.2.2. Reanalysis weather data

Reanalysis datasets were obtained from two sources: the European Center for Medium-Range Weather Forecasts (ECMWF), platform AgrERA5, part of the Copernicus project

(Boogaard et al., 2020), and the Global Modeling and Assimilation Office (GMAO), platform MERRA-2.

AgERA5 is a daily reanalysis dataset provided by ECMWF, available from 1979 to the present, with a focus on providing data for agricultural and agroecological studies (Chevuru et al., 2023; Van Tricht et al., 2023). It is provided at a spatial resolution of 0.1° × 0.1° (approximately 11 km × 11 km) (Boogaard et al., 2020) and is derived by forcing hourly ECMWF ERA5 data at the surface level. AgERA5 includes at wide range of atmospheric and surface variables. For this study, the following variables were downloaded from the Copernicus Climate Change Service (C3S) Climate Data Store (CDS) website: R_s (J $m^{-2}d^{-1}$), T_{min} and T_{max} (K), dew point temperature (T_{dew}, K), RH_9 (%), and wind speed measured at 10 m height (u_{10}, m s^{-1}).

MERRA also has a version tailored for agricultural studies, known as (AgMERRA). However, this dataset was not used in the present study due to its limited temporal coverage (1980-2010) (Galmarini et al., 2024; Ruane et al., 2015). Instead, the more recent product MERRA-2, developed by NASA to replace the original MERRA using a fixed assimilation system (Rienecker et al., 2011), was used, as it spans from 1980 to the present. MERRA-2 provides daily weather data at a spatial resolution of 0.5º x 0.625º (Global Modeling and Assimilation Office (GMAO), 2015a, 2015b). All variables required for the calculation of FAO-PM ET_o were downloaded: T_{min} (K), T_{max} (K), T_{dew} (K), RH_9 (%), u_{10} (m s^{-1}), R_s (J m^{-2} d^{-1}), and vapor pressure (hPa). The appropriate conversion of units was therefore performed on both datasets, with the wind speed at 10 meters adjusted to 2 meters in accordance with the recommendation of FAO 56 (Allen et al., 1998). Further details on the data assimilation system and performance metrics for AgrERA5 are reported by (Hersbach et al., 2020) and for MERRA-2 by (Gelaro et al., 2017).

The datasets were accessed using a script written in Python version 3.11 (Van Rossum & Drake, 2009). The MERRA-2 reanalysis data featured fewer grid centroids (36) compared to the AgERA5 (356), due to differences in spatial resolution between the two data sets. Both datasets were organized to cover the same period as the observed weather data, from January 2021 to May 2024 (Table 5.1). The Euclidean distance (straight line between two points) was calculated between each grid centroid and the weather station locations (Mardia et al., 1979). A filtering process was applied, and each grid centroid was classified based on its proximity to the weather stations. Following other approaches in the literature, the nearest grid point to each station was selected for use in this study (Paredes et al., 2021; Pelosi & Chirico, 2021; Soulis et al., 2025; Vanella et al., 2022). Although other methods exist, e.g. multiple linear regression (Paredes, Martins, et al., 2018) or triangle-based bi-linear interpolation method (Pelosi, 2023), these approaches have not been shown to outperform the simpler and widely adopted method of using the nearest grid point to the targeted station.

3.3. Computation of the FAO-Penman Monteith ET_o

The FAO Penman-Monteith equation is the most widely used method in agriculture for estimating the reference crop evapotranspiration (PM-ET_o) (Allen et al., 1998; Pereira et al., 2025). It allows for an accurate determination of the climatic demand conditions as it integrates various meteorological variables. The daily ET_o is estimated as follows:

$$ET_o = \frac{0.408\,\Delta\,(R_n - G) + \gamma\,\frac{900}{T + 273}\,u_2\,(e_s - e_a)}{\Delta + \gamma\,(1 + 0.34\,u_2)} \quad (1)$$

where Δ is the slope vapor pressure curve (kPa $^{o}C^{-1}$); R_n is the net radiation at the crop surface (MJ m^{-2} d^{-1}); G is the soil heat flux density (MJ m^{-2} d^{-1}), which is negligible at

daily steps, T is the air temperature at 2 m height (°C); u_2 is the wind speed at 2 m height (m s^{-1}); e_s is the saturation vapor pressure (kPa); e_a is the actual vapor pressure (kPa), $e_s - e_a$ is the vapor pressure deficit (kPa); and γ is the psychrometric constant (kPa $°C^{-1}$).

The net radiation at the crop surface (R_n, MJ m^{-2} d^{-1}) is calculated as the difference between the net shortwave radiation (R_{ns}, MJ m^{-2} d^{-1}) and the net longwave radiation (R_{nl}, MJ m^{-2} d^{-1}), where R_{ns} is calculated as $(1 - \alpha) R_s$, assuming an albedo (α) value of 0.23 for the green grass reference crop and R_{nl} is calculated as follows:

$$R_{nl} = \sigma \left[\frac{T_{max,K}^4 + T_{min,K}^4}{2}\right] \left(0.34 - 0.14\sqrt{e_a}\right) \left(1.35 \frac{R_s}{R_{so}} - 0.35\right) \quad (2)$$

where σ is the Stefan-Boltzmann constant (4.903 x 10^{-9} MJ K^{-4} d^{-1}), and T_{max} and T_{min} are the daily maximum and minimum temperatures (K), respectively. The mean e_s for a day is calculated as the average of the vapor pressure at the maximum and minimum temperature while e_a is estimated from the RH_{max} and RH_{min} as follows:

$$e_a = \frac{e^o(T_{min}) \frac{RH_{max}}{100} + e^o(T_{max}) \frac{RH_{min}}{100}}{2} \quad (3)$$

where $e°(T_{min})$ (kPa) and $e°(T_{max})$ (kPa) are the saturation vapor pressure at the daily minimum and maximum air temperature, respectively, and RH_{max} (%) and RH_{min} (%) are the maximum and minimum relative humidity, respectively.

The wind speed data (u_2, m s^{-1}) at the standard height of two meters above the ground level is obtained from that measured at height z (m) through the following logarithmic transformation:

$$u_2 = u_z \frac{4.87}{\ln(67.8\, z - 5.42)} \quad (4)$$

where u_Z is the wind speed measured at z meters above the ground surface (m s^{-1}), and z is the height of the measurement above the ground surface (m).

3.4. Calculation of ET_o using only temperature data (FAO-PMT)

Several approaches were used to estimate T_{dew}, u_2 and R_s to overcome missing data or data with poor quality. The predictors and the combination of approaches used in the current study are detailed in Figure 5.2. For e_a computation, and therefore the prediction of T_{dew}, the first approach used was straightforward and assumed T_{min} as the best predictor for T_{dew} (Allen et al., 1998; Pereira et al., 2025). A second approach used either T_{min} (for moist-subhumid sites), or the $T_{mean} - a_D$ (for humid sites) with a_D=2, both depending on the location aridity index (AI) (Paredes et al., 2021; Pereira et al., 2025; Todorovic et al., 2013). Therefore, the first step was to calculate the already mentioned AI for each location. The third approach consisted of the numerically optimization of the value of a_D by minimizing the Root Mean Squared Error (RMSE) using the "L-BFGS-B" algorithm (See Supplementary material S1). To overcome the missing u_2 data, two predictors were used, the average local or regional ($u_{2\ avg}$) or the world average value ($u_{2\ def}$ = 2 m s^{-1}) (Allen et al., 1998; Pereira et al., 2025).

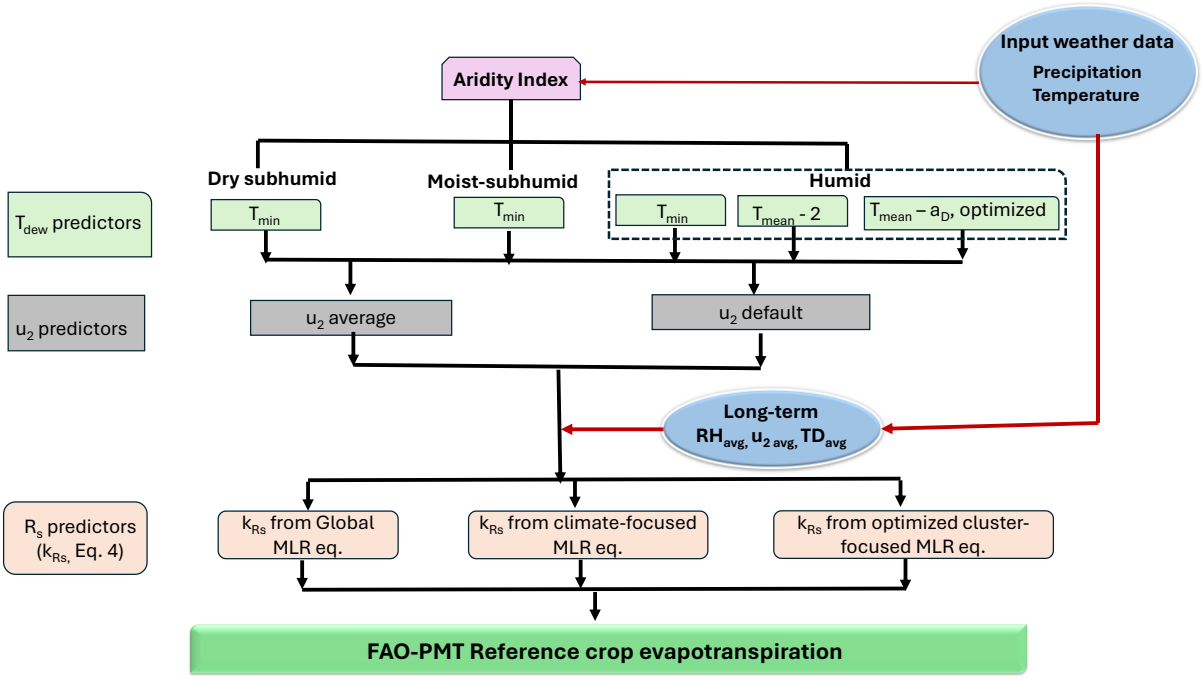

Figure 5.2. Flowchart of the approaches used to estimate reference crop evapotranspiration using the FAO-PM method based on temperature only (PMT). (MLR – multiple linear regression).

The shortwave radiation was estimated using the following equation (Hargreaves & Samani, 1982):

$$R_s = k_{Rs}\,(T_{max} - T_{min})^{0.5}\,R_a \qquad (5)$$

where k_{Rs} is the empirical adjustment coefficient ($°C^{-0.5}$), T_{max} and T_{min} are the maximum and minimum air temperature (°C), and R_a is the extraterrestrial radiation (MJ m^{-2} d^{-1}).

The estimation of k_{Rs} was carried out using three different approaches (Figure 5.2). The first two were based on the use of pre-established multiple linear regression (MLR) equations derived from long-term data collected from 555 weather stations across the Mediterranean. These MLR equations were derived by testing the average daily temperature difference (TD_{avg}), the daily average local or regional wind speed (u_2 avg), and the daily average relative humidity (RH_{avg}) as predictors of k_{Rs} using a set of goodness-of-fit indicators as detail by Paredes et al. (2020). Therefore, one MLR global

application across all climate types (global), and the other tailored to specific climate conditions (climate-focused), based on the AI (Paredes et al., 2020; Paredes & Pereira, 2019; Pereira et al., 2025), as follows:

Global equation (all climate types): $$k_{Rs} = 0.365 - 0.0099\ TD_{avg} + 0.0194\ u_{2\ avg} - 0.0017\ RH_{avg} \quad (6)$$

Climate focused equations:

Humid climates (AI>1.0) $$k_{Rs} = 0.519 - 0.0104\ TD_{avg} + 0.0188\ u_{2\ avg} - 0.0035\ RH_{avg} \quad (7a)$$

Moist locations (0.50 ≤AI <1.00) $$k_{Rs} = 0.396 - 0.0105\ TD_{avg} + 0.0186\ u_{2\ avg} - 0.0021\ RH_{avg} \quad (7b)$$

where TD_{avg} is the average daily temperature difference $T_{max} - T_{min}$, $u_{2\ avg}$ is the daily average local or regional wind speed, and RH_{avg} is the daily average relative humidity, all computed using a long-term data set.

The third approach was developed to improve k_{Rs} estimates and, consequently, the $ET_{o\ PMT}$ estimates. New adjusted MLR equations were derived at the cluster level (cluster-focused) using the same k_{Rs} predictors as in the previous approaches (TD_{avg}, HR_{avg}, $u_{2\ avg}$). The optimization was performed using the "L-BFGS-B" algorithm, aiming to minimizing the root mean square error (RMSE) between the ET_o and the $ET_{o\ PMT}$ (see supplementary S1 algorithm with the aim of minimize the root mean square error (RMSE) between the ET_o and the ET_o PMT (see Supplementary material S1). Therefore, k_{Rs} was considered treated as a cluster-specific constant of proportionality, derived through MLR using long-term mean values of the referred predictors. Due to the relatively short weather dataset (< 20 years), it was divided into calibration and validation subsets, comprising 70 % and 30 % of the data, respectively.

All the approaches were applied at two levels: individually at each site, and across groups of sites as defined by the cluster analysis (Section 2.5).

3.5. Data quality assurance and quality checking (QAQC)

All the weather datasets used in this study were subjected to prior quality assurance and control procedures to ensure consistency, integrity and quality for ET_o calculations. This step is mandatory to avoid error propagation into ET_o calculations. To this end, a custom script was developed to analyze data behavior through visual diagnostic tools including Q-Q plots and the normal probability plots (qqnorm), to identify data patterns and trends. Given the tropical location of the study, outliers were removed by applying a threshold of 3.5 times the interquartile range (IQR) below the first quartile (Q1) and above the third quartile (Q3) (Di Ciaccio et al., 2012; Dodge, 2008). This procedure aimed to exclude extreme values likely resulting from measurement errors that could significantly bias the analysis. Subsequently, the datasets were tested for mean homogeneity, trend, and variance homogeneity tests, following established statistical procedures (Allen, 1996; Levene, 1960; Montgomery & Runger, 2011; Pereira et al., 2025).

Wind speed data were specifically examined for prolonged periods of nearly constant and low values (≤0.5 m s^{-1}), which may indicate anemometer malfunction or a numerical 'offset' in the sensor calibration.

Shortwave radiation data (R_s, MJ m^{-2} d^{-1}) were evaluated following the procedure recommended by (Allen, 1996, 2008). The R_s values were compared with estimated clear-sky solar radiation (R_{so}, MJ m^{-2} d^{-1}) for each location, with R_{so} calculated as follows (Allen et al., 1998; Pereira et al., 2025):

$$R_{so} = R_a\,(0.75 + (2 \times 10^{-5}\,z)) \qquad (8)$$

where R_a is the extraterrestrial radiation (MJ m^{-2} d^{-1}) and z is the weather station altitude (m) (Table 5.1). R_a calculation method is detailed in (Allen et al., 1998).

The R_s/R_{so} ratio was calculated as the highest recorded observation within each 15-day period. This ratio was then used to adjust the remaining R_s observations by dividing each observed R_s by the ratio calculated for the highest record in that period. This procedure was systematically applied across the entire dataset for each weather station. All calculations and analyses were carried out using R statistical software version 2025.05.1 +513 (R Core Team, 2024). This tool performs functions similar to those of the agweather-qaqc software (Dunkerly et al., 2024).

Relative humidity values were plotted against air temperature throughout the day to check for inverse behavior. RH_{max} values were inspected to determine whether they approached saturation or were no more than 3-5% higher in the early morning or during rain events, indicating the need to recalibrate the sensors. In addition, RH records were evaluated for consistency on rainy days, when RH values should typically exceed 95%.

A rigorous data filtering process was applied, retaining only those dates with complete records for all variables required for ET_o estimation (Equation 1). This ensured homogeneity across all sites. Once homogenized, the data were subjected to the Shapiro–Wilk test to assess the normality of distributions for subsequent analyses. To identify relationships between sites, a comparative analysis of climatic variables was performed using the non-parametric Kruskal-Wallis test (Alvo & Yu, 2018; Conover, 1999), followed by pairwise comparisons using the Bonferroni method using a significance level of 0.01 ($\alpha = 0.01$ indicates a 1% maximum probability of committing a Type I error across all comparisons when performing multiple statistical tests). This approach provided a robust evaluation of whether significant differences existed among sites. The same data filtering process was applied for the cluster analysis, ensuring that only data common to all sites were used. The sites were then normalized and grouped, and a distance matrix was calculated. A dendrogram based on site altitude guided the selection of site groups

(Kassambara, 2017). The optimal number of clusters was determined using the Elbow method, which suggested K=5 (K represents the number of clusters into which the data was divided), indicating that the data naturally grouped into five distinct clusters (Syakur et al., 2018; Thorndike, 1953). Hierarchical clustering then identified the four final site groups.

3.6. Bias correction of reanalysis-based ET_o estimates

To improve the accuracy of ET_o estimates derived from reanalysis data ($ET_{o\ rean}$) at both individual sites and cluster levels and to support the subsequent application of gridded data for regional ET_o estimation (Céspedes et al., 2025; Garbanzo, Céspedes, et al., 2024, 2025; Garbanzo, do Rosário Cameira, et al., 2025), four correction methods were implemented. Rather than adjusting the underlying meteorological variables used in the calculation of ET_o, these correction techniques were applied directly to the reanalysis-based ET_o estimates (Paredes, Martins, et al., 2018). The corrections methods included: linear model (LM) adjustment, slope correction, robust linear modelling, and simple bias correction. Each correction was applied at both the individual site level and across groups of sites defined by the cluster analysis. Further details on each correction method are provided below:

(A) The adjusted linear model correction (ALM_c) involved fitting a linear regression between $ET_{o\ rean}$ (y) and $ET_{o\ obs}$ (X) as follows:

$$y = \beta_0 + \beta_1 \cdot X + \varepsilon \quad (9)$$

where β_0 is the regression intercept, β_1 is the slope, and ε represents random error term (Bapat, 2012).

The resulting intercept and slope values were then used to adjust the ET_o for each site. The $ET_{o\ rean}$ values were corrected for both systematic bias and scale error (Montgomery & Runger, 2011) by subtracting the intercept and dividing by the slope.

(B) The slope correction (S_c) method involved fitting a simple linear regression (LM) model between the $ET_{o\ rean}$ and $ET_{o\ obs}$ values, with the intercept of 0 ($\beta_0 = 0$). Once the model was fitted, the slope was calculated and applied as a correction factor. Each $ET_{o\ rean}$ value was adjusted by dividing it by the estimated slope (ET_o / slope = $ET_{o\ rean\_adjusted}$) (Bapat, 2012). This correction was applied individually to each site and aimed to compensate for systematic bias identified in the relationship between reanalysis and observed data.

(C) The robust linear model correction (RLM_c) followed a similar principle to the slope correction, but employed a robust linear regression instead of the ordinary least squares method. Unlike standard linear regression, which minimizes the sum of squared residuals, RLM_c minimizes a loss function that is less sensitive to large deviations (Bapat, 2012; Huber & Ronchetti, 2009). In this study, the Huber M-estimator was used, implemented through the 'rlm' function in the R software version 2025.05.1 +513. Fitting was carried out using integrated weighted least squares (IWLS). The Huber function addresses a convex optimization problem and provides parameter estimates that are more robust in the presence of outliers. As with the slope correction, the new β_1^{rlm} (means the updated or robust slope coefficient obtained from this Huber-based fitting procedure) was used to fit $ET_{o\ rean}$, reducing the influence of extreme values on the correction process, which are common in tropical regions. Therefore, the corrected $ET_{o\ rean}$ is estimated as follows:

$$\mathrm{ET_{o\ rean\ corr}} = \frac{\mathrm{ET_{o\ rean}}}{\beta_{1\ \mathrm{rlm}}} \quad (10)$$

(D) A simplified bias correction was applied to adjust $ET_{o\ rean}$ at different sites. The simplified BIAS correction ($BIAS_c$) was calculated as follows:

$$\mathrm{BIASc} = \frac{1}{n}\sum_{i=1}^{n}\left(\mathrm{ET_{o\ rean,i}} - \mathrm{ET_{o\ obs,i}}\right) \quad (11)$$

where n is the number of observations per site, $ET_{o\ rean,i}$ represents the reanalysis values for the *i-th* observation, and $ET_{o\ obs,i}$ is the corresponding observed value. The new estimated $ET_{o\ rean\_corrBIAS}$ was calculated by subtracting $BIAS_c$ from each daily $ET_{o\ rean}$ values. This correction aimed to eliminate systematic deviations inherent to the original estimates.

3.7. Accuracy assessment

To assess the accuracy of the tested approaches, a set of goodness-of-fit indicators (Paredes et al., 2021; Pereira et al., 2015) was employed to compare the observed (O_i = $ET_{o\ obs}$) and estimated (P_i =$ET_{o\ PMT}$ or $ET_{o\ REAN}$) values. The regression coefficient (b_0) of a forced-to-the-origin (FTO) linear regression was used to assess the proportionality between the estimated and observed ET_o values. A value of b_0 close to 1.0 indicates that the estimated and observed ET_o values are statistically similar. A $b_0 < 1$ suggests underestimation, while a $b_0 > 1$ suggests overestimation. The coefficient of determination (R^2) from an ordinary least squares (OLS) linear regression was used to assess the degree of dispersion of the O_i and P_i pairs along the regression line. R^2 represents the proportion of variance in the observed data that is explained by the estimation approach. Values of R^2 approaching 1 indicate a strong linear relationship between the observed and predicted values, and hence a better model fit. To quantify estimation errors, the root mean square

error (RMSE) was calculated, providing an overall measure of the differences between O_i and P_i. Additionally, the normalized root mean square error (NRMSE, %) was calculated as the RMSE divided by the mean of the observations ($\bar{O}$). Lower RMSE and/or NRMSE values indicate greater estimation accuracy. Two further indicators were used to assess the systematic bias of the estimates, the BIAS and the percentage bias (PBIAS, %). BIAS was calculated as the average difference between the observed and predicted values, while PBIAS was obtained by dividing BIAS by the sum of the O_i. The positive values of BIAS and PBIAS indicate a tendency towards overestimation, whereas negative values indicate underestimation. Values close to zero suggest lower systematic bias in the model's predictions (Montgomery & Runger, 2011). All goodness-of-fit indicators were calculated using R statistical software (R Core Team, 2024).

3.8. Spatial variability of ET_o in Guinea-Bissau

As Figure 1 clearly shows, there are few weather stations in the country, most of which are in western Guinea-Bissau. Furthermore, the distribution of stations varies greatly between regions. Following a thorough evaluation of the two reanalysis datasets, the one demonstrating superior performance was selected to estimate ETo at all gridded centroids across the country, to overcome this lack of data.

Initially, ET_o was calculated using the raw reanalysis data. These values were subsequently corrected using the most appropriate method identified in the study, with adjustments applied to each centroid based on its proximity to the most influential weather station. The mean annual cumulative ET_o for the period 2021–2023 was then estimated and mapped using ordinary kriging. Spatial autocorrelation analysis was conducted using the Global Moran's I statistic, together with Z-score and P-value calculations for the annual ET_o (Table 5.S8), following a methodology similar to that used for soil salinity

mapping by (Garbanzo, Céspedes, et al., 2025). All special analyses were carried out using ArcMap 10.8.2 and the Geostatistical Analyst (GS+) tool. In addition, RStudio version 2025.05.1 +513 was used to compute the goodness-of-fit indicators for the interpolated maps.

4. *Results and discussion*

4.1. QAQC assessment

The results of the tests for mean homogeneity, trend, and variance homogeneity of the ground-truth data relative to T_{max} and T_{min}, RH, and u_2 are shown in Table 5.2. The results of the Mann–Kendall test showed that none of the variables exhibited statistically significant trends, as the z-values were close to zero and the p-values were greater than 0.05. The Wilcoxon Rank-Sum test was then used to compare the central tendencies of the data from different locations. All variables yielded p-values above the 0.05 significance threshold, indicating that there were no significant differences in median values between the locations being compared. The analysis of the equality of variances across different locations (Levene's test) showed that all p-values exceeded 0.05, suggesting homoscedasticity (equal variances) across the dataset. Overall, the results of the statistical tests demonstrate that the analyzed meteorological variables are stable over time and comparable between locations. They also show that the variables exhibit consistent variability and are unaffected by outliers or measurement errors at all sites. Therefore, they can be used to estimate ET_o.

Table 5.2. Statistical test applied-mean homogeneity (Mann-Kendal test), trend analysis (Wilcoxon rank-sum test), and variance homogeneity (Levene's test) for weather variables used in for calculation the ET_o in Guinea-Bissau.

Variable	Mann–Kendall Test		Wilcoxon Rank Test		Levene's Test	
	Z-Value	*p*-Value	Rank–W	*p*-Value	F-Value	*p*-Value
RH_{Avg}	0.09	0.47	124.70	0.43	1.56	0.27
RH_{Max}	1.22	0.25	96.30	0.27	3.51	0.30
RH_{Min}	0.07	0.55	141.10	0.52	3.14	0.34
T_{avg}	1.02	0.44	97.40	0.37	0.58	0.54
T_{max}	1.57	0.21	77.05	0.14	1.39	0.47
T_{min}	−0.07	0.56	133.90	0.62	1.17	0.44
Wind speed	1.64	0.11	68.10	0.07	2.94	0.23

Additionally, R_s was checked and corrected as necessary, and examples of this correction are presented in Figure 5.3. These examples demonstrate the need for R_s correction due to inadequate pyranometer sensor calibration.

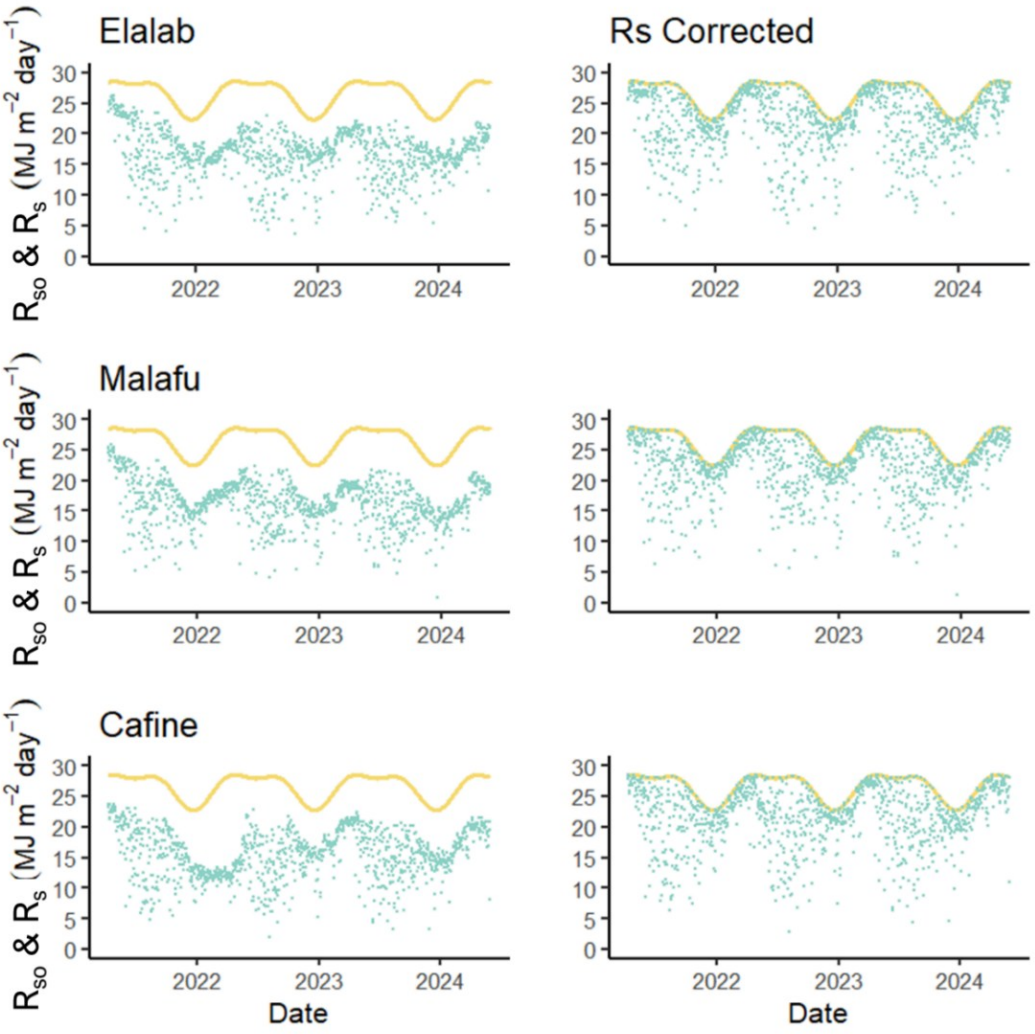

Figure 5.3. Examples of daily shortwave radiation (Rs) measured data (●) and estimated Rso dynamics (—) before and after correction in different locations of Guinea-Bissau—Elalab (north), Malafu (central), and Cafine (south).

4.2. Meteorological characteristics of the studied sites

A high variability in the different weather variables used for the calculation of ET_o was observed among the different sites in GB (Table 5.3). The sites with the significantly ($\alpha = 0.01$) highest temperatures were Bissora, Cacheu, and Buba. The sites with the lowest temperatures were Bissora, Cacheu, and Malafu. The results indicate that Bissora and Cacheu have the highest thermal amplitude among the studied locations, while Bubaque has the lowest thermal amplitude significantly ($\alpha = 0.01$). This trend was similar when the average daily temperature difference (TD) was analyzed. From one perspective, the

site with the significantly (α = 0.01) highest RH value was Cafine, which was the most humid site in the country. On the other hand, Bissora had significantly lower RH values (RH_{min}: 49.9% and RH_{avg}: 67.3%; α = 0.01), and was therefore considered the least humid site compared to the others. Buba presented contrasting humidity conditions. Djobel was the windiest location ($u_{2\ avg}$ = 2.1 m s^{-1}), while Bissora was the least windy location ($u_{2\ avg}$=0.7 m s^{-1}), both with significant differences (α = 0.01) relative to the other sites.

Table 5.3. Weather characterization of various locations in Guinea-Bissau based on the mean daily maximum (T_{max}), minimum (T_{min}), and average temperature difference (TD_{avg}); maximum (RH_{max}), minimum (RH_{min}), and average (RH_{avg}) relative humidity; and average wind speed ($u2_{\ avg}$) for the period 2021–2023.

Site	T_{min} °C	T_{max} °C	TD_{avg} °C	RH_{max} %	RH_{min} %	RH_{avg} %	$u_{2\ avg}$ m s^{-1}
Cafine	22.9b	31.7d	9.5 bc	99.1a	68.9a	78.8 a	1.3c
Malafu	21.5f	33.3bc	13.3 ab	98.6b	62.2bc	75.2 b	0.8f
Djobel	22.5bcd	32.7c	10.8 b	98.8b	59.8cd	77.7 a	2.1a
Enchugal	21.8de	33.1bc	12.1 ab	93.7c	57.8de	70.5 c	0.9e
Buba	22.6cde	33.3ab	12.1 ab	99.2ab	55.8e	75.0 b	1.6c
Elalab	22.6bc	31.9d	10.5 b	92.9cd	56.1e	71.3 c	1.7b
Cacheu	21.5ef	33.4ab	13.2 a	92.7d	55.5e	70.1 c	1.1d
Bubaque	24.3a	30.8e	6.8 c	92.3d	67.5ab	76.8 ab	0.8f
Bissora	20.3f	34.2a	14.8 a	89.4e	49.9f	67.3 c	0.7g
S.Domingo	19.8f	33.7a	13.9a	94.8c	49.3f	71.9c	0.8f
Quebil	22.2cd	33.2ab	11.0b	88.7e	40.4g	64.6d	0.8f
Shp_wilk	<0.01	<0.01	<0.01	<0.01	<0.01	< 0.01	<0.01
n	492	492	492	492	492	492	492
α	< 0.01	< 0.01	< 0.01	< 0.01	< 0.01	< 0.01	< 0.01

Note: means followed by the same letter do not represent significant differences; n = number of common days for all sites compared. α = Bonferroni test with an α = 0.01 using Kruskal–Wallis test. Shp_wilk = Shapiro–Wilk test.

The dendrogram generated by the cluster analysis identified three distinct groups based on the accumulated precipitation and ET_o at each site (Figure 5.4). These groups were

formed according to their position in the dendrogram and the geographical proximity of the sites. The first cluster included Buba and Cafine; the second included Malafu, Cacheu, and Enchugal; and the third included Elalab, Djobel, and S. Domingos. These clusters represent the southern, central and northern regions, respectively. As mentioned above, Bissora presented contrasting weather conditions, and did not fit into any cluster within the analysis. Its inland-like location resulted in distinct weather characteristics. Bubaque was also not included in the cluster analysis as it is located on an island. Quebil was excluded from the cluster analysis due to a lack of observations relating to sensor malfunction problems, which began in mid-2022. However, it was included in the ET_o estimates using the available weather data.

In Guinea-Bissau, there is considerable climatic variability between different sites and this study demonstrated sensitivity in identifying moist sub-humid and humid areas, regions with greater thermal amplitude, and sites with variable wind patterns (Table 5.2). Tropical climates are variable, because they are frequently influenced by tropical storms (Broccoli & Manabe, 1990; Hartshorn, 2013). These regions typically experience two well-defined seasons, namely the rainy season and the dry season, but with high interannual variability (Frank & Young, 2007). Subsistence agriculture is highly dependent on the behavior of the rainy season, particularly for the Mangrove Swamp Rice production in the country (Garbanzo, Cameira, et al., 2024; Garbanzo, do Rosário Cameira, et al., 2025; Linares, 2002). However, this seasonality is becoming increasingly unpredictable, with global warming exacerbating variability, particularly in rainfall distribution patterns and intensity (Mendes et al., 2025; Mendes & Fragoso, 2023). As a result, these areas are becoming increasingly vulnerable, making sustainable agricultural production more challenging (Céspedes et al., 2025; Temudo & Cabral, 2023). Appropriate management of water resources is therefore necessary.

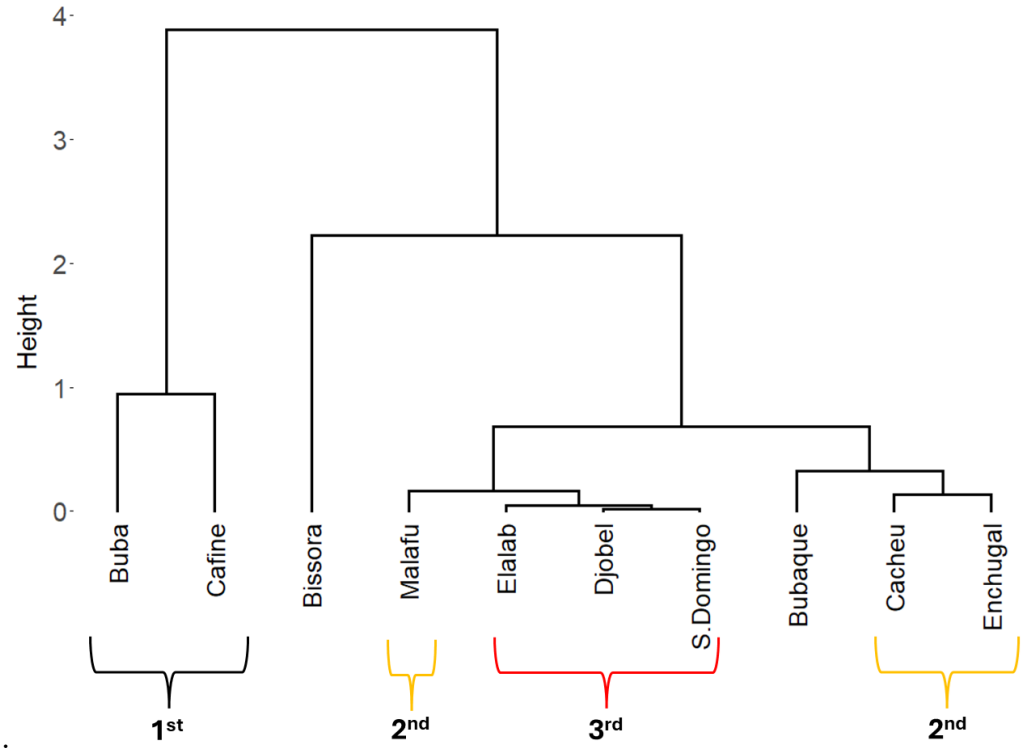

Figure 5.4. Dendrogram of a hierarchical clustering of the selected sites. Clustering was performed using cumulative rainfall and ET_o for 2021-2023 and site elevation, considering their spatial distribution in Guinea-Bissau.

4.3. FAO-PM ET_o using temperature data only

As previously stated, one of the new approaches for humid climates consisted of optimizing the a_D value used in the prediction of T_{dew} from $T_{mean.}$ The results showed that a_D values ranged from 2.5 ºC to 5.0 ºC, depending on the location, with an average a_D of 4.8 ºC when used alongside with $u_{2\ avg}$. When the $u_{2\ def}$ was used instead, the optimized a_D values ranged from 1.5 to 5.0 ºC, with an average of 4.5 ºC. These results are consistent with those reported by (Qiu et al., 2021) for humid climates in China, with a_D values of 5.14±1.33ºC. Similarly, (Paredes, Fontes, et al., 2018) reported a_D values ranging from 1.5 ºC to 4 ºC for the humid oceanic islands of the Azores, Portugal.

The new cluster-focused MLR equations, which were derived from observed weather datasets by minimizing RMSE, are presented in Table 5.4. The statistical indicators

related relating to the test and validation datasets are presented in Table 5.S3 of the Supplemental material. All the considered variables (TD_{avg}, $u_{2\ avg}$, and HR_{avg}) contribute differently to the estimation of k_{Rs} but play complementary roles. As with the global (Equation 6) and climate-focused MLR equations (Equations 7a and 7b), and in line with the findings of (Paredes & Pereira, 2019), TD_{avg} has a negative regression coefficient associated with the loss of long-wave radiation when TD_{avg} is high. The impact of $u_{2\ avg}$ on k_{Rs} values is positive and may be related to the transport of air moisture masses in windy conditions, leading to a clearer atmosphere. The impact of RH_{avg} on the k_{Rs} value is negative, representing the influence of cloudiness and air moisture. This is consistent with previous findings in other parts of the world (Almorox et al., 2018; Paredes, Fontes, et al., 2018; Paredes & Pereira, 2019; Pereira et al., 2025). It should be noted that the cluster-focused MLR regression to the origin presents a small range of 0.409–0.416, while the regression coefficients are relatively similar among the clusters (Table 5.4). The other two locations, which were not within the three clusters, present slightly different regression coefficients. Table 5.4 shows the k_{Rs} values estimated for each cluster.

Table 5.4. Cluster-focused optimized predictive multi-linear regression equations for estimating k_{Rs} values and respective values.

	Cluster	Predictive equations	k_{Rs}	Minimized RMSE ($^oC^{-0.5}$)	Eq.
1	**Cafine, Buba, Quebil**	$k_{Rs} = 0.410097 - 0.009323\ TD_{avg} + 0.021961\ u_{2_{avg}} - 0.001902\ RH_{avg}$	0.196	7.9×10^{-7}	(12)
2	**Enchugal, Cacheu, Malafu**	$k_{Rs} = 0.415814 - 0.009169\ TD_{avg} + 0.022404\ u_{2_{avg}} - 0.001868\ RH_{avg}$	0.183	1.1×10^{-6}	(13)
3	**Djobel, Elalab, S. Domingo**	$k_{Rs} = 0.409351 - 0.009369\ TD_{avg} + 0.021829\ u_{2_{avg}} - 0.001911\ RH_{avg}$	0.208	5.6×10^{-7}	(14)
-	**Bissora**	$k_{Rs} = 0.418652 - 0.009110\ TD_{avg} + 0.022572\ u_{2_{avg}} - 0.001855\ RH_{avg}$	0.174	9.4×10^{-7}	(15)
-	**Bubaque**	$k_{Rs} = 0.416080 - 0.009035\ TD_{avg} + 0.022784\ u_{2_{avg}} - 0.001840\ RH_{avg}$	0.232	2.9×10^{-6}	(16)

k_{Rs} – short-wave radiation empirical adjustment coefficient ($°C^{-0.5}$); TD_{avg} – long term average temperature difference, i.e. ($T_{max} - T_{min}$); $u_{2\ avg}$ – long term average local wind speed ($m\ s^{-1}$) measured at 2 m height; RH_{avg} – long term average relative humidity.

The goodness-of-fit indicators for the different approaches tested for estimating ET_o using ground-truth temperature and u_2 data, i.e. the FAO-PMT ET_o approach, are shown in Table 5.5, and the ranges of each indicator are presented in Table S4. It was found that the climate type of the site influenced the results. For the moist sub-humid locations, i.e. those sites located in the north of GB, the best predictor for k_{Rs} was, as expected, the value derived from the optimized LMR value (Table 5.5); for u_2 the best predictor was the regional/local average u_2 ($u_{2\ avg}$) value. This combination resulted in no tendency to over- or underestimation of ET_o (b_0 = 0.98) and yielded acceptable errors in estimates, with RMSE of 0.80 mm d^{-1} and NRMSE of 16.5%. However, small and no significant differences in estimates were found obtained when $u_{2\ def}$ was a used as predictor, with RMSE of 1.08 mm d^{-1} and NRMSE of 22.5%.

The second-best approach was to use either the global (Eq. 6) or the climate focused MLR (Eq. 7a and 7b) to estimate k_{Rs} in combination with the $u_{2\ def}$. For this set of sites, there was no significant difference ($p<0.05$) between using the climate-focused equations and using the global MLR, with RMSE of 1.04 mm d^{-1} and 1.00 mm d^{-1}, and NRMSE of 21.5% and 20.5%, respectively (Table 5.5). The results also showed that using $u_{2\ avg}$ did not improve predictions of k_{Rs} when either global or climate-focused MLR equations are were used. This is because it led to an increase in RMSE and NRMSE, which was not only statistically significant but also resulted in a large underestimation of ET_o, with b_0 values decreasing to 0.82 and 0.79 when the global and climate-focused MLR equations were used, respectively.

Table 5.5. Goodness-of-fit indicators used to compare PM-ET_o with $ET_{o\ PMT}$ when using T_{min} or the T_{mean} a predictor of T_{dew}, when k_{Rs} was calibrated for each site, when computed with the global Equation 6, or with the climate-focused Equations 7a and 7b, when using the default or the average local u_2 value, for the eleven sites of Guinea-Bissau.

Climate	Predictors			Goodness of fit indicators					
	T_{dew}	k_{Rs}	u_2	b_0 *	R^2 *	RMSE * (mm d^{-1})	NRMSE * (%)	BIAS *	PBIAS * (%)
Moist sub-humid	T_{min}	Global	Default	0.93 abc	0.96 a	1.00 ab	20.59 ab	-0.28 bc	-5.83 abc
			Avg	0.82 ab	0.97 a	1.13 ab	23.62 ab	-0.78 a	-16.40 ab
		Climate	Default	0.90 abc	0.96 a	1.04 ab	21.5 ab	-0.42 abc	-8.4 abc
			Avg	0.79 a	0.97 a	1.24 a	25.73 a	-0.91 ab	-19.17 a
		Optm	Default	1.07 c	0.97 a	1.08 ab	22.53 ab	0.43 c	9.28 c
			Avg	0.98 bc	0.98 a	**0.80** b	**16.49** b	-0.01 bc	-0.33 bc
Humid	T_{min}	Global	Default	0.92 abcde	0.97 a	0.87 abcde	18.61 abcde	-0.36 abcde	-6.78 abcde
			Avg	0.82 abc	0.98 ab	1.03 abc	22.01 abc	-0.76 abc	-16.22 abc
		Climate	Default	0.97 bcde	0.97 ab	0.86 abcde	18.32 abcde	-0.06 bcde	-1.22 bcde
			Avg	0.88 abcde	0.98 ab	0.87 abcde	18.63 abcde	-0.48 abcde	-10.22 abcde
		Optm	Default	1.07 e	0.97 ab	0.91 abcde	19.31 abcde	0.38 e	8.12 e
			Avg	0.98 cde	0.98 ab	**0.68 de**	**14.60** de	-0.01 cde	-0.21 cde
	T_{mean} - 2	Global	Default	0.86 ab	0.98 ab	1.12 ab	23.82 ab	-0.86 ab	-18.33 ab
			Avg	0.78 a	0.98 ab	1.20 a	25.43 a	-0.97 a	-20.68 a
		Climate	Default	0.86 abcd	0.98 ab	0.95 abcde	21.11 abcde	-0.57 abcd	-12.15 abcd
			Avg	0.85 abcd	0.98 ab	0.99 abcde	21.14 abcde	-0.66 abcd	-14.03 abcd
		Optm	Default	0.97 bcde	0.98 ab	0.72 bcde	15.42 bcde	-0.09 bcde	-1.83 bcde
			Avg	0.96 abcde	0.98 ab	**0.71 cde**	**15.10** cde	-0.14 abcde	-2.95 abcde
	T_{mean}-a_D (a_D opt)	Global	Default	0.91 abcde	0.98 ab	1.02 abcde	16.64 abcd	-0.33 abcde	-6.91 abcde
			Avg	0.82 abcd	0.98 ab	1.02 abcd	21.72 abcde	-0.75 abcd	-15.91 abcd
		Climate	Default	0.95 abcde	0.98 ab	0.72 abcde	15.31 cde	-0.15 abcde	-3.10 abcde
			Avg	0.91 abcde	0.98 ab	0.78 cde	16.63 abcde	-0.33 abcde	-6.91 abcde
		Optm	Default	0.99 de	0.98 ab	0.70 cde	14.90 cde	0.03 de	0.57 de
			Avg	0.99 cde	0.98 b	**0.67 e**	**14.33** e	0.02 cde	0.47 de

T_{dew} = dew point temperature; k_{Rs} =shortwave radiation empirical adjustment coefficient; u_2 = wind speed at 2 m height; Global = global multiple linear regression (Equation (6)); Climate = climate-focused multiple linear regression (Equations (7a) or (7b)); Optm = cluster-focused multi-linear regression (Equations (12)–(16)); Notes: means followed by the same letter are not significantly different ($\alpha < 0.05$) according to the Kruskal–Wallis test; The most effective approach is highlighted in grey, while bold numbers indicate the least error in estimates.

The results for the humid sites (Table 6.5) showed that, similarly to the moist sub-humid sites, the best predictor was the one resulting from the optimized MLR combined with the $u_{2\ avg}$. However, there was no significant difference ($p<0.05$) in the RMSE values using the tested T_{dew} predictors, i.e., T_{min} or the adjusted T_{mean} with either a_D=2 or calibrated a_D value, with RMSE of 0.68 mm d^{-1}, 0.71 mm d^{-1}, and 0.67 mm d^{-1}, respectively. When analyzing the results in terms of NRMSE, using the adjusted a_D value led to statistically different values, but there were few improvements in the results: NRMSE was 14.3%, compared to 14.6% with T_{min} and 15.1% with T_{mean}-2. There were also few differences in the other goodness-of-fit indicators, except for b_0, which showed a clear tendency towards underestimation when $u_{2\ avg}$ was used with either the global or the climate-focused MLR. These results showed that optimizing the predictors leads to very good results, but this approach is only possible when a good data set is available, hence uncommonly. Moreover, for the optimization approach (L-BFGS-B) applied in all the studied sites (Supplementary S1), there was a general tendency for slight underestimation when using u_{2avg}, distinguishing these results from other studies that relied on trial-and-error calibration of the T_{dew} and R_s predictors (Paredes et al., 2020; Raziei & Pereira, 2013; Todorovic et al., 2013).

The global LMR and the $u_{2\ deaf}$, results showed the advantage of optimizing the a_D value when using T_{mean}-a_D as T_{dew} predictor in relation to the use of the a_D = 2 ºC, as the latter leads to a clear under-estimation of ET_o (b_0=0.88) and higher RMSE (0.89 mm d^{-1} *vs* 0.71 mm d^{-1}). The use of T_{min} as the T_{dew} predictor also revealed also good results with an RMSE of 0.83 mm d^{-1}. Overall, the results for the humid climates showed a limited advantage in adjusting the T_{mean} as a T_{dew} predictor, when combined with the use of the global or climate-focused equations using through the u_2 default value, with NRMSE ranging from 16.6% to 23.8% and 15.3% to 21.1%, respectively.

The results of using the climate-focused LMR equations showed that these had an advantage over the global equation, but it was not statistically significant ($\alpha > 0.05$). This advantage resulted from a decrease in the underestimation, as well as in the RMSE and NRMSE. In such cases, it is beneficial to use T_{mean} rather than T_{min} the T_{dew} predictor considering that there are lower errors in the ET_o estimates. As with the global LMR, there is a slight advantage in adjusting the a_D value. However, the improvements were not significant, and therefore, the T_{min} should be used as a predictor of T_{dew} in humid climates, with these findings agreeing with those of FAO56rev (Pereira et al., 2025).

Selected examples of comparison results between $ET_{o\ PMT}$ and PM-ET_o when the analysis is focused at the cluster level are shown in Figure 5.5 and Table 5.S5. Examples also include the locations that were excluded from, the clusters Bissora (moist sub-humid) and Bubaque (humid). The scatter plots in Figure 5.5 demonstrate the strong correlation between $ET_{o\ PMT}$ using $u_{2\ def}$ and the various MLR equations, as well as PM-ET_o. The plots show that $ET_{o\ PMT}$ slightly underestimates PM-ET_o in Clusters 1 and 2, as well as in Bissora, when either the global or climate-focused equations are used to predict k_{Rs}. Furthermore, using the cluster-focused equations did not offer any advantages in these locations as the RMSEs were higher. Conversely, Cluster 3 and Bubaque show high underestimation when using the same predictors for k_{Rs} estimation, demonstrating the advantage of using cluster-focused equations in this case.

Table 5.S5 provides the results of the goodness-of-fit indicators for all approaches when the analysis was performed at the cluster level. The results show, as in the previous analysis, that the best approach was to optimize the predictors of T_{dew} and k_{Rs} (i.e. a_D and cluster-focused MLR). Therefore, the results are discussed with a focus on the previous simplified approaches. The first cluster included only locations with humid climates, and the results showed that using T_{min} relative to T_{mean}-2 as a predictor of T_{dew} was

advantageous. Additionally, there was a clear advantage from using the climate-focused MLR alongside $u_{2\ def}$. For the second cluster, which included both humid and moist sub-humid locations, the results showed that the best approach was to use T_{dew} predictors according to the AI, alongside with the climate-focused MLR equations and $u_{2\ def}$. The use of $u_{2\ avg}$ yielded a higher RMSE and a stronger tendency to underestimate ET_o. The third cluster comprised only moist sub-humid locations and showed the poorest results in terms of errors of all the clusters. In this case, the second-best approach was to use $u_{2\ def}$ alongside either the global or climate-focused MLR, as there were no significant differences. For Bissora (moist sub-humid), the second-best approach was to use the climate-focused equation with $u_{2\ def}$, while for Bubaque, despite being classified as humid, T_{min} was a better predictor of T_{dew}, with $u_{2\ def}$ being the best predictor over $u_{2\ avg}$.

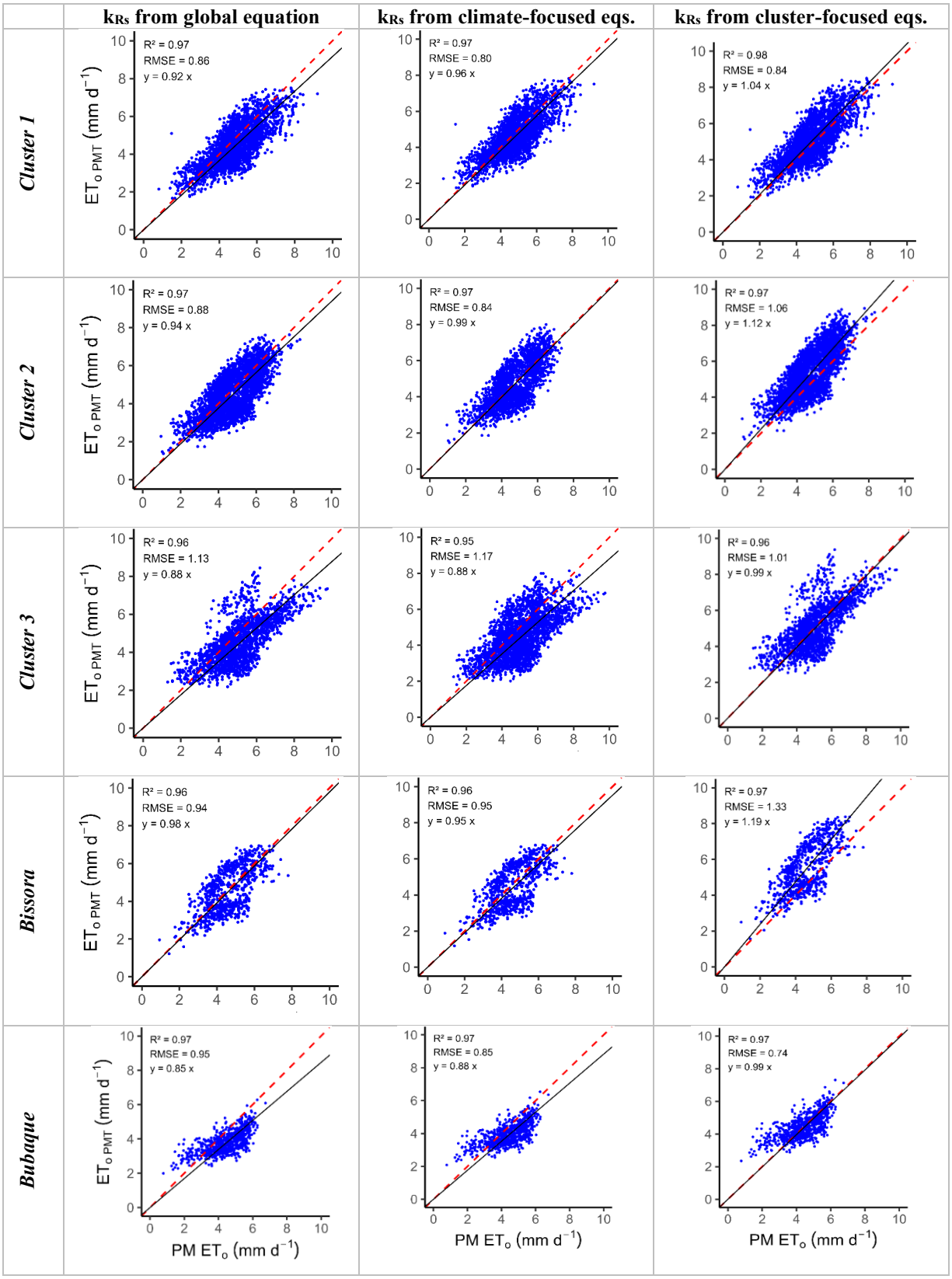

Figure 5.5. Comparing $ET_{o\ PMT}$ with PM-ET_o for each cluster and locations when using T_{dew}=T_{min}, the default u_2 value and the different MLR equations for estimating k_{Rs}. Included are the FTO regression equation, the OLS determination coefficient R^2 and the RMSE.

As mentioned previously, the cluster-focused optimized MLR equations using numerical models outperformed the global and climate-focused MLR equations for the set of sites, whether considering individual sites or clusters (Figure 5.6). Some sites exhibited similar RMSE values when using the climate-focused MLR and the global equation. However, the box-and-whiskers plot revealed variations where the metrics overlapped, indicating that while these standard approaches may be effective for certain sites, they are not suitable for most of them (Figure 5.6). The metrics indicate that the best adjustments for estimating ET_o using temperature alone were achieved by applying either $T_{dew}=T_{min}$ or $T_{dew} = T_{mean} - a_D$ criterion with optimized a_D, $u_{2\ def}$, and using the cluster-focused MLR to estimate k_{Rs} for each site or group of sites. The results for T_{min} showed a wider spread of RMSE values (Figure 5.6), possibly because humid and moist sub-humid sites were considered together. In contrast, for the other two predictors using T_{mean}, the spread was smaller, because only humid sites were considered.

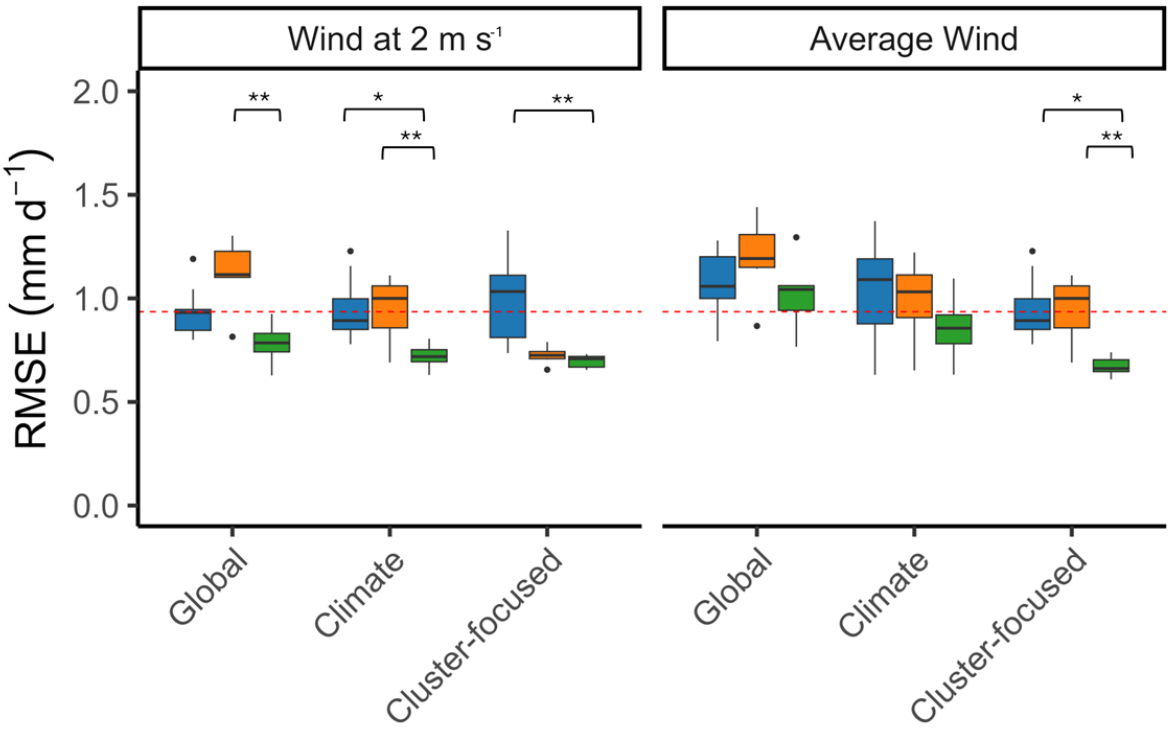

Figure 5.6. Box-and-whiskers plots of the root mean square errors of ET_o estimations using the PMT approach with different predictors for T_{dew} (T_{min} (blue), T_{mean}-2 (orange), or T_{mean}−a_D with a_D optimized (green)), using either the default 2 m s−1 or the local average wind speed as predictors, and using as the k_{Rs} predictor either the global, climate-focused or the cluster-focused equations, for the various sites in Guinea-Bissau. Means followed by an asterisk (*) are significantly different ($\alpha < 0.05$) and those followed by two asterisks (**) are highly significantly different ($\alpha < 0.01$) according to the Kruskal–Wallis test.

The results of the current study when using any of the MLR equations were within the range of those reported for several sites in Africa, such as the study performed by (Djaman et al., 2016) in Tanzania and Kenya when using the PMT approach with $u_{2\ avg}$ and the default predictors of T_{dew} and R_s (RMSE ranging 0.64 mm d^{-1} to 1.09 mm d^{-1}). A study performed in Côte d'Ivoire (Koudahe et al., 2018) reported RMSE ranging from 0.43 mm d^{-1} to 0.89 mm d^{-1} when using PMT with the default values for the different predictors (Allen et al., 1998). A study performed at several sites in Ghana (Landeras et al., 2018), reported RMSE values ranging from 0.58 to 1.11 mm d^{-1} when using PMT, while RMSE

decreased when using Artificial Neural Networks (ANNs) and Gene Expression Programming (GEP) to 0.53-0.84 mm d^{-1} and 0.51-0.79 mm d^{-1}, respectively. The study performed in humid climates of Uganda by (Djaman et al., 2017) tested several approaches to cope with missing data and reported that the PMT with default values for the predictors of k_{Rs} and T_{dew} and $u_{2\ avg}$ outperformed the other approaches with an RMSE ranging from 0.69 mm d^{-1} to 1.34 mm d^{-1}. Better results were reported in a study applied to Burkina Faso with an RMSE 0.53 mm d^{-1} and a tendency to overestimate ET_o (PBIAS=6%) when the PMT approach was used, optimizing the R_s and T_{dew} predictors and using the u_{2avg} value (Yonaba et al., 2023). The globally applied study by (Almorox et al., 2018) reported a RMSE for several humid locations in Hungary, ranging from 0.63 mm d^{-1} for Aw of climates as in GB, when using the default predictors for T_{dew} and u_2 and calibrated or default k_{Rs} values. In the current study, using the same approach, RMSE was 0.79 mm d^{-1} and 0.85 mm d^{-1} for humid and moist sub-humid sites, respectively. (Trajkovic et al., 2020) for several humid locations in Hungary, reported a wide range of RMSE from 0.10 mm d^{-1} to 0.81 mm d^{-1} when using the default k_{Rs} and T_{dew} predictors values with $u_{2\ avg}$. Other studies such as those by (Todorovic et al., 2013) and (Raziei & Pereira, 2013) for sub-humid and humid climates in the Mediterranean basin and in Iran, respectively, also reported better results when calibrating k_{Rs}, $u_{2\ avg}$, and using the different T_{dew} predictors. Furthermore, the results of the current study when using the LMR equations with the PMT approach are in line with those reported by (Paredes et al., 2020) for the humid and moist sub-humid climates.

Enhancing the accuracy of ET_o estimation can be challenging, particularly when analyzing sites with high climate variability and limited weather data availability. The FAO-PMT ET_o approach, which uses global and climate-focused MLR equations, showed good accuracy, particularly when considering each site individually,

demonstrating that there is no significant advantage in developing cluster-focused MLR equations or optimizing a_D. However, when performing the analysis at the cluster level, there was a consistent trend toward improved performance with this optimization, despite the robustness of the approach needing to be further tested using a wider set of weather data. Overall, due to the simplicity of the approach, the use of the global and/or the climate-focused LMRs as predictors of k_{Rs} is advocated despite their tendency to underestimate ET_o, in combination with the $u_{2\ default}$ when it leads to less underestimation. Furthermore, these approaches demonstrated their potential as valuable tools for improving water use efficiency in the absence of accurate data, as they can serve as a baseline for estimating water and salt balances using different models (Garbanzo, Céspedes, et al., 2024; Garbanzo, do Rosário Cameira, et al., 2025; Liu, Paredes, et al., 2022; Ramos et al., 2024). Future applications of the method would benefit from enhanced ground observation networks, particularly in data-scarce regions like central and eastern GB, to strengthen calibration and reduce potential uncertainties.

4.4. ET_o estimation using different reanalysis datasets

Analysis of wind speed data from AgERA5 ($u_{2\ ERA5}$) and MERRA-2 ($u_{2\ MERRA}$) revealed significant discrepancies with u_2 observations (results not shown), as reported in previous studies assessing reanalysis data (Martins et al., 2017; Paredes, Martins, et al., 2018). This led to ET_o estimation using reanalysis data that excluded this variable. Two approaches were then used, one replaced $u_{2\ ERA5}$ and $u_{2\ MERRA}$ with the $u_{2\ def}$ value, while the other used the $u_{2\ avg}$ value. The results show that the estimation of ET_o using raw AgERA5 reanalysis data ($ET_{o\ ERA5}$) exhibited significant variability compared to the ET_o values calculated from ground truth (observed, $ET_{o\ OBS}$) data (Figure 5.7 and Figure 5.S7), particularly when the default u_2 was used in the $ET_{o\ ERA5}$ estimations.

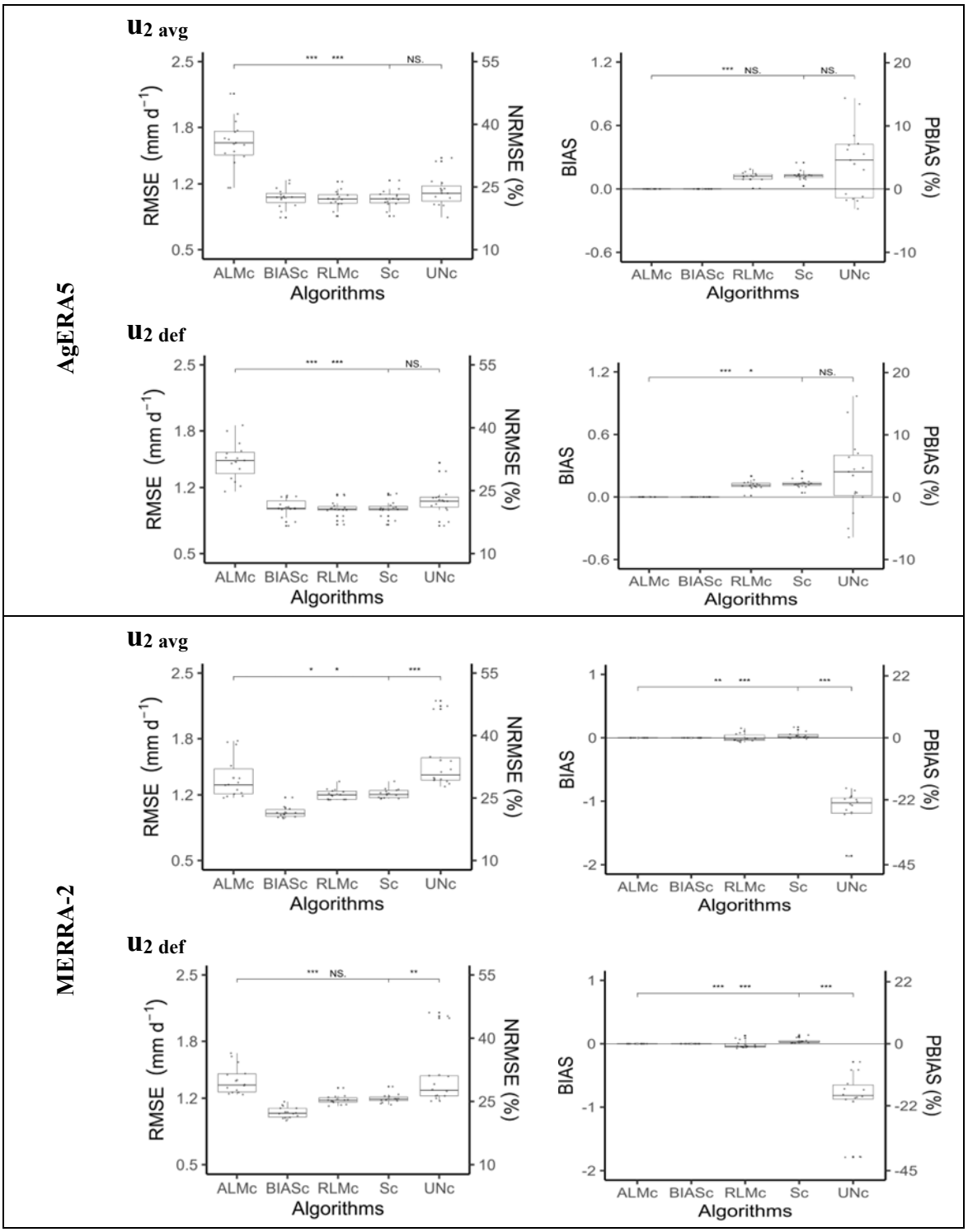

Figure 5.7. Comparison of ET_o estimated with ground truth (observed) data and with AgERA5 and MERRA-2 reanalysis datasets when raw (UN_c) data were used and after using the diverse bias correction methods (S_c, RLM_c, $Bias_c$, and ALM_c). The local average ($u_{2\ avg}$) or the default value of 2 m s^{-1} ($u_{2\ def}$) was used instead of the reanalysis wind speed data. (UN_c = uncorrected bias; bias correction methods: S_c = slope, RLM_c = robust linear model; $Bias_c$ = bias correction; ALM_c = adjusted linear model). Means followed by an asterisk (*) are significantly different ($\alpha < 0.05$) and those followed by two or three asterisks (** or ***) are highly significantly different ($\alpha < 0.01$) according to the Kruskal–Wallis test, NS = not statistically significant.

Using raw (uncorrected) reanalysis data with $u_{2\ avg}$ to estimate ET_o showed a wide range of regression coefficients b_0 (0.90 – 1.18) (Table 5.S6) and PBIAS (-7.72 – 21.14) (Figure 5.7), but most sites did not show an under- or overestimation tendency (b_0 near 1.0 and PBIAS near 0%) (Figure 5.S7). When $u_{2\ def}$ was used, however, the b_0 and PBIAS values varied in a wider range, with two groups of sites, one with an under-estimation tendency (b_0<0.90, PBIAS), and the other with an over-estimation tendency (b_0>1.10, PBIAS). In both approaches, R^2 was generally above 0.95, showing that $ET_{o\ ERA5}$ was able to explain most of the $ET_{o\ OBS}$ variance. When analyzing the errors due to using $u_{2\ avg}$, the RMSE ranged from 0.84 to 1.48 mm d^{-1}. This value decreased slightly when $u_{2\ def}$ was used instead (RMSE from 0.80 to 1.46 mm d^{-1}), corresponding to NRMSE ranging from 17.9% to 31.9% and 17.9% to 31.8%, respectively.

After applying different bias correction methods to the $ET_{o\ ERA5}$ data, the results showed a general decrease in the RMSE values and as expected, in PBIAS and BIAS (Figure 5.7) and as well as in b_0 (Table 5.S6). The analysis of the BIAS and PBIAS metrics revealed that $BIAS_c$ and ALM_c effectively removed the under- and over-estimation of the $ET_{o\ ERA5}$ data. However, the ALM_c ability to explain the variability in the data was lower than that of the other bias correction methods, suggesting lower predictive performance. This is evident in the decrease in R^2 from 0.96 to 0.90 and 0.92 when using $u_{2\ avg}$ or $u_{2\ def}$, respectively (Table 5.S6). Although ALM_c removed the bias of the reanalysis data, it failed to reduce the estimation errors.

Analyzing the set of goodness-of-fit indicators (Figure 5.7 and Table 5.S6), it was found that the different bias correction methods exhibited further differences in accuracy, with the simple $BIAS_c$ method performing the best. The average RMSE values were very similar for $BIAS_c$ (1.05 mm d^{-1} or 0.99 mm d^{-1} when using $u_{2\ avg}$ and $u_{2\ def}$, respectively), RLM_c (1.04 mm d^{-1} or 0.97 mm d^{-1}), and S_c (1.04 mm d^{-1} or 0.98 mm d^{-1}). This small

difference in NRMSE indicated that these bias correction methods were not significantly different ($\alpha < 0.05$). Similarly, the mean NRMSE values were 22.0%, 21.7%, and 21.7% respectively (Table 5.S6). For ALMc, the bias correction was successfully applied; however, the RMSE was higher (> 1.3 mm d^{-1}) than that of the other correction methods in both AgERA5 and MERRA-2, indicating lower accuracy. Using the $u_{2\ def}$ value resulted in slightly higher accuracy for all bias correction methods, but this was not statistically significant (NS). Overall, the $BIAS_c$ was the simplest and most effective, leading to significant differences ($\alpha = 0.05$) compared to using raw data. This makes it a practical option for calculating ET_o using AgERA5 and MERRA-2 data with either $u_{2\ avg}$ or $u_{2\ def}$.

Using raw MERRA-2 data to estimate ET_o ($ET_{o\ MERRA}$) produced greater variability and a marked under-estimation (Figure 5.7) and less precision (Table 5.S6). Comparing the two data sets (Figure 5.7), the superiority of using raw AgERA5 becomes evident, i.e., the results indicate that MERRA-2 underperforms compared to AgERA5 . Similar results were reported by (Soulis et al., 2025) for the estimation of annual ET_o in Greece. The differences in performance between the reanalysis datasets may be due to the coarser resolution of the MERRA-2 dataset, which makes it difficult to adequately capture climate variability within GB. When $u_{2\ avg}$ and $u_{2\ def}$ were used, the latter performed slightly better but did not reach statistical significance.

The results show that, for operational use, the $ET_{o\ MERRA}$ needs to be bias-corrected (see Figure 5.7). As with $ET_{o\ ERA5}$, the results also highlight that ALM_c and $BIAS_c$ were the only methods that effectively removed the bias. The RMSE was 1.57 mm d^{-1} when raw data were used, and it decreased to 1.38 mm d^{-1} with the ALMc method and to 1.01 mm d^{-1} with the BIASc method. As with the AgERA5 data, ALMc's ability to explain the variability in the data was lower than that of the other bias correction methods, showing

a smaller reduction in RMSE (see Table 5.S6). $BIAS_c$ was the best bias correction method, as it improved all accuracy indicators.

The results of the current study using raw reanalysis data are comparable to those reported in the literature. Tiruye et al., (2024) reported a tendency for overestimation when using ERA5-Land for the Tana Basin in Ethiopia, which has a subtropical climate, with RMSE ranging from 0.54 mm d^{-1} to 1.82 mm d^{-1}. Lopez-Guerrero et al., (2023) reported RMSE ranging from 0.49 mm d^{-1} to 0.88 mm d^{-1} for Egypt, Morocco, and Tunisia. Nouri & Homaee, (2022) reported an NRMSE ranging from 11% to 20% for ET_o estimates on a monthly timescale for the humid sites of Iran. Various studies have been carried out for Italy and Portugal. For example, (Vanella et al., 2022) reported an NRMSE ranging from 15% to 47% when using two ERA5 products, depending on the time scale. Other studies carried out in Italy using ERA5-Land datasets reported a tendency towards underestimation and generally lower RMSE; for instance, Pelosi et al., (2020) reported an RMSE ranging from 0.44 to 1.04 mm d^{-1}, with NRMSE values lower than 14%, and (Ippolito et al., 2024) reported RMSE ranging from 0.42 to 1.26 mm d^{-1}. Paredes, Martins, et al., (2018) reported better results using ERA-Interim for mainland Portugal, with RMSE > 0.75 mm d^{-1} for most sites, combined with a tendency of underestimation. After simple bias correction the RMSE decreased to a range of 0.50-0.75 mm d^{-1} for most sites (Paredes, Martins, et al., 2018).

There are few studies in the literature that have used MERRA-2 to estimate ET_o. The results of the current study are comparable with those reported by (Nouri & Homaee, 2022), with lower NRMSE values ranging from 10 to 20% at humid sites in Iran.

Overall, the results of the analysis of the gridded datasets emphasize the need for bias correction to enhance the accuracy of ET_o estimates derived from reanalysis products in

data-scarce regions. Furthermore, a comparison of the results from AgERA5 and MERRA-2 (Figure 5.7, Table 5.S6) with the FAO-PMT approach (section 3.2, Table 5.5) shows that the latter performs better and therefore can be used to estimate ET_o when temperature data is available.

The results of the current study suggest that AgERA5 data could be used with caution for estimating ET_o, particularly when the observed weather data are unavailable. Further caution is needed, particularly for studying climate variability and change, as previously reported (Mendes et al., 2025; Mendes & Fragoso, 2023, 2024). To allow for a more thorough evaluation of the accuracy of the gridded dataset, it is advisable to continue collecting meteorological data over a longer period and between regions. The method can be adapted to other regions, but local ground data are key to improving accuracy. Further long-term studies are encouraged, particularly in areas with limited station coverage, where expanding or recovering weather observations could reduce uncertainties.

4.5. ET_o mapping

Figure 5.8 shows the spatial variability of the mean annual $ET_{o\ ERA5}$ in the country after applying the best bias correction method ($BIAS_c$). The results show that the spatial distribution of the annual ET_o presents strong spatial coherence and continuity (Table 5.S8). The fitted exponential variogram with a nugget of 10 mm, sill of 17.8 km, and an extensive range of 240.3 km indicates a well-structured spatial dependence on the regional scale. Autocorrelation results support this, with a Global Moran's I of 0.84, a Z-score of 20.71, and $p < 0.001$, confirming significant spatial clustering of ET_o values. The model achieved excellent annual accuracy, with errors less than 2.5% of the observed NRMSE mean and minimal bias (BIAS = 0.14, negligible PBIAS). These values indicate both high precision and negligible systematic errors in the estimation. The high R^2 (0.87)

and Spearman correlation (ρ = 0.94) further validate the model's reliability across spatial domains.

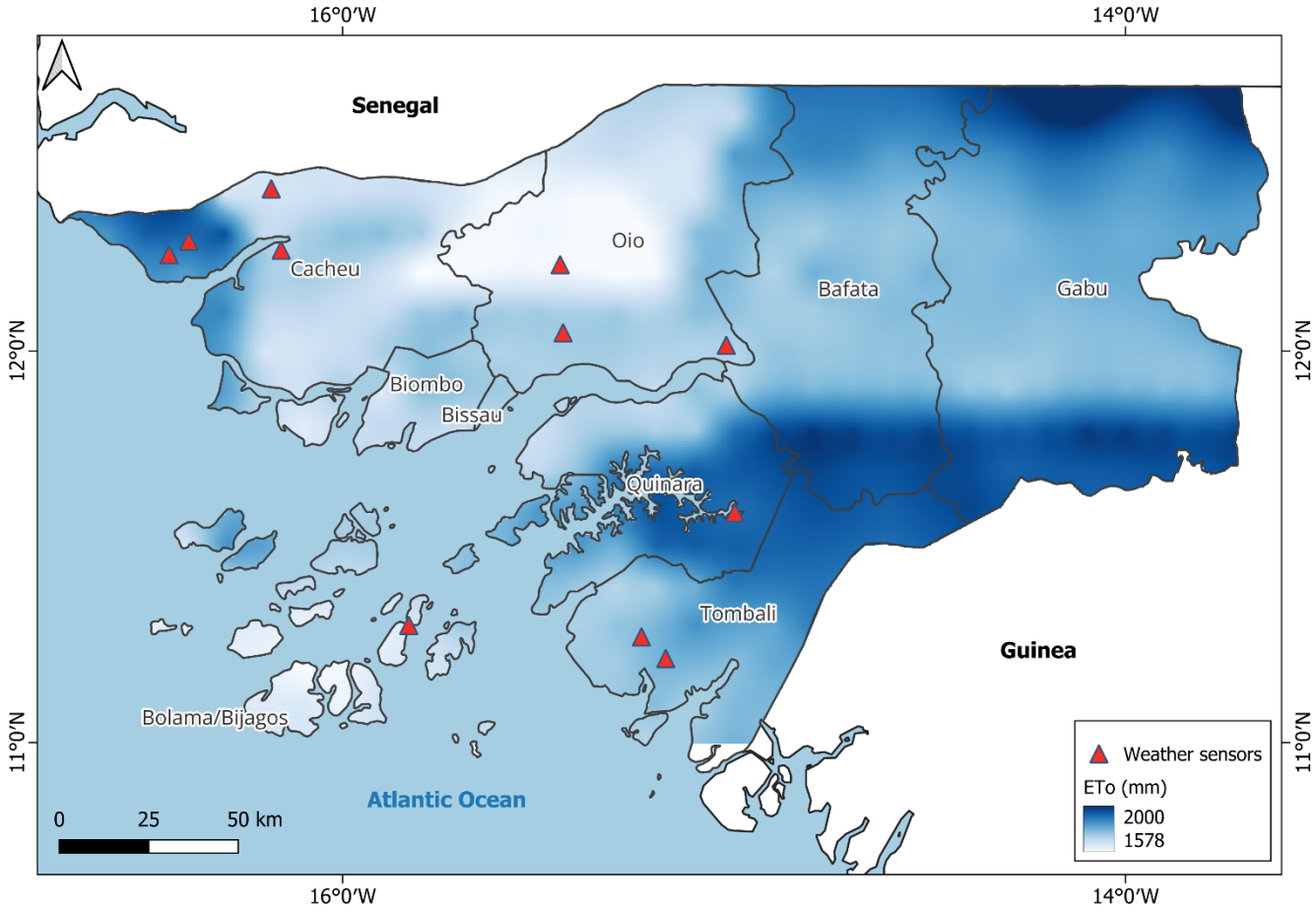

Figure 5.8. Spatial distribution of annual ET_o estimated using bias corrected AgERA5 data, in Guinea-Bissau.

In practice, the ET_o map is consistent with the observed patterns in the country, where southern areas have higher temperature and ET_o, while some inland locations have lower ET_o values. This reflects the typical variability observed in tropical regions, where climatic and topographic conditions contribute to significant spatial differences in ET_o. The results of this study highlight the value of gridded climate datasets such as AgERA5, after appropriate bias correction, for regional scale agroclimatic applications. For regions of the Guinea-Bissau where ground-based meteorological data are sparse, corrected satellite-derived ET_o maps can provide important support for water management

planning, drought monitoring and sustainable agricultural management. However, it is advisable to collect more observational data to further support the findings of the current study.

5. Conclusions

The approach developed in this study is an important tool for Guinea-Bissau (GB), where limited government investment in sensors hinders the rapid acquisition of accurate meteorological data. The findings of the present study underscore that the PMT approach yielded more accurate ET_o estimates than either of the reanalysis products, even after its bias correction. However, in the absence of observed temperature data, AgERA5 data could be used as an alternative source, although caution is advised due to known biases and uncertainties associated with ET_o estimation from this reanalysis product. When using the PMT approach it can be concluded that T_{min} is an adequate predictor of T_{dew} in both moist sub-humid and humid climates. Therefore, there is no need to use corrected T_{mean} to predict $T_{dew,}$ as this does not significantly affect ET_o estimates. Furthermore, the u_2 default value of 2 m s^{-1} was found to be the best predictor when coupled with either the global or the climate-focused equations for estimating ET_o. The newly proposed cluster-focused equations improve the accuracy of ET_o compared to the global or climate-focused equations but require further validation for GB. More broadly, this study demonstrates the suitability of the user-friendly approaches outlined in FAO56rev, particularly in regions where access to comprehensive weather information is limited.

The study provides a robust framework for enhancing agricultural practices and fostering resilience in areas grappling with climatic and environmental challenges. In the case of GB specifically, the approximate datasets and tools provided by the developed approaches could greatly benefit organizations working to improve the country's social

and food security, such as international cooperation projects and GB's development ministries.

However, the approach explored in this study could be further enhanced by expanding the ground-truth database to include more years of observations. It is important to test the global and climate-focused equations with more data from tropical countries, especially those with high rainfall and climate variability. This is particularly relevant for regions between 0° and 20° N latitude, which experience the greatest climate variability and have not been the focus of previous studies. Overall, it is essential to refine the tools further to improve the estimation of ET_o in regions where investment in specialized equipment is low. Nevertheless, this work provides a foundation for calculating water and salt balances in MSR production in Guinea-Bissau and other West African countries where this system exists.

6. *Supplementary material*

6.1. **Supplementary S1.** Numerical method for deriving the cluster-focused multiple linear regression (MLR) equations to estimate k_{Rs} (Eq. 4)

The goal is to minimize an objective function $f(k_{Rs})$ subject to box constraints using the "L-BFGS-B" method (Byrd et al., 1995). The objective function $f(k_{Rs})$ is the RMSE calculated as a function of the parameter k_{Rs}.

$$min_{Krs} RMSE(k_{Rs}) = f(k_{Rs})$$

Eq. A1

Where:
$RMSE$ = root mean square error.
K_{rs} = radiation adjustment coefficient.

Objective function

$$f(K_{rs}) = min_{0.05 \le kRs \le 0.25} = \sqrt{\frac{1}{n}\sum_{i=1}^{n}(ET_{o\,i} - ET_{o\,PMT\,i})^2}$$

Eq. A2

Where:
$min_{\,0.05 \le kRs \le 0.25}$ = The minimization is subject to box constraints using the "L-BFGS-B" Algorithm.
ETo_i = Evapotranspiration calculated with all weather variables for observation i..
$ET_{o\,PMT\,i}$ = Evapotranspiration calculated using temperature difference with k_{Rs} for observation i.

The "L-BFGS-B" Algorithm.

This aims to solve.

$$min_{\,\emptyset}\, f(\emptyset)$$

Eq. A3

Subject to

$$\emptyset_L \le \emptyset \le \emptyset_U$$

Eq A4.

Where:
$f(\emptyset)$ = is the objective function to be minimized ($RMSE(k_{Rs})$).
$\emptyset$ = is the vector of parameters (k_{Rs}).
$\emptyset_L$ and $\emptyset_U$ are the lower and upper bunds of the parameters, respectively.

Algorithm steps:

1) Initialize: start with an initial guess $\emptyset_0$ within bounds (0.17 as it is the default k_{Rs} value).
2) Compute gradient: calculate $\nabla f(\emptyset_k)$.
3) Search direction: determine P_k using limited-memory approximation of the inverse Hessian.
4) Line search and update: Find and appropriate step size $\propto_k$ and update $\emptyset_{k+1}$.
5) Projection: Ensure the updated parameters $\emptyset_{k+1}$ stay withing bounds by projecting onto the feasible region.

$$\emptyset_{k+1} = Proj\left(\emptyset_k - \propto_k H_k \nabla f(\emptyset_k)\right)$$

Eq A5.

Where:
H_k = is the approximation of the inverse Hessian matrix.
$\propto_k$ = is the step size determined by line search.
$Proj$ = denotes the projection operator ensuring $\emptyset_{k+1}$ remains

6.2. **Supplementary B.** Climate characterization and data QAQC.

Table 5.S2. Aridity index for GB calculated with data from FAO CLIMWAT 2.0 weather data.

Region	**CLIMWAT Weather station**	**ET_p**	**Rainfall**	**AI**	**Classification**	**Nearest stations**
-	**-**	**mm**	**mm**	**Index**	**-**	**-**
South	Buba	1539.4	2133	1.39	Humid	Cafine Quebil Buba Malafu Enchugal Bubaque
	Catio	1641.3	2629	1.60		
	Bolama	1691.9	2076	1.23		
Central	Bissau	1584.8	1650	1.04	Humid	
North	Zinguincor (Senegal)	1777.6	1235.1	0.69	Moist, sub-humid	Bissora S. Domingos Cacheu Elalab Djobel

6.3. **Supplementary C.** Goodness of fit indicators and standard deviation for predicting ET_o in sites.

Table 5.S3 presents the goodness-of-fit indicators and standard deviations of the data used to calibrate the multiple linear regression equations, which were optimized using the L-BFGS-B numerical method. The table includes metrics for predictions made in both the moist sub-humid and humid regions, as well as for scenarios where estimators such as T_{dew} and wind speed (u_2) were unavailable, using either average ($u_{2\ avg}$) values or a default ($u_{2\ def}$) of 2 m s^{-1}. The equations were calibrated using 70% of the dataset from each meteorological station, and the remaining 30% was used to validate the calibrated equations. Subsequently, the validated equations were applied to 100% of the dataset for the development of this study.

Table 5.S3. Goodness-of-fit indicators and the standard deviation of ET_o estimation when using the PMT approach relative to the test and validation of the cluster-focused multiple linear regression equations for estimating the radiation coefficient (k_{Rs}) (Eqs. 12-16) and using different predictors for dew point temperature (T_{dew}) and wind speed (u_2).

Climate	Predictors			Goodness of fit indicators and standard deviation											
	T_{dew}	k_{Rs}	u_2	b_0	SD	R^2	SD	RMSE (mm d^{-1})	SD	NRMSE (%)	SD	BIAS	SD	PBIAS (%)	SD
				Testing (70% data set)											
Moist sub humid	T_{min}	**Optm**	Default	0.98	0.01	0.97	0.01	0.92	0.134	19.1	3.06	0.00	0.04	-0.04	0.85
			Avg	0.98	0.01	0.98	0.01	0.77	0.174	16.0	3.11	0.00	0.04	-0.04	0.79
Humid	T_{min}	**Optm**	Default	0.98	0.00	0.97	0.00	0.78	0.053	16.7	1.16	-0.01	0.02	-0.17	0.44
			Avg	0.98	0.01	0.98	0.00	0.67	0.061	14.3	1.50	-0.02	0.06	-0.56	1.33
	T_{mean} - 2	**Optm**	Default	0.97	0.02	0.98	0.00	0.70	0.043	14.9	1.25	-0.05	0.07	-1.17	1.53
			Avg	0.97	0.02	0.98	0.00	0.68	0.051	14.4	1.41	-0.05	0.07	-1.16	1.51
	T_{mean}-a_D (a_D opt)	**Optm**	Default	0.98	0.01	0.98	0.00	0.67	0.045	14.3	1.19	0.00	0.01	0.09	0.30
			Avg	0.99	0.03	0.98	0.00	0.67	0.049	14.3	1.31	0.04	0.11	0.86	2.20
				Validation (30% data set)											
Moist sub humid	T_{min}	**Optm**	Default	0.98	0.006	0.97	0.01	0.85	0.117	17.8	2.44	-0.01	0.03	-0.11	0.62
			Avg	0.98	0.014	0.98	0.01	0.72	0.131	15.1	2.40	-0.01	0.05	-0.33	1.10
Humid	T_{min}	**Optm**	Default	0.99	0.005	0.97	0.00	0.79	0.057	16.7	1.17	-0.01	0.02	-0.17	0.44
			Avg	0.98	0.018	0.98	0.00	0.67	0.068	14.3	1.50	-0.03	0.06	-0.56	1.33
	T_{mean} - 2	**Optm**	Default	0.98	0.006	0.98	0.00	0.67	0.045	14.3	1.19	0.00	0.01	0.09	0.30
			Avg	0.99	0.026	0.98	0.00	0.67	0.049	14.3	1.31	0.04	0.11	0.86	2.20
	T_{mean}-a_D (a_D opt)	**Optm**	Default	0.99	0.005	0.97	0.00	0.79	0.057	16.7	1.17	-0.01	0.02	-0.17	0.44
			Avg	0.98	0.018	0.98	0.00	0.67	0.068	14.3	1.50	-0.03	0.06	-0.56	1.33

Table 5.S4. Ranges of the goodness-of-fit indicators relative to comparing PM-ET_o with $ET_{o\ PMT}$ when using T_{min} or the T_{mean} as predictor of T_{dew}, when k_{Rs} was computed with the global Eq. (6), with the climate-focused Eqs (7a, 7b), or the cluster-focused Eqs. (12-16) when using the default or the average local u_2 value, for the eleven sites of Guinea-Bissau.

Climate	Predictors			Goodness of fit indicators (ranges)					
	T_{dew}	k_{Rs}	u_2	b_0	R^2	RMSE (mm d^{-1})	NRMSE (%)	BIAS	PBIAS (%)
Moist sub humid	T_{min}	Global	Default	0.86-0.98	0.95-0.98	0.86-1.19	18.0-23.8	-0.7- -0.03	-13.0- -0.8
			Avg	0.76-0.87	0.95-0.98	0.99-1.26	19.6-27.5	-1.0-0.6	-22.7 - -11.7
		Climate	Default	0.83-0.95	0.95-0.98	0.89-1.22	18.6-24.5	-0.8- -0.15	-15.9- -3.35
			Avg	0.73-0.85	0.95-0.98	1.09-1.37	21.7-30.0	-1.2-0.7	-25.6 - -13.7
		Cluster	Default	0.96-1.19	0.95-0.98	0.77-1.33	14.7-29.0	-0.07-0.93	-1.32-20.24
			Avg	0.92-1.04	0.96-0.98	0.67-1.08	14.6-21.6	-0.30-0.25	-6.62-5.15
Humid	T_{min}	Global	Default	0.85-1.00	0.97-0.98	0.80-0.94	16.8-21.5	-0.58-0.04	-13.3-1.2
			Avg	0.76-0.88	0.95-0.98	0.79-1.28	17.3-27.3	-0.9-0.1	-18.9-1.5
		Climate	Default	0.88-1.12	0.97-0.98	0.78-1.04	16.3-22.2	-0.41-0.57	-9.4-12.5
			Avg	0.80-1.01	0.95-0.98	0.63-1.09	13.8-23.3	-1.1- -0.6	-23.5 – 11.0
		Cluster	Default	0.98-1.14	0.97-0.98	0.74-1.09	15.7-23.8	0.06-0.68	1.5-15.1
			Avg	0.95-1.03	0.97-0.98	0.61-0.77	12.8-16.8	-0.18-0.20	-3.93-4.3
	T_{mean} - 2	Global	Default	0.77-0.88	0.97-0.98	0.81-1.30	17.7-26.9	-1.05- -0.5	-22.5 - - 10.8
			Avg	0.72-0.86	0.95-0.98	0.87-1.44	18.9-30.8	-1.3 - - 0.6	-27.5 - -13.3
		Climate	Default	0.81-1.01	0.97-0.98	0.69-1.11	15.1-23.0	-0.8-0.08	-17.7-1.9
			Avg	0.77-1.00	0.95-0.98	0.65-1.22	14.3-26.1	-1.0-0.0	-22.3-0.6
		Cluster	Default	0.92-1.03	0.97-0.98	0.66-0.79	13.7-16.9	-0.30-0.22	-5.8-4.7
			Avg	0.92-1.03	0.97-0.98	0.62-0.79	13.0-17.0	-0.2-0.17	-6.4- 3.64
	T_{mean}-a_D (a_D opt)	Global	Default	0.87-0.99	0.97-0.98	0.63-0.92	13.7-18.4	-0.5-0.02	-10.6-0.49
			Avg	0.75-0.89	0.95-0.98	0.77-1.29	16.7-24.0	-0.9-0.1	-19.2-2.5
		Climate	Default	0.92-1.00	0.97-0.98	0.63-0.80	13.2-17.2	-0.3-0.04	-6.0-0.96
			Avg	0.80-1.01	0.95-0.98	0.63-1.10	13.8-23.8	-1.1- -0.5	-24.0 - - 10.4
		Cluster	Default	0.97-1.00	0.97-0.98	0.66-0.73	13.7-16.6	-0.01-0.05	-0.01-1.08
			Avg	0.96-1.04	0.97-0.98	0.61-0.74	12.7-16.8	-0.16-0.09	-3.3-5.28

Default – u_2 = 2 m s^{-1} SD= standard deviation; R^2 = coefficient of determination; RMSE = root mean square error; NRMSE = normalized root mean square error.

Table S5. Accuracy of different PMT approaches analysed at cluster level. $ET_{o\ PMT}$ estimated when using T_{min} or the T_{mean} as predictor of T_{dew}, ther k_{Rs} were computed with the global Eq. (6). or with the climate-focused Eqs (7a, 7b), or the cluster-focused Eqs. (12-16) when using the default or the average local u_2 value for the eleven sites of Guinea-Bissau.

Cluster (AI)	Predictors			Goodness of fit indicators and standard deviation						
	T_{dew}	k_{Rs}	u_2	b_0	R^2	RMSE (mm d^{-1})	NRMSE (%)	BIAS	PBIAS (%)	
Cluster 1st (humid)	T_{min}	Global	Deft	0.92	0.97	0.86	17.91	-0.35	-7.2	Def – u2 = 2 m s^{-1} SD= standard deviation; Optim = optimized with the " L-BFGS-B" algorithm.
			Avg	0.86	0.98	0.97	20.02	-0.63	-13.1	
		Climate	Def	0.96	0.97	0.80	16.64	-0.14	-3.0	
			Avg	0.90	0.98	0.84	17.32	-0.42	-8.7	
		Optim	Def	1.04	0.98	0.84	17.41	0.27	5.6	
			Avg	0.99	0.98	0.72	14.87	0.01	0.3	
	T_{mean} - 2	Global	Def	0.80	0.98	1.14	23.63	-0.88	-18.3	
			Avg	0.79	0.98	1.19	24.58	-0.95	-19.6	
		Climate	Deft	0.85	0.98	0.97	20.08	-0.66	-13.62	
			Avg	0.84	0.98	1.00	20.71	-0.71	-14.7	
		Optim	Deft	0.94	0.98	0.73	15.21	-0.20	-4.2	
			Avg	0.94	0.98	0.73	15.18	-0.23	-4.8	
	T_{mean}-a_D (a_t optim)	Global	Deft	0.91	0.98	0.80	16.55	-0.35	-7.4	
			Avg	0.85	0.98	0.95	19.59	-0.62	-12.9	
		Climate	Deft	0.95	0.98	0.72	14.90	-0.15	-3.0	
			Avg	0.78	0.98	1.23	25.53	-0.98	-20.4	
		Optim	Deft	0.99	0.98	0.70	14.49	0.02	0.5	
			Avg	0.99	0.98	0.68	14.18	0.02	0.5	
Cluster 2nd (humid+moist)	T_{min}	Global	Deft	0.94	0.97	0.88	18.41	-0.23	-4.9	
			Avg	0.80	0.98	1.12	23.47	-0.89	-18.6	
		Climate	Deft	0.99	0.97	0.84	17.78	0.01	0.12	
			Avg	0.85	0.98	0.93	19.61	-0.67	-14.1	
		Optim	Deft	1.12	0.97	1.06	22.22	0.61	12.9	
			Avg	0.99	0.98	0.65	13.73	0.03	0.6	
	T_{min} (moist) & T_{mean} – 2 (humid)	Global	Deft	0.79	0.98	1.17	24.57	-0.94	-19.7	
			Avg	0.76	0.98	1.30	27.26	-1.11	-23.4	
		Climate	Deft	0.85	0.98	0.95	20.04	-0.65	-13.8	
			Avg	0.82	0.98	1.04	21.99	-0.82	-17.3	
		Optim	Deft	0.99	0.98	0.71	14.95	0.03	0.5	
			Avg	0.97	0.98	0.67	14.11	-0.07	-1.5	
	T_{min} (moist) & T_{mean} – a_D (humid)	Global	Deft	0.90	0.98	0.79	16.58	-0.39	-8.3	
			Avg	0.79	0.98	1.13	23.75	-0.92	-19.3	
		Climate	Deft	0.86	0.96	1.07	22.30	-0.52	-10.8	
			Avg	0.80	0.96	1.27	26.35	-0.87	-18.1	
		Optim	Deft	1.00	0.98	0.71	14.94	0.04	0.9	
			Avg	1.00	0.98	0.64	13.56	0.05	1.0	
Cluster 3rd (moist)	T_{min}	Global	Deft	0.88	0.96	1.13	22.29	-0.53	-10.5	
			Avg	0.86	0.96	1.15	22.65	-0.60	-11.8	
		Climate	Def	0.88	0.95	1.17	23.40	-0.51	-10.3	
			Avg	0.84	0.96	1.22	24.46	-0.70	-14.1	
		Optim	Def	0.99	0.96	1.01	19.91	0.05	1.0	
			Avg	0.98	0.96	0.99	19.49	-0.01	-0.2	
Bissora (moist)	T_{min}	Global	Deft	0.98	0.96	0.94	20.42	-0.04	-0.8	
			Avg	0.76	0.98	1.26	27.47	-1.04	-22.7	
		Climate	Def	0.95	0.96	0.95	20.71	-0.15	-3.4	
			Avg	0.73	0.98	1.37	29.97	-1.17	-25.6	
		Optim	Def	1.19	0.97	1.33	28.99	0.93	20.2	
			Avg	0.99	0.98	0.67	14.67	0.02	0.4	
Bubaque (humid)	T_{min}	Global	Deft	0.85	0.97	0.95	21.50	-0.58	-13.3	
			Avg	0.79	0.97	1.11	25.29	-0.82	-18.7	
		Climate	Def	0.88	0.97	0.85	19.28	-0.41	-9.4	
			Avg	0.83	0.97	0.98	22.22	-0.64	-14.5	
		Optim	Def	0.99	0.97	0.74	16.79	0.07	1.5	
			Avg	0.95	0.97	0.74	16.79	-0.12	-2.6	
	T_{mean} - 2	Global	Def	0.79	0.97	1.13	25.56	-0.83	-18.9	
			Avg	0.78	0.97	1.17	26.54	-0.89	-20.2	
		Climate	Deft	0.83	0.97	0.99	22.58	-0.66	-14.9	
			Avg	0.82	0.97	1.02	23.22	-0.70	-15.8	
		Optim	Deft	0.94	0.97	0.75	16.98	-0.16	-3.6	
			Avg	0.94	0.97	0.75	17.03	-0.15	-3.5	
	T_{mean}-a_D (a_D optim)	Global	Deft	0.90	0.97	0.81	18.45	-0.29	-6.6	
			Avg	0.81	0.97	1.06	23.98	-0.73	-16.6	
		Climate	Deft	0.94	0.97	0.76	17.27	-0.13	-2.9	
			Avg	0.85	0.97	0.93	21.21	-0.55	-12.5	
		Optim	Deft	0.97	0.97	0.73	16.60	0.00	0.0	
			Avg	0.96	0.97	0.74	16.81	-0.05	-1.1	

6.4. Supplementary D. Correlation between ET_o estimated with weather observations and with AgeERA5 and MERRA-2 reanalysis data.

Table 5.S6. Goodness-of-fit indicators relative to the estimation of ET_o when using AgERA5 and MERRA-2 reanalysis data compared to observed ground measurements.

Bias correction methods	PBias (%)	SD	Bias	SD	R^2	SD	RMSE (mm d^{-1})	SD	NRMSE (%)	SD
	AgERA5									
	$u_{2\ avg}$									
UN_c	5.17	7.22	0.2	0.34	0.96	0.01	1.12	0.17	23.6	3.9
ALM_c	0.00	0.00	0.0	0.00	0.90	0.03	1.63	0.27	34.0	5.7
$BIAS_c$	0.00	0.00	0.0	0.00	0.95	0.01	1.05	0.11	22.0	2.3
RLM_c	2.41	0.82	0.1	0.04	0.96	0.01	1.04	0.09	21.7	1.6
S_c	2.59	0.88	0.1	0.05	0.96	0.01	1.04	0.09	21.7	1.7
	$u_2 = 2\ m\ s^{-1}$									
UN_c	4.54	7.98	0.2	0.37	0.96	0.01	1.07	0.17	22.4	3.9
ALM_c	0.00	0.00	0.0	0.00	0.92	0.02	1.48	0.20	31.0	4.3
$BIAS_c$	0.00	0.00	0.0	0.00	0.96	0.01	0.99	0.10	20.7	2.0
RLM_c	2.39	0.78	0.1	0.04	0.96	0.01	0.97	0.08	20.3	1.4
S_c	2.66	0.81	0.1	0.04	0.96	0.01	0.98	0.09	20.4	1.5
	MERRA-2									
	$u_{2\ avg}$									
UN_c	-24.27	6.88	-1.18	0.39	0.94	0.00	1.57	0.33	32.51	5.44
ALM_c	0.00	0.00	0.00	0.00	0.93	0.02	1.38	0.22	28.71	3.94
$BIAS_c$	0.00	0.00	0.00	0.00	0.96	0.00	1.01	0.06	21.11	0.86
RLM_c	0.01	1.37	0.00	0.07	0.94	0.00	1.21	0.06	25.14	0.97
S_c	0.79	1.09	0.04	0.06	0.94	0.00	1.21	0.05	25.32	0.95
	$u_2 = 2\ m\ s^{-1}$									
UN_c	-18.63	9.61	-0.91	0.51	0.94	0.01	1.44	0.35	29.88	5.95
ALM_c	0.00	0.00	0.00	0.00	0.93	0.01	1.39	0.15	28.93	2.39
$BIAS_c$	0.00	0.00	0.00	0.00	0.96	0.01	1.05	0.06	21.95	1.54
RLM_c	-0.30	1.26	-0.01	0.06	0.94	0.01	1.18	0.05	24.67	1.11
S_c	0.93	0.78	0.05	0.04	0.94	0.01	1.20	0.05	24.94	1.17

SD= standard deviation; UN_c – raw data or uncorrected bias; bias correction methods: S_c- Slope, RLM_c – Robust linear model; $Bias_c$ - Bias; ALM_c – Adjusted linear model

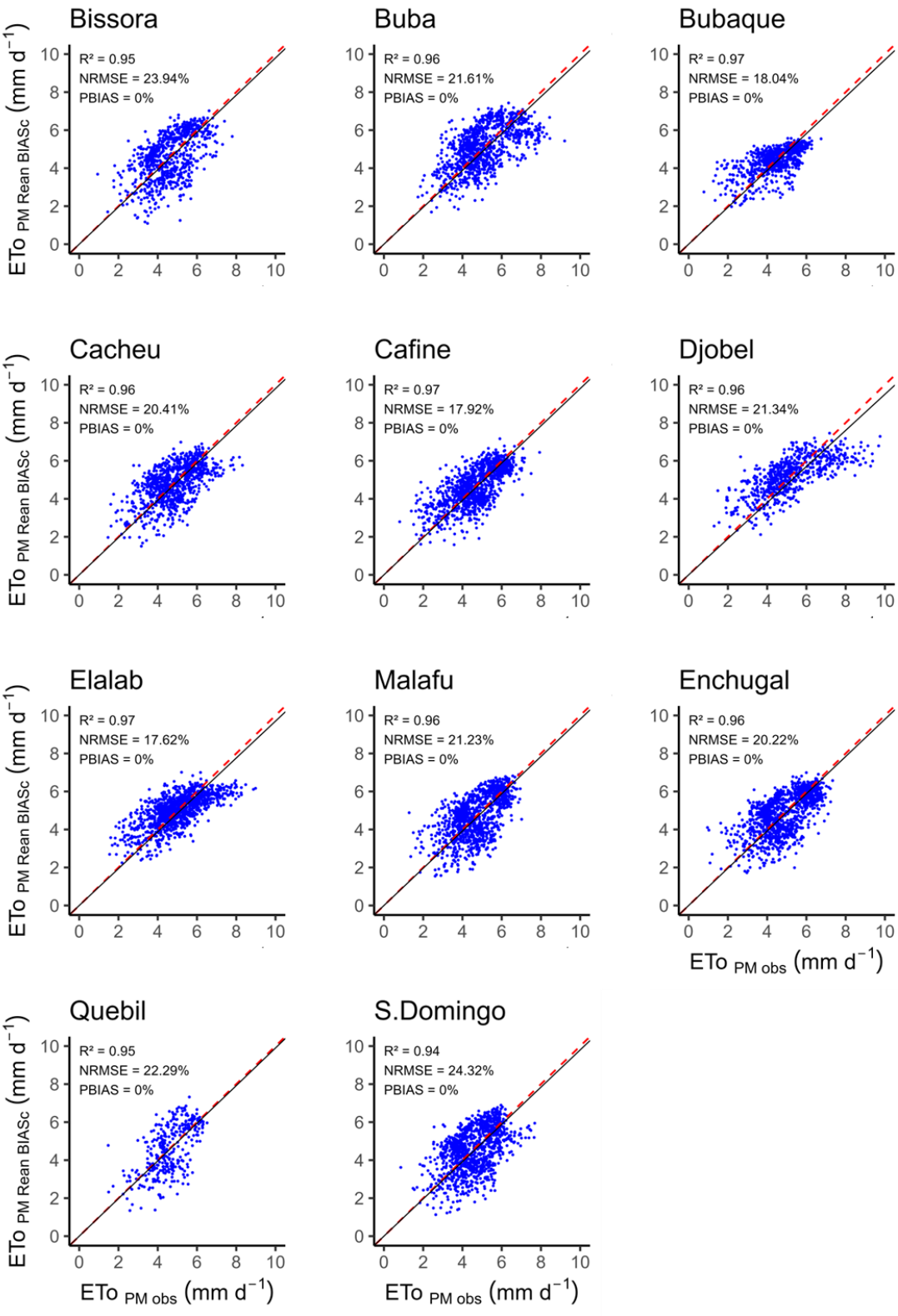

Figure 5.S7. Comparing ET_o estimated with observed weather data and with AgERA5 after bias correction for the eleven sites in Guinea-Bissau.

6.5. **Supplementary E.** Spatial distribution of annual ET_o in GB.

Table 5.S8. Geostatistical parameters used to calculate the interpolation annual ET_o with AgERA5 in GB.

Metric	Annual ET_o	Units
GS+ metrics		
Variogram Model	Exponential	-
Nugget	10	mm y^{-1}
Sill	17870	m
Range	240300	m
Autocorrelation metrics		
Global Moran's I	0.84	index
Variance	0.001677	mm y^{-1}
Z - score	20.714055	mm y^{-1}
p-value*	< 000.1	index
Goodness-of-fit indicators		
RMSE	40.5	mm y^{-1}
NRMSE	2.3	%
BIAS	0.14	-
PBIAS	0.008	%
R^2	0.87	-
ρ	0.94	-

ρ = Pearson correlation

Chapter 6

Modeling soil water and salinity dynamics in mangrove swamp rice production system of Guinea Bissau, West Africa

This chapter was published in Agricultural Water Management.

Garbanzo, G., Cameira, M. do R., Paredes, P., Temudo, M., Ramos T. 2025. Modeling soil water and salinity dynamics in mangrove swamp rice production system of Guinea Bissau, West Africa. Agricultural Water Management, 313, 109494. https://doi.org/10.1016/j.agwat.2025.109494

Keywords:

HYDRUS-1D, Optimal Growing Period, Rainfall Variability, Groundwater Depth, Salinity Stress, Salt-free period.

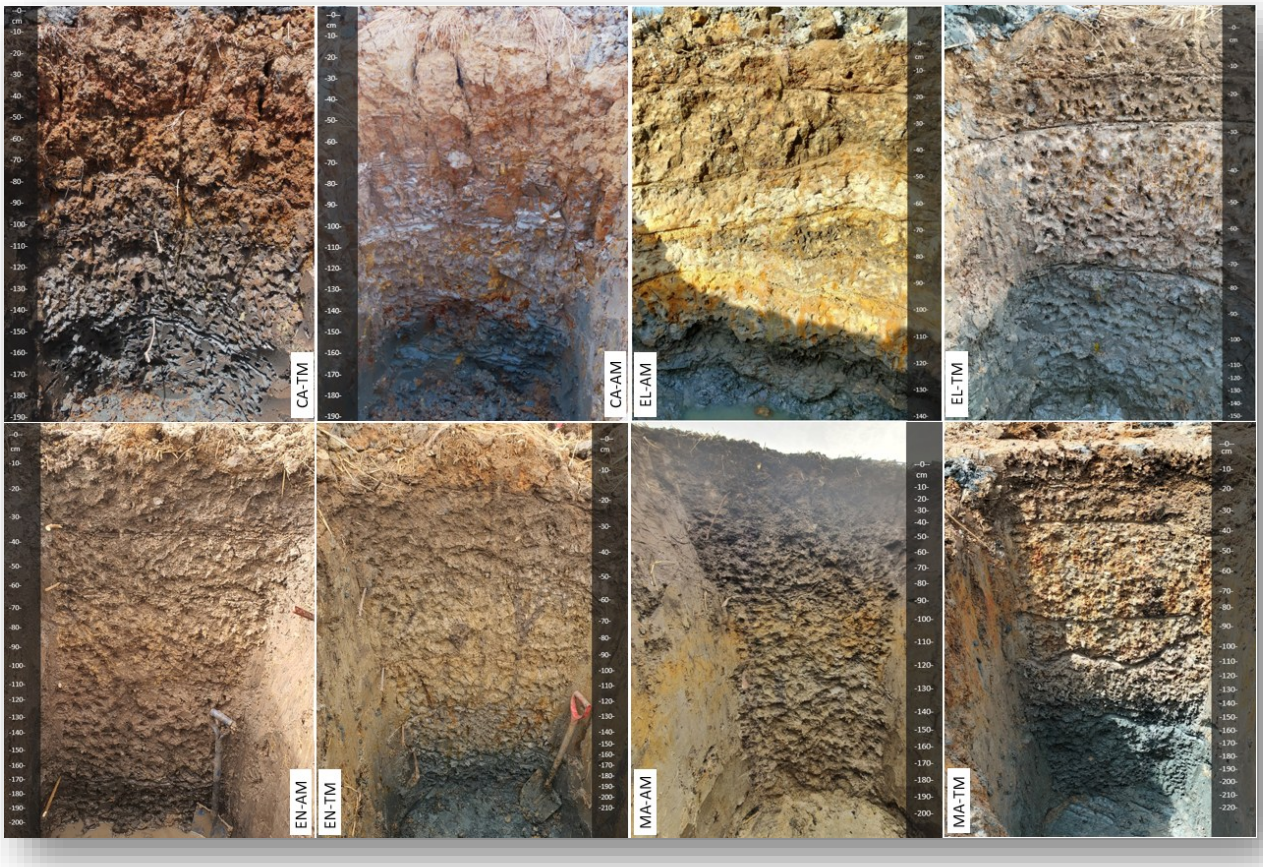

1. *Abstract*

Mangrove swamp rice production (MSRP) is of fundamental importance for the livelihoods, food security, and nutritional well-being of coastal populations in West Africa. However, this system faces increasing challenges due to its reliance on sufficient and well-distributed rainfall to maintain feasible soil salinity levels for rice production during the growing season. This study examines the dynamics of soil water and salts using field observations collected from four different MSRP fields in Guinea-Bissau during two growing seasons, along with simulations using the HYDRUS-1D model. Several rainfall and groundwater depth scenarios were also considered to identify the key factors contributing to soil salinity at the study sites. The results helped identify the main factors influencing soil salinity during the study period and estimate the potential impacts on crop yields, which could decline by up to 60%. Key factors influencing soil salinity included the amount and distribution of seasonal rainfall, groundwater depth, and groundwater quality. The analysis of modeled scenarios also provided insights into effective management strategies for coping with soil salinization, particularly by assessing: a) where and when more productive, long-cycle rice varieties can still be cultivated; b) where salt-tolerant rice varieties have to be chosen. Additionally, the results reinforce the need for the regular maintenance of dikes and other drainage structures to avoid brackish water entrance and guaranty minimum rice growth conditions. Future research will explore adopting this practice in field with modern water management, with the model enabling precise analysis of impact on sustainability.

2. *Introduction*

Mangrove swamp rice production (MSRP) refers to rice cultivation on former mangrove soils that have been anthropogenically modified for agricultural use. This practice typically occurs near saltwater rivers in areas previously covered by mangrove forests, which have been transformed into rice paddies through deforestation, dike and bunds construction, plots creation, and soil desalination (Baggie et al., 2018; Balasubramanian et al., 2007; Garbanzo et al., 2024a). In West Africa, the MSRP region extends from Senegal to Sierra Leone and plays a vital role in ensuring food security. In Guinea-Bissau, MSRP areas represent approximately 49% of the country's crop production (The Republic of Guinea-Bissau, 2018), forming the basis of the population's diet.

While the MSRP system is not particularly conservation-friendly for mangrove forests, it remains the only viable option for local communities in these African regions to sustain food production, given the higher fertility of mangrove soils compared to upland areas (Jnr, 2014). However, MSRP faces significant challenges, primarily due to its reliance on rainfall (2,500-1,500 mm) to leach salt from the rootzone, ensuring suitable conditions for rice growth. As variability in rainfall patterns driven by climate change makes the desalination of paddy fields increasingly difficult, rice production is negatively impacted (Mendes and Fragoso, 2023; Temudo et al., 2022). Irrigation is not feasible because freshwater resources are either unavailable or farmers lack the financial means to access necessary technologies (Martiarena and Temudo, 2023; Temudo and Cabral, 2023). Additionally, paddy fields are influenced by tidal movements that affect groundwater dynamics, saline water intrusion, and soil salinity buildup as salts are drawn up to the soil surface layer due to strong evaporation rates during the dry season (Garbanzo et al., 2024a). These challenges characterize MSRP as a highly complex system, and

understanding its dynamics is crucial for ensuring the sustainability of this production system.

Although soil salinization in MSRP areas exhibits significant spatial variability (Sylla et al., 1995), the landscape can be categorized into two distinct zones: tidal mangrove fields (TM) and associated mangrove fields (AM) (Baggie et al., 2018; Garbanzo et al., 2024a). TM are the ones closer to the main dike, were previously covered by mangroves forest, and tend to experience higher levels of salinization. In contrast, AM are situated further inland, in areas that were once mangrove-covered and have been cultivated for decades or even centuries or are located near the first main dike prior to agricultural expansion driven by population growth; they have lower salinization levels primarily influenced by brackish groundwater during the dry season. Soil salinization management in MSRP areas remains largely empirical, based on local knowledge and practices, many of which are not well-suited to the changing socio-environmental conditions (Martiarena and Temudo, 2023).

MSRP in Guinea-Bissau is also not supported with fertilizers input. As a result, and given that rice is sensitive to salinity stress (Ayers and Westcot, 1985; Minhas et al., 2020), yields are generally low. According to the USDA (2024), average yields in Guinea-Bissau (2019-2024) were only about 1.7 tonnes ha^{-1}, compared to 3.6 tonnes ha^{-1} in neighboring Senegal. For traditional rice-producing countries like India (4.2 tonnes ha^{-1}), Bangladesh (4.6 tonnes ha^{-1}), Vietnam (6.0 tonnes ha^{-1}), Spain (6.5 tonnes ha^{-1}), and China (7.1 tonnes ha^{-1}), the differences are even more pronounced (FAO, 2023). Nonetheless, the yields from MSRP are much higher than those obtained through other rice cropping systems practiced in the country: upland slash-and-burn and freshwater inland swamp cultivation (Garbanzo et al., 2024a). Traditionally, in this low-external inputs system, soil fertility and the control of toxicity, particularly during dry season when aerobic conditions prevail,

were achieved through the regular entrance of brackish water. This practice also improved weeds' control and reduced the labor input by eliminating the need for ploughing, which is a great advantage in times of increased youth migration and engagement in education (Cossa, 2023). Although this practice has been almost abandoned due to increasingly irregular rainfall patterns, some development projects have reintroduced it through the installation of modern water management infrastructures using PVC drainage tubes (see https://universsel.org/). With an improved understanding of soil water-salt dynamics, these innovations may facilitate the reimplementation of traditional brackish water management practices.

Therefore, more effective soil, water, and crop management practices are crucial for improving both the rice yields and the livelihoods of local communities in a context of drastic socio-environmental transformations. Numerical Modeling, using tools such as the HYDRUS software package (Šimůnek et al., 2024, 2016), SWAP (Heinen et al., 2024, 2020), RZWQM (Ma et al., 2001), SALTMED (Ragab, 2002), and WAVES (Yu et al., 2021), can offer a better understanding of soil water-salt dynamics in complex systems and valuable solutions for coping with soil salinity. These modeling tools can incorporate site-specific soil, water, and crop parameters, while accounting for time-varying field conditions, including soil salinity levels, groundwater dynamics, and rainfall patterns. By doing so, they can provide insights on the impacts of these factors on crop yields, with minimal effort and resources, aiding in the development of improved management guidelines for rice production in salt-affected areas.

Examples of applications of numerical modeling tools for saline water management have been extensively reported in the literature, including studies on interactions with shallow saline groundwater systems (Karimov et al., 2014; Xu et al., 2013), evaluation of soil salinity control measures (Guo et al., 2024; Ramos et al., 2023), the impacts of irrigation

water quality on crop growth (Kanzari et al., 2024; Phogat et al., 2018; Stulina et al., 2005), and disentangling the relationships with nutrient management (Phogat et al., 2018; Ramos et al., 2023). Most of these studies have focused on addressing complex soil salinization issues in arid to semi-arid regions, which are among the most severely affected by human-induced salinization (Hopmans et al., 2021). However, findings from these regions cannot be directly extrapolated to MSRP areas. Although MSRP systems exhibit comparable complexities in salinization processes, their presence in humid climates significantly alters salt dynamics and salinity build-up. In humid climates, higher rainfall and frequent leaching events reduce the accumulation of salts compared to arid or semi-arid conditions. However, in MSRP systems, the interaction between tidal inflows, poor drainage, and alternating wet-dry conditions creates a unique salinity dynamic. These factors influence the timing and extent of salt accumulation differently than in drier regions, making it necessary to treat them as distinct systems in terms of salinity modeling and management. This distinct climatic context demands tailored research and a deeper understanding of these unique conditions to develop effective management strategies. To date, this remains a critical knowledge gap in existing research on soil salinity in MSRP areas; a gap that this study aims to address.

The specific objectives of this study are therefore: (i) to calibrate and validate the HYDRUS-1D model for simulating soil-water dynamics and salt transport in the tidal and associated mangrove fields in Guinea-Bissau; (ii) to compute the soil-water balance and evaluate the impact of soil-water management on rice yields at each study site; and (iii) to assess the effects of changing groundwater dynamics and rainfall conditions on rice yields. The findings of this study are instrumental in enhancing rice production in Guinea-Bissau but also in other MSRP regions across West Africa.

3. Material and methods.

3.1. Study area

This study was conducted in three paddy rice field of three villages of Guinea-Bissau. Elalab (12°14'48.5"N, 16°26'30.3"W), Djobel (12°16'51.3"N, 16°23'34.4"W), and Cafine (11°12'40.4"N, 15°10'26.7" W) (Fig. 6.1). In Cafine, both tidal and associated areas were studied, whereas only associated areas were considered in Elalab and Djobel due to the smaller field dimensions and the need to ensure the security of dataloggers and sensors. According to the Köppen climate classification, the region's climate is classified as tropical monsoon (Aw), characterized by heavy rainfall during the wet season (Beck et al., 2018). Rainfall typically begins in June in the southern regions of Guinea-Bissau (Cafine, Djobel) and in July in the northern regions (Elalab), ending by late September or October (Fig. 6.1). Average annual rainfall ranges from approximately 1,500 mm in the north to 2,500 mm in the south. Moreover, average annual temperatures are between 24 °C and 27 °C, with minimal variation throughout the year (Garbanzo et al., 2024b).

The soils exhibit hypersaline conditions, with salinity increasing in the deeper horizons. They are classified as Inceptisols with Vertic features, characterized by limited pedogenetic development (D'Amico et al., 2024; Teixeira, 1962). Generally, tidal mangrove soils have rich clay content, whereas associated mangrove soils are predominantly sandy (Garbanzo et al., 2025). Soil profiles tend to be deeper in the southern regions compared to the northern areas. The soils also present ustic moisture regimes, remaining dry for more than 90 consecutive days. Additionally, MSR soils have undergone physical and chemical modifications induced by local farmers' interventions, having originally been mangrove forests converted for rainwater harvesting and prevention of tidal water intrusion during rice cultivation. Table 6.1 shows the main

physical and chemical properties of the soils in the study areas. The methodologies used for soil characterization can be found in Merkohasanaj et al. (2025).

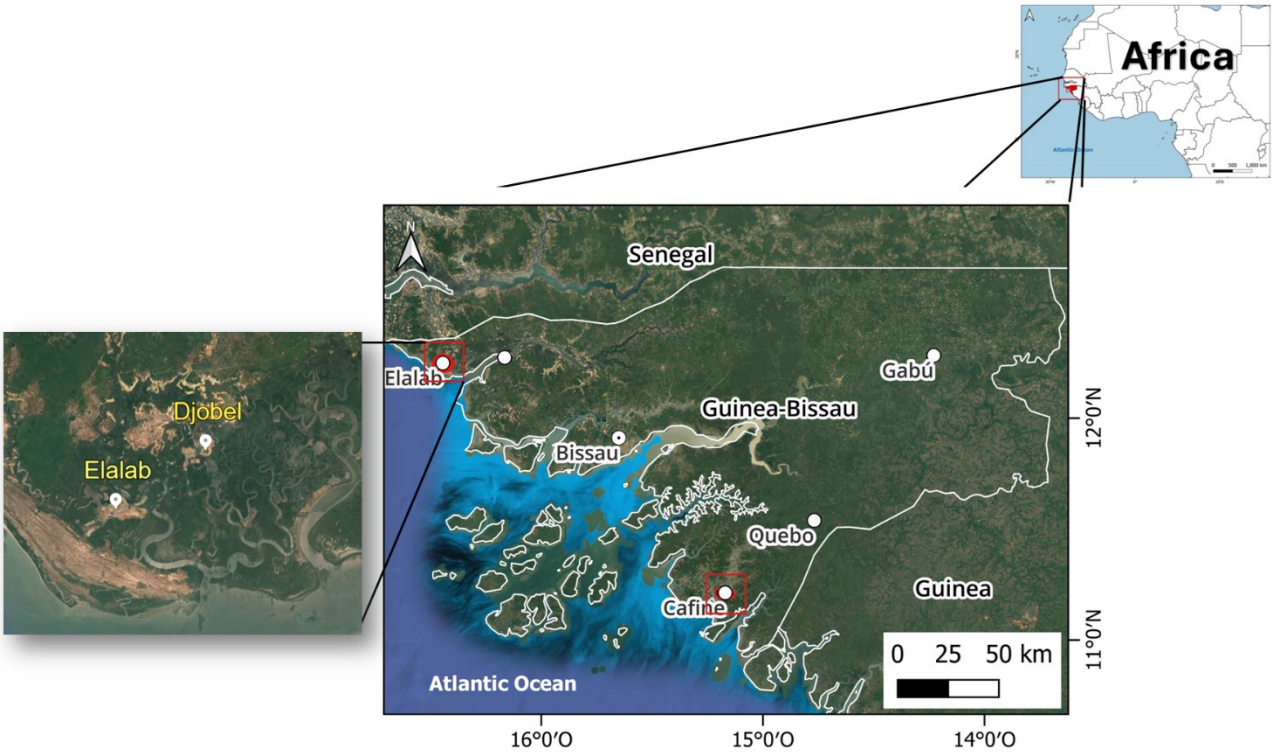

Fig. 6.1. Locations of the study sites in Guinea-Bissau, West Africa.

Table 6.1. Soil physical properties of mangrove swamp rice fields in Guinea-Bissau.

Location	Depth [m]	Sand [%] (2.0-0.05 mm)	Silt [%] (0.05-0.002 mm)	Clay [%] (<0.002 mm)	ρ_b [g cm^{-3}]	OC [%]	θ_{FC} [cm^3 cm^{-3}]	θ_{WP} [cm^3 cm^{-3}]	EC_e [dS m^{-1}]
Cafine TM	0.0 – 0.39	19	39	42	1.09	1.37	0.327	0.214	17.4
	0.39 – 0.63	36	24	40	1.16	1.08	0.254	0.210	28.5
	0.63 – 0.85	48	28	24	0.87	1.53	0.428	0.315	118.3
Cafine AM	0.0 – 0.30	17	38	45	1.17	1.04	0.371	0.190	16.0
	0.30 – 0.48	12	31	57	1.15	0.58	0.454	0.301	12.3
	0.48 – 0.74	31	32	37	0.98	0.70	0.476	0.215	22.6
	0.74 – 1.18	40	35	25	0.62	0.91	0.574	0.272	105.7
Djobel AM	0.0 – 0.25	19	50	31	1.20	0.29	0.127	0.088	24.2
	0.25 – 0.50	23	55	22	1.40	0.37	0.175	0.098	13.9
	0.50 – 0.75	15	49	36	1.55	0.27	0.122	0.091	16.4
Elalab AM	0.0 – 0.13	68	13	19	1.53	0.75	0.211	0.100	35.1
	0.13 – 0.40	44	21	35	1.65	0.47	0.341	0.131	34.4
	0.40 – 0.53	94	2	4	1.52	0.09	0.136	0.063	21.1
	0.55 – 0.70	84	7	9	1.51	0.08	0.094	0.062	54.2

TM, tidal mangrove; AM, Associated mangrove; OC, Organic carbon; ρ_b, bulk density; θ_{FC}, volumetric water content at field capacity. θ_{WP}, volumetric water content at wilting point, EC_e, electrical conductivity of the saturation paste extract.

Data collection

The paddies were continuously monitored between 2022 and 2023 to study the dynamics of water and salts. Teros 12 sensors (Meter Group, USA) were used to measure soil water contents (SWC) and bulk electrical conductivity (EC_b). The relationships between EC_b data, the electrical conductivity of the saturation paste extract (EC_e), and the electrical conductivity of the soil solution (EC_{sw}) were as follows (Hilhorst, 2000):

$$EC_e = \frac{80\ \theta\ EC_b}{\theta_s(\varepsilon_b - 4.1)} \quad (1)$$

$$EC_{sw} = \frac{\varepsilon_w\ EC_b}{\varepsilon_b} \quad (2)$$

$$\varepsilon_w = 80.3 - 0.37(T_{soil} - 20) \quad (3)$$

$$EC_e = EC_{sw}\frac{\theta}{\theta_s} \quad (4)$$

where θ is the volumetric soil water content [$L^3\ L^{-3}$], θ_s is the saturation water content [$L^3\ L^{-3}$], ε_b is the dielectric permittivity of the bulk soil [dS m^{-1}], ε_w is the dielectric permittivity of the soil pore water [dS m^{-1}], and T_{soil} is the soil temperature (ºC). The sensors were installed at soil depths of 0.07, 0.15, 0.25 and 0.35 m, positioned at the center of the rice cultivation plots at each of the four sites. Each sensors took measurement every 20 minutes. The reliability of sensors measurements (16 unit) was assessed in the laboratory before installation and subsequently in the field after deployment (Figure. 6.S1 of the supplementary material). For this purpose, soil cores (100 cm^3) were periodically collected (soil depths of 0.0 – 0.10, 0.10-0.20 m) for measuring volumetric soil water contents (SWC). At the same time, disturbed soil samples were collected to determine soil salinity, which was assessed by measuring the electrical conductivity of a 1:5 soil-to-water extract ($EC_{1:5}$) and converting it to the EC_e (Sonmez et al., 2008) considering the texture (fine, medium fine) of soil horizons where sensors were installed, as follows:

$$EC_e = 7.36\, EC_{1:5} + 0.24 \quad (6.5)$$

In addition, Hydros 21 groundwater level sensors (Meter Group, USA) were installed at a depth of 2.0 m to monitor groundwater depth (GWD) next to the sensor Teros 12. In Cafine, GWD ranged from 0 to 1.89 m in tidal areas and 0 to 1.77 m in associated areas, with electrical conductivity (EC_{gw}) averaging 48.3 dS m^{-1} in tidal areas and 47.2 dS m^{-1} in associated areas. In Djobel, GWD ranged from 0 to 1.78 m and EC_{gw} averaged 17.7 dS m^{-1}. In Elalab, GWD ranged from 0 to 1.35 m, with an average EC_{gw} of 54.1 dS m^{-1}. Meteorological data including air temperature, relative humidity (RH), rainfall, solar radiation, and wind speed (u_2) were collected daily using Atmos 41 sensors (Meter Group, USA). The years 2022 and 2023 were characterized by high rainfall in Elalab and Djobel, while both years represented normal rainfall conditions in Cafine (Figure. 6.2).

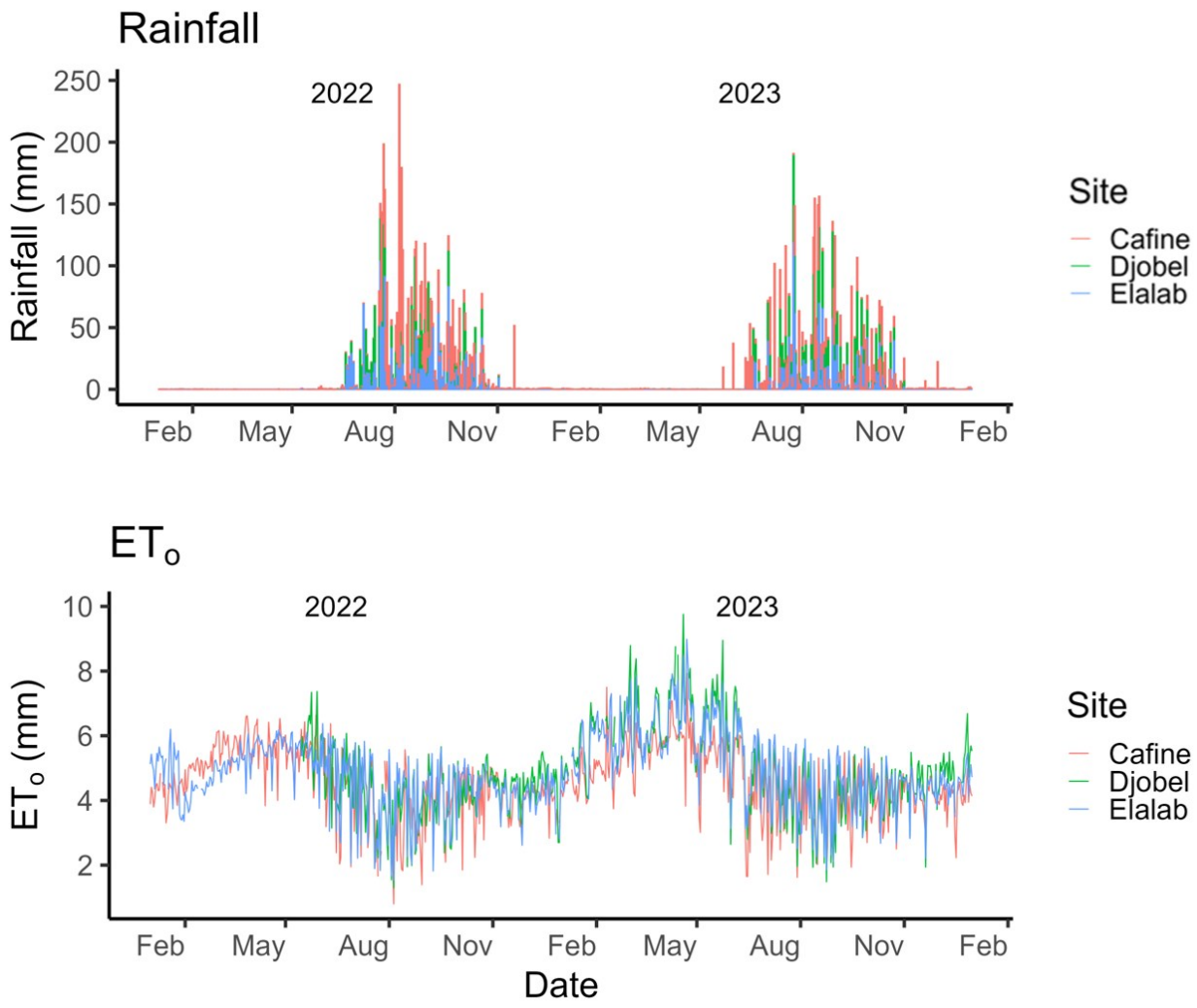

Figure. 6.2. Daily rainfall measurements and computed FAO-56 Penman Monteith reference evapotranspiration (ET_o) at the study sites.

The rice varieties Yakassau and Caublack were cultivated in Cafine, Edjur in Djobel, while in Elalab Yakai Tomor was used, as these were the varieties used by farmers in the fields where the sensors were installed. Table 6.2 outlines the crop growth stages for each variety, location, and growing season. Typically, the rice-growing season in the study areas extended from early August to late November, with the southern region having a longer growing period due to higher rainfall compared to the northern region. Rice transplanting generally began around the first week of September, with priority given to areas with fresher and more abundant clean water. However, the timing of

transplanting varied as farmers relied on traditional methods, such as salinity taste-testing, while also considering labor availability and optimization of waterlogging levels before planting. The most critical stages for rice growth occurred shortly after transplanting in early September and during the flowering and grain filling. The latter occurred in late October in the northern regions and mid-November in the southern areas, coinciding with the final period of the rainy season. This period is particularly important for key phenological stages such as flowering and grain filling, when the crop is most vulnerable to environmental stress, making it crucial to maintain minimal soil salinity levels during these times (Figure. 6.3). Lastly, during the late-season period the grains enter a drying phase, with harvest timings varying across villages, among varieties and availability of labor groups.

Table 6.2. Dates of the crop growth stages measured, and yield obtained at each site for the 2022 and 2023 seasons.

Site & Ecology	Rice variety	Year	Crop growth stages				Yield
			Initial	Crop development	Mid-season	Late-season	Average (kg ha^{-1})
Cafine	Yakasau	2022	28/09-09/10	10/10-16/11	17/11-02/12	03/12-15/12	1807
TM		2023	04/10-15/10	16/10-20/11	21/11-11/12	12/12-17/12	(± 21%)
Cafine	Caublack	2022	28/09-06/10	07/10-03/11	04/11-21/11	22/11-27/11	1750
AM		2023	20/09-01/10	02/10-06/11	07/11-27/11	28/11-07/12	(± 11%)
Djobel	Edjur	2022	20/09-01/10	02/10-30/10	31/10-16/11	17/11-22/11	2073
AM		2023	05/09-16/09	17/09-22/10	23/10-13/11	14/11-20/11	(± 8.2%)
Elalab	Tomor	2022	23/09-04/10	05/10-26/10	27/10-26/11	27/11-09/12	1703
AM		2023	15/09-26/09	27/09-31/10	01/11-30/11	01/12-12/12	(± 20%)

TM, tidal mangrove; AM, Associated mangrove.

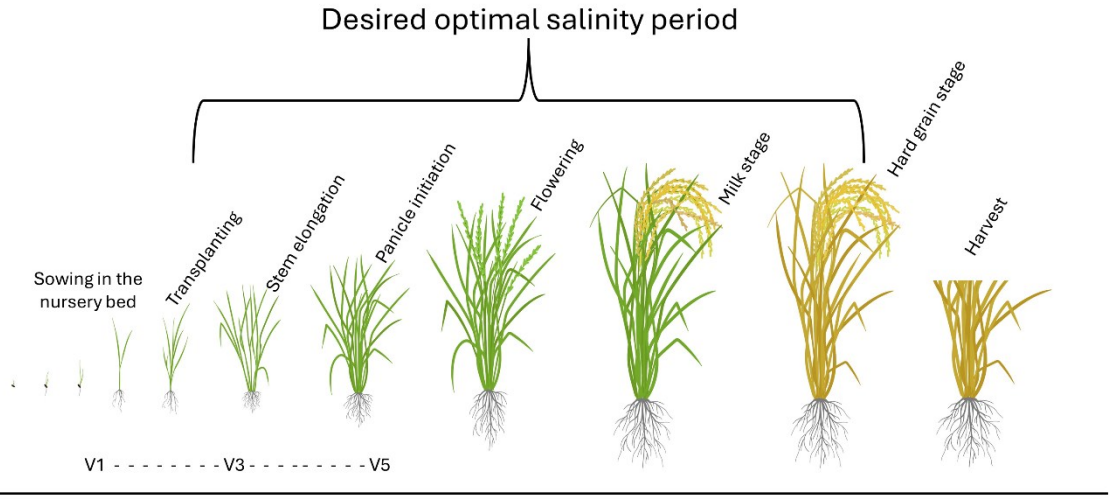

	Germination				Vegetative Growth					Reproductive				Ripening							
DOY	209	218	225	232	239	246	253	260	267	274	285	286	295	309	316	326	338	344	350	356	365
Week	4	1	2	3	4	1	2	3	4	1	2	3	4	1	2	3	4	1	2	3	4
Month	July	August				September				October				November				December			

*Doy =days of the year.

Figure. 6.3. The phenological stages of rice observed in the study sites during the 2022 and 2023 seasons.

3.2. Modeling approach

3.2.1. Model description

The HYDRUS-1D model (Šimůnek et al., 2016, 2024) was used to numerically simulate one-dimensional water flow and solute transport in variably-saturated porous media by solving the Richards and the Fickian-based convention-dispersion equation (CDE), respectively. The soil hydraulic properties were described by the Mualem-van Genuchten functional relationships (Mualem, 1976; van Genuchten, 1980), as follows:

$$S_e(h) = \frac{\theta(h)-\theta_r}{\theta_s-\theta_r} = \frac{1}{(1+|\alpha h|^{\eta})^m} \tag{6.6}$$

$$K(h) = K_s S_e^{\ell}\left[1-\left(1-S_e^{1/m}\right)^m\right]^2 \tag{6.7}$$

where Se is the effective saturation [-], h is the soil pressure head [cm], θ_r and θ_s represent the residual and saturated soil water contents [L^3 L^{-3}], respectively, α [L^{-1}] and

η [-] are empirical shape parameters, K_s is the saturated hydraulic conductivity [L T^{-1}], l is a parameter related to the pore connectivity/tortuosity [-], and m=1-1/η.

The sink term in the water flow equation is the root water uptake (RWU) and was formulated based on the macroscopic approach proposed by Feddes et al. (1978). In this approach, potential root water uptake (PRWU), which corresponds to potential crop transpiration (T_c, L T^{-1}), is distributed across the root zone. PRWU may be reduced by the presence of stress factors, such as water availability and salt content, thereby defining the actual water uptake rate by the roots, or the actual transpiration rate (T_c act, L T^{-1}). In the model proposed by Feddes et al. (1978), water uptake by the roots occurs at the potential rate when the soil pressure head h is between h2 and h3, decreases linearly when h > h2 and h < h3, and becomes zero when h > h1 and h < h4 (subscripts 1 to 4 represent different pressure thresholds). On the other hand, root water uptake reductions due to salinity stress are described with the threshold and slope function proposed by Maas (1990). According to this function, water uptake is at its maximum when the EC_e is below the crop's salinity tolerance threshold (EC_e threshold, dS m^{-1}). Above this threshold, water uptake decreases linearly with increasing salinity, at a rate determined by a specific slope (s, % per dS m^{-1}). Both reduction functions were combined under the assumption that the effects of water and salinity stress are multiplicative (van Genuchten, 1997). Soil salinity was represented by the EC_{sw}, which was simulated in the CDE model as a non-reactive tracer. The model assumes a conversion factor of EC_{sw} / EC_e = 2.

For each site, the crop water-yield linear function proposed by Doorenbos and Kassam, (1979) was further applied to evaluate the impact of soil water and salinity stresses on crop yields, as follows:

$$\left(1 - \frac{Y_a}{Y_m}\right) = K_y \left(1 - \frac{ET_{c\ act}}{ET_c}\right) \quad (8)$$

where Y_a and Y_m are the actual and maximum crop yields [tonnes ha^{-1}], respectively; $ET_{c\ act}$ and ET_c are the actual and potential seasonal crop evapotranspiration [mm], respectively; and K_y is the yield response factor describing the reduction in relative yield due to the relative reduction in ET caused by soil water and salinity stresses.

3.2.2. Model setup, calibration, and validation

The soil water contents and fluxes and salt transport in the four case studies during the 2022 and 2023 growing seasons were modelled with HYDRUS-1D. For each season, simulations run from May 15th (day 1) to December 31th (day 231). At each location, the soil domain was modelled as a 1D column with a depth of 2.0 m, discretized into 101 nodes. Initial conditions were set by the SWC and EC_{sw} measurements at different depths the start of the rice-growing season.

The upper boundary conditions were defined by soil evaporation (E_s), and rainfall (rice fields are not irrigated), while the bottom boundary condition was set as the measured GWD. Daily weather data were used to calculate the reference evapotranspiration (ET_o, mm) using the FAO56 Penman-Monteith equation (Allen et al., 1998). The crop evapotranspiration (ET_c) was then computed using the crop coefficients (K_c) proposed by Pereira et al., (2021) for rice (flooded - anticipated cut-off), with values of 1.05 for the initial stage, 1.20 for the mid-season stage, and 0.80 for the end-season stage. A dual K_c approach ($K_c = K_{cb} + K_e$) was used for ET_c partitioning, with the T_c component calculated using the basal crop coefficient (K_{cb}) for each growth stage, as proposed by Pereira et al. (2021), and the Es component, computed as $E_s = ET_c - T_c$. The K_{cb} values for the initial, mid-season, and end-season stages were 0.15, 1.15, and 0.70, respectively. The K_c and K_{cb} values were corrected for local climate conditions of relative

humidity and wind velocity (RH and u_2) and crop height following the FAO56 procedure (Allen et al., 1998).

For root water uptake, T_c reductions due to water stress were calculated using the parameters h1= 100 cm, h2= 55 cm, h3=−160 to −250 cm, and h4=−15000 cm (Li et al., 2014). T_c reductions due to salt stress considered a EC_e threshold of 3.0 dS m^{-1}, and a s rate value of 12% per dS m^{-1} (Minhas et al., 2020), with these parameters applied throughout the entire crop season. For assessment of yield impacts, the K_y value was set to 1.25 (Monteiro et al., 2013), also for the entire crop season. The root depth was determined to vary between 0.3 and 0.5 m, depending on the location, as measured in the field.

The calibration process involved adjusting the simulated SWC and ECsw values to the correspondent daily observations at different depths (0.07, 0.15, 0.25 and 0.35 m) using the numerical inversion procedure proposed by Šimůnek and van Genuchten (1996). The calibration parameters were the soil hydraulic parameters (θr, θs, α, η, Ks) and soil dispersivity (λ). Weighting coefficients for the different data points in the objective function were assumed to be 1 (González et al., 2015). The parameter l was set to 0.5 (Mualem, 1976). Calibration was carried out sequentially for each layer, iterating through all four layers and restarting the process until the deviations between the measured and simulated data were minimized and stabilized. Ultimately, to improve model fitting, the Ks and λ parameters underwent additional manual tunning. For each location, the 2023 experimental dataset was used for model calibration, while model validation was conducted using the calibrated parameters and the 2022 datasets.

The goodness-of-fit indicators used to evaluate the accuracy of model simulations were: The coefficient of determination (R2), that measures the proportion of variance explained by the model, with values close to 1 indicating a high degree of linear fit (Taylor, 1990). The mean absolute error (MAE) and the root mean square error (RMSE) that quantify the average deviation between the measured and model-predicted values (Plevris et al., 2022). MAE provides a direct measure of error, while RMSE penalizes larger errors more heavily, providing sensitivity to the model's performance (Hodson, 2022; Steurer et al., 2021). Moreover, the normalized RMSE (NRMSE) was calculated to compare the relative error to the mean of the observation. Additionally, the BIAS was evaluated, serving as an indicator to both the direction and magnitude of systematic error. Similarly, the percentage Bias (PBIAS) was computed, to estimate the predictions' tendency (Montgomery and Runger, 2011). A negative PBIAS value reflects an underestimation, while positive values indicate overestimation of predicted data (Huber and Ronchetti, 2009). The goodness-of-fit indicators were calculated as follows:

$$R^2 = 1 - \frac{\sum_{i=1}^{n}(O_i - P_i)^2}{\sum_{i=1}^{n}(O_i - \bar{O})^2} \quad (9)$$

$$MAE = \frac{1}{n}\sum_{i=1}^{n}(O_i - P_i) \quad (10)$$

$$RMSE = \sqrt{\frac{1}{n}\sum_{i=1}^{n}(O_i - P_i)^2} \quad (11)$$

$$NRMSE = \frac{RMSE}{\bar{O}} \cdot 100 \quad (12)$$

$$BIAS = \frac{1}{n}\sum_{i=1}^{n}(P_i - O_i) \quad (13)$$

$$PBIAS = 100 \cdot \frac{\sum_{i=1}^{n}(P_i - O_i)}{\sum_{i=0}^{n} O_i} \quad (14)$$

where O_i and P_i represent the observed and the model-predicted values, respectively, $\bar{O}$ is the mean of the observations.

Metrics were computed using R software version 2024.04.1 (R Core Team, 2024). For soil salinity, the EC_e served as reference for computing the goodness-of-fit indicators and analysis of results.

3.3. Modeling scenarios

For each study site, two GWD and three rainfall scenarios were considered, in order to evaluate their impacts on soil salinity and rice growth. The scenario analysis focused on the following aspects:

- ✓ EC_e levels throughout the simulation, with particular attention to the growing season.
- ✓ The number of days in the year when EC_e remained below the $EC_{e\ threshold}$.
- ✓ Impacts of soil salinity on crop transpiration ($1 - T_{c\ act} / T_c$) and crop yields ($1 - Y_a / Y_m$).

- ✓ The window of opportunity for growing rice, defined as the salt-free period (Guei et al., 1997).
- ✓ Identification of sites where cultivation is feasible only with salt-tolerant rice varieties.

The first GWD scenario reflected field conditions observed from sensor measurements in 2023. According to the site, initial GWDs ranged from 1.35 to 1.89 m. As the soil became saturated, these depths gradually became shallower, and a water layer was formed at the soil surface. The second GWD scenario simulated a shallower GWD, representing conditions typically associated with dike breaches or saltwater infiltration, often caused by inadequate maintenance or significant tidal events. In this case, the initial GWD was set at 0.5 m and progressively rose to the soil surface with the onset of the rainy season.

The three rainfall scenarios were based on historical daily rainfall data from the AgERA5 dataset, provided by the European Center for Medium-Range Weather Forecasts (ECMWF) platform, part of the Copernicus project (Boogaard et al., 2020). Rainfall data from 1979 to 2023 were analyzed, focusing on the centroid (pixel) closest to the meteorological station used in this study. Calibration was performed by comparing rainfall data from 2021 to 2023 using several correction schemes, including simple bias correction, slope correction, and linear scaling correction (Teutschbein and Seibert, 2012). The linear scaling correction proved to be the most effective, with a 90-day correction period (Figure. 6.S2 of the supplemental material). This method was applied to the rainfall datasets, leading to the selection of three distinct rainfall scenarios corresponding to the 20th (low), 50th (medium) and 80th (high) percentiles of total annual rainfall for each year. The corresponding years for each scenario were as follows: for Cafine, 1995, 1980, and 2018; for Djobel, 1980, 1988, and 1995; for Elalab, 1994, 1979, and 2000, respectively (Figure. 6.4).

Full meteorological reanalysis data for these years were also downloaded to calculate ET_o using the FAO56 Penman-Monteith method (Allen et al., 1998). A simple BIAS correction was then applied, calibrated, and validated for Guinea-Bissau (Garbanzo et al., 2025b). This data was subsequently used for calculating ET_c and the soil water balance following the same methodological approach outlined above. Crop growth data for the main rice varieties in each village were also considered (Table 6.2).

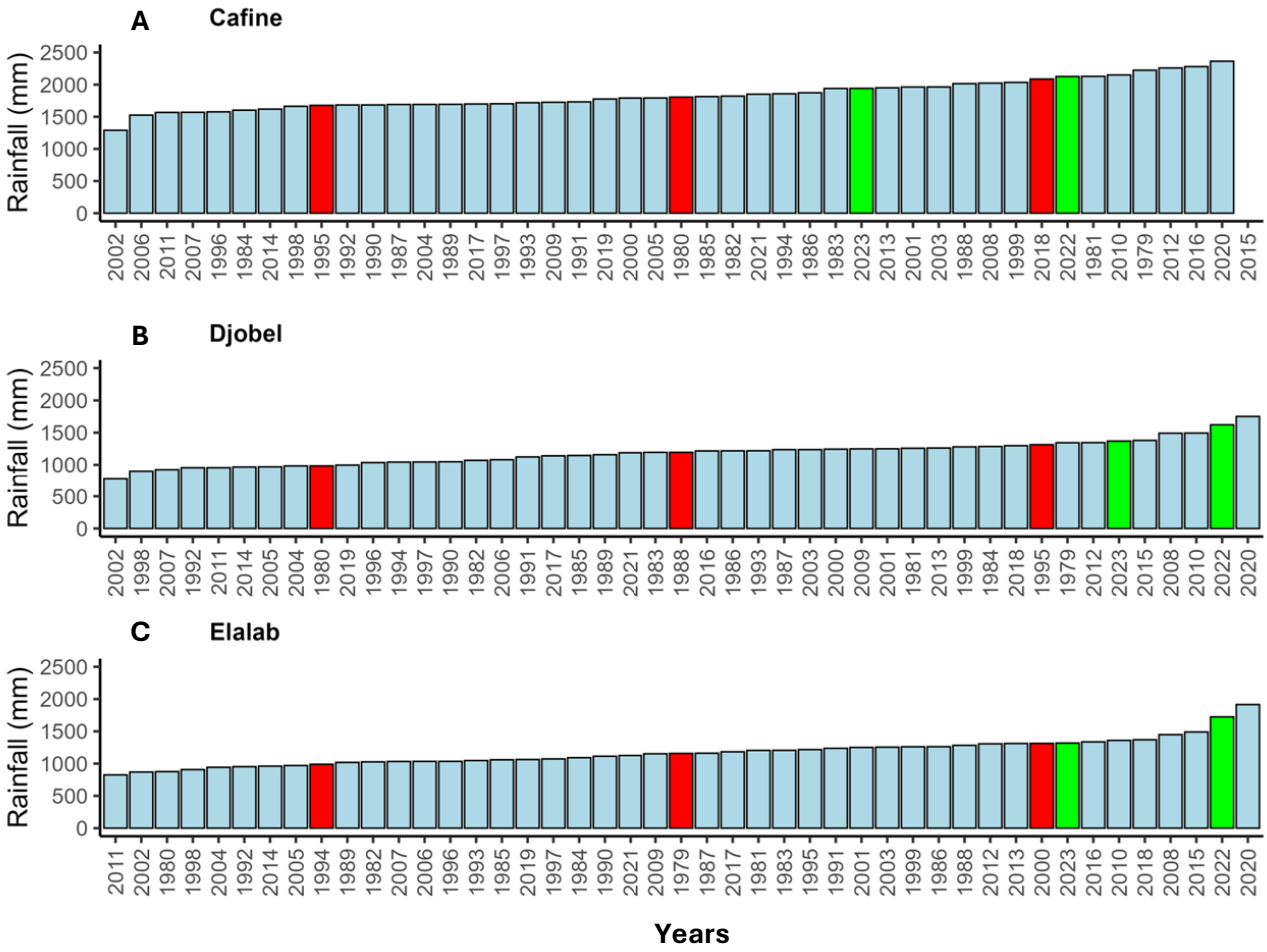

Figure. 6.4. Rainfall scenarios in Cafine (A), Elalab (B), and Djobel (C) based on AgERA 5 reanalysis data.

4. *Results* and discussion

4.1. Model performance

Figure. 6.5 presents the measured and simulated SWC for four study sites, with the calibrated parameters detailed in Table 6.3. For all sites, initial SWC values were low but increased with the onset of the rainy season. Eventually, SWC reached saturation, forming a surface water layer that created favorable conditions for rice transplanting and growth. SWC remained close to saturation until the end of the rainfall season, after which they decreased at most sites, facilitating grain drying and harvesting. The Elalab site was an exception to this pattern, since the SWC values in the upper soil layers declined before the transplanting period. This anomaly can be explained by farming operations that were taking place at the time, which probably changed the soil physical properties in the monitored area and affected sensor readings. According to the observations, soil compaction may have reduced saturation values. Despite this, SWC remained relatively stable for the rest of the growing season, suggesting that Elalab's conditions were like those in the other fields, with SWC near saturation and the formation of a surface water layer. Therefore, data from Elalab were retained in the study.

The HYDRUS-1D model effectively simulated measured values during both the calibration and validation periods, as indicated by the goodness-of-fit metrics presented in Table 6.4. Across all sites, the R^2 values exceeded 0.97, demonstrating that the model was able to explain most of the variance of measured data. The MAE and RMSE ranged from 0.015 to 0.082 $m^3\ m^{-3}$ and 0.027 to 0.099 $m^3\ m^{-3}$, respectively. NRMSE values were generally low. Nevertheless, the highest estimation errors were consistently measured at the Elalab site, likely due to the issues discussed earlier. BIAS and PBIAS values were near zero at all sites, indicating no significant over- or underestimation of measured

values, except at Elalab. Thus, despite variations in model fit quality, consistent trends were measured across all four study sites for all goodness-of-fit indicators during both calibration and validation periods, suggesting the model achieved a robust overall performance.

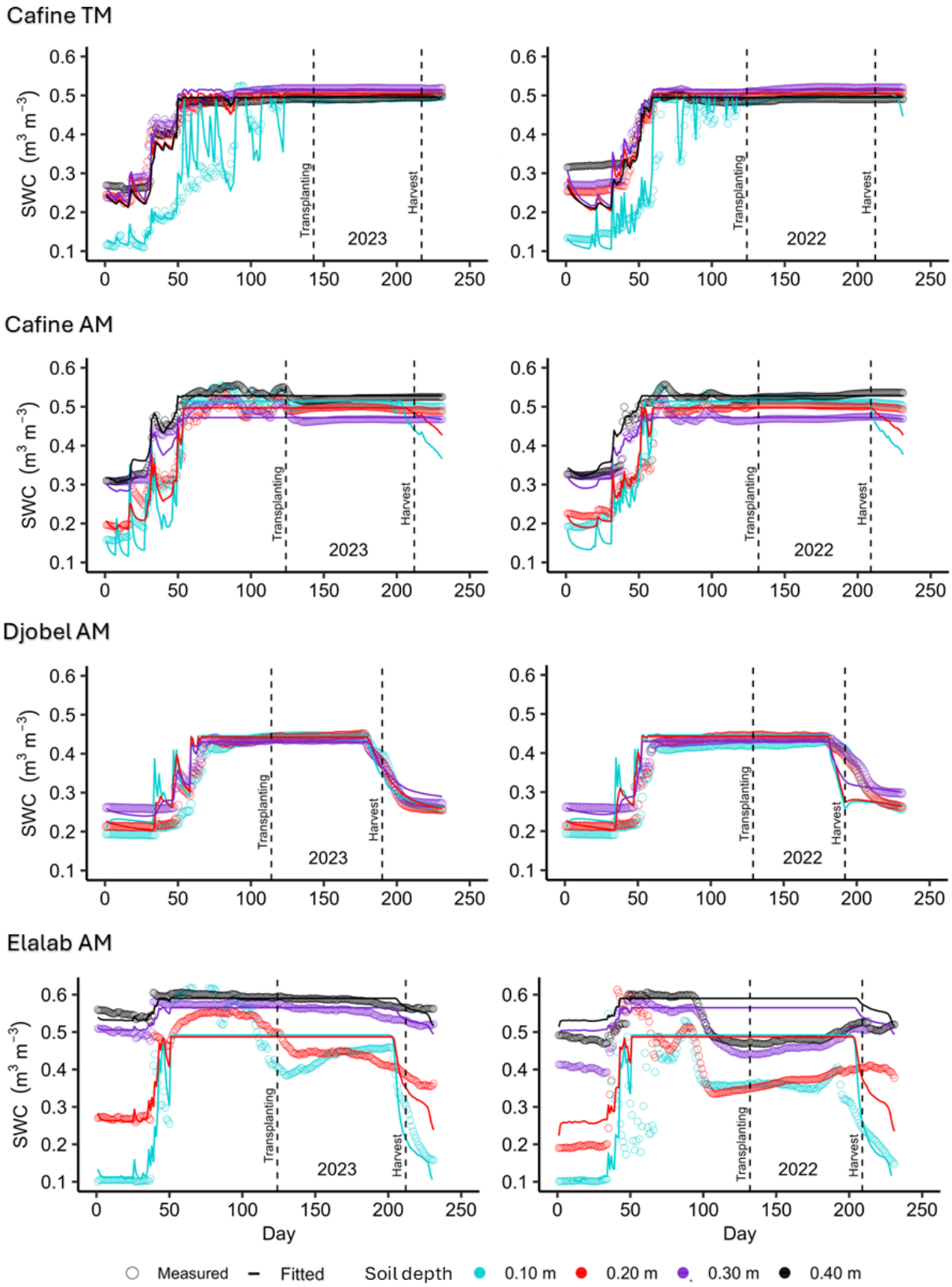

Figure. 6.5. Measured and simulated soil water contents (SWC) in the four study sites during 2023 (calibration) and 2022 (validation). TM, tidal mangrove; AM, Associated mangrove.

Table 6.3. Calibrated soil hydraulic and solute transport parameters.

Village	Soil Depth (m)	θ_r ($m^3\ m^{-3}$)	θ_s ($m^3\ m^{-3}$)	α (cm^{-1})	η (-)	K_s ($cm\ d^{-1}$)	λ (cm)
Cafine TM	0.0 – 0.1	0.070	0.505	0.045	2.45	36.1	15
	0.1 – 0.2	0.090	0.505	0.021	2.60	78.0	60
	0.2 – 0.3	0.095	0.515	0.024	2.50	190.0	90
	0.3 – 0.4	0.095	0.495	0.045	1.90	106.0	90
Cafine AM	0.0 – 0.1	0.004	0.514	0.039	1.55	32.5	55
	0.1 – 0.2	0.064	0.497	0.031	1.59	78.0	55
	0.2 – 0.3	0.090	0.472	0.010	1.65	12.0	60
	0.3 – 0.4	0.004	0.528	0.009	1.60	5.1	60
Djobel AM	0.0 – 0.1	0.088	0.446	0.020	1.35	6.0	40
	0.1 – 0.2	0.098	0.443	0.013	1.60	8.1	40
	0.2 – 0.3	0.091	0.430	0.022	1.38	3.6	45
Elalab AM	0.0 – 0.1	0.006	0.492	0.025	2.40	374.0	35
	0.1 – 0.2	0.008	0.487	0.020	1.75	203.0	60
	0.2 – 0.3	0.054	0.565	0.010	1.25	316.0	90
	0.3 – 0.4	0.050	0.590	0.008	1.38	49.0	90

TM, tidal mangrove; AM, Associated mangrove; θ_r and θ_s, residual and saturated water contents, respectively; α and η, empirical shape parameters; K_s, saturated hydraulic conductivity; ℓ, pore connectivity/tortuosity parameter; λ, soil dispersivity.

Table 6.4. Goodness-of-fit for the comparison of measured and simulated soil water contents at the four study sites.

Study sites	R^2 (-)	MAE ($m^3\ m^{-3}$)	RMSE ($m^3\ m^{-3}$)	NRMSE (%)	BIAS (-)	PBIAS (%)
Calibration (2023)						
Cafine TM	0.99	0.016	0.027	6.18	-0.01	-0.33
Cafine AM	0.99	0.019	0.029	6.31	0.01	1.57
Djobel AM	0.99	0.017	0.031	8.56	-0.01	-3.07
Elalab AM	0.99	0.031	0.046	9.42	-0.01	-0.77
Validation (2022)						
Cafine TM	0.99	0.016	0.030	6.72	0.01	0.25
Cafine AM	0.99	0.015	0.028	6.07	0.01	0.72
Djobel AM	0.99	0.025	0.040	10.93	-0.01	-1.31
Elalab AM	0.97	0.082	0.099	20.52	-0.06	-12.8

TM, tidal mangrove; AM, Associated mangrove; R^2, coefficient of determination; MAE, mean absolute error; RMSE, root means square error; NRMSE, normalized root mean square error; PBIAS, percent Bias.

Similarly, HYDRUS-1D simulations effectively captured the overall trend of soil salinization across the study sites, with high EC_e values at the beginning of the rainy season gradually decreasing to levels more suitable for rice cultivation (Figure. 6.6). The goodness-of-fit indicators were satisfactory (Table 6.5), with R^2 values consistently above 0.82. The MAE and RMSE values exhibited large variation in the four study sites, ranging from 0.39 to 4.01 dS m^{-1} and 0.49 to 5.72 dS m^{-1}, respectively. At the Elalab site, as expected, the poorer fit of the model to measured SWC data also affected EC_e simulations, leading to higher estimation errors. However, the model successfully captured the same trends of field data. There was a consistent tendency to underestimate measured EC_e values across all study sites, as indicated by the negative BIAS and PBIAS values.

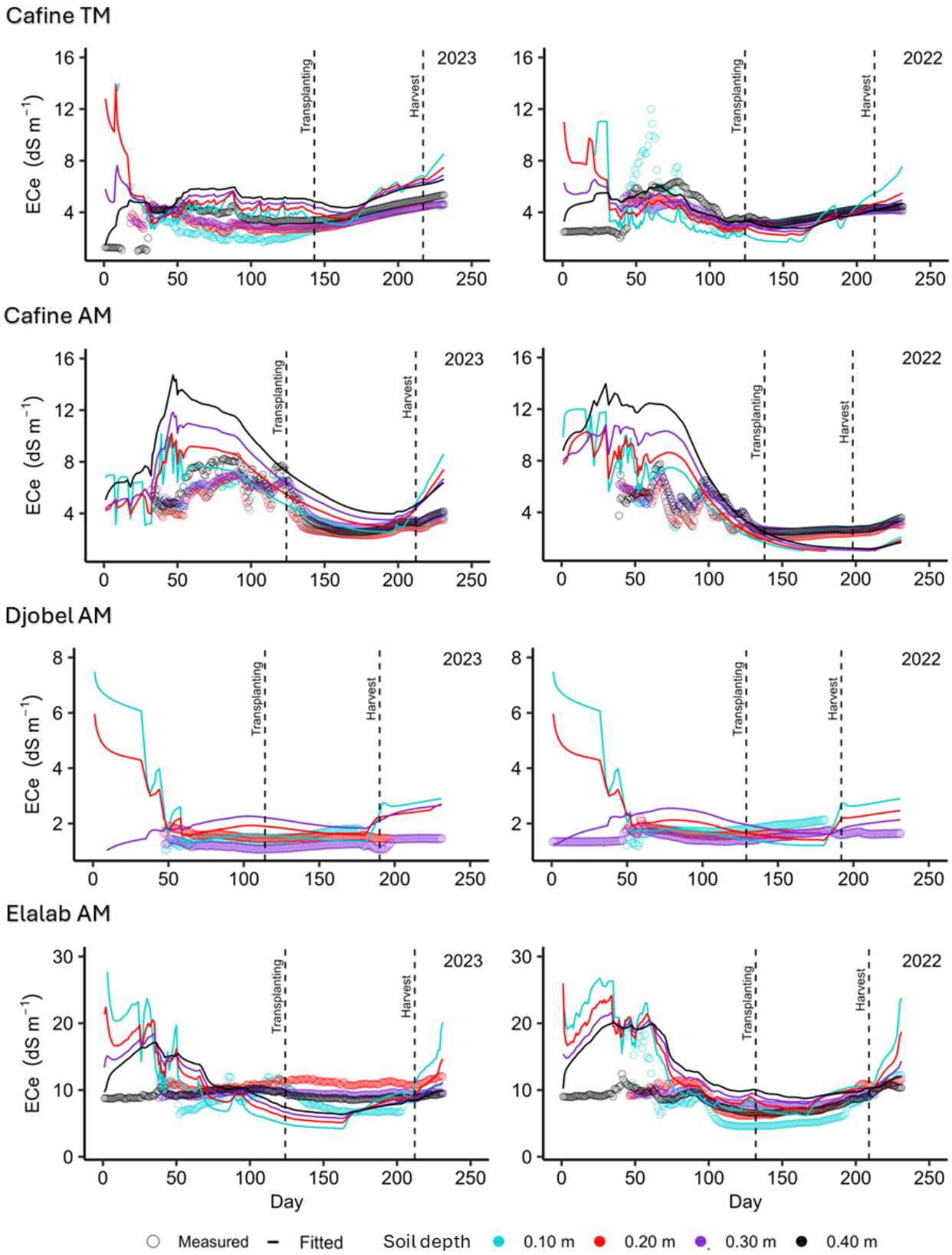

Figure. 6.6. Measured and simulated values of electrical conductivity of the saturation paste extract (EC_e) at the four study sites during 2023 (calibration) and 2022 (validation). TM, tidal mangrove; AM, Associated mangrove.

Table 6.5. Goodness-of-fit for the comparison of measured and simulated values of the electrical conductivity of the saturation paste extract (EC_e) at the four study sites.

Study sites	R^2 [-]	MAE [dS m^{-1}]	RMSE [dS m^{-1}]	NRMSE [%]	BIAS [-]	PBIAS [%]
Calibration (2023)						
Cafine TM	0.95	1.50	1.68	34.84	-1.42	-29.41
Cafine AM	0.94	2.06	2.70	41.88	-1.98	-30.69
Djobel AM	0.93	0.52	0.65	35.79	-0.47	-25.93
Elalab AM	0.90	4.01	5.72	46.26	-3.96	-32.96
Validation (2022)						
Cafine TM	0.92	0.77	1.20	32.34	0.28	7.56
Cafine AM	0.82	1.88	2.57	62.37	-0.51	-12.48
Djobel AM	0.93	0.39	0.49	27.41	-1.88	-10.34
Elalab AM	0.85	3.23	4.09	42.34	-0.21	-0.209

TM, tidal mangrove; AM, Associated mangrove; R^2, coefficient of determination; MAE, mean absolute error; RMSE, root means square error; NRMSE, normalized root mean square error; PBIAS, percent Bias.

The HYDRUS-1D model has been widely used to evaluate irrigation water management in paddy fields (Li et al., 2015, 2014; Mo'allim et al., 2018; Shekhar et al., 2020), but few studies so far have focused on salinity management (Phogat et al., 2010). Additionally, the model has been extensively applied to soil salinity management in various agricultural systems with shallow saline groundwater conditions (Forkutsa et al., 2009; Guo et al., 2024; Karimov et al., 2014; Ramos et al., 2023), which may partially resemble those in the study areas. While these applications have provided valuable insights into addressing various management challenges, the modeling approach typically used, simulating EC_{sw} as a non-reactive tracer, remains relatively simplistic.

As a result, deviations between model results and observations may become more pronounced when omitted processes become relevant. In this study, model performance was generally acceptable across all sites. However, a closer analysis of Figure. 6.6 reveals larger deviations between model results and measured data across all sites during the non-

growing season compared to the growing period. Simulated EC_e values were generally higher than the measured data, suggesting that precipitation and dissolution processes, which were not accounted for in the modeling approach, may have played a significant role during the dry period. Salt precipitation, influenced by both rainfall water and soil chemistry, affects soil-solution salinity. In arid regions, calcite precipitation often occurs during irrigation at low leaching fractions, reducing the salt load by 5–25% at the bottom of the root zone and lowering EC_{sw} throughout most of the root zone, except for the upper layer. When irrigation water contains elevated concentrations of sulfate and calcium, gypsum precipitation can also significantly reduce root zone EC_{sw} (Hopmans et al., 2021; Letey et al., 2011). Although the study sites were not irrigated, the dry conditions that led to salt accumulation in the soil profile during the non-growing season further promoted salt precipitation, as observed in situ (Garbanzo et al., 2024b; Merkohasanaj et al., 2025).

An additional factor reducing EC_{sw} below the levels predicted by simulation models during the non-growing season dry period is the nonlinearity between water EC and actual salt concentration (Letey et al., 2011). While the EC-to-salt concentration ratio decreases with increasing concentration, the model keeps assuming a EC_{sw} increase as SWCs decrease (Ramos et al., 2011). Further issues related to conversion factors include the $EC_{sw}/EC_e = 2$ relationship used in HYDRUS-1D. This ratio, based on a common approximation for soil water contents near field capacity in medium-textured soils, may vary for soils with different textures and moisture levels (Skaggs et al., 2006), such as the dry condition observed at the beginning of the simulation period and the saturated conditions measured later during the growing season. Moreover, this relationship differs from those used for converting soil sensor data, potentially introducing inconsistencies when comparing measured and simulated datasets.

Lastly, as in any modeling application, goodness-of-fit depends on the quality of the measured data. In extremely dry conditions, sensors used to measure SWC and EC_b may be less reliable (Corwin and Lesch, 2005). Water is the primary medium for electrical current conduction, and ion mobility is also significantly reduced at lower SWCs. Additionally, the relationship between SWC and EC_b becomes highly nonlinear outside the sensor's calibration range, complicating the accurate interpretation of sensor data. Furthermore, in dry soils, the contact between electrodes and the soil is less effective, increasing electrical resistance at the interface and resulting in inaccurate readings.

4.2. Salinity impact on rice yields

Table 6.6 summarizes the soil water balance for the four study sites during the 2022 and 2023 rice growing seasons, calculated using HYDRUS-1D. It also details the estimated effects of osmotic stress on crop transpiration rates and their subsequent impacts on rice yields. Precipitation is reported for the pre-season (from the start of simulations to the transplanting date at each site and growing season) and the growing season itself. Because plots are surrounded by bunds, which allow for the full capture and retention of rainwater, total precipitation is considered to be effectively harvested and used within the system. However, due to the characteristics of MSRP systems, the soil water balance for the growing season includes infiltrated water as an input, as water may originate during the pre-season, instead of the effective precipitation term typically used in soil water balance analyses. The soil water balance closing errors are small, ranging from 0.0% (Elalab AM field, 2022) to 3.31% (Elalab AM fields, 2023), being primarily due to rounding in intermediate calculations.

As shown in Section 3.1, soil salinity in the monitored sites tends to increase significantly during the dry season as salts are transported upwards from the saline

groundwater table due to high soil evaporation. In tidal areas, salinity further increases when the soil surface is temporarily submerged by seawater. With the onset of the rainy season, soil salinity in the rice fields decreases to levels suitable for cultivation. Longer rainy seasons and greater rainfall enhance the leaching of salt from surface layers, creating favorable conditions for rice growth.

Djobel AM fields exhibited the most favorable conditions for rice cultivation during both years. This site is located further away from the coast (Figure. 6.1) and recorded the lowest EC_{gw} values (17.7 dS m^{-1}) compared to the other sites. Despite the high silt content in the soils, which can hinder salt leaching, the substantial rainfall both before the growing season (1,003–1,325 mm) and during the growing season (362–242 mm) efficiently leached salts and maintained EC_e values below the defined threshold (3.0 dS m^{-1}) during both growing periods. Therefore, root water uptake and rice yields were unaffected by osmotic stress.

In Cafine, salt dynamics differed significantly between tidal and associated areas. Initial EC_e and EC_{gw} values were slightly higher in the tidal area compared to the associated area. In 2022, higher rainfall (>2,600 mm) was sufficient to leach salts from the associated area but not the tidal area, primarily due to higher infiltration rates in the associated area. Additionally, from the middle of the growing season onward (Figure. 6.6), significant capillary rise fluxes in the tidal area caused salts to move upward into the root zone, adversely affecting crop yields. In 2023, lower rainfall levels led to reduced pre-season leaching in both areas. While the amount of infiltrated water during the growing period was comparable to the previous year, the reduced pre-season rainfall was less effective at removing salts, further impacting crop yields.

Elalab exhibited the most challenging conditions for rice cultivation. The GWD was shallower (0–1.35 m) and more saline (ECgw of 54.1 dS m^{-1}) compared to other sites. Despite substantial rainfall both before (1,091–1,508 mm) and during (282–366 mm) each growing season, along with sandy soils that could potentially promote drainage, the rainfall was insufficient to lower root-zone EC_e values below the defined threshold (3.0 dS m^{-1}) in either growing period. As a result, root water uptake was significantly affected, leading to an estimated yield reduction of 44% to 60% compared to rice grown under optimal conditions.

Table 6.6. Soil water balanced during the 2022 and 2023 rice growing season.

Villages	P		Growing season									
	P_{NGS}	P_{GS}	I	CR	ΔSS	T_c	$T_{c\ act}$	E_s	DP	$1-T_{c\ act}/T_c$	$1-ET_{c\ act}/ET_c$	$1-Y_a/Y_m$
	[mm]		[mm]							[-]		
Cafine TM												
2022	2376	287	337	210	0	249	223	128	197	0.11	0.07	0.09
2023	1419	442	309	141	0	241	176	114	168	0.27	0.18	0.23
Cafine AM												
2022	2314	339	800	0	0	217	216	106	498	0.01	0.01	0.01
2023	1393	467	722	6	4	267	231	119	386	0.13	0.09	0.12
Djobel AM												
2022	1325	242	529	1	50	217	216	106	272	0.00	0.00	0.00
2023	1003	363	694	18	25	267	267	124	355	0.00	0.00	0.00
Elalab AM												
2022	1508	282	316	87	39	290	151	100	191	0.48	0.36	0.44
2023	1091	366	369	91	47	312	102	127	295	0.67	0.48	0.60

TM, tidal mangrove; AM, Associated mangrove; P, precipitation; P_{NGS}, precipitation in non-growing season; P_{GS}, precipitation in growing season; I, Infiltration; CR, capillary rise; T_c, potential crop transpiration; $T_{c\ act}$, actual crop transpiration; E_s, soil evaporation; DP, deep drainage, ΔSS, variation in soil water storage; ET_c, potential crop evapotranspiration, $ET_{c\ act}$, actual crop evapotranspiration; Y_a, actual yield; Y_m, maximum yield.

4.3. Rainfall and groundwater depth scenarios

Table 6.7 summarizes the results of modeling scenarios that account for low, medium, and high rainfall seasons, as well as shallow and observed GWD conditions. Table 6.7 presents the mean rootzone electrical conductivity (EC_e mean) during the growing season, the number of days with EC_e below the salinity tolerance threshold (3.0 dS m^{-1}) for both the growing season and the entire simulation period, and the relative effects of soil salinity on crop evapotranspiration rates and crop yields. For all the scenarios, the most adverse conditions consistently occurred with lower seasonal rainfall and shallower GWD.

Consistent with field monitoring results, Djobel demonstrated the most favorable conditions for rice production in every scenario since the EC_e mean generally remained below the salinity tolerance threshold. Furthermore, in cases where EC_e exceeded the defined threshold (low and medium rainfall with shallow GWD scenarios), the impacts on crop yields were minimal (<6%). Although rainfall distribution and root water uptake significantly influence these outcomes, it is reasonable to assume that under the measured GWD conditions, the salt-free period could be extended. This extension may allow for earlier rice transplantation, anticipating the growing season to mitigate potential salinity issues at its end (Figure. 6.7). However, under shallow GWD conditions, this strategy may fail, as the salt-free period might be shorter than the period used to define the growing season. In the worst-case scenario (low rainfall and shallow GWD), no salt-free period occurs, though, as noted, the impacts on crop yields remain minimal.

In the Cafine AM site, conditions for rice cultivation were acceptable for most scenarios. Although only the most favorable scenario exhibited a mean EC_e below the

salinity tolerance threshold and a salt-free period extending beyond the growing season (Figure. 6.S3, supplemental material), the impacts on crop yields were relatively minor (<10%) in most scenarios, except under the worst-case conditions (low and medium rainfall with shallow GWD). In contrast, scenarios for the Cafine TM site consistently failed to provide satisfactory conditions for rice cultivation (Figure. 6.S4, supplemental material), with yield reductions ranging from 19% to 46%. At the Elalab site (Figure. 6.S5, supplemental material), conditions were even more unfavorable, with estimated yield reductions ranging from 58% to 82%.

Table 6.7. Estimated salt-free period for different rainfall (low, medium, and high) and groundwater depth (shallow and measured GWD) scenarios and corresponding impacts on crop yields ($EC_{e\ threshold}$ = 3.0 dS m^{-1}).

Scenarios	$EC_{e\ mean}$ [dS m^{-1}]	Nº Days $EC_e < EC_{e\ threshold}$		$1-T_{c\ act}/T_c$ [-]	$1-ET_{c\ act}/ET_c$ [-]	$1-Y_a/Y_m$ [-]
		Growing season	Simulation period			
Cafine TM						
Low rainfall x $GWD_{observed}$	5.2	0	0	0.28	0.20	0.25
Low rainfall x $GWD_{shallow}$	7.6	0	0	0.53	0.37	0.46
Medium rainfall x $GWD_{observed}$	4.8	0	0	0.22	0.16	0.19
Medium rainfall x $GWD_{shallow}$	6.8	0	0	0.43	0.30	0.38
High rainfall x $GWD_{observed}$	4.3	0	0	0.21	0.15	0.19
High rainfall x $GWD_{shallow}$	6.1	0	0	0.42	0.29	0.37
Cafine AM						
Low rainfall x $GWD_{observed}$	5.1	0	0	0.22	0.16	0.20
Low rainfall x $GWD_{shallow}$	8.1	0	0	0.48	0.34	0.43
Medium rainfall x $GWD_{observed}$	4.2	0	0	0.11	0.08	0.10
Medium rainfall x $GWD_{shallow}$	6.7	0	0	0.37	0.26	0.33
High rainfall x $GWD_{observed}$	2.7	55	82	0.07	0.05	0.07
High rainfall x $GWD_{shallow}$	4.5	0	0	0.18	0.13	0.16
Djobel AM						
Low rainfall x $GWD_{observed}$	2.4	69	129	0.01	0.01	0.01
Low rainfall x $GWD_{shallow}$	3.9	0	0	0.07	0.05	0.06
Medium rainfall x $GWD_{observed}$	2.0	76	142	0.00	0.00	0.00
Medium rainfall x $GWD_{shallow}$	3.1	45	45	0.02	0.02	0.02
High rainfall x $GWD_{observed}$	1.8	78	153	0.00	0.00	0.00
High rainfall x $GWD_{shallow}$	2.7	64	64	0.01	0.01	0.01
Elalab AM						
Low rainfall x $GWD_{observed}$	10.3	0	0	0.74	0.55	0.69
Low rainfall x $GWD_{shallow}$	11.5	0	0	0.88	0.65	0.82
Medium rainfall x $GWD_{observed}$	8.9	0	0	0.63	0.47	0.58
Medium rainfall x $GWD_{shallow}$	15.4	0	0	0.80	0.59	0.74
High rainfall x $GWD_{observed}$	8.6	0	0	0.66	0.50	0.62
High rainfall x $GWD_{shallow}$	9.8	0	0	0.83	0.62	0.77

TM, tidal mangrove; AM, Associated mangrove; $EC_{e\ mean}$, mean EC_e in the rootzone; T_c, potential crop transpiration; $T_{c\ act}$, actual crop transpiration; ET_c, potential crop evapotranspiration, $ET_{c\ act}$, actual crop evapotranspiration; Y_a, actual yield; Y_m, maximum yield.

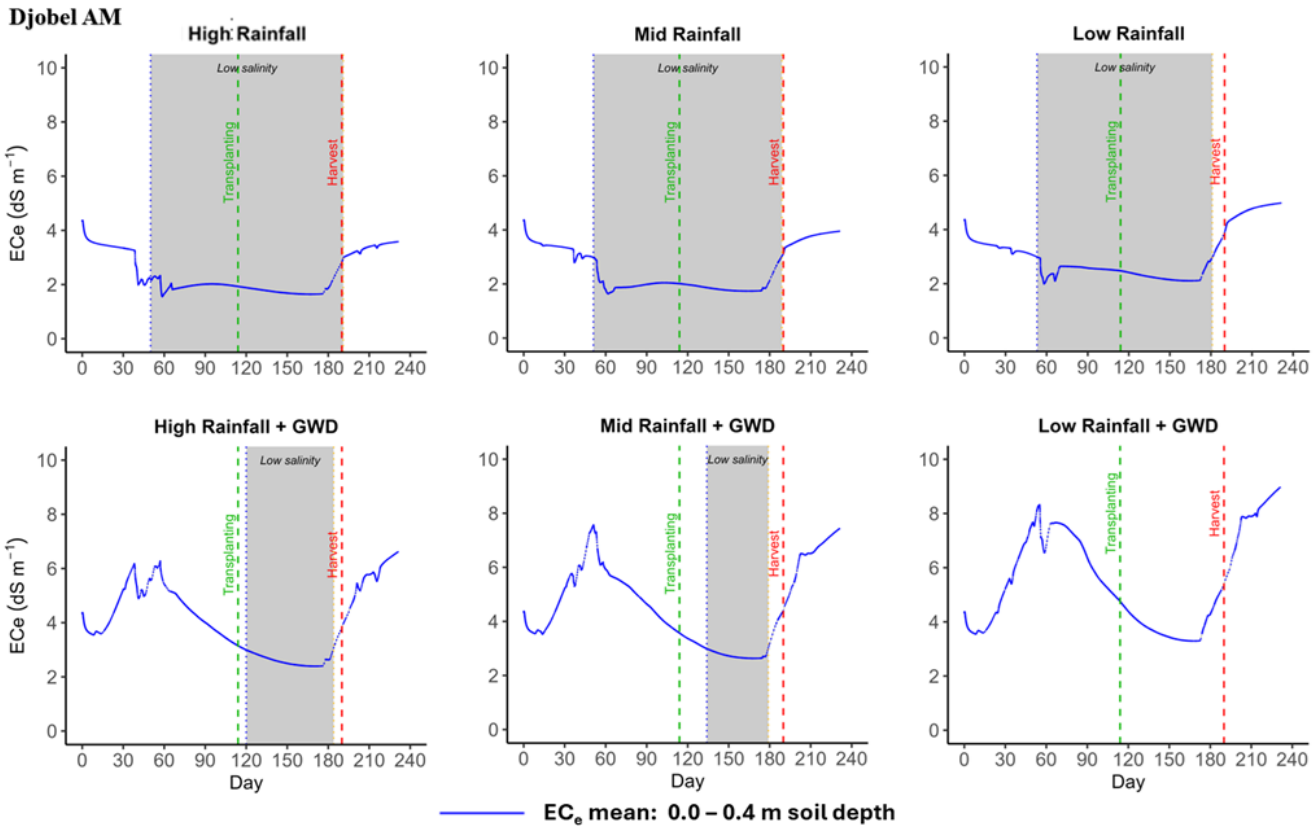

Figure. 6.7. Salt-free period (grey area) for the rainfall scenarios (low, medium, and high) and groundwater depth (GWD identifies shallow groundwater depth) conditions at the Djobel Associated Mangrove (AM) site ($EC_{e\ threshold}$ = 3.0 dS m^{-1}).

The scenario analysis emphasizes the need for cultivating salt-tolerant rice varieties in Cafine TM (and eventually Cafine AM) and Elalab. Due to the lack of specific information on the $EC_{e\ thresholds}$ for the varieties grown in these areas (Yakasau, Caublack, Edjur, and Tomor), the commonly accepted threshold limit for rice (3.0 dS m^{-1}) was used in the present study. However, since some of these varieties may exhibit higher salinity tolerance than the defined threshold, additional simulation scenarios were conducted, considering an $EC_{e\ threshold}$ of 5.0 dS m^{-1} for both Cafine locations and 10 dS m^{-1} for Elalab (Table 6.8). These $EC_{e\ thresholds}$ are provided solely for illustrative purposes, as they are defined based on a review of existing literature review (Fageria, 1985; Haque et al., 2021;

IRRI, n.d.; Reddy et al., 2017), since the crop tolerance thresholds values for local varieties are unknown.

Although the mean EC_e rootzone values remain unchanged, the use of salt-tolerant crop varieties in Cafine TM and Cafine AM offers a promising opportunity to boost crop production by mitigating the effects of salinity on yields. Furthermore, under the measured GWD conditions, the period during which salinity levels remain below the assigned threshold is prolonged in both locations. In Cafine TM, this extension facilitates the scheduling of transplanting dates with a reduced risk of salinity affecting rice yields (Figure. 6.8), similarly to the conditions measured in Djobel. On the other hand, in Cafine AM, improvements in salt conditions are evident only toward the end of the cropping season (Figure. 6.9). In Elalab, the rice-growing conditions also improve around the middle of the cropping season (Figure. 6.10). However, crop yields are inevitably reduced, by 19% to 48%, due to persistently high salinity levels at this site.

Table 6.8. Estimated salt-free period for different rainfall (low, medium, and high) and groundwater depth (shallow and measured GWD) scenarios and corresponding impacts on crop yields.

Scenarios	$EC_{e\ mean}$	Nº Days $EC_e < EC_{e\ threshold}$		$1-T_{c\ act}/T_c$	$1-ET_{c\ act}/ET_c$	$1-Y_a/Y_m$
	[dS m^{-1}]	Growing season	Simulation period	[-]	[-]	[-]
Cafine TM ($EC_{e\ threshold}$ = 5.0 dS m^{-1})						
Low rainfall x $GWD_{observed}$	5.5	37	61	0.08	0.06	0.07
Low rainfall x $GWD_{shallow}$	7.8	0	0	0.27	0.19	0.23
Medium rainfall x $GWD_{observed}$	4.9	53	84	0.12	0.09	0.11
Medium rainfall x $GWD_{shallow}$	7.0	0	0	0.36	0.26	0.32
High rainfall x $GWD_{observed}$	4.4	52	94	0.08	0.05	0.07
High rainfall x $GWD_{shallow}$	6.4	0	0	0.26	0.18	0.23
Cafine AM ($EC_{e\ threshold}$ = 5.0 dS m^{-1})						
Low rainfall x $GWD_{observed}$	5.0	47	54	0.10	0.07	0.09
Low rainfall x $GWD_{shallow}$	8.0	0	0	0.28	0.20	0.25
Medium rainfall x $GWD_{observed}$	4.1	63	75	0.06	0.04	0.07
Medium rainfall x $GWD_{shallow}$	6.6	11	15	0.20	0.14	0.18
High rainfall x $GWD_{observed}$	2.6	78	105	0.07	0.05	0.06
High rainfall x $GWD_{shallow}$	4.4	54	69	0.14	0.10	0.13
Elalab AM ($EC_{e\ threshold}$ = 10.0 dS m^{-1})						
Low rainfall x $GWD_{observed}$	12.1	19	19	0.34	0.25	0.31
Low rainfall x $GWD_{shallow}$	13.7	0	0	0.52	0.39	0.48
Medium rainfall x $GWD_{observed}$	10.2	59	77	0.21	0.16	0.19
Medium rainfall x $GWD_{shallow}$	12.2	11	11	0.39	0.29	0.36
High rainfall x $GWD_{observed}$	10.1	50	87	0.27	0.20	0.26
High rainfall x $GWD_{shallow}$	11.8	31	36	0.47	0.35	0.43

TM, tidal mangrove; AM, Associated mangrove; $EC_{e\ mean}$, mean EC_e in the rootzone; T_c, potential crop transpiration; $T_{c\ act}$, actual crop transpiration; ET_c, potential crop evapotranspiration, $ET_{c\ act}$, actual crop evapotranspiration; Y_a, actual yield; Y_m, maximum yield.

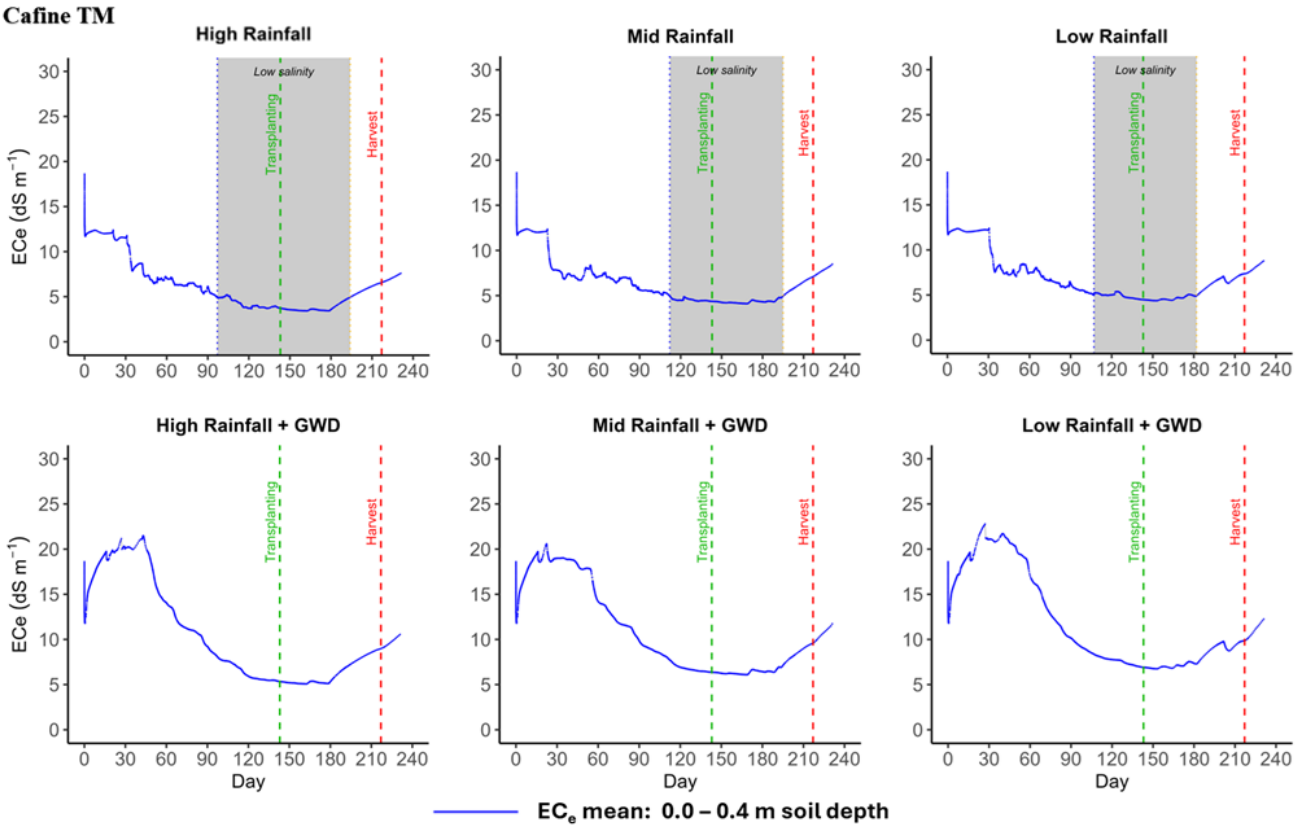

Figure. 6.8. Salt-free period (grey area) under varying rainfall scenarios (low, medium, and high) and groundwater depth (GWD identifies shallow groundwater depth) conditions at the Cafine Tidal Mangrove (TM) site ($EC_{e\ threshold}$ = 5.0 dS m^{-1}).

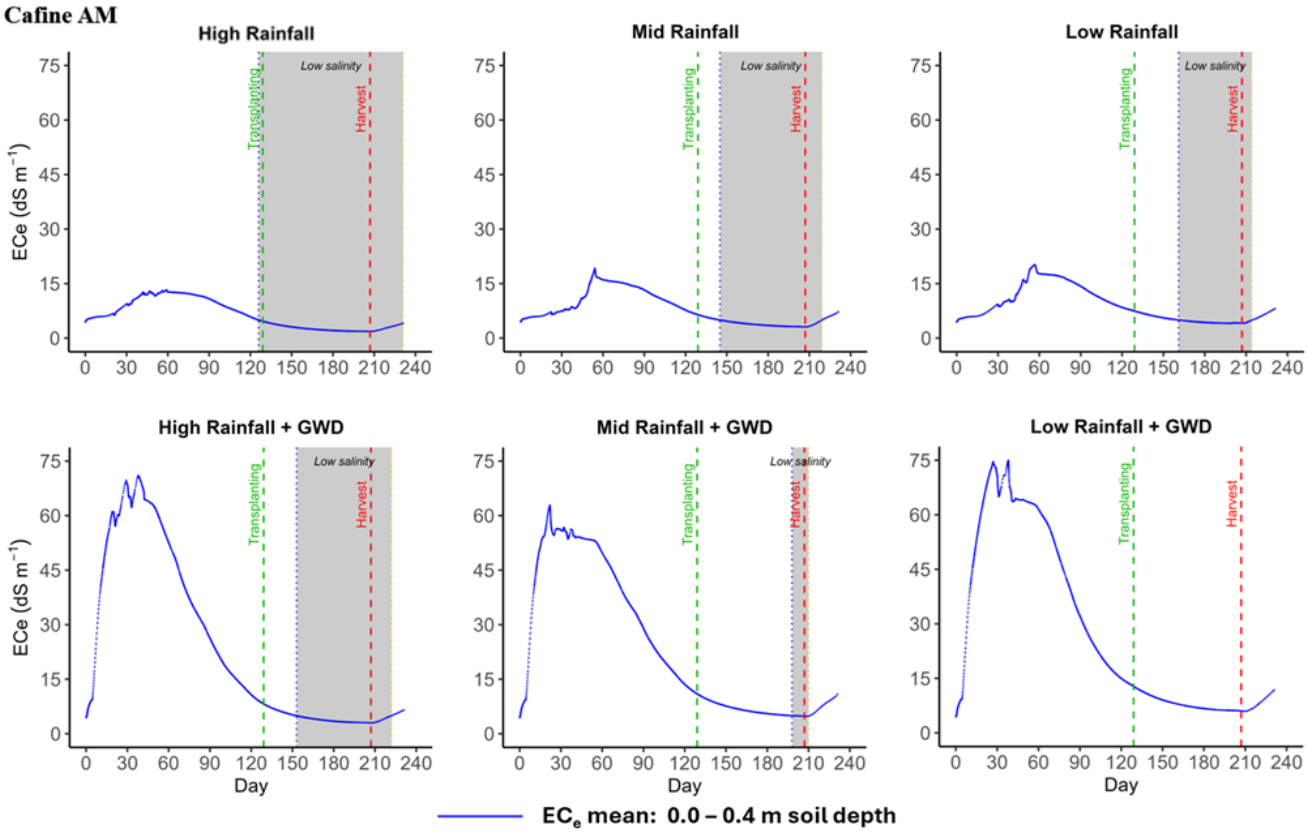

Figure. 6.9. Salt-free period (grey area) under varying rainfall scenarios (low, medium, and high) and groundwater depth (GWD identifies shallow groundwater depth) conditions at the Cafine Associated Mangrove (AM) site ($EC_{e\ threshold}$ = 5.0 dS m^{-1}).

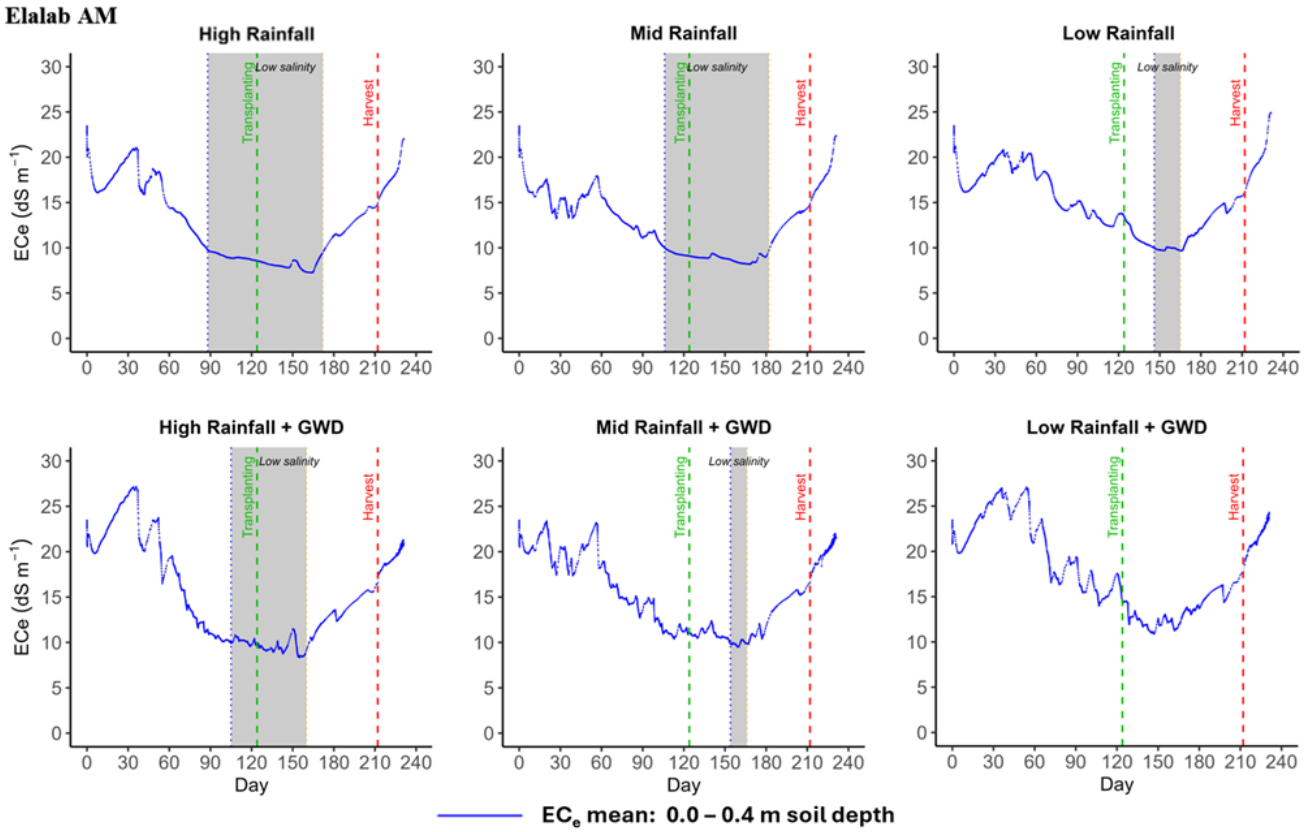

Figure. 6.10. Salt-free period (grey area) under varying rainfall scenarios (low, medium, and high) and groundwater depth (GWD identifies shallow groundwater depth) conditions at the Elalab Associated Mangrove (AM) site ($EC_{e\ threshold}$ = 10.0 dS m^{-1}).

4.4. Driving mechanisms for salinity build-up in MSRP

The findings of this study provide quantitative insights into the issues reported by (Bos et al., 2006) and Van Ghent and Ukkerman, (1993), who highlighted the likelihood of salinity problems in MRSP areas resulting from saline water intrusion and the upward movement of salts from deeper soil layers through capillary fluxes. These factors often lead to severe disruptions or complete loss of annual rice production. Despite the challenges discussed earlier, model simulations effectively captured the dynamics of soil water and salinity in MSRP field. During the non-growing season, SWCs are low, leading to significant salt accumulation in the root zone. This salinity build-up primarily results from salts transported upward by capillary fluxes driven by soil evaporation. In tidal

areas, tidal effects can also cause additional salt deposition on the soil surface. At the onset of the rainy season, soil salinity gradually decreases to levels suitable for rice cultivation. The extent of this reduction depends on the seasonal rainfall amount and distribution, groundwater depth, and groundwater salinity.

Seasonal rainfall provides the primary mechanism for flushing salts from the root zone. In the monitored period and modeling scenarios, years with the highest rainfall consistently produced the most favorable conditions for rice growth. However, prolonged dry spells can allow salts to migrate back into the root zone through upward fluxes. In irrigated paddy fields located in salt-affected areas, this issue would be more easily handled with irrigation (Kitamura et al., 2006; Marcos et al., 2018; Sugimori et al., 2008; Zeng et al., 2003). In contrast, MSRP systems, which rely solely on rainfall, depend heavily on well-distributed rainfall to prevent salinity build-up and avoid osmotic stress that could compromise crop yields. This challenge was particularly evident in the soil water balance estimates for the Cafine and Elalab sites.

Similar to other agricultural systems with shallow groundwater, the depth of the groundwater influences the effectiveness of salt leaching (Guo et al., 2024; Karimov et al., 2014; Liu et al., 2022; Narjary et al., 2021; Ramos et al., 2023). The shallower the groundwater, the more difficult it becomes to flush salts away from the root zone, and the stronger the upward fluxes during dry spells in the growing season when rainfall fails. In this study, the modeled scenario with a shallower initial GWD always presented worse conditions for salt leaching than those scenarios with deeper initial GWD, in cases of dikes' degradation and/or occurrence of significant high and strong tidal events. Naturally, the closer the agricultural fields are to the shoreline, the higher the risk of saline water intrusion, the worse the quality of groundwater, and the higher the risk of more salts moving upward and soil salinity build-up.

4.5. Soil salinity management in MSRP systems

Rice is classified as a sensitive crop to salinity-stress (Ayers and Westcot, 1985; Minhas et al., 2020). Thus, in MSRP it is essential to reduce soil salinity to levels suitable for rice production. However, as demonstrated in this study, the inter- and intra-annual variability of rainfall amounts and distribution significantly affects salt dynamics, posing serious challenges to rice cultivation under rainfed agriculture. During drought conditions, elevated soil salinity will inevitably impact rice yields. In a climate change context, prospects are further uncertain. While the MSRP systems rely solely on rainfall to lower soil salinity, adopting improved management practices is recommended to mitigate salinity and support sustainable rice production. However, although the principles for cultivating crops in saline environments are well understood and promote the use of specialized crop-soil-water management techniques, it is crucial to acknowledge that profit margins for agriculture under saline conditions are typically low, and saline soils always present a risk of crop failure (Minhas et al., 2020). Consequently, while some practices and strategies can enhance rice production in the study areas, they alone cannot close the significant yield gap between low external-inputs agriculture in these marginal regions and the more productive edaphoclimatic regions, namely of Asia, where rice is cultivated with mechanization, irrigation, a heavy use of agrochemical and the so-called high yielding varieties (HYV), which would not survive under Guinea-Bissau's MSRP fields.

This study clearly illustrates the importance of identifying the optimal window for growing rice in associated and tidal mangrove areas. While, in most sites, this period does not exactly correspond to a salt-free period as defined by Guei et al., (1997), it remains the only time when conditions for growing rice are most favorable. Depending on the

amount of rainfall, rice transplantation in some locations (e.g., Djobel) could occur earlier than the dates considered in this study. This would prevent salinity from impacting crop growth at the end of the growing cycle as rainfall ceases. Alternatively, since the dry period is essential for drying grains, to bring forward to transplant earlier would also enable the cultivation of more productive rice varieties with longer growing cycles. For this reason, establishing a monitoring network for soil salinity levels is crucial.

In some locations, soil salinity levels never drop below the threshold defined in literature as the tolerance limit for rice. In such cases, and depending on the amount of rainfall, the impacts on the crop throughout the season may be minor (e.g. Cafine AM). However, in other situations, rice production may only be viable by growing salinity-tolerant varieties (e.g., Cafine TM, Elalab AM). This could explain the preferences of farmers for certain rice varieties, which are locally described as highly resistant to salinity (Temudo, 2011). However, precise information on the EC_e thresholds of these varieties is still lacking, highlighting a significant gap in understanding their full potential under saline conditions. Gaining knowledge of the local EC_e thresholds will help identify optimal salinity tolerance levels and improve rice cultivation strategies in the country by leveraging the potential of local rice varieties.

To mitigate global warming impact on MSRP it is crucial to keep the groundwater table at deeper levels at the start of the rainfall season, thereby facilitating early salt leaching and minimizing soil salinity levels. For this purpose, an increase in the width and height of the main dike, the regular maintenance of MSR fields' dikes and related drainage structures is mandatory. Additionally, the selection of the most salt- and drought-tolerant local varieties for risk-prone areas and a better adaptation of the agricultural calendar to present rainfall distribution conditions are also the most needed adaptation measures.

5. *Conclusions*

This study simulated the soil water and salinity dynamics in the mangrove swamp rice production system of Guinea-Bissau, which is essential for food security but faces several environmental challenges due to the critical role of rainfall in the viability of rice production. The HYDRUS-1D model was successfully used to describe the salt dynamics in four locations, with RMSE varying from 0.49 to 5.72 dS m^{-1} and NRMSE values ranging from 27.4% to 62.3%. The main factors influencing soil salinity involving seasonal rainfall amount and distribution, and groundwater depth and quality. Management strategies to address soil salinity were also discussed, such as the possibility of growing longer and more productive varieties in certain areas or the need to cultivate salt-tolerant varieties in others. The maintenance and improvement of drainage structures was found to be critical for minimizing salinity issues in paddy fields.

While these findings may help improve the livelihoods of local populations, rice production in GB faces additional limitations that keep production levels behind those of similar areas worldwide, particularly in the absence of support from governmental and external entities. Future studies should focus on refining groundwater management strategies, particularly regarding the maintenance of optimal groundwater levels to mitigate the impact of salinity stress on rice growth. Additionally, further research is needed to determine the salinity tolerance thresholds of locally adapted rice varieties, as these thresholds were shown to vary significantly across the studied sites. Understanding these thresholds will be crucial for developing targeted cultivation strategies, ensuring the optimal transplanting period, and improving rice production. Considering the potential reintroduction of brackish water during the dry season in fields with modern water management infrastructures, the model developed is going to be further improved to this aim in collaboration with some of the country's organizations.

6. *Supplementary material*

6.1. **Supplementary A.** Sensor Calibration

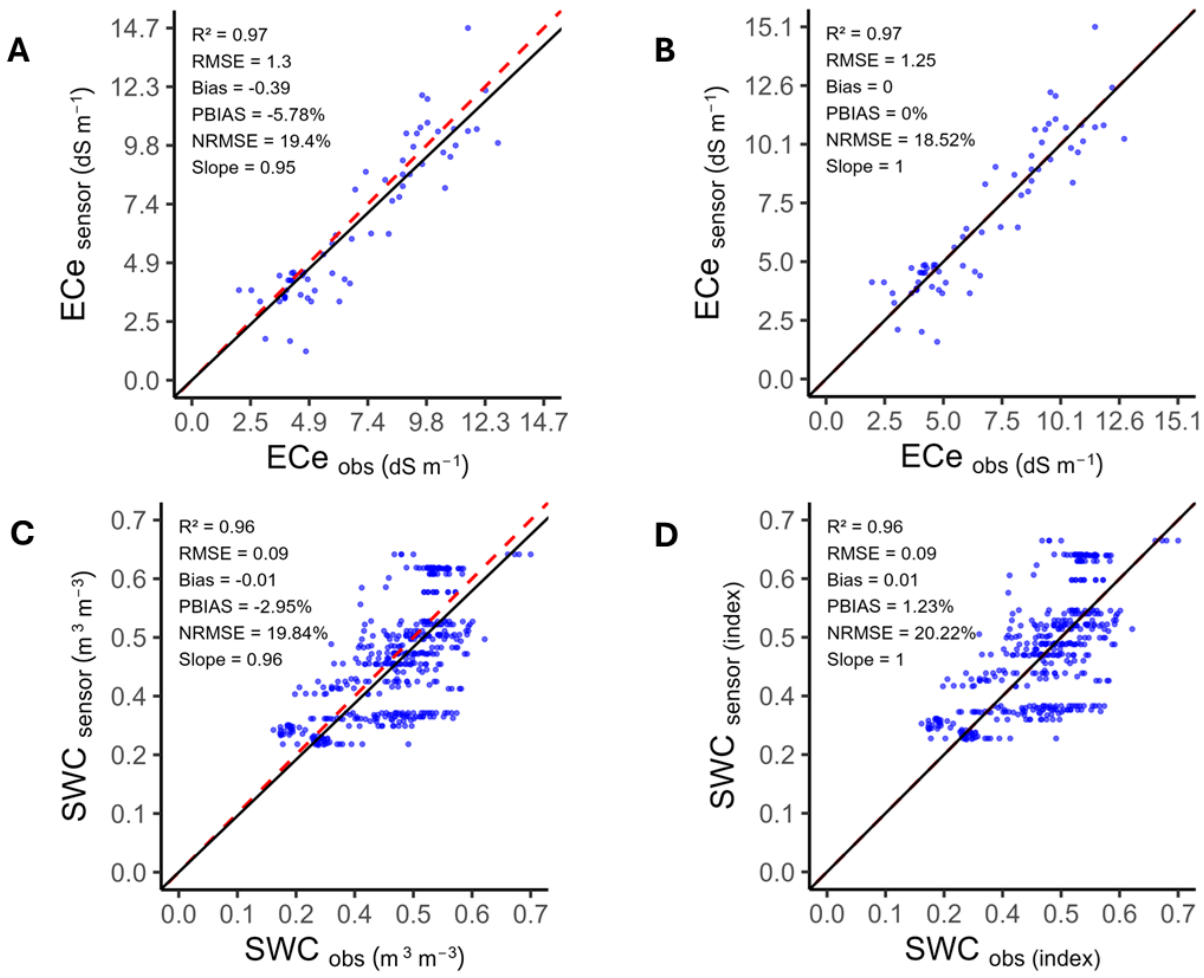

Figure. 6.S1. Comparison of volumetric water content and electrical conductivity values using sensor Teros 12 and observed / laboratory information.

6.2. **Supplementary B.** Rainfall correction

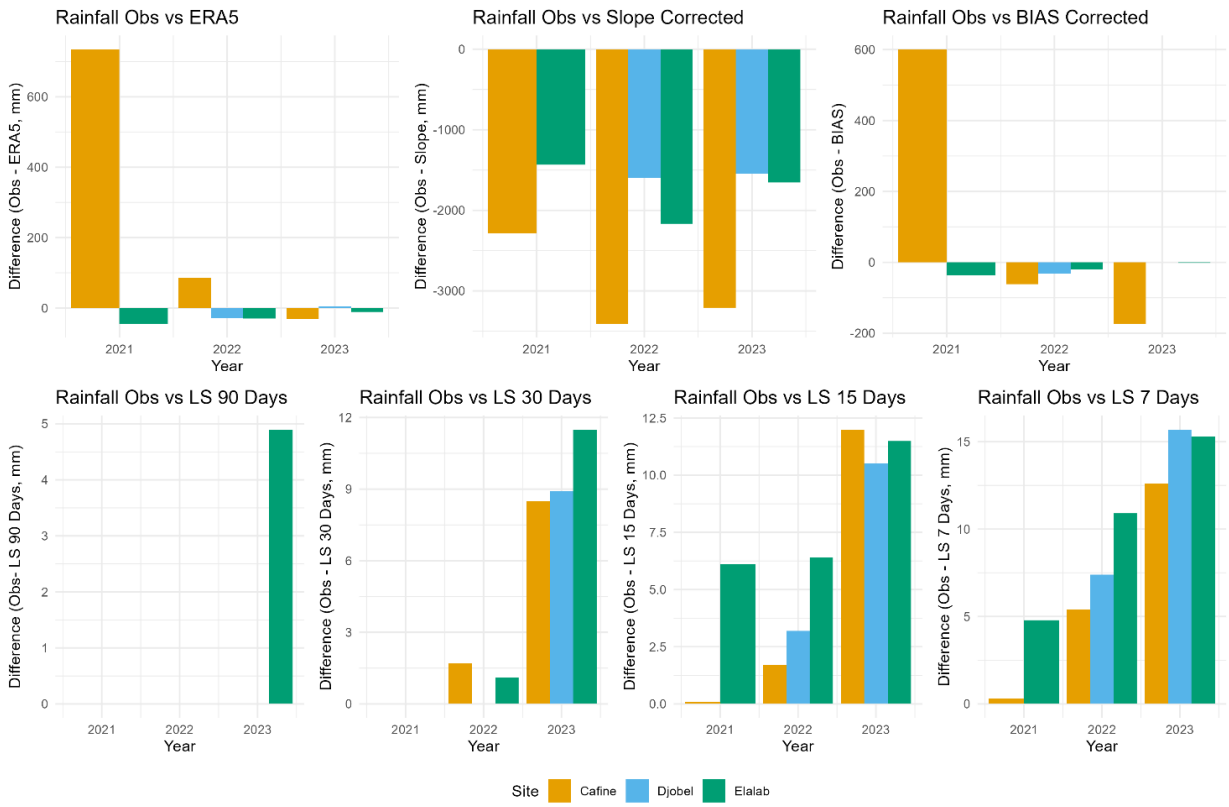

Figure. 6.S2. Calibration of ERA 5 reanalysis using slope, bias and linear scaling correction for rainfall in Guinea-Bissau, west Africa.

6.3. Supplementary C. Modeling conditions at the Cafine Tidal site.

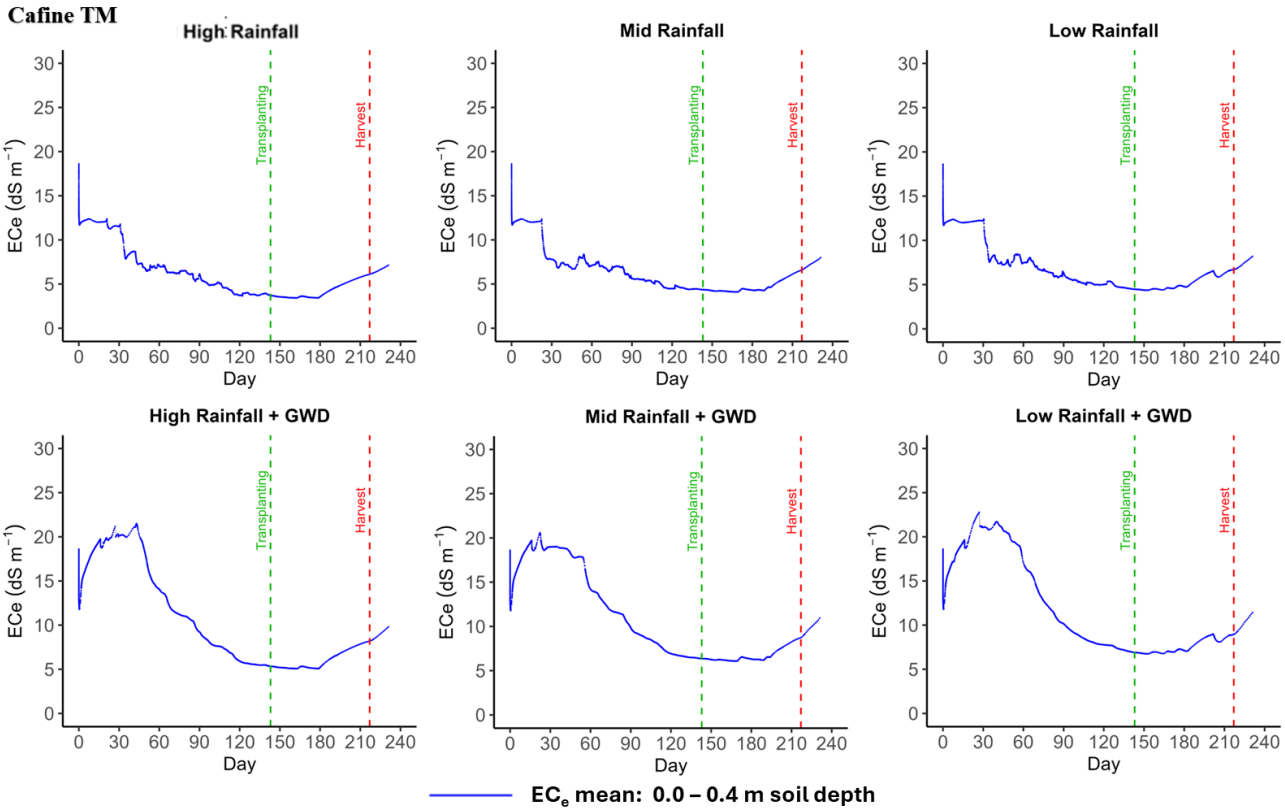

Figure. 6.S3. Salt-free period (grey area) under varying rainfall scenarios (low, medium, and high) and groundwater depth (GWD identifies shallow groundwater depth) conditions at the Cafine Tidal site ($EC_{e\ threshold}$ = 3.0 dS m^{-1}).

6.4. Supplementary D. Modeling conditions at the Cafine Associated site.

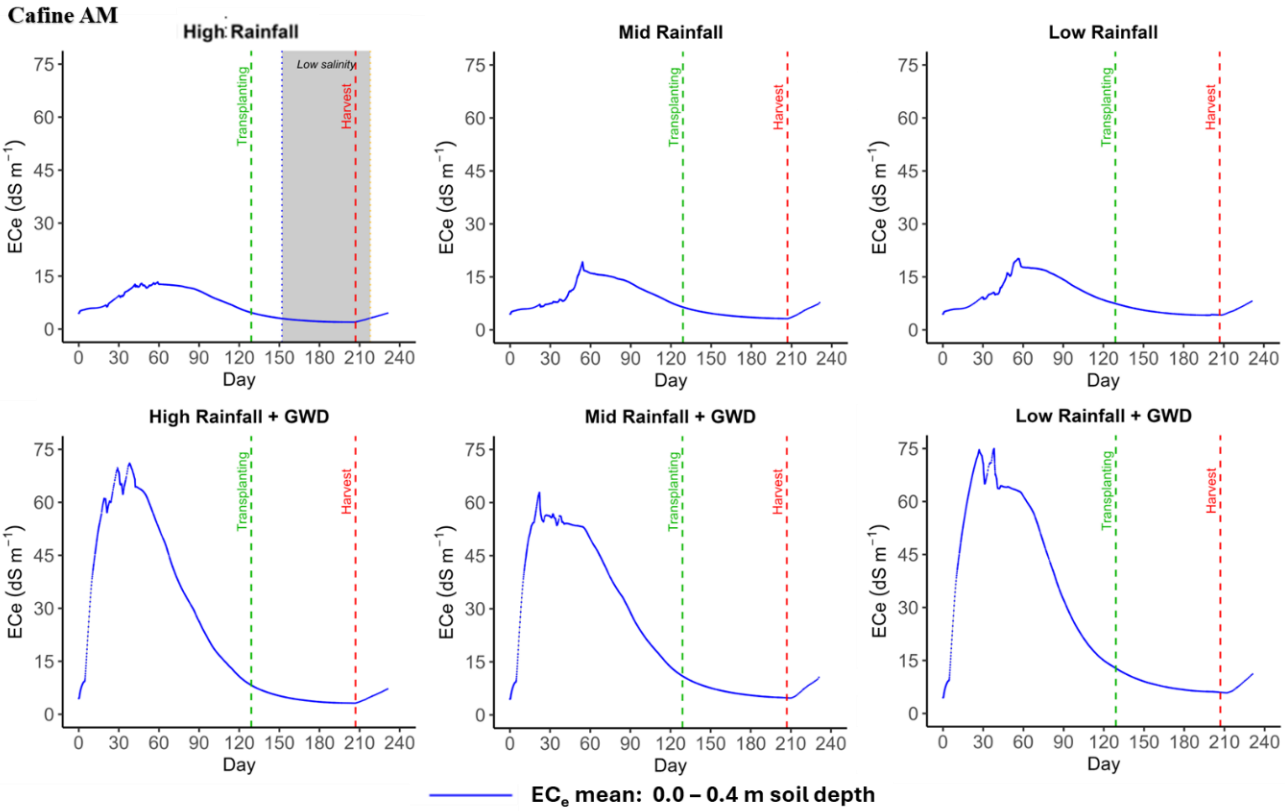

Figure. 6.S4. Salt-free period (grey area) under varying rainfall scenarios (low, medium, and high) and groundwater depth (GWD identifies shallow groundwater depth) conditions at the Cafine Associated site ($EC_{e\ threshold}$ = 3.0 dS m^{-1}).

6.5. Supplementary B. Modeling conditions at the Elalab Associated site.

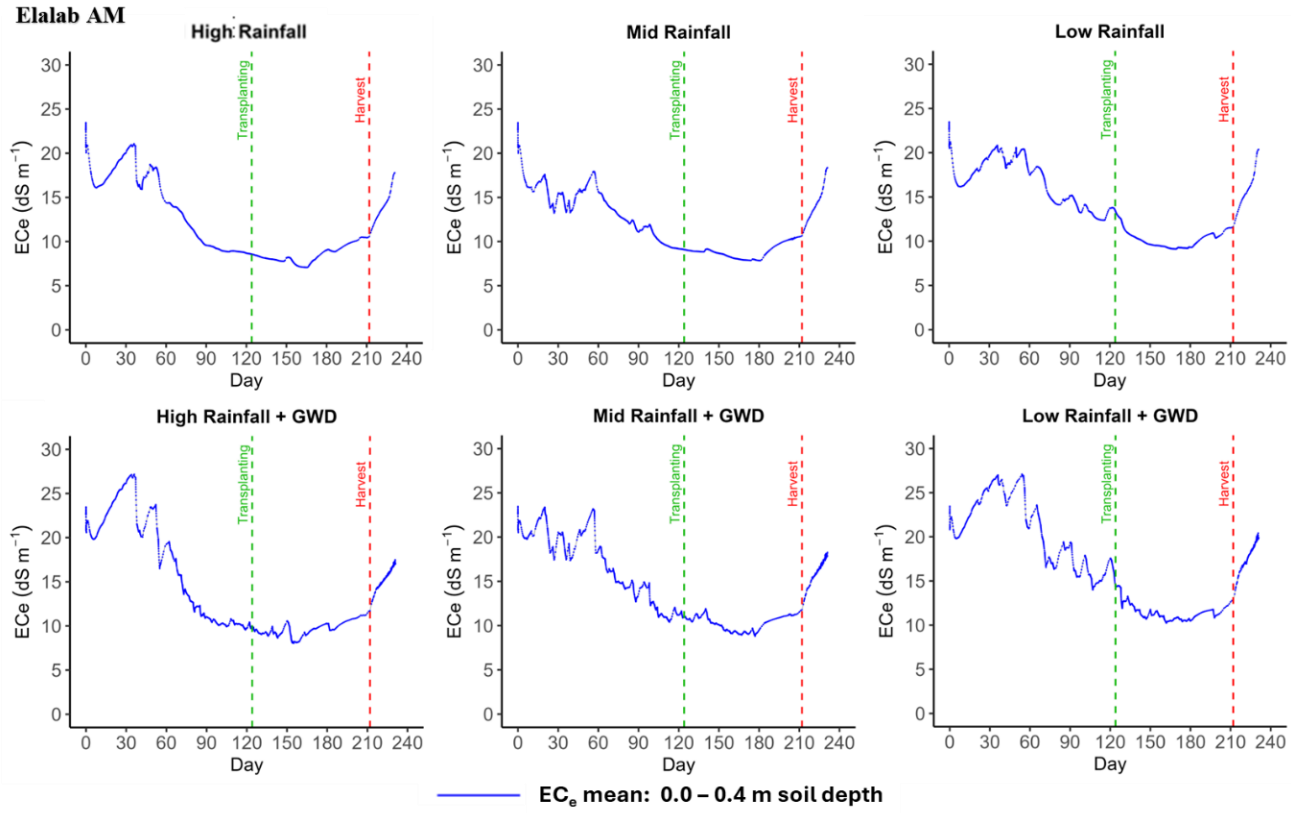

Figure. 6.S5. Salt-free period (grey area) under varying rainfall scenarios (low, medium, and high) and groundwater depth (GWD identifies shallow groundwater depth) conditions at the Elalab Associated site ($EC_{e\ threshold}$ = 3.0 dS m^{-1}).

Chapter 7

General Discussion and Conclusions

7. Discussion

7.1. Integrating Chapter Findings: understanding of Soil Properties, Water Management, and Salinity in MSRP

This thesis introduces a novel approach for characterizing the physicochemical properties of soils in mangrove swamp rice fields and quantifying the soil hydro-saline balance. Considering a regional perspective by evaluating rice production management in different coastal villages in the northern and southern regions of GB, using the rice fields of Elalab and Cafine – Cafal villages respectively, as case studies. In some instances, existing information from the Oio region (more at the center of the coastal area) was also considered, with Enchugal serving as a case study to examine the spatial distribution of salinity. The results underscore the importance of integrating agro-ecological site descriptions to elucidate the influence of environmental constraints on water regulation and salinity dynamics on a regional scale. Distinctive micro-environments are generated by differences in rainfall distribution, soil composition and tidal regimes, and these inform and support local farmers' management decisions. This comprehensive approach enables a comparative understanding of system characteristics at a national level.

Chapter 2 provided an in-depth analysis of the structural and functional features of the Mangrove Swamp Rice Production (MSRP) system, emphasizing the challenges arising from insufficient knowledge regarding soil and water management practices. The analysis identified recurrent dike failures, inadequate agricultural infrastructure and spatio-temporal variability in rainfall as key factors that necessitate the adoption of site-specific management strategies by both farmers and institutional actors. The three main constraints were the lack of information on weather variables, irregular rainfall distribution, and limited knowledge of land and water management. Understanding the

environmental and infrastructure challenges helps to recognize where the MSRP system is vulnerable and how local communities have come up with practical ways to adapt and handle those challenges.

Insights derived from farmer interviews, initially presented in Chapter 2 and further substantiated by the analyses in Chapter 3, reveal that the management of the MSRP system is predominantly governed by indigenous, experience-based knowledge embedded within specific ethnic traditions. Notably, communities in the northern regions demonstrate greater proficiency in water management than those in the south (Figure 3.7), largely due to adaptive modifications in plot geometry and bund construction aimed at maximizing water retention (Figures 3.5 and 3.6). The Chapter 3 findings suggest that the configuration and scale of plots and bunds in northern sites are more effective at regulating water levels than their southern counterparts.

This opened the possibility of studying the distribution of salt both at the plot and whole field levels. Results showed that salt concentrations could reach levels exceeding hypersalinity in tidal mangrove areas (TM) (Figure 4.6). In contrast, other regions of the rice fields, such as the associated mangrove (AM), showed low or negligible salt concentrations. This suggests that it is highly probable that the AM plots exhibit lower levels of hypersalinity compared to TM ones, which aligns with the literature reviewed in Chapter 2. Despite this contrast, local farmers tend to favor TM areas for cultivation, because they value their higher soil fertility and superior rice yields, even though such sites are more exposed to environmental risks.

Furthermore, this thesis introduces practical applications using two types of maps to optimize system management. The first set of soil plasticity maps introduced in Chapter 3, serve as operational tools to support decision-making during land preparation. These

maps enable farmers to determine the optimal water content for tillage, allowing them to align their labor input with the most suitable moisture conditions for ploughing. This study demonstrated significant variation in soil texture and plastic limits both within a single village and between different villages, providing farmers with valuable insights for their management decisions.

The second analytical tool, presented in Chapter 4, focuses on identifying spatial gradients of soil salinity and distinguishing between areas of low and high salt concentration. Building directly upon the framework established in Chapter 3, this study employs soil texture as a covariate to improve the accuracy of identifying saline site. Accurate identifying these areas enables more targeted plot management, allowing desalination techniques to be explicitly applied to the most hypersaline locations. A practical example would be selecting salt-tolerant rice varieties and planting them in these hypersaline areas. However, this system is vulnerable to dike breaches (See Video: https://www.youtube.com/watch?v=niwk9uxXQC0), which must be quickly repaired, as such breaches lead to increased salt concentrations, crop production failure, and hunger in the following year. Therefore, accurately identifying saline sites would improve the management of the MSRP, where either desalination techniques or salt-tolerant varieties could be applied to specific sites, enabling site-specific production strategies within the system.

Then, Chapters 2, 3, and 4 provide essential data for the development of the saline water balance model for the MSRP system. Chapter 2 identifies key constraints related to rainfall variability and EC_e, highlighting the importance of incorporating low, medium, and high rainfall scenarios into the saline balance analysis. Chapter 3 contributes critical parameters for model calibration, including the physical characteristics of the study sites and detailed information on the rice varieties cultivated by local farmers. These include

the most widely used varieties, their phenological stages, and typical planting and harvesting schedules. In addition, chapter 4 presents the identification of saline zones and observed EC_e concentrations present within the MSRP system. This information is basic for the parameterization and calibration of the Hydrus-1D model and for constructing realistic rainfall scenarios to simulate the system's response under varying environmental conditions.

Since the hydro-saline balance model was designed to simulate realistic conditions for rice cultivation, it was essential to incorporate crop-specific parameters such as crop transpiration (ET_c) and soil evaporation (E_s). Chapter 5 of this thesis focuses on the calculation of daily reference crop evapotranspiration (ET_o) using the FAO Penman-Monteith (FAO-PM) method, which is a key variable in determining ET_c. ET_o is therefore an analytical input for quantifying the saline water balance in the MSRP. This chapter introduces a practical tool developed for farmers and agricultural technicians in GB, allowing ET_o to be estimated using only temperature data. That means, temperature is one of the most accessible and easy-to-measure meteorological variables, as it does not require specialized equipment and thermometers could be available in rural areas. With careful daily temperature readings, it is possible to indirectly calculate ET_o, making this method particularly useful in data-scarce regions. In summary, the main outputs of this chapter were the estimation of ET_o for each site using a simplified and accurate approach, and the potential use of gridded weather data in the absence of weather station observations.

The thesis is also linked to other research lines within the Malmon project, such as the analysis of physicochemical characteristics discussed by Merkohasanaj et al. (2025) and the rice crop monitoring work discussed by Céspedes et al. (2025). These collaborations

establish a strong interdisciplinary nexus, fostering the integration of soil science, agronomy, and environmental monitoring within a unified research framework.

The physicochemical studies of soil profiles were essential for developing chapter 6. Merkohasanaj et al. (2025) involved detailed analyses of the soil's chemical and physical properties, providing valuable insights into the soil's fertility, salinity, and water retention capacity. Complementarily, Céspedes et al. (2025) conducted an in-depth characterization of rice plant growth dynamics, the outcomes of which were instrumental in the construction and calibration of the HYDRUS-1D monitoring model employed in this research.

Finally, Chapter 6 explores how water and dissolved salts move through the soil, introducing the hypothesis that the rice varieties cultivated by local farmers are well adapted to the specific conditions of the MSRP system. This adaptation may allow the plants to uptake water more efficiently, even under saline conditions. In this part of the thesis, all previously generated outputs are integrated as inputs to construct the saline water balance. This framework is then used to analyze different scenarios in depth, focusing on how rainfall patterns and fluctuations in groundwater levels influence water availability and salinity dynamics within the system.

However, Chapter 6 did not include an analysis to determine the salinity threshold of rice varieties in GB. This is a significant research gap, as understanding the salinity threshold of rice varieties is crucial for selecting the most suitable varieties for cultivation in different areas of GB. This underscores the need for further investigation into water and solute balances in MSRP soils, and inspires future studies in this area.

7.2. *Addressing knowledge Gaps: Spatial variability and salt accumulation in MSRP*

This study aligns with findings from existing literature on the identification and characterization of salt content in the system. First, it was found that the cations responsible for soil salinity in MSRP are Na and Mg, which is consistent with the finding of Andreetta et al., (2016), D'Amico et al., (2024), Merkohasanaj et al., (2022, 2025). Their concentration varied depending on proximity to the village, with some areas showing hypersaline characteristics as described by Sylla (1994) and Sylla et al. (1995). However, despite the high salt content in these sites under initial conditions, rice cultivation is still possible, provided that highly salt-tolerant varieties (e.g., Emana Manai, as discussed in Chapter 2) are used, along with a significant amount of freshwater harvested to dilute the salt concentrations. This strategy enables the establishment of a free-salt period, as described by Guei et al., (1997). As discussed in Chapter 6, the present study represents a significant contribution to the field. It provides a comprehensive understanding of water and solute movement dynamics in MSRP soils, which is crucial for adequate soil and water management in rice cultivation. This study is the first numerical approach to addressing the theoretical gaps identified by previous studies, and its findings are expected to guide and inspire future research in this area.

Current tools to improve prediction and parameter calibration for better forecasting variables, such as EC_e and shortwave radiation, were studied using the latter for ET_o prediction. Firstly, machine learning algorithms worked exceptionally well for predicting EC_e using soil texture variables and satellite indices. It is essential to highlight that algorithms such as Random Forest were far more effective than deep learning techniques, such as convolutional neural networks. On the one hand, this aligns with other studies on

salinity (e.g., Kaplan et al., 2023; Yang et al., 2023; Zhao et al., 2023). On the other hand, numerical solutions were essential for calibrating the shortwave radiation adjustment parameter (k_{Rs}) required to predict ET_o using temperature data only (Paredes et al., 2018, 2020; Paredes & Pereira, 2019). The L-BFGS-B algorithm (Byrd et al., 1995) was modeled and calibrated using the RMSE as the adjustment parameter. This approach minimized error, allowing for precise calibration of the k_{Rs} parameter for each location or sites cluster.

Rainfall variation affects rice growth as it can result in poor dilution of salts in the plots. Field observations and continuous monitoring revealed that salts do not have an active outlet through plot drainage, as few sites can drain water, and no drainage systems are designed explicitly for this purpose. While northern and southern Balanta regions (e.g., Enchugal village in Oio and Cafine-Cafale villages in Tombali) implement drainage to plow the soil, this practice is rare in the northern region of S. Domingos, among the Felupe and Baiote (e.g., Elalab and Djobel villages). This discrepancy is primarily due to each area's varying amounts of rainfall. Typically, farmers close all possible outlets of the bunds, increase their height, and aim to capture as much rainwater as possible.

However, this management practice does not effectively remove excess salts from the system. In contrast, regions with high salt concentrations (e.g., Cafine – Cafal, and Enchugal) employ drainage systems to flush out excess salts. (Fayrap & Koç, 2012; Xiao Pang et al., 2010), allowing for more efficient salinity management (Minhas et al., 2020; Ramos et al., 2023, 2024). MSRP operates under a completely different system, where such drainage practices are not applied in all cases. For example, in sites like Elalab, farmers prefer to plow with water, which increases the force required for plowing, rather than flushing freshwater. As a result, the lack of an effective drainage system in the plots

of many drought-prone regions leads to productivity relying solely on leaching and salt dissolution.

Maps were generated at the medium scale of the plot level to identify hypersalinity within the MSRP. However, this study also identified significant small-scale variations within the system. Chapter 3 determined, through 3D models, the heterogeneity found in the plots. This highlights that salt accumulation occurs heterogeneously among the plots and in the case of large ones, this variation can affect rice production at a plot level. This means that farmers struggle to control water levels inside them, which can involve the reduction of plot size as observed in the case study in Elalab.

7.3. Study limitations and implications for future research in MSRP

This study was hampered by lack of prior research on rice growth and site characterization. This hindered the development of the baseline information essential for creating numerical models and simulations. For example, historical climate data for the regions under study was scarce and knowledge about the current rice varieties and their phenological development was limited.

The availability of laboratories and research equipment in the country was also limited. This delayed the analysis of soil physicochemical characteristics, as well as extending the time required to conduct the studies. This restricted the direct analysis of EC_e, and only data for $EC_{1:5}$ and $EC_{1:25}$, could be generated as these were more easily measured in the field and the country's laboratories. However, the conversion of $EC_{1:5}$ and $EC_{1:25}$ to EC_e present a problem with formulas calibrated by Sonmez et al. (2008). These formulas were designed for saline soils, not hypersaline soils, as presented in this study. This gap could be addressed by future research aimed at developing calibrated formulas for hypersaline

soils could address this gap, allowing for the transformation of EC from various solutions to EC_e.

Local rice varieties remain poorly characterized, requiring further research to determine growth aspects and salinity tolerance. Specifically, the salinity-tolerant varieties in MSRP have not yet been studied to assess their EC_e threshold. Chapter 6 explores an approach to observing tolerance levels without affecting rice production. This knowledge gap should be further investigated in future research in the country.

This study is limited to specific case studies within the country, focusing on rice fields from two villages in the south (Cafine and Cafal), one in the central region (Enchugal), and two in the north (Elalab and Djobel). Due to budget constraints and the considerable time required for analysis, only three rice fields were thoroughly examined for their physicochemical characteristics and spatial distribution. While this information approximates the behavior of salt concentration on rice fields in each region, it is essential to note that some sites within these regions may exhibit different characteristics than those observed in this study. Therefore, future research should consider expanding the number of case study sites for a more comprehensive understanding.

Conclusions and future research

It was concluded that the physicochemical properties of the rice field soils are highly variable, with significant differences observed between associated mangrove soils and tidal mangrove soils. Most of the soils were classified as Inceptisols with Vertic characteristics. Various deposits of saltwater river sediments were identified, which influence the porosity of each soil horizon, and thereby affect the amount of water stored in the soil. However, this water is not fully available to the plants due to hypersalinity, which negatively impacts rice production, particularly in years with low precipitation, an early end to the rainy season, and/or prolonged dry spells.

This study demonstrated that farmers have extensive knowledge of salt management in different plots. Simulations showed that rice transplanting was synchronized with the salt dilution in the plot, proving that farmers store sufficient water to complete the rice growth cycle. However, farmers face significant challenges in dry years because it is difficult to predict whether a certain year will be rainy or dry. Therefore, it is essential to use all harvested water efficiently, as observed in the northern regions where plots are smaller and more homogeneous.

The plots are predominantly saline and hypersaline, and water harvesting is the primary method for desalinization. In several village in the southern and central regions, farmers leach excess salts from the soil, but this practice is only possible in areas where plots are equipped with drainage systems. However, such drainage designs are not feasible for all farmers, as many rice fields are designed specifically for rainwater harvesting. Therefore, the greater the capacity of water harvesting system, the lower the risk of production losses due to salinization.

Allowing brackish water into the rice fields will depend on the salt concentration of the river and the timing of the practice. Solute and water movement simulations, determined that the groundwater is highly saline, and the initial condition at a depth of 0.50 m would negatively affect rice production. If the initial water level was more significant than 1.50 m in depth, the salinity of the groundwater did not affected the crop. Therefore, if this practice is carried out, the groundwater level must be below 1.50 m in May. This means that if brackish water is allowed in, it should be done before March. This practice could be implemented in the Oio region or in the south of the country. However, it is not recommended in the northern region. Further research is needed in this area particularly in the Oio region, where freshwater availability is higher than in other parts of the country.

Sustainable rice cultivation in MSRP of GB depends on adapting farming practices to biophysical conditions and addressing soil salinity challenges under climate change. This study emphasizes the critical role of Na^{+} and Mg^{2+} in soil salinity. It demonstrates that machine learning algorithms, such as Random Forest, can effectively map the spatial distribution of salinity, offering valuable insights for identifying hypersaline areas. Such precision is essential for developing targeted interventions, including water management strategies and drainage systems, to optimize rice cultivation and mitigate soil salinization. Future research should focus on long-term monitoring, enhancing the understanding of cation interactions in soil salinity, and validating the model across diverse environments. This approach will improve agricultural productivity and resilience, aligning with global sustainability goals.

Furthermore, effective water management, including optimizing groundwater levels, drainage structures, and salt-tolerant rice varieties, is essential for sustaining productivity under variable rainfall conditions. The simulations conducted using the HYDRUS-1D model and machine learning techniques provide valuable tools for predicting salinity

patterns in regions of Guinea-Bissau. Adjusting global models with more data from tropical countries, especially those with high rainfall and climatic variability, is essential. Expanding data collection and refining these models for tropical climates will strengthen agricultural resilience and food security in West Africa, offering a solid framework for sustainable rice cultivation.

Some questions remain for future investigation, including: What specific strategies can be employed to effectively mitigate the risks associated with dike breaches in the Mangrove Swamp Rice Production (MSRP) system? How can the findings of this study be applied to rice cultivation in other coastal regions with similar environmental conditions outside Guinea-Bissau? Additionally, what further research is needed to comprehensively understand the long-term impacts of soil salinity on the growth and yield of different rice varieties within the MSRP system? Addressing these questions will be crucial for advancing sustainable rice cultivation practices and ensuring food security in vulnerable regions.

This thesis contributes advancing scientific knowledge on salt dynamics in MSRP. Through a multidisciplinary approach, it provides empirical and visual evidence, as well as a biophysical characterization of the agroecosystem, integrating local farmers' knowledge in the country. The study identified Na^{+} and Mg^{2+} as the primary cations responsible for soil salinization in MSRP fields, along with the presence of hypersaline zones within rice paddies. Machine learning techniques, such as Random Forest, were calibrated and applied to map these saline areas with high precision. Likewise, numerical methods, including L-BFGS-B, were employed to optimize cluster-focused predictive multi-linear regression equations for estimating K_{rs} values. Another relevant contribution was the estimation of reference evapotranspiration (ET_o) under data-scarce conditions, with particular applicability to regions between 0° and 20°N latitude in West Africa,

which experience high climate variability and remain understudied. Finally, this thesis characterized for the first time in the context of GB the "salt-free period" proposed by Guei et al. (1997), showing that this period is dynamic and strongly influenced by rainfall patterns and groundwater depth.

References list

References for Chapter 1

Adefurin, O. and SJ Zwart, 2016. A detailed map of rice production areas in mangrove ecosystems in West-Africa in 2013 – Mapping of mangrove rice systems using Landsat 8 satellite imagery and secondary data. AfricaRice GIS Report – 2. Africa Rice Center, Cotonou, Benin.

Agurla, S., Gahir, S., Munemasa, S., Murata, Y., & Raghavendra, A. S. (2018). Mechanism of Stomatal Closure in Plants Exposed to Drought and Cold Stress. In M. Iwaya-Inoue, M. Sakurai, & M. Uemura (Eds.), Survival Strategies in Extreme Cold and Desiccation: Adaptation Mechanisms and Their Applications (pp. 215-232.). Springer Singapore. https://doi.org/10.1007/978-981-13-1244-1_12

Anugrah, M.A., Kendarto, D.R., Suryadi, E., Dwiratna, S., 2020. Water balance modelling to estimate water needs of the new rice field expansion area in buru district, maluku. Int. J. Emerg. Trends Eng. Res. 8, 5612–5618. https://doi.org/10.30534/ijeter/2020/114892020

Balasubramanian, V., Sie, M., Hijmans, R. J., & Otsuka, K. (2007). Increasing Rice Production in Sub-Saharan Africa: Challenges and Opportunities. Advances in Agronomy, 94, 55–133. https://doi.org/10.1016/S0065-2113(06)94002-4

Bazrafshan, A., Shorafa, M., Mohammadi, M. H., Zolfaghari, A. A., van de Craats, D., & van der Zee, S. E. A. T. M. (2020). Comparison of the individual salinity and water deficit stress using water use, yield, and plant parameters in maize. Environmental Monitoring and Assessment, 192(7), 448. https://doi.org/10.1007/s10661-020-08423-x

Corwin, D.L., 2021. Climate change impacts on soil salinity in agricultural areas. Eur. J. Soil Sci. 72, 842–862. https://doi.org/10.1111/ejss.13010

Dokoohaki, H., Gheysari, M., Mousavi, S.F., Zand-Parsa, S., Miguez, F.E., Archontoulis, S. V., Hoogenboom, G., 2016. Coupling and testing a new soil water module in DSSAT CERES-Maize model for maize production under semi-arid condition. Agric. Water Manag. 163, 90–99. https://doi.org/10.1016/j.agwat.2015.09.002

Écoutin, J.-M., Barry, M., S., B., Charles-Dominique, E., Journet, O., Penot, E., Ruë, O., Souaré, D., & Sow, M. (1999). Aménagement technique du milieu. In M. C. Cormier-Salem (Ed.), Rivières du Sud: societes et mangroves ouestafricaines (pp. 209–268). IRD.

Espírito-Santo, J. (1949). Notas sobre a cultura do arroz entre os balantas. Boletim Cultural Da Guiné Portugues, 4(14), 197–232.

Fofana, I., Goundan, A., & Mangne, L. (2014). Impact Simulation of ECOWAS Rice Self-Sufficiency Policy.

https://ebrary.ifpri.org/utils/getfile/collection/p15738coll2/id/128894/filename/129105.pdf

Guei, R. G., Dixon, C. A., & Sampong, M. A. (1997). Strategies and approaches to mangrove swamp rice varietal improvement in West Africa. African Crop Science Journal, 5(2), 209–217. https://doi.org/10.4314/acsj.v5i2.27863

Hawthorne, W. (2001). Nourishing a stateless society during the slave trade: The rise of balanta paddy-rice production in Guinea-Bissau. Journal of African History, 42(1), 1–24. https://doi.org/10.1017/s0021853700007696

Kronzucker, H.J., Coskun, D., Schulze, L.M., Wong, J.R., Britto, D.T., 2013. Sodium as nutrient and toxicant. Plant Soil 369, 1–23. https://doi.org/10.1007/s11104-013-1801-2

Letey, J., Feng, G.L., 2007. Dynamic versus steady-state approaches to evaluate irrigation management of saline waters. Agric. Water Manag. 91, 1–10.

Lourenço, P., Cabral, A. I. R., Oom, D., Vasconcelos, M. J. P., Catarino, L., & Temudo, M. P. (2009). Re-growth of mangrove forests of Guinea-Bissau. In I. S. on R. S. of 33rd Environment (Ed.), International Symposium on Remote Sensing of Environment "Sustaining the Millennium Development Goals" (Stresa, La, pp. 4–8).

Mendes, O., & Fragoso, M. (2023). Assessment of the Record-Breaking 2020 Rainfall in Guinea-Bissau and Impacts of Associated Floods. Geosciences, 13(2), 25. https://doi.org/10.3390/geosciences13020025

Middleton, N., Thomas, D., Arnoldo, E., 1992. World atlas of desertification, Land Degradation & Development.

Ministry of Natural Resources and Environment. (2006). National programme of action of adaptation to climate changes (Issue December). http://unfccc.int/resource/docs/napa/gnb01.pdf

Ragab, R., 2002. A holistic generic integrated approach for irrigation, crop and field management: The SALTMED model. Environ. Model. Softw. 17, 345–361. https://doi.org/10.1016/S1364-8152(01)00079-2

Rosa, R.D., Ramos, T.B., Pereira, L.S., 2016. The dual Kc approach to assess maize and sweet sorghum transpiration and soil evaporation under saline conditions: Application of the SIMDualKc model. Agric. Water Manag. 177, 77–94. https://doi.org/10.1016/j.agwat.2016.06.028

Schwarz, C. (1993). Os ecossistemas orizícolas da Guiné–Bissau. Comunicações, 13(1), 367–388.

Shelia, V., Šimunek, J., Boote, K., Hoogenbooom, G., 2018. Coupling DSSAT and HYDRUS-1D for simulations of soil water dynamics in the soil-plant-atmosphere system. J. Hydrol. Hydromechanics 66, 232–245. https://doi.org/10.1515/johh-2017-0055

Šimůnek, J., van Genuchten, M.T., Šejna, M., 2016. Recent Developments and Applications of the HYDRUS Computer Software Packages. Vadose Zo. J. 15, vzj2016.04.0033. https://doi.org/10.2136/vzj2016.04.0033

Singh, A., 2021. Soil salinization management for sustainable development: A review. J. Environ. Manage. 277, 111383. https://doi.org/10.1016/j.jenvman.2020.111383

Sparks, D.L., 2003a. 4 - Soil Solution-Solid Phase Equilibria, in: Sparks, D.L. (Ed.), Environmental Soil Chemistry (Second Edition). Academic Press, Burlington, pp. 115–132. https://doi.org/https://doi.org/10.1016/B978-012656446-4/50004-9

Sparks, D.L., 2003b. 10 - The Chemistry of Saline and Sodic Soils, in: Sparks, D.L. (Ed.), Environmental Soil Chemistry (Second Edition). Academic Press, Burlington, pp. 285–300. https://doi.org/https://doi.org/10.1016/B978-012656446-4/50010-4

Temudo, M. P. (2011). Planting Knowledge, Harvesting Agro-Biodiversity: A Case Study of Southern Guinea-Bissau Rice Farming. Human Ecology, 39(3), 309–321. https://doi.org/10.1007/s10745-011-9404-0

Temudo, M. P., & Cabral, A. I. (2017). The Social Dynamics of Mangrove Forests in Guinea-Bissau, West Africa. Human Ecology, 45(3), 307–320. https://doi.org/10.1007/s10745-017-9907-4

van Dam, J.C., Groenendijk, P., Hendriks, R.F.A., Kroes, J.G., 2008. Advances of Modeling Water Flow in Variably Saturated Soils with SWAP. Vadose Zo. J. 7, 640–653. https://doi.org/10.2136/vzj2007.0060

Van de Craats, D., Van der Zee, S.E.A.T.M., Sui, C., Van Asten, P.J.A., Cornelissen, P., Leijnse, A., 2020. Soil sodicity originating from marginal groundwater. Vadose Zo. J. 19, 1–14. https://doi.org/10.1002/vzj2.20010

Van Ghent, P. A. M., & Ukkerman, R. (1993). The Balanta rice farming system in Guinea Bissau. Selected Papers of the Ho Chi Minh …, 1250 mm, 103–122. https://doi.org/http://content.alterra.wur.nl/Internet/webdocs/ilri-publicaties/publicaties/Pub53/pub53-h6.pdf

References for Chapter 2

Abreu, F., Correia, A., 1993. Aspectos Agro-climáticos da Guiné Bissau. Comunicações, Intituto de Invesigacion Científica Tropical 63, 33–45.

Adesina, A.A., Seidi, S., 1995. Farmers' perceptions and adoption of new agricultural technology: analysis of modern mangrove rice varieties in Guinea Bissau. Quarterly Journal of International Agriculture 34, 358–371.

Africa Rice., 2011. Lessons from the rice crisis: Policies for food security in Africa. Cotonou, Benin.

African Union., 2023. Compact Guinee-Bissau pour l'alimentation et l'agriculture. African Union.

Agegnehu, G., Amede, T., Erkossa, T., Yirga, C., Henry, C., Tyler, R., Nosworthy, M.G., Beyene, S., Sileshi, G.W., 2021. Extent and management of acid soils for sustainable crop production system in the tropical agroecosystems: a review. Acta Agriculturae Scandinavica, Section B — Soil & Plant Science 71, 852–869. https://doi.org/10.1080/09064710.2021.1954239

Agurla, S., Gahir, S., Munemasa, S., Murata, Y., Raghavendra, A.S., 2018. Mechanism of Stomatal Closure in Plants Exposed to Drought and Cold Stress, in: Iwaya-Inoue, M., Sakurai, M., Uemura, M. (Eds.), Survival Strategies in Extreme Cold and Desiccation: Adaptation Mechanisms and Their Applications. Springer Singapore, Singapore, pp. 215-232. https://doi.org/10.1007/978-981-13-1244-1_12

Alberto, M.C.R., Quilty, J.R., Buresh, R.J., Wassmann, R., Haidar, S., Correa, T.Q., Sandro, J.M., 2014. Actual evapotranspiration and dual crop coefficients for dry-seeded rice and hybrid maize grown with overhead sprinkler irrigation. Agricultural Water Management 136, 1–12. https://doi.org/10.1016/j.agwat.2014.01.005

Allen, R.G., Pereira, L.S., Raes, D., Smith, M., 1998. Crop Evapotranspiration. FAO Irrigation and Drainage Paper No. 56. 300 p.

Andreetta, A., Huertas, A.D., Lotti, M., Cerise, S., 2016. Land use changes affecting soil organic carbon storage along a mangrove swamp rice chronosequence in the Cacheu and Oio regions (northern Guinea-Bissau). Agriculture, Ecosystems & Environment 216, 314–321. https://doi.org/10.1016/j.agee.2015.10.017

Andriesse, W., Fresco, L.O., 1991. A characterization of rice-growing environments in West Africa. Agriculture, Ecosystems & Environment 33, 377–395. https://doi.org/10.1016/0167-8809(91)90059-7

Andrieu, J., 2018. Land cover changes on the West-African coastline from the Saloum Delta (Senegal) to Rio Geba (Guinea-Bissau) between 1979 and 2015. European Journal of Remote Sensing 51, 314–325. https://doi.org/10.1080/22797254.2018.1432295

Ayers, R.S., Westcot, D.W., 1985a. Water quality for agriculture. FAO, Roma, Italy.

Ayers, R.S., Westcot, D.W., 1985b. Water Quality for Agriculture. Irrigation and Drainage Paper 29. 174 p.

Balasubramanian, V., Sie, M., Hijmans, R.J., Otsuka, K., 2007. Increasing Rice Production in Sub-Saharan Africa: Challenges and Opportunities. Advances in Agronomy 94, 55–133. https://doi.org/10.1016/S0065-2113(06)94002-4

Bazrafshan, A., Shorafa, M., Mohammadi, M.H., Zolfaghari, A.A., van de Craats, D., van der Zee, S.E.A.T.M., 2020. Comparison of the individual salinity and water deficit stress using water use, yield, and plant parameters in maize. Environmental Monitoring and Assessment 192, 448. https://doi.org/10.1007/s10661-020-08423-x

Bivar, M., Temudo, M.P., 2014. Rice, cows and envy: agriculture and change among young rice producers in Guinea-Bissau (No. 086), Future Agricultures.

Bos, D., Grigoras, I., Ndiaye, A., 2006. Land cover and avian biodiversity in rice fields and mangroves of West Africa. Dakar.

Bouman, B. a. M., Lampayan, R.M., Tuong, T.P., 2007. Water Management in Irrigated Rice: Coping with Water Scarcity, International Rice Research Institute. International Rice Research Institute, Los baños, Philippines.

Bouman, B.A.M., 2007. A conceptual framework for the improvement of crop water productivity at different spatial scales. Agricultural Systems 93, 43–60. https://doi.org/10.1016/j.agsy.2006.04.004

Bouman, B.A.M., Humphreys, E., Tuong, T.P., Barker, R., 2007. Rice and Water, in: Advances in Agronomy. Academic Press, pp. 187-237. https://doi.org/10.1016/S0065-2113(04)92004-4

Cabral, A., 1954a. Acerca da Utilizaçao da terra na Africa negra. Boletim Cultural da Guiné Portugues.

Cabral, A., 1954b. A propósito de mecanizaçao da agricultuta na Guine Portuguesa. Boletim Cultural da Guiné Portugues.

Caeiro, R.M., 2019. From Learning to Doing: Diffusion of Agricultural Innovations in Guinea-Bissau (No. 26065), O13,O31,O33,Q16. Cambridge.

Castro, A., 1950. Notas sobre algumas variedades de arroz em cultura na Guiné. Boletim Cultural da Guiné Portuguesa 5, 347–378.

Chauhan, B.S., Jabran, K., Mahajan, G., 2017. Rice Production Worldwide, Rice Production Worldwide. Springer International Publishing, Cham. https://doi.org/10.1007/978-3-319-47516-5

Choudhury, B.U., Singh, A.K., Pradhan, S., 2013. Estimation of crop coefficients of dry-seeded irrigated rice–wheat rotation on raised beds by field water balance method in the Indo-Gangetic plains, India. Agricultural Water Management 123, 20–31. https://doi.org/10.1016/j.agwat.2013.03.006

Clerget, B., Bueno, C., Quilty, J.R., Correa Jr., T.Q., Sandro, J., 2014. Modifications in development and growth of a dual-adapted tropical rice variety grown as either a flooded or an aerobic crop. Field Crops Research 155, 134–143. https://doi.org/10.1016/j.fcr.2013.09.013

Cooper, S., McConkey, S., 2005. Guinea Bissau. Practical Neurology 5, 184–185. https://doi.org/10.1111/j.1474-7766.2005.00307.x

Cormier-Salem, M., 1999. Rivières du Sud. Sociétés et Mangroves Ouest Africaines, Institut d. ed. Paris.

Cornelissen, P., Van der Zee, S.E.A.T.M., Leijnse, A., 2020. Role of degradation concepts for adsorbing contaminants in context of wastewater irrigation. Vadose Zone Journal 19, 1–18. https://doi.org/10.1002/vzj2.20064

Cossa, V., 2023. Experimentação com variedades e densidades de sementeira de arroz no agroecossistema de mangal de bolanha salgada no Sul de Guiné-Bissau (Workshop). Bissau, Guinea Bissau.

Da Silva, C., 1993. Os ecosistemas Orizicolas na Guiné Bissau. Comunicações, Intituto de Invesigacion Científica Tropical 367–388.

D'Amico, M.E., Barbieri, M., Khair, D.A. El, Comolli, R., 2023. Mangrove rice productivity and pedogenic trends in Guinea Bissau, West Africa. Journal of Soils and Sediments. https://doi.org/10.1007/s11368-023-03608-6

Dias, G.A., Vasconcelos, M.J., Catarino, L., 2022. Examining the Socioeconomic Benefits of Oysters: A Provisioning Ecosystem Service from the Mangroves of Guinea-Bissau, West Africa. Journal of Coastal Research 38, 355–360. https://doi.org/10.2112/JCOASTRES-D-21-00055.1

Diaz, M.B., Roberti, D.R., Carneiro, J.V., Souza, V. de A., de Moraes, O.L.L., 2019. Dynamics of the superficial fluxes over a flooded rice paddy in southern Brazil. Agricultural and Forest Meteorology 276–277, 107650. https://doi.org/10.1016/j.agrformet.2019.107650

Doorenbos, J., Kassam, A.H., 1979. Yield Response to water. FAO Irrigation and Drainage Paper No. 33. 193 p.

Dore, M.H.I., 2005. Climate change and changes in global precipitation patterns: What do we know? Environment International 31, 1167–1181. https://doi.org/10.1016/j.envint.2005.03.004

Dossou-Yovo, E.R., Devkota, K.P., Akpoti, K., Danvi, A., Duku, C., Zwart, S.J., 2022. Thirty years of water management research for rice in sub-Saharan Africa: Achievement and perspectives. Field Crops Research 283, 108548. https://doi.org/10.1016/j.fcr.2022.108548

Écoutin, J.-M., Barry, M., S., B., Charles-Dominique, E., Journet, O., Penot, E., Ruë, O., Souaré, D., Sow, M., 1999. Aménagement technique du milieu, in: Cormier-Salem, M.C. (Ed.), Rivières Du Sud: Societes et Mangroves Ouestafricaines. IRD, Paris, pp. 209–268.

Espírito-Santo, J., 1949. Notas sobre a cultura do arroz entre os balantas. Boletim Cultural da Guiné Portugues 4, 197–232.

Espírito-Santo, J, 1949. Notas sobre a cultura do arroz entre os Balantas. Boletim Cultural da Guiné Portuguesa 4, 197–232.

Espírito-Santo, J., 1948. Nomes vernáculos de algumas plantas da Guiné Portuguesa. Boletim Cultural da Guiné Portuguesa 3, 983–1036.

FAO., 2021. Global map of salt-affected soils (GSASmap) [WWW Document]. URL https://www.fao.org/soils-portal/data-hub/soil-maps-and-databases/global-map-of-salt-affected-soils/en/ (accessed 12.15.23).

Farooq, M.S., Fatima, H., Rehman, O.U., Yousuf, M., Kalsoom, R., Fiaz, S., Khan, M.R., Uzair, M., Huo, S., 2023. Major challenges in widespread adaptation of aerobic rice system and potential opportunities for future sustainability. South African Journal of Botany 159, 231–251. https://doi.org/10.1016/j.sajb.2023.06.017

Fernandes, R.M., 2012. O Informal e o Artesanal : Pescadores e Revendedeiras de peixe na Guiné-Bissau. Universidade de Coimbra.

Fernández, F., Hoeft, R., 2021. Managing soil pH and crop nutrients, in: Illinois Extension (Ed.), Agronomy Handbook. Illinois, pp. 91-112.

Ferreira, 1968. Problemas e perpectivas do desenvolvimento rural da Guiné. Universidade técnica de Lisboa, Lisboa, Portugal.

Ferreira, A., Rolim, J., Paredes, P., Cameira, M. do R., 2023. Methodologies for Water Accounting at the Collective Irrigation System Scale Aiming at Optimizing Water Productivity. Agronomy 13, 1938. https://doi.org/10.3390/agronomy13071938

Fofana, I., Goundan, A., Mangne, L., 2014. Impact Simulation of ECOWAS Rice Self-Sufficiency Policy. Dakar.

Food and Agriculture Organization of the United Nations, 2023. FAO-STAT data base, last accessed on September 15, 2023 [WWW Document]. FAO, Rome, Italy. URL https://www.fao.org/faostat/en/#data

Food and Agriculture Organization of the United Nations., 2018. FAO Rice Market Monitor. [WWW Document]. Seguimiento del mercado del arroz de la FAO (SMA). URL https://www.fao.org/markets-and-trade/commodities/rice/rmm/en/

Fukai, S., Mitchell, J., 2022. Factors determining water use efficiency in aerobic rice. Crop and Environment 1, 24–40. https://doi.org/10.1016/j.crope.2022.03.008

Garbanzo, G., Céspedes, J., Sandoval, J., Temudo, M., Paredes, P., Cameira, M. do R., 2024. Moving toward the Biophysical Characterization of the Mangrove Swamp Rice Production System in Guinea Bissau: Exploring Tools to

Improve Soil- and Water-Use Efficiencies. Agronomy 14, 335. https://doi.org/10.3390/agronomy14020335

Genuchten, M.T. van, Hoffman, G.J., 1984. Analysis of crop salt tolerance data, in: Shainberg, I., Shalhever, J. (Eds.), Soil Salinity under Irrigation Processes and Management. Springer Verlag, pp. 258–271.

Ghassemi 1940-, F. (Fereidoun), Jakeman, A.J., Nix, H.A., Studies., A.N.University.C. for R. and E., 1995. Salinization of Land and Water Resources: Human Causes, Extent, Management and Case Studies, TA - TT -. CAB International ;, Wallingford, Oxon, UK.

Giri, B., Kapoor, R., Wu, Q.S., Varma, A., 2022. Structure and Functions of Pedosphere, Structure and Functions of Pedosphere. Springer Nature Singapore, Singapore. https://doi.org/10.1007/978-981-16-8770-9

Grieve, C.M., Grattan, S.R., Maas, E. V, 2012. Plant Salt Tolerance, in: Wallender, W.W.;, Tanji, K.K. (Eds.), Agricultural Salinity. Assessment and Management. ASCE, Reston VA., pp. 405–459.

Guei, R.G., Dixon, C.A., Sampong, M.A., 1997. Strategies and approaches to mangrove swamp rice varietal improvement in West Africa. African Crop Science Journal 5, 209–217. https://doi.org/10.4314/acsj.v5i2.27863

Hawthorne, W, 2001. Nourishing a stateless society during the slave trade: the rise of balanta paddy-rice production in Guinea-Bissau. The Journal of African History 42, 1–24. https://doi.org/10.1017/S0021853700007696

Hawthorne, WALTER, 2001. Nourishing a stateless society during the slave trade: the rise of balanta paddy-rice production in Guinea-Bissau. The Journal of African History 42, 1–24. https://doi.org/10.1017/S0021853700007696

Hoffman, G.J., Shannon, M.C., 2007. 4. Salinity, in: Lamm, F.R., Ayars, J.E., F.S., N. (Eds.), Microirrigation for Crop Production Design, Operation, and Management. Elsevier B.V., pp. 131-160. https://doi.org/10.1016/S0167-4137(07)80007-2

Hopmans, J.W., Qureshi, A.S., Kisekka, I., Munns, R., Grattan, S.R., Rengasamy, P., Ben-Gal, A., Assouline, S., Javaux, M., Minhas, P.S., Raats, P.A.C., Skaggs, T.H., Wang, G., De Jong van Lier, Q., Jiao, H., Lavado, R.S., Lazarovitch, N., Li, B., Taleisnik, E., 2021. Critical knowledge gaps and research priorities in global soil salinity, in: Advances in Agronomy. Elsevier, pp. 1-191. https://doi.org/10.1016/bs.agron.2021.03.001

Idris, O.A., Opute, P., Orimoloye, I.R., Maboeta, M.S., 2022. Climate Change in Africa and Vegetation Response: A Bibliometric and Spatially Based Information Assessment. Sustainability 14, 4974. https://doi.org/10.3390/su14094974

Kargas, G., Londra, P., Sgoubopoulou, A., 2020. Comparison of Soil EC Values from Methods Based on 1:1 and 1:5 Soil to Water Ratios and ECe from Saturated Paste Extract Based Method. Water 12, 1010. https://doi.org/10.3390/w12041010

Koehring, J., 1980. Guinea Bissau rice production. Department of Agricultural Experimentation, Bissau, Guinea Bissau.

Kraehmer, H., Thomas, C., Vidotto, F., 2017. Rice Production in Europe, in: Rice Production Worldwide. Springer International Publishing, Cham, pp. 93-116. https://doi.org/10.1007/978-3-319-47516-5_4

Kroes, J., Van Dam, J., Bartholomeus, R., Groenendijk, P., Heinen, M., Hendriks, R., Mulder, R., Supit, I., Van Walsul, P., 2017. SWAP version 4. Wageningen Environmental Research, Wageningen. https://doi.org/10.18174/416321

Kyle, S., 2015. Working Paper Rice Sector Policy Options in Guinea bissau (No. January). Cornell University, Department of Applied Economics and Management., New York, USA. https://doi.org/10.22004/ag.econ.250010

Lea, J.D. (Zach), 1993. Applied Policy Analysis of the Rice Marketing Subsector of Guinea-Bissau. Journal of International Food & Agribusiness Marketing 4, 23–40. https://doi.org/10.1300/J047v04n04_02

Linares, O.F., 2002. African rice (Oryza glaberrima): History and future potential. Proceedings of the National Academy of Sciences 99, 16360–16365. https://doi.org/10.1073/pnas.252604599

Linares, O.F., 1981. From tidal swamp to inland valley: on the social organization of wet rice cultivation among the Diola of Senegal. Africa 51, 557–595. https://doi.org/10.2307/1158828

Liu, M., Paredes, P., Shi, H., Ramos, T.B., Dou, X., Dai, L., Pereira, L.S., 2022a. Impacts of a shallow saline water table on maize evapotranspiration and groundwater contribution using static water table lysimeters and the dual Kc water balance model SIMDualKc. Agricultural Water Management 273, 107887. https://doi.org/10.1016/j.agwat.2022.107887

Liu, M., Shi, H., Paredes, P., Ramos, T.B., Dai, L., Feng, Z., Pereira, L.S., 2022b. Estimating and partitioning maize evapotranspiration as affected by salinity using weighing lysimeters and the SIMDualKc model. Agricultural Water Management 261, 107362. https://doi.org/10.1016/j.agwat.2021.107362

Luning, H.A., 1984. Rice research and development in West Africa: problems and perspectives. Netherlands Journal of Agricultural Science 32, 193–204. https://doi.org/10.18174/njas.v32i3.16896

Maas, E. V, Hoffman, G.J., 1977. Crop salt tolerance-current assessment. Journal of the Irrigation and Drainage Division 103, 115–134.

Machado, R., Serralheiro, R., 2017. Soil Salinity: Effect on Vegetable Crop Growth. Management Practices to Prevent and Mitigate Soil Salinization. Horticulturae 3, 30. https://doi.org/10.3390/horticulturae3020030

Mallareddy, M., Thirumalaikumar, R., Balasubramanian, P., Naseeruddin, R., Nithya, N., Mariadoss, A., Eazhilkrishna, N., Choudhary, A.K., Deiveegan, M., Subramanian, E., Padmaja, B., Vijayakumar, S., 2023. Maximizing Water

Use Efficiency in Rice Farming: A Comprehensive Review of Innovative Irrigation Management Technologies. Water 15, 1802. https://doi.org/10.3390/w15101802

Marius, C., Lucas, J., 1982. Evolution geochimique et exemple d´aménagement des mangroves au Senegal (Casamance). Oceanologica Acta 1, 10.

Martiarena, M.L., Temudo, M.P., 2023. Endogenous learning and innovation in African smallholder agriculture: lessons from Guinea-Bissau. The Journal of Agricultural Education and Extension 1–19. https://doi.org/10.1080/1389224X.2023.2169480

Marzouk, Y., 1991. Histoire des conceptions hydrauques etatiques et paysannes en basse Cassamance, Senegal, 1960 - 1990, in: Dupré, G. (Ed.), Savoirs Paysans et Développement. Karthala-Orstom, Paris, pp. 61-97.

McGeorge, W.T., 1954. Diagnosis and Improvement of Saline and Alkaline Soils, Agricultur. ed, Soil Science Society of America Journal. United States Department of Agriculture. https://doi.org/10.2136/sssaj1954.03615995001800030032x

Medina, N., 2008. O ecossistema orizícola na Guiné-Bissau: principais constrangimentos à produção na zona (regiões de biombo, cacheu e oio) e perspectivas. Universidade Técnica de Lisboa.

Mendes, O., Fragoso, M., 2023. Assessment of the Record-Breaking 2020 Rainfall in Guinea-Bissau and Impacts of Associated Floods. Geosciences 13, 25. https://doi.org/10.3390/geosciences13020025

Merkohasanaj, M., Cortez, N., Goulao, L., Andreetta, A., 2022. Characterisation of physical-chemical and fertility dynamics of mangrove soils from Guinea-Bissau in different agroecological conditions underlying paddy rice cultivation ao cultivo do arroz. Revista de Ciencias Agrarias 45, 267–271. https://doi.org/https://doi.org/10.19084/rca.28424

Minhas, P.S., Qadir, M., Yadav, R.K., 2019. Groundwater irrigation induced soil sodification and response options. Agricultural Water Management 215, 74–85. https://doi.org/10.1016/j.agwat.2018.12.030

Minhas, P.S., Ramos, T.B., Ben-Gal, A., Pereira, L.S., 2020. Coping with salinity in irrigated agriculture: Crop evapotranspiration and water management issues. Agricultural Water Management 227, 105832. https://doi.org/10.1016/j.agwat.2019.105832

Ministry of Natural Resources and Environment., 2006. National programme of action of adaptation to climate changes. Bissau, Guinea Bissau.

Miranda, I., 1993. Pesquisa Orizícola Guineense. Comunicações, Intituto de Invesigacion Científica Tropical 97–114.

Moratiel, R., Martínez-Cob, A., 2013. Evapotranspiration and crop coefficients of rice (Oryza sativa L.) under sprinkler irrigation in a semiarid climate determined

by the surface renewal method. Irrigation Science 31, 411–422. https://doi.org/10.1007/s00271-011-0319-8

Mota, T., 1954. Guiné portuguesa, Vol 1. ed. Agência Geral do Ultramar, Lisboa.

Naidoo, G., 2023. The mangroves of Africa : A review. Marine Pollution Bulletin 190, 114859. https://doi.org/10.1016/j.marpolbul.2023.114859

Nie, L., Peng, S., 2017. Rice Production in China, in: B.S. Chauhan et al. (eds.) (Ed.), Rice Production Worldwide. Springer International Publishing, Berlin, Germany, pp. 33–52. https://doi.org/10.1007/978-3-319-47516-5

Njipouakouyou, S., LonaTchedná, J., Mendes, O., Mendes, C.L., 2019. A comparative investigation of evapotranspiration (Et) obtained from two methods and determining a best cultivation period. case of Bafata-Guinea Bissau. International Journal of Current Research 11, 1468–1470. https://doi.org/https://doi.org/10.24941/ijcr.34115.02.2019

Nuijten, E., Temudo, M., Richards, P., Okry, F., Teeken, B., Mokuwa, A., Struik, P.C., 2013. Towards a new approach for understanding interactions of technology with environment and society in small-scale rice farming., in: Realizing Africa's Rice Promise. CABI, UK, pp. 355-366. https://doi.org/10.1079/9781845938123.0355

Nuijten, E., van Treuren, R., Struik, P.C., Mokuwa, A., Okry, F., Teeken, B., Richards, P., 2009. Evidence for the Emergence of New Rice Types of Interspecific Hybrid Origin in West African Farmers' Fields. PLoS ONE 4, e7335. https://doi.org/10.1371/journal.pone.0007335

Oosterbaan, R.J., 2000. SALTMOD: Description of Principles, User Manual, and Examples of Application.

Oosterbaan, RJ.;, Vos, J., 1980. Rice polders in the acid sulfate soils of the bolanhas in the mangroves of Guinea-Bissau, International Institute for Land Reclamation and Improvement. Wageningen, The Netherlands.

Oue, H., Laban, S., 2020. Water use of rice and mung bean cultivations in a downstream area of an irrigation system in South Sulawesi in the 2nd dry season. Paddy and Water Environment 18, 87–98. https://doi.org/10.1007/s10333-019-00766-7

Padhy, S.R., Dash, P.K., Bhattacharyya, P., 2022. Challenges, opportunities, and climate change adaptation strategies of mangrove-agriculture ecosystem in the Sundarbans, India: a review. Wetlands Ecology and Management 30, 191–206. https://doi.org/10.1007/s11273-021-09844-2

Penot, E., 1998. La riziculture de mangrove balante de la région Tombali (Guinée-Bissau) ou l'adaptation d'une société rizicole africaine à travers un siècle de changements majeurs, in: Leplaideur, A., Chéneau-Loquay, A. (Eds.), Les Rizicultures de l'Afrique de l'Ouest - Partie III : Les Modèles Inondés Endogènes. ORSTOM, CIRAD-CA, Montpellier, pp. 251–258.

Penot, E., 1995. La riziculture de mangrove balante de la region de Tombali en Guinée-Bissau, ou l'adaptation d'une société rizicole africaine traditionnelle à travers un siècle de changements majeurs. Séminaire « Riziculture en Afrique de l'Ouest ».

Penot, E., 1994. La riziculture de mangrove de la société balant dans la région de Tombali (Guinée-Bissau), in: Cormier-Salem, M.-C. (Ed.), Dynamique et Usages de La Mangrove Dans Les Pays Des Rivières Du Sud, Du Sénégal à La Sierra Leone. ORSTOM, Paris, pp. 209–222.

Penot, E., 1992. L'économie d'une société rizicole traditionnelle en pleine mutation : la société balante de la région de Tombali en Guinée Bissau, Education et Développement interculturels. Bissau, Guinea Bissau.

Pereira, L.S., Cordery, I., Iacovides, I., 2012. Improved indicators of water use performance and productivity for sustainable water conservation and saving. Agricultural Water Management 108, 39–51. https://doi.org/10.1016/j.agwat.2011.08.022

Pereira, L.S., Gonçalves, J.M., Dong, B., Mao, Z., Fang, S.X., 2007. Assessing basin irrigation and scheduling strategies for saving irrigation water and controlling salinity in the upper Yellow River Basin, China. Agricultural Water Management 93, 109–122. https://doi.org/10.1016/j.agwat.2007.07.004

Ragab, R., 2002. A holistic generic integrated approach for irrigation, crop and field management: the SALTMED model. Environmental Modelling & Software 17, 345–361. https://doi.org/10.1016/S1364-8152(01)00079-2

Rengasamy, P., 2016. Soil Salinization. Oxford Research Encyclopedia of Environmental Science 1–31. https://doi.org/10.1093/acrefore/9780199389414.013.65

Rhoades, J., Kandiah, A., Mashali, A., 1992. The use of saline waters for crop production, FAO Irrigation and Drainage Paper 48. Roma, Italy.

Rodrigues, G.C., Pereira, L.S., 2009. Assessing economic impacts of deficit irrigation as related to water productivity and water costs. Biosystems Engineering 103, 536–551. https://doi.org/10.1016/j.biosystemseng.2009.05.002

Rodrigues, J., Carrapiço, F., 1990. Studies on rice production using Azolla as biofertilizer in Guinea-Bissau, in: Polsinelli, M., Materassi, R., Vicenzini, M. (Eds.), Nitrogen Fixation: Developments in Plant and Soil Sciences. Proceedings of the Fifth International Symposium on Nitrogen Fixation with Non-Legumes, Florence, Italy, pp. 541-542.

Röhrig, F., Bougouma, K., Schiek, B., Ghosh, A., Ramirez-Villegas, J., Achicanoy, H., Esquivel, A., Saavedra, C., Diekjürgen, D., Grosjean, G., 2021. WFP Critical Corporate Initiative: Climate Response Analysis for Adaptation Guinea Bissau. The Alliance of Bioversity and The International Center for Tropical Agriculture; World Food Programme 76.

Rosa, R.D., Paredes, P., Rodrigues, G.C., Alves, I., Fernando, R.M., Pereira, L.S., Allen, R.G., 2012. Implementing the dual crop coefficient approach in interactive

software. 1. Background and computational strategy. Agricultural Water Management 103, 8–24. https://doi.org/10.1016/j.agwat.2011.10.013

Rosa, R.D., Ramos, T.B., Pereira, L.S., 2016. The dual Kc approach to assess maize and sweet sorghum transpiration and soil evaporation under saline conditions: Application of the SIMDualKc model. Agricultural Water Management 177, 77–94. https://doi.org/10.1016/j.agwat.2016.06.028

Secretary of State for Environment and Tourism., 2014. Fifth National Report to the Convention on Biological Diversity. Bissau, Guinea Bissau.

Seidi, S., 1998. An Economic Analysis of Mangrove Rice Research, Extension and Seed Production in Guinea-Bissau: Preliminary Evidence from the Tombali Region. Etudes et recherches saheliennes 1, 33–39.

Šimůnek, J., Suarez, D.L., 1994. Two-dimensional transport model for variably saturated porous media with major ion chemistry. Water Resources Research 30, 1115–1133. https://doi.org/10.1029/93WR03347

Šimůnek, J., Van Genuchten, M.Th., Šejna, M., 2016. Recent Developments and Applications of the HYDRUS Computer Software Packages. Vadose Zone Journal 15, 1–25. https://doi.org/10.2136/vzj2016.04.0033

Soullier, G., Demont, M., Arouna, A., Lançon, F., Mendez del Villar, P., 2020. The state of rice value chain upgrading in West Africa. Global Food Security 25, 100365. https://doi.org/10.1016/j.gfs.2020.100365

Sousa, J., Campos, R., Mendes, O., Duarte Lopes, P., Matias, M., Rosa, A.P., Mendes Fernandes, R., Cruz, C., Indjai, B., Infande, A., da Costa, M., Salvaterra, G., Lourenço, J., Tavares, D., Camala, D., Ainslie, A., Catarino, L., 2023. The (dis)engagement of mangrove forests and mangrove rice in academic and non-academic literature on Guinea-Bissau–a systematic review protocol. PLOS ONE 18, e0284266. https://doi.org/10.1371/journal.pone.0284266

Sparks, D.L., 2003a. Soil Solution-Solid Phase Equilibria, in: Sparks, D.L. (Ed.), Environmental Soil Chemistry. Elsevier, Burlington, pp. 115–132. https://doi.org/10.1016/B978-012656446-4/50004-9

Sparks, D.L., 2003b. The Chemistry of Saline and Sodic Soils, in: Sparks, D.L. (Ed.), Environmental Soil Chemistry. Elsevier, Burlington, pp. 285-300. https://doi.org/10.1016/B978-012656446-4/50010-4

Strawn, D., Bohn, H., O'Connor, G., 2015. Salt-Affected soils, in: Soil Chemistry. John Wiley & Sons, Ltd, Oxford, UK, pp. 333-350.

Sylla, M., 1994. Soil salinity and acidity: spatial variabily and effects on rice production in west africa's mangrove zone. Wageningen University and Research.

Sylla, M., Stein, A., van Breemen, N., Fresco, L.O., 1995. Spatial variability of soil salinity at different scales in the mangrove rice agro-ecosystem in West Africa. Agriculture, Ecosystems & Environment 54, 1–15. https://doi.org/10.1016/0167-8809(95)00594-I

Teeken, B., Nuijten, E., Temudo, M.P., Okry, F., Mokuwa, A., Struik, P.C., Richards, P., 2012. Maintaining or Abandoning African Rice: Lessons for Understanding Processes of Seed Innovation. Human Ecology 40, 879–892. https://doi.org/10.1007/s10745-012-9528-x

Teeken, B., Temudo, M.P., 2021. Varietal selection in marginal agroecological niches and cultural landscapes: the case of rice in the Togo Hills. Agroecology and Sustainable Food Systems 45, 1109–1138. https://doi.org/10.1080/21683565.2021.1878405

Teixeira, D.S., 1962. Os solos da Guiné Portuguesa. Carta general caracteristicas, formação e utilização, 1st ed, Junta de investigaçoes do ultramar. Junta de Investigações do Ultramar, Lisboa.

Temudo, M.P., 2011. Planting Knowledge, Harvesting Agro-Biodiversity: A Case Study of Southern Guinea-Bissau Rice Farming. Human Ecology 39, 309–321. https://doi.org/10.1007/s10745-011-9404-0

Temudo, M.P., 1998. Inovação e mudança em sociedades rurais africanas gestão de recursos naturais, saber local e instituições de desenvolvimento induzido estudo de caso na Guiné-Bissau. Universidade Técnica de Lisboa.

Temudo, M.P., Cabral, A.I., 2017. The Social Dynamics of Mangrove Forests in Guinea-Bissau, West Africa. Human Ecology 45, 307–320. https://doi.org/10.1007/s10745-017-9907-4

Temudo, M.P., Cabral, A.I.R., 2023. Climate change as the last trigger in a long-lasting conflict: the production of vulnerability in northern Guinea-Bissau, West Africa. The Journal of Peasant Studies 50, 315–338. https://doi.org/10.1080/03066150.2021.1996355

Temudo, M.P., Cabral, A.I.R., Reis, P., 2022. The Sea Swallowed our Houses and Rice Fields: The Vulnerability to Climate Change of Coastal People in Guinea-Bissau, West Africa. Human Ecology 50, 835–850. https://doi.org/10.1007/s10745-022-00352-2

Temudo, M.P., Figueira, R., Abrantes, M., 2015. Landscapes of bio-cultural diversity: shifting cultivation in Guinea-Bissau, West Africa. Agroforestry Systems 89, 175–191. https://doi.org/10.1007/s10457-014-9752-z

Temudo, M.P., Oom, D., Pereira, J.M., 2020. Bio-cultural fire regions of Guinea-Bissau: Analysis combining social research and satellite remote sensing. Applied Geography 118, 102203. https://doi.org/10.1016/j.apgeog.2020.102203

Temudo, M.P., Santos, P., 2017. Shifting environments in Eastern Guinea-Bissau, West Africa: The length of fallows in question. NJAS: Wageningen Journal of Life Sciences 80, 57–64. https://doi.org/10.1016/j.njas.2016.12.001

Tesio, F., Camerini, F., Maucieri, G., Bertini, C., Cerise, S., 2021. Mangrove rice biodiversity valorization in Guinea Bissau. A bottom-up approach. Experimental Agriculture 57, 244–254. https://doi.org/10.1017/S001447972100017X

The Republic of Guinea-Bissau., 2018. Framework Convention on Climate Change. National Communication. Bissau.

The World Bank, 2023. The Climate Change Knowledge Product [WWW Document]. The world Bank. URL https://climateknowledgeportal.worldbank.org/download-data

Thiam, S., Villamor, G.B., Kyei-Baffour, N., Matty, F., 2019. Soil salinity assessment and coping strategies in the coastal agricultural landscape in Djilor district, Senegal. Land Use Policy 88, 104191. https://doi.org/10.1016/j.landusepol.2019.104191

Ukpong, I.E., 1997. Vegetation and its relation to soil nutrient and salinity in the Calabar mangrove swamp, Nigeria. Mangroves and Salt Marshes 1, 211–218. https://doi.org/https://doi.org/10.1023/A:1009952700317

Ukpong, I.E., 1995. An Ordination Study of Mangrove Swamp Communities in West Africa. Vegetatio 116, 147–159.

Van Dam, J.C., Groenendijk, P., Hendriks, R.F.A., Kroes, J.G., 2008. Advances of Modeling Water Flow in Variably Saturated Soils with SWAP. Vadose Zone Journal 7, 640–653. https://doi.org/10.2136/vzj2007.0060

Van de Craats, D., Van der Zee, S.E.A.T.M., Sui, C., Van Asten, P.J.A., Cornelissen, P., Leijnse, A., 2020. Soil sodicity originating from marginal groundwater. Vadose Zone Journal 19, 1–14. https://doi.org/10.1002/vzj2.20010

Van der Knaap, M., 2019. Rice-fish farming in Sub-Saharan Africa. FAO Aquaculture Newsletter 1.

Van Ghent, P.A.M., Ukkerman, R., 1993. The Balanta rice farming system in Guinea Bissau, Projet PRIVAT. WUR, Wageningen, The Netherlands. https://doi.org/http://content.alterra.wur.nl/Internet/webdocs/ilri-publicaties/publicaties/Pub53/pub53-h6.pdf

van Oort, P.A.J., 2018. Mapping abiotic stresses for rice in Africa: Drought, cold, iron toxicity, salinity and sodicity. Field Crops Research 219, 55–75. https://doi.org/10.1016/j.fcr.2018.01.016

van Oort, P.A.J., Zwart, S.J., 2018. Impacts of climate change on rice production in Africa and causes of simulated yield changes. Global Change Biology 24, 1029–1045. https://doi.org/10.1111/gcb.13967

Vasconcelos, M.J., Cabral, A.I.R., Melo, J.B., Pearson, T.R.H., Pereira, H. de A., Cassamá, V., Yudelman, T., 2015. Can blue carbon contribute to clean development in West-Africa? The case of Guinea-Bissau. Mitigation and Adaptation Strategies for Global Change 20, 1361–1383. https://doi.org/10.1007/s11027-014-9551-x

Verburg, Kirsten., 1996. SWIM v2. 1 user manual.

Wolanski, E., Cassagne, B., 2000. Salinity intrusion and rice farming in the mangrove-fringed Konkoure River delta, Guinea. Wetlands Ecology and Management 8, 29–36. https://doi.org/10.1023/A:1008470005880

World Bank Group., 2019. Guinea Bissau : Unlocking diversification to unleash agriculture growth. Bissau, Guinea Bissau.

Zwart, S.J., 2013. Assessing and improving water productivity of irrigated rice systems in Africa., in: Wopereis, M.C.S., Johnson, D.E., Ahmadi, N., Tollens, E., Jalloh, A. (Eds.), Realizing Africa's Rice Promise. Wallingford UK, pp. 265-275. https://doi.org/https://doi.org/10.1079/9781845938123.0265

References for Chapter 3

A. Kirkby, E., Nikolic, M., White, P.J., Xu, G., 2023. Mineral nutrition, yield, and source–sink relationships, in: Marschner's Mineral Nutrition of Plants. Elsevier, pp. 131-200. https://doi.org/10.1016/B978-0-12-819773-8.00015-0

Adhikari, K., Kheir, R.B., Greve, M.B., Bøcher, P.K., Malone, B.P., Minasny, B., McBratney, A.B., Greve, M.H., 2013. High-Resolution 3-D Mapping of Soil Texture in Denmark. Soil Science Society of America Journal 77, 860–876. https://doi.org/10.2136/sssaj2012.0275

Andreetta, A., Huertas, A.D., Lotti, M., Cerise, S., 2016. Land use changes affecting soil organic carbon storage along a mangrove swamp rice chronosequence in the Cacheu and Oio regions (northern Guinea-Bissau). Agric Ecosyst Environ 216, 314–321. https://doi.org/10.1016/j.agee.2015.10.017

Andrieu, J., 2018. Land cover changes on the West-African coastline from the Saloum Delta (Senegal) to Rio Geba (Guinea-Bissau) between 1979 and 2015. Eur J Remote Sens 51, 314–325. https://doi.org/10.1080/22797254.2018.1432295

Arvidsson, J., Bölenius, E., 2006. Effects of soil water content during primary tillage – laser measurements of soil surface changes. Soil Tillage Res 90, 222–229. https://doi.org/10.1016/j.still.2005.09.005

ASTM Committee D4318-17 on Soil and R Rock, 2010. Standard test methods for liquid limit, plastic limit, and plasticity index of soils. ASTM international. https://doi.org/10.1520/D4318-00

Baggie, I., Sumah, F., Zwart, S.J., Sawyerr, P., Bandabla, T., Kamara, C.S., 2018. Characterization of the mangrove swamp rice soils along the Great Scarcies River in Sierra Leone using principal component analysis. Catena (Amst) 163, 54–62. https://doi.org/10.1016/j.catena.2017.11.026

Balasubramanian, V., Sie, M., Hijmans, R.J., Otsuka, K., 2007. Increasing Rice Production in Sub-Saharan Africa: Challenges and Opportunities. Advances in Agronomy 94, 55–133. https://doi.org/10.1016/S0065-2113(06)94002-4

Beck, H.E., Zimmermann, N.E., McVicar, T.R., Vergopolan, N., Berg, A., Wood, E.F., 2018. Present and future Köppen-Geiger climate classification maps at 1-km resolution. Sci Data 5, 180214. https://doi.org/10.1038/sdata.2018.214

Boekel, P., Peerlkamp, P.L., 1956. Soil consistency as a factor determining the soil structure of clay soils. Netherlands Journal of Agricultural Science 4, 122–125. https://doi.org/10.18174/njas.v4i1.17792

Bos, D., Grigoras, I., Ndiaye, A., 2006. Land cover and avian biodiversity in rice fields and mangroves of West Africa. Dakar.

Casagrande, A., 1958. Notes on the Design of the Liquid Limit Device. Géotechnique 8, 84–91. https://doi.org/10.1680/geot.1958.8.2.84

Chapman, H.D., 2016. Cation-Exchange Capacity, in: Methods of Soil Analysis, Part 2: Chemical and Microbiological Properties. pp. 891-901. https://doi.org/10.2134/agronmonogr9.2.c6

Chauhan, B.S., Jabran, K., Mahajan, G., 2017. Rice Production Worldwide, Rice Production Worldwide. Springer International Publishing, Cham. https://doi.org/10.1007/978-3-319-47516-5

Chen, Y., 2013. New Approaches for Calculating Moran's Index of Spatial Autocorrelation. PLoS One 8, e68336. https://doi.org/10.1371/journal.pone.0068336

Cresswell, H.P., Painter, D.J., Cameron, K.C., 1991. Tillage and water content effects on surface soil physical properties. Soil Tillage Res 21, 67–83. https://doi.org/10.1016/0167-1987(91)90006-J

Davidson, J., 2009. "We Work Hard": Customary Imperatives of the Diola Work Regime in the Context of Environmental and Economic Change. Afr Stud Rev 52, 119–141. https://doi.org/10.1353/arw.0.0179

Dexter, A.R., Bird, N.R.A., 2001. Methods for predicting the optimum and the range of soil water contents for tillage based on the water retention curve. Soil Tillage Res 57, 203–212. https://doi.org/10.1016/S0167-1987(00)00154-9

Dossou-Yovo, E.R., Devkota, K.P., Akpoti, K., Danvi, A., Duku, C., Zwart, S.J., 2022. Thirty years of water management research for rice in sub-Saharan Africa: Achievement and perspectives. Field Crops Res 283, 108548. https://doi.org/10.1016/j.fcr.2022.108548

Écoutin, J.-M., Barry, M., S., B., Charles-Dominique, E., Journet, O., Penot, E., Ruë, O., Souaré, D., Sow, M., 1999. Aménagement technique du milieu, in: Cormier-Salem, M.C. (Ed.), Rivières Du Sud: Societes et Mangroves Ouestafricaines. IRD, Paris, pp. 209–268.

Espinosa, J., Molina, E., 1999. Acidez y Encalado de los Suelos, 1 ed. ed. International Plan Nutrition Institute.

Espírito-Santo, J., 1949. Notas sobre a cultura do arroz entre os balantas. Boletim Cultural da Guiné Portugues 4, 197–232.

Fandé, M.B., Ponte Lira, C., Penha-Lopes, G., 2022. Using TanDEM-X Global DEM to Map Coastal Flooding Exposure under Sea-Level Rise: Application to Guinea-Bissau. ISPRS Int J Geoinf 11, 225. https://doi.org/10.3390/ijgi11040225

Food and Agriculture Organization of the United Nations., 2018. FAO Rice Market Monitor. [WWW Document]. Seguimiento del mercado del arroz de la FAO (SMA). URL https://www.fao.org/markets-and-trade/commodities/rice/rmm/en/

Garbanzo, G., Cameira, R., Temudo, M., Paredes, P., 2024. Mangrove swamp rice production system of Guinea Bissau: Identification of main constraints

associated with salinity and rainfall variability. Submitted to Agronomy for publication 30.

Garbanzo-León, J.G., Alemán-Montes, B., Alvarado-Hernández, A., Henríquez-Henríquez, C., 2017. Validación de modelos geoestadísticos y convencionales en la determinación de la variación espacial de la fertilidad de suelos del Pacífico Sur de Costa Rica. Investigaciones Geográficas 2017, 20–41. https://doi.org/10.14350/rig.54706

García del Toro, E.M., Más-López, M.I., 2019. Changes in Land Cover in Cacheu River Mangroves Natural Park, Guinea-Bissau: The Need for a More Sustainable Management. Sustainability 11, 6247. https://doi.org/10.3390/su11226247

Grattan, S.R., Grieve, C.M., 1992. Mineral element acquisition and growth response of plants grown in saline environments. Agric Ecosyst Environ 38, 275–300. https://doi.org/10.1016/0167-8809(92)90151-Z

Haigh, S.K., Vardanega, P.J., Bolton, M.D., 2013. The plastic limit of clays. Géotechnique 63, 435–440. https://doi.org/10.1680/geot.11.P.123

Hawthorne, W., 2001. Nourishing a stateless society during the slave trade: the rise of balanta paddy-rice production in Guinea-Bissau. The Journal of African History 42, 1–24. https://doi.org/10.1017/S0021853700007696

Hongliang Fang, Shunlin Liang, McClaran, M.P., van Leeuwen, W.J.D., Drake, S., Marsh, S.E., Thomson, A.M., Izaurralde, R.C., Rosenberg, N.J., 2005. Biophysical characterization and management effects on semiarid rangeland observed from Landsat ETM+ data. IEEE Transactions on Geoscience and Remote Sensing 43, 125–134. https://doi.org/10.1109/TGRS.2004.839813

Keller, T., Arvidsson, J., Dexter, A., 2007. Soil structures produced by tillage as affected by soil water content and the physical quality of soil. Soil Tillage Res 92, 45–52. https://doi.org/10.1016/j.still.2006.01.001

Keller, T., Dexter, A.R., 2012. Plastic limits of agricultural soils as functions of soil texture and organic matter content. Soil Research 50, 7. https://doi.org/10.1071/SR11174

Kraehmer, H., Thomas, C., Vidotto, F., 2017. Rice Production in Europe, in: Rice Production Worldwide. Springer International Publishing, Cham, pp. 93-116. https://doi.org/10.1007/978-3-319-47516-5_4

Kunhikrishnan, A., Thangarajan, R., Bolan, N.S., Xu, Y., Mandal, S., Gleeson, D.B., Seshadri, B., Zaman, M., Barton, L., Tang, C., Luo, J., Dalal, R., Ding, W., Kirkham, M.B., Naidu, R., 2016. Functional Relationships of Soil Acidification, Liming, and Greenhouse Gas Flux, in: Advances in Agronomy. pp. 1-71. https://doi.org/10.1016/bs.agron.2016.05.001

Kyle, S., 2015. Working Paper Rice Sector Policy Options in Guinea bissau (No. January). Cornell University, Department of Applied Economics and Management., New York, USA. https://doi.org/10.22004/ag.econ.250010

Linares, O.F., 2002. African rice (Oryza glaberrima): History and future potential. Proceedings of the National Academy of Sciences 99, 16360–16365. https://doi.org/10.1073/pnas.252604599

Linares, O.F., 1981. From tidal swamp to inland valley: on the social organization of wet rice cultivation among the Diola of Senegal. Africa 51, 557–595. https://doi.org/10.2307/1158828

Marius, C., Lucas, J., 1991. Holocene mangrove swamps of West Africa sedimentology and soils. Journal of African Earth Sciences (and the Middle East) 12, 41–54. https://doi.org/10.1016/0899-5362(91)90056-5

Martiarena, M.L., Temudo, M.P., 2023. Endogenous learning and innovation in African smallholder agriculture: lessons from Guinea-Bissau. The Journal of Agricultural Education and Extension 1–19. https://doi.org/10.1080/1389224X.2023.2169480

Martínez-López, J., Bertzky, B., Willcock, S., Robuchon, M., Almagro, M., Delli, G., Dubois, G., 2021. Remote Sensing Methods for the Biophysical Characterization of Protected Areas Globally: Challenges and Opportunities. ISPRS Int J Geoinf 10, 384. https://doi.org/10.3390/ijgi10060384

Mendes, O., Fragoso, M., 2023. Assessment of the Record-Breaking 2020 Rainfall in Guinea-Bissau and Impacts of Associated Floods. Geosciences (Basel) 13, 25. https://doi.org/10.3390/geosciences13020025

Merkohasanaj, M., Cortez, N., Goulao, L., Andreetta, A., 2022. Characterisation of physical-chemical and fertility dynamics of mangrove soils from Guinea-Bissau in different agroecological conditions underlying paddy rice cultivation ao cultivo do arroz. Revista de Ciencias Agrarias 45, 267–271. https://doi.org/https://doi.org/10.19084/rca.28424

Miranda, I., 1993. Pesquisa Orizícola Guineense. Comunicações, Intituto de Invesigacion Científica Tropical 97–114.

Mosleh, Z., Salehi, M.H., Jafari, A., Borujeni, I.E., Mehnatkesh, A., 2016. The effectiveness of digital soil mapping to predict soil properties over low-relief areas. Environ Monit Assess 188, 195. https://doi.org/10.1007/s10661-016-5204-8

Nambiar, K.K.M., Gupta, A.P., Fu, Q., Li, S., 2001. Biophysical, chemical and socio-economic indicators for assessing agricultural sustainability in the Chinese coastal zone. Agric Ecosyst Environ 87, 209–214. https://doi.org/10.1016/S0167-8809(01)00279-1

Obour, P.B., Lamandé, M., Edwards, G., Sørensen, C.G., Munkholm, L.J., 2017. Predicting soil workability and fragmentation in tillage: a review. Soil Use Manag 33, 288–298. https://doi.org/10.1111/sum.12340

O'Kelly, B.C., Vardanega, P.J., Haigh, S.K., 2018. Use of fall cones to determine Atterberg limits: a review. Géotechnique 68, 843–856. https://doi.org/10.1680/jgeot.17.R.039

Penot, E., 1995. La riziculture de mangrove balante de la region de Tombali en Guinée-Bissau, ou l'adaptation d'une société rizicole africaine traditionnelle à travers un siècle de changements majeurs. Séminaire « Riziculture en Afrique de l'Ouest ».

Penot, E., 1992. L'économie d'une société rizicole traditionnelle en pleine mutation : la société balante de la région de Tombali en Guinée Bissau, Education et Développement interculturels. Bissau, Guinea Bissau.

Poggio, L., Gimona, A., 2017. 3D mapping of soil texture in Scotland. Geoderma Regional 9, 5–16. https://doi.org/10.1016/j.geodrs.2016.11.003

Posit team, 2023. RStudio: Integrated Development Environment for R. [WWW Document]. URL http://www.posit.co/

Raimundo Lopes, N.D., Li, T., Qian, D., Matomela, N., Sá, R.M., 2022. Factors influencing coastal land cover change and corresponding impact on habitat quality in the North-western Coastline of Guinea-Bissau (NC-GB). Ocean Coast Manag 224, 106181. https://doi.org/10.1016/j.ocecoaman.2022.106181

Sambú, F.B., 2003. Variabilidade Climática da Precipitação na Região da Guiné-Bissau: Situação Sinóptica e a Influencia dos Sistemas Convectivos. Universidade de Évora.

Santos, C., Mourato, J.M., 2022. 'I was born here, I will die here': climate change and migration decisions from coastal and insular Guinea-Bissau. Geogr Ann Ser B 1–19. https://doi.org/10.1080/04353684.2022.2154689

Schoeneberger, P., Wysocki, E.C.B., Staff, S.S., 2012. Field book for describing and sampling soils, Version 3.0. Natural, Natural Resources Conservation Service, National Soil Survey Center. https://doi.org/10.1038/258254a0

Schwarz, C., 1993. Os ecossistemas orizícolas da Guiné–Bissau. Comunicações 13, 367–388.

Sharma, B., Bora, P.K., 2003. Plastic Limit, Liquid Limit and Undrained Shear Strength of Soil—Reappraisal. Journal of Geotechnical and Geoenvironmental Engineering 129, 774–777. https://doi.org/10.1061/(ASCE)1090-0241(2003)129:8(774)

Singh, M., Kalra, N., Chakraborty, D., Kamble, K., Barman, D., Saha, S., Mittal, R.B., Pandey, S., 2008. Biophysical and socioeconomic characterization of a water-stressed area and simulating agri-production estimates and land use planning under normal and extreme climatic events: a case study. Environ Monit Assess 142, 97–108. https://doi.org/10.1007/s10661-007-9911-z

Sivakumar, V., O'Kelly, B.C., Henderson, L., Moorhead, C., Chow, S.H., 2015. Measuring the plastic limit of fine soils: an experimental study. Proceedings of the Institution of Civil Engineers - Geotechnical Engineering 168, 53–64. https://doi.org/10.1680/geng.14.00004

Soil Survey Staff., 2022a. Keys to soil taxonomy, 13th ed, Soil Conservation Service. Natural Resourses Conservation Service,.

Soil Survey Staff., 2022b. Kellogg soil survey laboratory methods manual, Soil Survey Investigations Report.

Sowers, G., 1965. Methods of Soil Analysis, Methods of Soil Analysis: Part 1 Physical and Mineralogical Properties, Including Statistics of Measurement and Sampling, Agronomy Monographs. American Society of Agronomy, Soil Science Society of America, Madison, WI, USA. https://doi.org/10.2134/agronmonogr9.1

Sylla, M., 1994. Soil salinity and acidity: spatial variabily and effects on rice production in west africa's mangrove zone. Wageningen University and Research.

Sylla, M., Stein, A., van Breemen, N., Fresco, L.O., 1995. Spatial variability of soil salinity at different scales in the mangrove rice agro-ecosystem in West Africa. Agric Ecosyst Environ 54, 1–15. https://doi.org/10.1016/0167-8809(95)00594-I

Teixeira, D.S., 1962. Os solos da Guiné Portuguesa. Carta general caracteristicas, formação e utilização, 1st ed, Junta de investigaçoes do ultramar. Junta de Investigações do Ultramar, Lisboa.

Temudo, M.P., 2018. Men wielding the plough: Changing patterns of production and reproduction among the Balanta of Guinea-Bissau. Journal of Agrarian Change 18, 267–280. https://doi.org/10.1111/joac.12222

Temudo, M.P., 2011. Planting Knowledge, Harvesting Agro-Biodiversity: A Case Study of Southern Guinea-Bissau Rice Farming. Hum Ecol 39, 309–321. https://doi.org/10.1007/s10745-011-9404-0

Temudo, M.P., 1998. Inovação e mudança em sociedades rurais africanas gestão de recursos naturais, saber local e instituições de desenvolvimento induzido estudo de caso na Guiné-Bissau. Universidade Técnica de Lisboa.

Temudo, M.P., Cabral, A.I., 2017. The Social Dynamics of Mangrove Forests in Guinea-Bissau, West Africa. Hum Ecol 45, 307–320. https://doi.org/10.1007/s10745-017-9907-4

Temudo, M.P., Cabral, A.I.R., 2023. Climate change as the last trigger in a long-lasting conflict: the production of vulnerability in northern Guinea-Bissau, West Africa. J Peasant Stud 50, 315–338. https://doi.org/10.1080/03066150.2021.1996355

Temudo, M.P., Cabral, A.I.R., Reis, P., 2022. The Sea Swallowed our Houses and Rice Fields: The Vulnerability to Climate Change of Coastal People in Guinea-Bissau, West Africa. Hum Ecol 50, 835–850. https://doi.org/10.1007/s10745-022-00352-2

Tesio, F., Camerini, F., Maucieri, G., Bertini, C., Cerise, S., 2021. Mangrove rice biodiversity valorization in Guinea Bissau. A bottom-up approach. Exp Agric 57, 244–254. https://doi.org/10.1017/S001447972100017X

Thiam, S., Villamor, G.B., Kyei-Baffour, N., Matty, F., 2019. Soil salinity assessment and coping strategies in the coastal agricultural landscape in Djilor district, Senegal. Land use policy 88, 104191. https://doi.org/10.1016/j.landusepol.2019.104191

Ukpong, I.E., 1997. Vegetation and its relation to soil nutrient and salinity in the Calabar mangrove swamp, Nigeria. Mangroves and Salt Marshes 1, 211–218. https://doi.org/https://doi.org/10.1023/A:1009952700317

Ukpong, I.E., 1995. An Ordination Study of Mangrove Swamp Communities in West Africa. Vegetatio 116, 147–159.

Unger, P., 1984. Soil tillage in Africa: needs and challenges. Land and Water Development Division. Food and Agriculture Organization of the United Nations, Roma, Italia.

Utomo, W.H., Dexter, A.R., 1981. Soil friability. Journal of Soil Science 32, 203–213. https://doi.org/10.1111/j.1365-2389.1981.tb01700.x

Van Ghent, P.A.M., Ukkerman, R., 1993. The Balanta rice farming system in Guinea Bissau, Projet PRIVAT. WUR, Wageningen, The Netherlands. https://doi.org/http://content.alterra.wur.nl/Internet/webdocs/ilri-publicaties/publicaties/Pub53/pub53-h6.pdf

van Oort, P.A.J., 2018. Mapping abiotic stresses for rice in Africa: Drought, cold, iron toxicity, salinity and sodicity. Field Crops Res 219, 55–75. https://doi.org/10.1016/j.fcr.2018.01.016

Zeraatpisheh, M., Ayoubi, S., Mirbagheri, Z., Mosaddeghi, M.R., Xu, M., 2021. Spatial prediction of soil aggregate stability and soil organic carbon in aggregate fractions using machine learning algorithms and environmental variables. Geoderma Regional 27, e00440. https://doi.org/10.1016/j.geodrs.2021.e00440

References for Chapter 4

Abbas, J.A.A., 2023. Soil salinity assessment by using spectral salinity indices in Al-Sweira project middle of the Iraqi alluvial plain. International Journal of Environmental Science and Technology 20, 10847–10860. https://doi.org/10.1007/s13762-022-04733-4

Abd El-Hamid, H.T., Alshehri, F., El-Zeiny, A.M., Nour-Eldin, H., 2023. Remote sensing and statistical analyses for exploration and prediction of soil salinity in a vulnerable area to seawater intrusion. Mar Pollut Bull 187, 114555. https://doi.org/10.1016/j.marpolbul.2022.114555

Ahmed, S., De Marsily, G., 1987. Comparison of geostatistical methods for estimating transmissivity using data on transmissivity and specific capacity. Water Resour Res 23, 1717–1737. https://doi.org/10.1029/WR023i009p01717

Ahmed, S., Sarker, S.K., Friess, D.A., Kamruzzaman, Md., Jacobs, M., Islam, Md.A., Alam, Md.A., Suvo, M.J., Sani, Md.N.H., Dey, T., Naabeh, C.S.S., Pretzsch, H., 2022. Salinity reduces site quality and mangrove forest functions. From monitoring to understanding. Science of The Total Environment 853, 158662. https://doi.org/10.1016/j.scitotenv.2022.158662

Aksoy, S., Yildirim, A., Gorji, T., Hamzehpour, N., Tanik, A., Sertel, E., 2022. Assessing the performance of machine learning algorithms for soil salinity mapping in Google Earth Engine platform using Sentinel-2A and Landsat-8 OLI data. Advances in Space Research 69, 1072–1086. https://doi.org/10.1016/j.asr.2021.10.024

Allaire-Leung, S.E., Gupta, S.C., Moncrief, J.F., 2000. Water and solute movement in soil as influenced by macropore characteristics. J Contam Hydrol 41, 283–301. https://doi.org/10.1016/S0169-7722(99)00079-0

Andreetta, A., Huertas, A.D., Lotti, M., Cerise, S., 2016. Land use changes affecting soil organic carbon storage along a mangrove swamp rice chronosequence in the Cacheu and Oio regions (northern Guinea-Bissau). Agric Ecosyst Environ 216, 314–321. https://doi.org/10.1016/j.agee.2015.10.017

Andrieu, J., Cormier-Salem, M.-C., Descroix, L., Sané, T., Diéye, E.H.B., Ndour, N., 2019. Correctly assessing forest change in a priority West African mangrove ecosystem: 1986–2010 An answer to Carney et al. (2014) paper "Assessing forest change in a priority West African mangrove ecosystem: 1986–2010." Remote Sens Appl 13, 337–347. https://doi.org/10.1016/j.rsase.2018.12.001

Ansel, J., Yang, E., He, H., Gimelshein, N., Jain, A., Voznesensky, M., Bao, B., Bell, P., Berard, D., Burovski, E., Chauhan, G., Chourdia, A., Constable, W., Desmaison, A., DeVito, Z., Ellison, E., Feng, W., Gong, J., Gschwind, M., Hirsh, B., Huang, S., Kalambarkar, K., Kirsch, L., Lazos, M., Lezcano, M., Liang, Y., Liang, J., Lu, Y., Luk, C.K., Maher, B., Pan, Y., Puhrsch, C., Reso, M., Saroufim, M., Siraichi, M.Y., Suk, H., Zhang, S., Suo, M., Tillet, P., Zhao, X., Wang, E., Zhou, K., Zou, R., Wang, X., Mathews, A., Wen, W., Chanan, G., Wu, P., Chintala, S., 2024. PyTorch 2: Faster Machine Learning

Through Dynamic Python Bytecode Transformation and Graph Compilation, in: Proceedings of the 29th ACM International Conference on Architectural Support for Programming Languages and Operating Systems, Volume 2. ACM, New York, NY, USA, pp. 929–947. https://doi.org/10.1145/3620665.3640366

Avdan, U., Kaplan, G., Küçük Matcı, D., Yiğit Avdan, Z., Erdem, F., Tuğba Mızık, E., Demirtaş, İ., 2022. Soil salinity prediction models constructed by different remote sensors. Physics and Chemistry of the Earth, Parts A/B/C 128, 103230. https://doi.org/10.1016/j.pce.2022.103230

Ayers, R.S., Westcot, D.W., 1985. Water Quality for Agriculture. Irrigation and Drainage Paper 29. 174 p.

Balasubramanian, V., Sie, M., Hijmans, R.J., Otsuka, K., 2007. Increasing Rice Production in Sub-Saharan Africa: Challenges and Opportunities. Advances in Agronomy 94, 55–133. https://doi.org/10.1016/S0065-2113(06)94002-4

Bannari, A., Guedon, A.M., El-Harti, A., Cherkaoui, F.Z., El-Ghmari, A., 2008. Characterization of Slightly and Moderately Saline and Sodic Soils in Irrigated Agricultural Land using Simulated Data of Advanced Land Imaging (EO-1) Sensor. Commun Soil Sci Plant Anal 39, 2795–2811. https://doi.org/10.1080/00103620802432717

Barreto, A.C., Ferreira Neto, M., Oliveira, R.P. de, Moreira, L.C.J., Medeiros, J.F. de, Sá, F.V. da S., 2023. Comparative analysis of spectral indexes for soil salinity mapping in irrigated areas in a semi-arid region, Brazil. J Arid Environ 209, 104888. https://doi.org/10.1016/j.jaridenv.2022.104888

Bazrafshan, A., Shorafa, M., Mohammadi, M.H., Zolfaghari, A.A., van de Craats, D., van der Zee, S.E.A.T.M., 2020. Comparison of the individual salinity and water deficit stress using water use, yield, and plant parameters in maize. Environ Monit Assess 192, 448. https://doi.org/10.1007/s10661-020-08423-x

Beck, H.E., Zimmermann, N.E., McVicar, T.R., Vergopolan, N., Berg, A., Wood, E.F., 2018. Present and future Köppen-Geiger climate classification maps at 1-km resolution. Sci Data 5, 180214. https://doi.org/10.1038/sdata.2018.214

Bell, D., Menges, C., Ahmad, W., van Zyl, J.J., 2001. The Application of Dielectric Retrieval Algorithms for Mapping Soil Salinity in a Tropical Coastal Environment Using Airborne Polarimetric SAR. Remote Sens Environ 75, 375–384. https://doi.org/10.1016/S0034-4257(00)00180-2

Bellon-Maurel, V., Fernandez-Ahumada, E., Palagos, B., Roger, J.-M., McBratney, A., 2010. Critical review of chemometric indicators commonly used for assessing the quality of the prediction of soil attributes by NIR spectroscopy. TrAC Trends in Analytical Chemistry 29, 1073–1081. https://doi.org/10.1016/j.trac.2010.05.006

Bishop, C.M., 1995. Neural Networks for Pattern Recognition. Clarendon Press, Oxford.

Boser, B.E., Guyon, I.M., Vapnik, V.N., 1992. A training algorithm for optimal margin classifiers, in: Proceedings of the Fifth Annual Workshop on Computational Learning Theory. ACM, New York, NY, USA, pp. 144–152. https://doi.org/10.1145/130385.130401

Bouaziz, M., Chtourou, M.Y., Triki, I., Mezner, S., Bouaziz, S., 2018. Prediction of Soil Salinity Using Multivariate Statistical Techniques and Remote Sensing Tools. Advances in Remote Sensing 07, 313–326. https://doi.org/10.4236/ars.2018.74021

Bouyoucos, G.J., 1926. Estimation of the colloidal material in soils. Science (1979) 64, 362–362. https://doi.org/10.1126/science.64.1658.362

Breiman, L., 2001. Random Forests 45, 5–32. https://doi.org/https://doi.org/10.1023/A:1010933404324

Buitinck, L., Louppe, G., Blondel, M., Pedregosa, F., Mueller, A., Grisel, O., Niculae, V., Prettenhofer, P., Gramfort, A., Grobler, J., Layton, R., Vanderplas, J., Joly, A., Holt, B., Varoquaux, G., 2013. API design for machine learning software: experiences from the scikit-learn project. Journal of Machine Learning Research.

Cabalceta, G., Molina, E., 2005. Niveles críticos de nutrimentos en suelos de Costa Rica utilizando la solución extractora Mehlich 3. Agronomía Costarricense 30, 31–44. https://doi.org/10.15517/rac.v30i2.6808

Cawse-Nicholson, K., Townsend, P.A., Schimel, D., Assiri, A.M., Blake, P.L., Buongiorno, M.F., Campbell, P., Carmon, N., Casey, K.A., Correa-Pabón, R.E., Dahlin, K.M., Dashti, H., Dennison, P.E., Dierssen, H., Erickson, A., Fisher, J.B., Frouin, R., Gatebe, C.K., Gholizadeh, H., Gierach, M., Glenn, N.F., Goodman, J.A., Griffith, D.M., Guild, L., Hakkenberg, C.R., Hochberg, E.J., Holmes, T.R.H., Hu, C., Hulley, G., Huemmrich, K.F., Kudela, R.M., Kokaly, R.F., Lee, C.M., Martin, R., Miller, C.E., Moses, W.J., Muller-Karger, F.E., Ortiz, J.D., Otis, D.B., Pahlevan, N., Painter, T.H., Pavlick, R., Poulter, B., Qi, Y., Realmuto, V.J., Roberts, D., Schaepman, M.E., Schneider, F.D., Schwandner, F.M., Serbin, S.P., Shiklomanov, A.N., Stavros, E.N., Thompson, D.R., Torres-Perez, J.L., Turpie, K.R., Tzortziou, M., Ustin, S., Yu, Q., Yusup, Y., Zhang, Q., 2021. NASA's surface biology and geology designated observable: A perspective on surface imaging algorithms. Remote Sens Environ 257, 112349. https://doi.org/10.1016/j.rse.2021.112349

Chaaou, A., Chikhaoui, M., Naimi, M., El Miad, A.K., Achemrk, A., Seif-Ennasr, M., El Harche, S., 2022. Mapping soil salinity risk using the approach of soil salinity index and land cover: a case study from Tadla plain, Morocco. Arabian Journal of Geosciences 15, 722. https://doi.org/10.1007/s12517-022-10009-5

Chuvieco, E., 2020. Fundamentals of Satellite Remote Sensing: an environmental approach. CRC Press. https://doi.org/10.1201/9780429506482

Cortes, C., Vapnik, V., 1995. Support-vector networks. Mach Learn 20, 273–297. https://doi.org/10.1007/BF00994018

Csillag, F., Pásztor, L., Biehl, L.L., 1993. Spectral band selection for the characterization of salinity status of soils. Remote Sens Environ 43, 231–242. https://doi.org/10.1016/0034-4257(93)90068-9

Cui, X., Han, W., Zhang, H., Dong, Y., Ma, W., Zhai, X., Zhang, L., Li, G., 2023. Estimating and mapping the dynamics of soil salinity under different crop types using Sentinel-2 satellite imagery. Geoderma 440, 116738. https://doi.org/10.1016/j.geoderma.2023.116738

Dakak, H., Dekkaki, H.C., Zouahri, A., Moussadek, R., Iaaich, H., Yachou, H., Ghanimi, A., Douaik, A., 2023. Soil Salinity Prediction and Mapping Using Electromagnetic Induction and Spatial Interpolation, in: The 2nd International Laayoune Forum on Biosaline Agriculture. MDPI, Basel Switzerland, p. 76. https://doi.org/10.3390/environsciproc2022016076

D'Amico, M.E., Barbieri, M., Khair, D.A. El, Comolli, R., 2024. Mangrove rice productivity and pedogenic trends in Guinea Bissau, West Africa. J Soils Sediments 24, 244–258. https://doi.org/10.1007/s11368-023-03608-6

Day, P.R., 2015. Particle Fractionation and Particle-Size Analysis. pp. 545–567. https://doi.org/10.2134/agronmonogr9.1.c43

Decoste, D., Schölkopf, B., 2002. Training Invariant Support Vector Machines. https://doi.org/https://doi.org/10.1023/A:1012454411458

Dehaan, R.L., Taylor, G.R., 2002. Field-derived spectra of salinized soils and vegetation as indicators of irrigation-induced soil salinization. Remote Sens Environ 80, 406–417. https://doi.org/10.1016/S0034-4257(01)00321-2

Dehni, A., Lounis, M., 2012. Remote Sensing Techniques for Salt Affected Soil Mapping: Application to the Oran Region of Algeria. Procedia Eng 33, 188–198. https://doi.org/10.1016/j.proeng.2012.01.1193

Dossou-Yovo, E.R., Devkota, K.P., Akpoti, K., Danvi, A., Duku, C., Zwart, S.J., 2022. Thirty years of water management research for rice in sub-Saharan Africa: Achievement and perspectives. Field Crops Res 283, 108548. https://doi.org/10.1016/j.fcr.2022.108548

Du, R., Chen, J., Zhang, Z., Chen, Y., He, Y., Yin, H., 2022. Simultaneous estimation of surface soil moisture and salinity during irrigation with the moisture-salinity-dependent spectral response model. Agric Water Manag 265, 107538. https://doi.org/10.1016/j.agwat.2022.107538

FAO, 2018. FAO Rice Market Monitor. [WWW Document]. Seguimiento del mercado del arroz de la FAO (SMA). Food and Agriculture Organization of the United Nations. URL https://www.fao.org/markets-and-trade/commodities/rice/rmm/en/ (accessed 10.10.23).

Farifteh, J., Van der Meer, F., Atzberger, C., Carranza, E.J.M., 2007. Quantitative analysis of salt-affected soil reflectance spectra: A comparison of two adaptive methods (PLSR and ANN). Remote Sens Environ 110, 59–78. https://doi.org/10.1016/j.rse.2007.02.005

Garbanzo, G., Cameira, M., Paredes, P., 2024a. The Mangrove Swamp Rice Production System of Guinea Bissau: Identification of the Main Constraints Associated with Soil Salinity and Rainfall Variability. Agronomy 14, 468. https://doi.org/10.3390/agronomy14030468

Garbanzo, G., Céspedes, J., Sandoval, J., Temudo, M., Paredes, P., Cameira, M. do R., 2024b. Moving toward the Biophysical Characterization of the Mangrove Swamp Rice Production System in Guinea Bissau: Exploring Tools to Improve Soil- and Water-Use Efficiencies. Agronomy 14, 335. https://doi.org/10.3390/agronomy14020335

Garbanzo, G., do Rosário Cameira, M., Paredes, P., Temudo, M., Ramos, T.B., 2025. Modeling soil water and salinity dynamics in mangrove swamp rice production system of Guinea Bissau, West Africa. Agric Water Manag 313, 109494. https://doi.org/10.1016/j.agwat.2025.109494

Geron, A., 2019. Hands-on machine learning with Scikit-Learn, Keras, and TensorFlow. Concepts, tools, and techniques to build intelligent systems, 2nd ed. O'Reilly Media, Inc, USA, .

Golabkesh, F., Ghanavati, N., Nazarpour, A., Babaei Nejad, T., 2021. Monitoring Soil Salinity Changes, Comparison of Different Maps and Indices Extracted from Landsat Satellite Images (Case Study: Atabieh, Khuzestan). Pol J Environ Stud 30, 1139–1154. https://doi.org/10.15244/pjoes/123503

Golestani, M., Mosleh Ghahfarokhi, Z., Esfandiarpour-Boroujeni, I., Shirani, H., 2023. Evaluating the spatiotemporal variations of soil salinity in Sirjan Playa, Iran using Sentinel-2A and Landsat-8 OLI imagery. Catena (Amst) 231, 107375. https://doi.org/10.1016/j.catena.2023.107375

Goodfellow, I., Bengio, Y., Courville, A., 2016. Convolutional Networks, in: Deep Learning. MIT Press, p. 810.

Hadjimitsis, D.G., Papadavid, G., Agapiou, A., Themistocleous, K., Hadjimitsis, M.G., Retalis, A., Michaelides, S., Chrysoulakis, N., Toulios, L., Clayton, C.R.I., 2010. Atmospheric correction for satellite remotely sensed data intended for agricultural applications: impact on vegetation indices. Natural Hazards and Earth System Sciences 10, 89–95. https://doi.org/10.5194/nhess-10-89-2010

Han, J., Kim, M., Mammadov, Z., Lee, S., Elzinga, E.J., Mammadov, G., Hwang, W., Ro, H.-M., 2024. Synergistic effect of climate change and water management: Historical and future soil salinity in the Kur-Araz lowland, Azerbaijan. Science of The Total Environment 907, 167720. https://doi.org/10.1016/j.scitotenv.2023.167720

Harris, S.A., 2014. Comments on the Application of the Holdridge System for Classification of World Life Zones as Applied to Costa Rica. Arctic and Alpine Research 5, 187–191.

Haykin, S., 1999. Neural networks. A comprehensive foundation, 2nd ed. Pearson Education , Ontario, Canada.

He, Y., Zhang, Z., Xiang, R., Ding, B., Du, R., Yin, H., Chen, Y., Ba, Y., 2023. Monitoring salinity in bare soil based on Sentinel-1/2 image fusion and machine learning. Infrared Phys Technol 131, 104656. https://doi.org/10.1016/j.infrared.2023.104656

Herrero, J., Castañeda, C., 2023. Comparing Two Saline-Gypseous Wetland Soils in NE Spain. Land (Basel) 12, 1990. https://doi.org/10.3390/land12111990

Herrero, J., Weindorf, D.C., Castañeda, C., 2015. Two Fixed Ratio Dilutions for Soil Salinity Monitoring in Hypersaline Wetlands. PLoS One 10, e0126493. https://doi.org/10.1371/journal.pone.0126493

Hodson, T.O., 2022. Root-mean-square error (RMSE) or mean absolute error (MAE): when to use them or not. Geosci Model Dev 15, 5481–5487. https://doi.org/10.5194/gmd-15-5481-2022

Holdridge, L.R., 1947. Determination of World Plant Formations From Simple Climatic Data. Science (1979) 105, 367–368. https://doi.org/10.1126/science.105.2727.367

Hopmans, J.W., Qureshi, A.S., Kisekka, I., Munns, R., Grattan, S.R., Rengasamy, P., Ben-Gal, A., Assouline, S., Javaux, M., Minhas, P.S., Raats, P.A.C., Skaggs, T.H., Wang, G., De Jong van Lier, Q., Jiao, H., Lavado, R.S., Lazarovitch, N., Li, B., Taleisnik, E., 2021. Critical knowledge gaps and research priorities in global soil salinity, in: Advances in Agronomy. Elsevier, pp. 1-191. https://doi.org/10.1016/bs.agron.2021.03.001

Hossain, M.S., Rahman, G.K.M.M., Solaiman, A.R.M., Alam, M.S., Rahman, M.M., Mia, M.A.B., 2020. Estimating Electrical Conductivity for Soil Salinity Monitoring Using Various Soil-Water Ratios Depending on Soil Texture. Commun Soil Sci Plant Anal 51, 635–644. https://doi.org/10.1080/00103624.2020.1729378

Howard, J., Gugger, S., 2020. Deep Learning for Coders with fastai and PyTorch: AI Applications Without a PhD. O'Reilly Media, Inc, Sebastopol, Canada.

Huan, X., Caramanis, C., Mannor, S., Smola, A., 2009. Robustness and Regularization of Support Vector Machines, Journal of Machine Learning Research.

Ivushkin, K., Bartholomeus, H., Bregt, A.K., Pulatov, A., Kempen, B., de Sousa, L., 2019. Global mapping of soil salinity change. Remote Sens Environ 231, 111260. https://doi.org/10.1016/j.rse.2019.111260

Ju, X., Gao, L., She, D., Jia, Y., Pang, Z., Wang, Y., 2024. Impacts of the soil pore structure on infiltration characteristics at the profile scale in the red soil region. Soil Tillage Res 236, 105922. https://doi.org/10.1016/j.still.2023.105922

Kalambukattu, J.G., Johns, B., Kumar, S., Raj, A.D., Ellur, R., 2023. Temporal remote sensing based soil salinity mapping in Indo-Gangetic plain employing machine-learning techniques. Proceedings of the Indian National Science Academy 89, 290–305. https://doi.org/10.1007/s43538-023-00157-x

Kaplan, G., Gašparović, M., Alqasemi, A.S., Aldhaheri, A., Abuelgasim, A., Ibrahim, M., 2023. Soil salinity prediction using Machine Learning and Sentinel – 2 Remote Sensing Data in Hyper – Arid areas. Physics and Chemistry of the Earth, Parts A/B/C 130, 103400. https://doi.org/10.1016/j.pce.2023.103400

Krause, P., Boyle, D.P., Bäse, F., 2005. Comparison of different efficiency criteria for hydrological model assessment. Advances in Geosciences 5, 89–97. https://doi.org/10.5194/adgeo-5-89-2005

Krizhevsky, A., Sutskever, I., Hinton, G.E., 2017. ImageNet classification with deep convolutional neural networks. Commun ACM 60, 84–90. https://doi.org/10.1145/3065386

Kuhn, M., Johnson, K., 2013. Applied Predictive Modeling, 1st ed. Springer New York, New York, NY. https://doi.org/10.1007/978-1-4614-6849-3

Latifi, H., Fassnacht, F., Koch, B., 2012. Forest structure modeling with combined airborne hyperspectral and LiDAR data. Remote Sens Environ 121, 10–25. https://doi.org/10.1016/j.rse.2012.01.015

LeCun, Y., Bengio, Y., Hinton, G., 2015. Deep learning. Nature 521, 436–44. https://doi.org/10.1038/nature14539

Li, X., Li, Y., Wang, B., Sun, Y., Cui, G., Liang, Z., 2022. Analysis of spatial-temporal variation of the saline-sodic soil in the west of Jilin Province from 1989 to 2019 and influencing factors. Catena (Amst) 217, 106492. https://doi.org/10.1016/j.catena.2022.106492

Linares, O.F., 1981. From tidal swamp to inland valley: on the social organization of wet rice cultivation among the Diola of Senegal. Africa 51, 557–595. https://doi.org/10.2307/1158828

Lipiec, J., Kuś, J., Słowińska-Jurkiewicz, A., Nosalewicz, A., 2006. Soil porosity and water infiltration as influenced by tillage methods. Soil Tillage Res 89, 210–220. https://doi.org/10.1016/j.still.2005.07.012

Liu, J., Yang, K., Tariq, A., Lu, L., Soufan, W., El Sabagh, A., 2023. Interaction of climate, topography and soil properties with cropland and cropping pattern using remote sensing data and machine learning methods. The Egyptian Journal of Remote Sensing and Space Sciences 26, 415–426. https://doi.org/10.1016/j.ejrs.2023.05.005

Liu, M., Lei, H., Wang, X., Paredes, P., 2025. High-resolution mapping of evapotranspiration over heterogeneous cropland affected by soil salinity. Agric Water Manag 308, 109301. https://doi.org/10.1016/j.agwat.2025.109301

Liu, Y., Wang, Y., Zhang, J., 2012. New Machine Learning Algorithm: Random Forest. pp. 246–252. https://doi.org/10.1007/978-3-642-34062-8_32

Lopes, C.L., Mendes, R., Caçador, I., Dias, J.M., 2020. Assessing salt marsh extent and condition changes with 35 years of Landsat imagery: Tagus Estuary case

study. Remote Sens Environ 247, 111939. https://doi.org/10.1016/j.rse.2020.111939

Louppe, G., Wehenkel, L., Sutera, A., Geurts, P., 2013. Understanding variable importances in forests of randomized trees, in: Proceedings of the 26th International Conference on Neural Information Processing Systems. Curran Associates Inc., Lake Tahoe, Nevada, pp. 431–439.

Marius, C., Lucas, J., 1991. Holocene mangrove swamps of West Africa sedimentology and soils. Journal of African Earth Sciences (and the Middle East) 12, 41–54. https://doi.org/10.1016/0899-5362(91)90056-5

Martiarena, M.L., Temudo, M.P., 2023. Endogenous learning and innovation in African smallholder agriculture: lessons from Guinea-Bissau. The Journal of Agricultural Education and Extension 1–19. https://doi.org/10.1080/1389224X.2023.2169480

Martins, V.S., Roy, D.P., Huang, H., Boschetti, L., Zhang, H.K., Yan, L., 2022. Deep learning high resolution burned area mapping by transfer learning from Landsat-8 to PlanetScope. Remote Sens Environ 280, 113203. https://doi.org/10.1016/j.rse.2022.113203

Mendes, O., Fragoso, M., 2024. Recent changes in climate extremes in Guinea-Bissau. African Geographical Review 1–19. https://doi.org/10.1080/19376812.2024.2359997

Mendes, O., Fragoso, M., 2023. Assessment of the Record-Breaking 2020 Rainfall in Guinea-Bissau and Impacts of Associated Floods. Geosciences (Basel) 13, 25. https://doi.org/10.3390/geosciences13020025

Metternicht, G.I., Zinck, J.A., 2003. Remote sensing of soil salinity: potentials and constraints. Remote Sens Environ 85, 1–20. https://doi.org/10.1016/S0034-4257(02)00188-8

Minhas, P.S., Ramos, T.B., Ben-Gal, A., Pereira, L.S., 2020. Coping with salinity in irrigated agriculture: Crop evapotranspiration and water management issues. Agric Water Manag 227, 105832. https://doi.org/10.1016/j.agwat.2019.105832

Mondal, P., Liu, X., Fatoyinbo, T.E., Lagomasino, D., 2019. Evaluating Combinations of Sentinel-2 Data and Machine-Learning Algorithms for Mangrove Mapping in West Africa. Remote Sens (Basel) 11, 2928. https://doi.org/10.3390/rs11242928

Muchate, N.S., Nikalje, G.C., Rajurkar, N.S., Suprasanna, P., Nikam, T.D., 2016. Plant Salt Stress: Adaptive Responses, Tolerance Mechanism and Bioengineering for Salt Tolerance. The Botanical Review 82, 371–406. https://doi.org/10.1007/s12229-016-9173-y

Mzid, N., Boussadia, O., Albrizio, R., Stellacci, A.M., Braham, M., Todorovic, M., 2023. Salinity Properties Retrieval from Sentinel-2 Satellite Data and Machine

Learning Algorithms. Agronomy 13, 716. https://doi.org/10.3390/agronomy13030716

Naidoo, G., 2023. The mangroves of Africa : A review. Mar Pollut Bull 190, 114859. https://doi.org/10.1016/j.marpolbul.2023.114859

Naimi, S., Ayoubi, S., Zeraatpisheh, M., Dematte, J.A.M., 2021. Ground Observations and Environmental Covariates Integration for Mapping of Soil Salinity: A Machine Learning-Based Approach. Remote Sens (Basel) 13, 4825. https://doi.org/10.3390/rs13234825

Navarro-Noya, Y.E., Valenzuela-Encinas, C., Sandoval-Yuriar, A., Jiménez-Bueno, N.G., Marsch, R., Dendooven, L., 2015. Archaeal Communities in a Heterogeneous Hypersaline-Alkaline Soil. Archaea 2015, 1–11. https://doi.org/10.1155/2015/646820

Paredes, P., Martins, D., Pereira, L., Cadima, J., Pires, C., 2018. Accuracy of daily estimation of grass reference evapotranspiration using ERA-Interim reanalysis products with assessment of alternative bias correction schemes. Agric Water Manag 210, 340–353. https://doi.org/10.1016/j.agwat.2018.08.003

Parker, J., 2004. Ecophysiology of salt-and waterlogging tolerance in selected species of Halosarcia. University of Western Australia.

Pedregosa, F., Varoquaux, G., Gramfort, A., Michel, V., Thirion, B., Grisel, O., Blondel, M., Prettenhofer, P., Weiss, R., Dubourg, V., Vanderplas, J., Passos, A., Cournapeau, D., Brucher, M., Perrot, M., Duchesnay, E., 2011. Scikit-learn: Machine Learning in Python. Journal of Machine Learning Research 12, 2825–2830.

Periasamy, S., Ravi, K.P., Tansey, K., 2022. Identification of saline landscapes from an integrated SVM approach from a novel 3-D classification schema using Sentinel-1 dual-polarized SAR data. Remote Sens Environ 279, 113144. https://doi.org/10.1016/j.rse.2022.113144

Pettorelli, N., Vik, J.O., Mysterud, A., Gaillard, J.-M., Tucker, C.J., Stenseth, N.Chr., 2005. Using the satellite-derived NDVI to assess ecological responses to environmental change. Trends Ecol Evol 20, 503–510. https://doi.org/10.1016/j.tree.2005.05.011

Planet Labs PBC, 2024. Planet Application Program Interface: In Space for Life on Earth [WWW Document]. Planet. URL https://api.planet.com/ (accessed 3.28.24).

Plevris, V., Solorzano, G., Bakas, N., Ben Seghier, M., 2022. Investigation of performance metrics in regression analysis and machine learning-based prediction models, in: 8th European Congress on Computational Methods in Applied Sciences and Engineering. CIMNE. https://doi.org/10.23967/eccomas.2022.155

Pongrac, B., Gleich, D., 2021. Regression Neural Network for Soil Moisture Estimation, in: 2021 7th Asia-Pacific Conference on Synthetic Aperture Radar (APSAR). IEEE, pp. 1–4. https://doi.org/10.1109/APSAR52370.2021.9688481

Pouladi, N., Jafarzadeh, A.A., Shahbazi, F., Ghorbani, M.A., 2019. Design and implementation of a hybrid MLP-FFA model for soil salinity prediction. Environ Earth Sci 78, 159. https://doi.org/10.1007/s12665-019-8159-6

QGIS Development Team, 2024. QGIS Geographic Information System [WWW Document]. QGIS Association. URL https://www.qgis.org (accessed 5.23.24).

R Core Team, 2024. R: A Language and Environment for Statistical Computing [WWW Document]. R Foundation for Statistical Computing, Vienna, Austria. URL https://www.R-project.org (accessed 3.30.24).

Ramos, T.B., Castanheira, N., Oliveira, A.R., Paz, A.M., Darouich, H., Simionesei, L., Farzamian, M., Gonçalves, M.C., 2020. Soil salinity assessment using vegetation indices derived from Sentinel-2 multispectral data. application to Lezíria Grande, Portugal. Agric Water Manag 241, 106387. https://doi.org/10.1016/j.agwat.2020.106387

Ramos, T.B., Gonçalves, M.C., van Genuchten, M.Th., 2024. Soil salinization in Portugal: An in-depth exploration of impact, advancements, and future considerations. Vadose Zone Journal. https://doi.org/10.1002/vzj2.20314

Rengasamy, P., Olsson, K., 1991. Sodicity and soil structure. Soil Research 29, 935. https://doi.org/10.1071/SR9910935

Rhoades, J.D., 1996. Salinity: Electrical Conductivity and Total Dissolved Solids, in: Methods of Soil Analysis. Part 3. Chemical Methods. . pp. 417–435.

Rodríguez, L.I., García, T., Unday, G., Jiménez, J., Rodríguez, M.M., Fernández, Y., 2023. Effects of Sodium Salinity on Rice (Oryza sativa L.) Cultivation: A Review. Sustainability 15, 1804. https://doi.org/10.3390/su15031804

Rosenblatt, F., 1967. Recent work on the theoretical model of biological memory [WWW Document]. URL https://bpb-us-e2.wpmucdn.com/websites.umass.edu/dist/a/27637/files/2016/01/rosenblatt-1967.pdf (accessed 5.23.24).

Roy, D.P., Huang, H., Boschetti, L., Giglio, L., Yan, L., Zhang, H.H., Li, Z., 2019. Landsat-8 and Sentinel-2 burned area mapping - A combined sensor multi-temporal change detection approach. Remote Sens Environ 231, 111254. https://doi.org/10.1016/j.rse.2019.111254

Salem, S.I., Higa, H., Ishizaka, J., Pahlevan, N., Oki, K., 2023. Spectral band-shifting of multispectral remote-sensing reflectance products: Insights for matchup and cross-mission consistency assessments. Remote Sens Environ 299, 113846. https://doi.org/10.1016/j.rse.2023.113846

Salmas, C.E., Ladavos, A.K., Skaribas, S.P., Pomonis, P.J., Androutsopoulos, G.P., 2003. Evaluation of Microporosity, Pore Tortuosity, and Connectivity of Montmorillonite Solids Pillared with LaNiOx Binary Oxide. A Combined Application of the CPSM Model, the αs-Plot Method and a Pore Percolation−Connectivity Model. Langmuir 19, 8777–8786. https://doi.org/10.1021/la034913t

Sarkar, S.K., Rudra, R.R., Sohan, A.R., Das, P.C., Ekram, K.M.M., Talukdar, S., Rahman, A., Alam, E., Islam, M.K., Islam, A.R.M.T., 2023. Coupling of machine learning and remote sensing for soil salinity mapping in coastal area of Bangladesh. Sci Rep 13. https://doi.org/10.1038/s41598-023-44132-4

Scudiero, E., Skaggs, T.H., Corwin, D.L., 2015. Regional-scale soil salinity assessment using Landsat ETM + canopy reflectance. Remote Sens Environ 169, 335–343. https://doi.org/10.1016/j.rse.2015.08.026

Shi, H., Hellwich, O., Luo, G., Chen, C., He, H., Ochege, F.U., Van de Voorde, T., Kurban, A., Maeyer, P. de, 2022. A Global Meta-Analysis of Soil Salinity Prediction Integrating Satellite Remote Sensing, Soil Sampling, and Machine Learning. IEEE Transactions on Geoscience and Remote Sensing 60, 1–15. https://doi.org/10.1109/TGRS.2021.3109819

Shrestha, R.P., Qasim, S., Bachri, S., 2021. Investigating remote sensing properties for soil salinty mapping: A case study in Korat province of Thailand. Environmental Challenges 5, 100290. https://doi.org/10.1016/j.envc.2021.100290

Siji, G.C., Sumathi, B., 2020. Grid Search Tuning of Hyperparameters in Random Forest Classifier for Customer Feedback Sentiment Prediction. International Journal of Advanced Computer Science and Applications 11. https://doi.org/10.14569/IJACSA.2020.0110920

Simonyan, K., Zisserman, A., 2014. Very Deep Convolutional Networks for Large-Scale Image Recognition.

Singh, A., 2021. Soil salinization management for sustainable development: A review. J Environ Manage 277, 111383. https://doi.org/10.1016/j.jenvman.2020.111383

Singh, S., 2024. Impact of hydraulic tortuosity on microporous and nanoporous media flow. Phys Rev E 109, 025106. https://doi.org/10.1103/PhysRevE.109.025106

Sirpa-Poma, J.W., Satgé, F., Resongles, E., Pillco-Zolá, R., Molina-Carpio, J., Flores Colque, M.G., Ormachea, M., Pacheco Mollinedo, P., Bonnet, M.-P., 2023. Towards the Improvement of Soil Salinity Mapping in a Data-Scarce Context Using Sentinel-2 Images in Machine-Learning Models. Sensors 23, 9328. https://doi.org/10.3390/s23239328

Soil Survey Staff., 2022. Keys to soil taxonomy, 13th ed, Soil Conservation Service. Natural Resources Conservation Service,.

Soil Survey Staff, 2022. Kellogg Soil Survey Laboratory Methods Manual. Soil Survey Investigations Report No. 42, Version 6.0.

Sonmez, S., Buyuktas, D., Okturen, F., Citak, S., 2008. Assessment of different soil to water ratios (1:1, 1:2.5, 1:5) in soil salinity studies. Geoderma 144, 361–369. https://doi.org/10.1016/j.geoderma.2007.12.005

Steurer, M., Hill, R.J., Pfeifer, N., 2021. Metrics for evaluating the performance of machine learning based automated valuation models. Journal of Property Research 38, 99–129. https://doi.org/10.1080/09599916.2020.1858937

Stulina, G., Cameira, M.R., Pereira, L.S., 2005. Using RZWQM to search improved practices for irrigated maize in Fergana, Uzbekistan. Agric Water Manag 77, 263–281. https://doi.org/10.1016/j.agwat.2004.09.040

Sun, G., Zhu, Y., Gao, Z., Yang, J., Qu, Z., Mao, W., Wu, J., 2022. Spatiotemporal Patterns and Key Driving Factors of Soil Salinity in Dry and Wet Years in an Arid Agricultural Area with Shallow Groundwater Table. Agriculture 12, 1243. https://doi.org/10.3390/agriculture12081243

Sylla, M., 1994. Soil salinity and acidity: spatial variability and effects on rice production in West Africa's mangrove zone. Wageningen University and Research: Wageningen, The Netherlands.

Sylla, M., Stein, A., van Breemen, N., Fresco, L.O., 1995. Spatial variability of soil salinity at different scales in the mangrove rice agro-ecosystem in West Africa. Agric Ecosyst Environ 54, 1–15. https://doi.org/10.1016/0167-8809(95)00594-I

Tan, J., Ding, J., Han, L., Ge, X., Wang, X., Wang, J., Wang, R., Qin, S., Zhang, Z., Li, Y., 2023. Exploring PlanetScope Satellite Capabilities for Soil Salinity Estimation and Mapping in Arid Regions Oases. Remote Sens (Basel) 15, 1066. https://doi.org/10.3390/rs15041066

Taylor, R., 1990. Interpretation of the Correlation Coefficient: A Basic Review. Journal of Diagnostic Medical Sonography 6, 35–39. https://doi.org/10.1177/875647939000600106

Temudo, M.P., Cabral, A.I., 2017. The Social Dynamics of Mangrove Forests in Guinea-Bissau, West Africa. Hum Ecol 45, 307–320. https://doi.org/10.1007/s10745-017-9907-4

Temudo, M.P., Cabral, A.I.R., Reis, P., 2022. The Sea Swallowed our Houses and Rice Fields: The Vulnerability to Climate Change of Coastal People in Guinea-Bissau, West Africa. Hum Ecol 50, 835–850. https://doi.org/10.1007/s10745-022-00352-2

Temudo, M.P., Figueira, R., Abrantes, M., 2015. Landscapes of bio-cultural diversity: shifting cultivation in Guinea-Bissau, West Africa. Agroforestry Systems 89, 175–191. https://doi.org/10.1007/s10457-014-9752-z

The Republic of Guinea-Bissau, 2018. Framework Convention on Climate Change. National Communication. Bissau, Guinea Bissau.

Thomas, G.W., 1996. Soil pH and Soil Acidity, in: Methods of Soil Analysis. Part 3. Chemical Methods. . pp. 475–490.

Timm, B.C., McGarigal, K., 2012. Fine-scale remotely-sensed cover mapping of coastal dune and salt marsh ecosystems at Cape Cod National Seashore using Random Forests. Remote Sens Environ 127, 106–117. https://doi.org/10.1016/j.rse.2012.08.033

Triki Fourati, H., Bouaziz, M., Benzina, M., Bouaziz, S., 2017. Detection of terrain indices related to soil salinity and mapping salt-affected soils using remote sensing and geostatistical techniques. Environ Monit Assess 189, 177. https://doi.org/10.1007/s10661-017-5877-7

Triki Fourati, H., Bouaziz, M., Benzina, M., Bouaziz, S., 2015. Modeling of soil salinity within a semi-arid region using spectral analysis. Arabian Journal of Geosciences 8, 11175–11182. https://doi.org/10.1007/s12517-015-2004-3

Tukey, J.W., 1949. Comparing Individual Means in the Analysis of Variance. Biometrics 5, 99. https://doi.org/10.2307/3001913

Ukpong, I.E., 1997. Vegetation and its relation to soil nutrient and salinity in the Calabar mangrove swamp, Nigeria. Mangroves and Salt Marshes 1, 211–218. https://doi.org/https://doi.org/10.1023/A:1009952700317

United Nations, 2024. The Sustainable Development Goals Report. New York, USA.

U.S. Salinity Laboratory Staff, 1954. Diagnosis and Improvement of Saline and Alkali Soils. USDA Handbook 60., Soil Science.

Valman, S.J., Boyd, D.S., Carbonneau, P.E., Johnson, M.F., Dugdale, S.J., 2024. An AI approach to operationalise global daily PlanetScope satellite imagery for river water masking. Remote Sens Environ 301, 113932. https://doi.org/10.1016/j.rse.2023.113932

Van Dam, J.C., Groenendijk, P., Hendriks, R.F.A., Kroes, J.G., 2008. Advances of Modeling Water Flow in Variably Saturated Soils with SWAP. Vadose Zone Journal 7, 640–653. https://doi.org/10.2136/vzj2007.0060

van de Craats, D., van der Zee, S.E.A.T.M., Sui, C., van Asten, P.J.A., Cornelissen, P., Leijnse, A., 2020. Soil sodicity originating from marginal groundwater. Vadose Zone Journal 19, 1–14. https://doi.org/10.1002/vzj2.20010

Van der Zee, S.E.A.T.M., Stofberg, S.F., Yang, X., Liu, Y., Islam, Md.N., Hu, Y.F., 2017. Irrigation and Drainage in Agriculture: A Salinity and Environmental Perspective. Current Perspective on Irrigation and Drainage 1–22. https://doi.org/10.5772/66046

Van Ghent, P.A.M., Ukkerman, R., 1993. The Balanta rice farming system in Guinea Bissau, Projet PRIVAT. WUR, Wageningen, The Netherlands.

https://doi.org/http://content.alterra.wur.nl/Internet/webdocs/ilri-publicaties/publicaties/Pub53/pub53-h6.pdf

Van Rossum, G., Drake, F., 2009. Python 3 Reference Manual. CreateSpace, Scotts Valley, CA.

Venugopal, V., Kumar, D.M., Selvaraj, V., Kumar, S.C.P., 2023. Analysis of Salinity Indices Using SVM Based Approach of Ballari Town, India. Mathematical Modelling of Engineering Problems 10, 1803–1810. https://doi.org/10.18280/mmep.100532

Wang, F., Yang, S., Wei, Y., Shi, Q., Ding, J., 2021. Characterizing soil salinity at multiple depth using electromagnetic induction and remote sensing data with random forests: A case study in Tarim River Basin of southern Xinjiang, China. Science of The Total Environment 754, 142030. https://doi.org/10.1016/j.scitotenv.2020.142030

White, S.M., Madsen, E.A., 2016. Tracking tidal inundation in a coastal salt marsh with Helikite airphotos: Influence of hydrology on ecological zonation at Crab Haul Creek, South Carolina. Remote Sens Environ 184, 605–614. https://doi.org/10.1016/j.rse.2016.08.005

Wilschefski, S., Baxter, M., 2019. Inductively Coupled Plasma Mass Spectrometry: Introduction to Analytical Aspects. Clinical Biochemist Reviews 40, 115–133. https://doi.org/10.33176/AACB-19-00024

Wolanski, E., Cassagne, B., 2000. Salinity intrusion and rice farming in the mangrove-fringed Konkoure River delta, Guinea. Wetl Ecol Manag 8, 29–36. https://doi.org/10.1023/A:1008470005880

Wu, W., Zucca, C., Muhaimeed, A.S., Al-Shafie, W.M., Fadhil Al-Quraishi, A.M., Nangia, V., Zhu, M., Liu, G., 2018. Soil salinity prediction and mapping by machine learning regression in Central Mesopotamia, Iraq. Land Degrad Dev 29, 4005–4014. https://doi.org/10.1002/ldr.3148

Wulder, M.A., Roy, D.P., Radeloff, V.C., Loveland, T.R., Anderson, M.C., Johnson, D.M., Healey, S., Zhu, Z., Scambos, T.A., Pahlevan, N., Hansen, M., Gorelick, N., Crawford, C.J., Masek, J.G., Hermosilla, T., White, J.C., Belward, A.S., Schaaf, C., Woodcock, C.E., Huntington, J.L., Lymburner, L., Hostert, P., Gao, F., Lyapustin, A., Pekel, J.-F., Strobl, P., Cook, B.D., 2022. Fifty years of Landsat science and impacts. Remote Sens Environ 280, 113195. https://doi.org/10.1016/j.rse.2022.113195

Xiao, Ji, Q., Chen, J., Zhang, F., Li, Y., Fan, J., Hou, X., Yan, F., Wang, H., 2023. Prediction of soil salinity parameters using machine learning models in an arid region of northwest China. Comput Electron Agric 204, 107512. https://doi.org/10.1016/j.compag.2022.107512

Xiao, S., Nurmemet, I., Zhao, J., 2023. Soil salinity estimation based on machine learning using the GF-3 radar and Landsat-8 data in the Keriya Oasis, Southern Xinjiang, China. Plant Soil. https://doi.org/10.1007/s11104-023-06446-0

Xiong, Y., Dai, Z., Long, C., Liang, X., Lou, Y., Mei, X., Nguyen, B.A., Cheng, J., 2024. Machine Learning-Based examination of recent mangrove forest changes in the western Irrawaddy River Delta, Southeast Asia. Catena (Amst) 234, 107601. https://doi.org/10.1016/j.catena.2023.107601

Yang, H., Wang, Z., Cao, J., Wu, Q., Zhang, B., 2023. Estimating soil salinity using Gaofen-2 imagery: A novel application of combined spectral and textural features. Environ Res 217, 114870. https://doi.org/10.1016/j.envres.2022.114870

Zeiler, M.D., Fergus, R., 2013. Visualizing and Understanding Convolutional Networks.

Zenna, N., Senthilkumar, K., Sie, M., 2017. Rice Production in Africa, in: Chauhan, B.S., Jabran, K., Mahajan, G. (Eds.), Rice Production Worldwide. Springer International Publishing, New York, USA, pp. 117–135. https://doi.org/10.1007/978-3-319-47516-5

Zhang, H., Hardy, D., Mylavarapy, R., Wang, J., 2014. Mehlich-3, in: Sikora F., Moore, K. (Eds.), Soil Test Methods from the Southeastern United States. Southern Cooperative Series Bulletin N.419, pp. 101–101.

Zhang, H., Fu, X., Zhang, Y., Qi, Z., Zhang, Hengcai, Xu, Z., 2023. Mapping Multi-Depth Soil Salinity Using Remote Sensing-Enabled Machine Learning in the Yellow River Delta, China. Remote Sens (Basel) 15, 5640. https://doi.org/10.3390/rs15245640

Zhang, L., Xue, Z., Zhang, Y., Ma, J., Li, H., 2022. Enhanced Generalized Regression Neural Network for Soil Moisture Estimation Over the Qinghai-Tibet Plateau. IEEE J Sel Top Appl Earth Obs Remote Sens 15, 3815–3829. https://doi.org/10.1109/JSTARS.2022.3166978

Zhang, Li, X., Zhou, S., Zhao, Y., Ren, J., 2023. Quantitative Study on Salinity Estimation of Salt-Affected Soils by Combining Different Types of Crack Characteristics Using Ground-Based Remote Sensing Observation. Remote Sens (Basel) 15, 3249. https://doi.org/10.3390/rs15133249

Zhang, Z., Niu, B., Li, X., Kang, X., Hu, Z., 2022. Estimation and Dynamic Analysis of Soil Salinity Based on UAV and Sentinel-2A Multispectral Imagery in the Coastal Area, China. Land (Basel) 11, 2307. https://doi.org/10.3390/land11122307

Zhao, W., Ma, F., Yu, H., Li, Z., 2023. Inversion Model of Salt Content in Alfalfa-Covered Soil Based on a Combination of UAV Spectral and Texture Information. Agriculture 13, 1530. https://doi.org/10.3390/agriculture13081530

Zhou, Y., Chen, S., Hu, B., Ji, W., Li, S., Hong, Y., Xu, H., Wang, N., Xue, J., Zhang, X., Xiao, Y., Shi, Z., 2022. Global Soil Salinity Prediction by Open Soil Vis-NIR Spectral Library. Remote Sens (Basel) 14, 5627. https://doi.org/10.3390/rs14215627

References for Chapter 5

Abdulsalam, M. K., Akpootu, D. O., Aliyu, S., & Isah, A. K. (2023). A Comparative Study for Estimating Reference Evapotranspiration Models over Kano, Nigeria. Journal of Energy Research and Reviews, 15(2), 12–25. https://doi.org/10.9734/jenrr/2023/v15i2303

Allen, R. G. (1996). Assessing Integrity of Weather Data for Reference Evapotranspiration Estimation. Journal of Irrigation and Drainage Engineering, 122(2), 97–106. https://doi.org/10.1061/(ASCE)0733-9437(1996)122:2(97)

Allen, R. G. (2008). Quality Assessment of Weather Data and Micrometeological Flux-Impacts on Evapotranspiration Calculation. Journal of Agricultural Meteorology, 64(4), 191–204. https://doi.org/10.2480/agrmet.64.4.5

Allen, R. G., Pereira, L. S., Raes, D., & Smith, M. (1998). Crop Evapotranspiration. Guidelines for computing crop water requirements, FAO irrigation and drainage paper 56. https://www.fao.org/4/X0490E/x0490e00.htm

Almorox, J., Senatore, A., Quej, V. H., & Mendicino, G. (2018). Worldwide assessment of the Penman–Monteith temperature approach for the estimation of monthly reference evapotranspiration. Theoretical and Applied Climatology, 131(1–2), 693–703. https://doi.org/10.1007/s00704-016-1996-2

Alvo, M., & Yu, P. L. H. (2018). A Parametric Approach to Nonparametric Statistics. Springer International Publishing. https://doi.org/10.1007/978-3-319-94153-0

Anwar, S. A., Malcheva, K., & Srivastava, A. (2023). Estimating the potential evapotranspiration of Bulgaria using a high-resolution regional climate model. Theoretical and Applied Climatology, 152(3–4), 1175–1188. https://doi.org/10.1007/s00704-023-04438-9

Bapat, R. B. (2012). Linear Algebra and Linear Models (3rd ed.). Springer. www.springer.com/series/223

Beck, H. E., Zimmermann, N. E., McVicar, T. R., Vergopolan, N., Berg, A., & Wood, E. F. (2018). Present and future Köppen-Geiger climate classification maps at 1-km resolution. Scientific Data, 5(1), 180214. https://doi.org/10.1038/sdata.2018.214

Boogaard, H., Schubert, J., De Wit, A., Lazebnik, J., Hutjes, R., & Van der Grijn, G. ,. (2020). Agrometeorological indicators from 1979 to present derived from reanalysis. Copernicus Climate Change Service (C3S) Climate Data Store (CDS). https://doi.org/10.24381/cds.6c68c9bb

Broccoli, A. J., & Manabe, S. (1990). Can existing climate models be used to study anthropogenic changes in tropical cyclone climate? Geophysical Research Letters, 17(11), 1917–1920. https://doi.org/10.1029/GL017i011p01917

Brown, D., de Sousa, K., & van Etten, J. (2023). ag5Tools: An R package for downloading and extracting agrometeorological data from the AgERA5 database. SoftwareX, 21, 101267. https://doi.org/10.1016/j.softx.2022.101267

Céspedes, J., Garbanzo, G., Cabral, A., Temudo, M., & Campagnolo, M. (2025). An approach to monitoring rice development in the mangrove swamp rice production system of Guinea-Bissau. (Submitted to International Journal of Applied Earth Observation and Geoinformation). International Journal of Applied Earth Observation and Geoinformation.

Chevuru, S., de Wit, A., Supit, I., & Hutjes, R. (2023). Copernicus global crop productivity indicators: An evaluation based on regionally reported yields. Climate Services, 30, 100374. https://doi.org/10.1016/j.cliser.2023.100374

Conover, W. J. (1999). Practical nonparametric statistics. Wiley.

Daly, C., Halbleib, M., Smith, J. I., Gibson, W. P., Doggett, M. K., Taylor, G. H., Curtis, J., & Pasteris, P. P. (2008). Physiographically sensitive mapping of climatological temperature and precipitation across the conterminous United States. International Journal of Climatology, 28(15), 2031–2064. https://doi.org/10.1002/joc.1688

Dee, D. P., Uppala, S. M., Simmons, A. J., Berrisford, P., Poli, P., Kobayashi, S., Andrae, U., Balmaseda, M. A., Balsamo, G., Bauer, P., Bechtold, P., Beljaars, A. C. M., van de Berg, L., Bidlot, J., Bormann, N., Delsol, C., Dragani, R., Fuentes, M., Geer, A. J., … Vitart, F. (2011). The ERA-Interim reanalysis: configuration and performance of the data assimilation system. Quarterly Journal of the Royal Meteorological Society, 137(656), 553–597. https://doi.org/10.1002/qj.828

Demchev, D. M., Kulakov, M. Yu., Makshtas, A. P., Makhotina, I. A., Fil'chuk, K. V., & Frolov, I. E. (2020). Verification of ERA-Interim and ERA5 Reanalyses Data on Surface Air Temperature in the Arctic. Russian Meteorology and Hydrology, 45(11), 771–777. https://doi.org/10.3103/S1068373920110035

Di Ciaccio, A., Coli, M., & Angulo Ibanez, J. M. (2012). Advanced Statistical Methods for the Analysis of Large Data-Sets. Springer Berlin Heidelberg. https://doi.org/10.1007/978-3-642-21037-2

Djaman, K., Rudnick, D., Mel, V. C., Mutiibwa, D., Diop, L., Sall, M., Kabenge, I., Bodian, A., Tabari, H., & Irmak, S. (2017). Evaluation of Valiantzas' Simplified Forms of the FAO-56 Penman-Monteith Reference Evapotranspiration Model in a Humid Climate. Journal of Irrigation and Drainage Engineering, 143(8). https://doi.org/10.1061/(ASCE)IR.1943-4774.0001191

Djaman, K., Tabari, H., Balde, A. B., Diop, L., Futakuchi, K., & Irmak, S. (2016). Analyses, calibration and validation of evapotranspiration models to predict grass-reference evapotranspiration in the Senegal river delta. Journal of Hydrology: Regional Studies, 8, 82–94. https://doi.org/10.1016/j.ejrh.2016.06.003

Dodge, Y. (2008). The concise encyclopedia of statistics. In The Concise Encyclopedia of Statistics. Springer New York. http://link.springer.com/10.1007/978-0-387-32833-1_200

Dunkerly, C., Huntington, J. L., McEvoy, D., Morway, A., & Allen, R. G. (2024). agweather-qaqc: An Interactive Python Package for Quality Assurance and Quality Control of Daily Agricultural Weather Data and Calculation of Reference Evapotranspiration. Journal of Open Source Software, 9(97), 6368. https://doi.org/10.21105/joss.06368

ECMWF. (2020). Fact sheet: Earth system data assimilation. European Center for Medium-Range Weather Forecasts. https://www.ecmwf.int/en/about/media-centre/focus/2020/fact-sheet-earth-system-data-assimilation

Ferreira, P. M. (2004). Guinea - Bissau. Between conflict and democracy. African Security Review, 13(4), 44–56. https://doi.org/10.1080/10246029.2004.9627317

Frank, W. M., & Young, G. S. (2007). The Interannual Variability of Tropical Cyclones. Monthly Weather Review, 135(10), 3587–3598. https://doi.org/10.1175/MWR3435.1

Galmarini, S., Solazzo, E., Ferrise, R., Srivastava, A. K., Ahmed, M., Asseng, S., Cannon, A. J., Dentener, F., De Sanctis, G., Gaiser, T., Gao, Y., Gayler, S., Gutierrez, J. M., Hoogenboom, G., Iturbide, M., Jury, M., Lange, S., Loukos, H., Maraun, D., … Zhao, C. (2024). Assessing the impact on crop modelling of multi- and uni-variate climate model bias adjustments. Agricultural Systems, 215, 103846. https://doi.org/10.1016/j.agsy.2023.103846

Garbanzo, G., Cameira, M., & Paredes, P. (2024). The Mangrove Swamp Rice Production System of Guinea Bissau: Identification of the Main Constraints Associated with Soil Salinity and Rainfall Variability. Agronomy, 14(3), 468. https://doi.org/10.3390/agronomy14030468

Garbanzo, G., Céspedes, J., Sandoval, J., Temudo, M., Paredes, P., & Cameira, M. do R. (2024). Moving toward the Biophysical Characterization of the Mangrove Swamp Rice Production System in Guinea Bissau: Exploring Tools to Improve Soil- and Water-Use Efficiencies. Agronomy, 14(2), 335. https://doi.org/10.3390/agronomy14020335

Garbanzo, G., Céspedes, J., Temudo, M., Cameira, M. do R., Paredes, P., & Ramos, T. (2025). Advances in soil salinity diagnosis for mangrove swamp rice production in Guinea Bissau, West Africa. Science of Remote Sensing, 11, 100231. https://doi.org/10.1016/j.srs.2025.100231

Garbanzo, G., do Rosário Cameira, M., Paredes, P., Temudo, M., & Ramos, T. B. (2025). Modeling soil water and salinity dynamics in mangrove swamp rice production system of Guinea Bissau, West Africa. Agricultural Water Management, 313, 109494. https://doi.org/10.1016/j.agwat.2025.109494

Gebremedhin, M. A., Lubczynski, M. W., Maathuis, B. H. P., & Teka, D. (2022). Deriving potential evapotranspiration from satellite-based reference

evapotranspiration, Upper Tekeze Basin, Northern Ethiopia. Journal of Hydrology: Regional Studies, 41, 101059. https://doi.org/10.1016/j.ejrh.2022.101059

Gelaro, R., McCarty, W., Suárez, M. J., Todling, R., Molod, A., Takacs, L., Randles, C. A., Darmenov, A., Bosilovich, M. G., Reichle, R., Wargan, K., Coy, L., Cullather, R., Draper, C., Akella, S., Buchard, V., Conaty, A., da Silva, A. M., Gu, W., … Zhao, B. (2017). The Modern-Era Retrospective Analysis for Research and Applications, Version 2 (MERRA-2). Journal of Climate, 30(14), 5419–5454. https://doi.org/10.1175/JCLI-D-16-0758.1

Global Modeling and Assimilation Office (GMAO). (2015a). MERRA-2 statD_2d_slv_Nx: 2d, Daily, Aggregated Statistics, Single-Level, Assimilation, Single-Level Diagnostics V5.12.4, Greenbelt, MD, USA, Goddard Earth Sciences Data and Information Services Center (GES DISC), The National Aeronautics and Space Administration (NASA). https://doi.org/10.5067/9SC1VNTWGWV3

Global Modeling and Assimilation Office (GMAO). (2015b). MERRA-2 tavg1_2d_flx_Nx: 2d,1-Hourly, Time-Averaged, Single-Level, Assimilation, Surface Flux Diagnostics V5.12.4, Greenbelt, MD, USA, Goddard Earth Sciences Data and Information Services Center (GES DISC). The National Aeronautics and Space Administration (NASA). https://doi.org/10.5067/7MCPBJ41Y0K6

Gourgouletis, N., Gkavrou, M., & Baltas, E. (2023). Comparison of Empirical ETo Relationships with ERA5-Land and In Situ Data in Greece. Geographies, 3(3), 499–521. https://doi.org/10.3390/geographies3030026

Hargreaves, G. H., & Samani, Z. A. (1982). Estimating Potential Evapotranspiration. Journal of the Irrigation and Drainage Division, 108(3), 225–230. https://doi.org/10.1061/JRCEA4.0001390

Hargreaves, G. L., Hargreaves, G. H., & Riley, J. P. (1985). Irrigation Water Requirements for Senegal River Basin. Journal of Irrigation and Drainage Engineering, 111(3), 265–275. https://doi.org/10.1061/(ASCE)0733-9437(1985)111:3(265)

Harris, Osborn, T. J., Jones, P., & Lister, D. (2020). Version 4 of the CRU TS monthly high-resolution gridded multivariate climate dataset. Scientific Data, 7(1), 109. https://doi.org/10.1038/s41597-020-0453-3

Harris, S. A. (2014). Comments on the Application of the Holdridge System for Classification of World Life Zones as Applied to Costa Rica. Arctic and Alpine Research, 5(3), 187–191. http://www.jstor.org/stable/1550169

Hartshorn, G. S. (2013). Tropical Forest Ecosystems. In Encyclopedia of Biodiversity (pp. 269–276). Elsevier. https://doi.org/10.1016/B978-0-12-384719-5.00146-5

Herrera, S., Cardoso, R. M., Soares, P. M., Espírito-Santo, F., Viterbo, P., & Gutiérrez, J. M. (2019). Iberia01: a new gridded dataset of daily precipitation and

temperatures over Iberia. Earth System Science Data, 11(4), 1947–1956. https://doi.org/10.5194/essd-11-1947-2019

Hersbach, H., Bell, B., Berrisford, P., Hirahara, S., Horányi, A., Muñoz-Sabater, J., Nicolas, J., Peubey, C., Radu, R., Schepers, D., Simmons, A., Soci, C., Abdalla, S., Abellan, X., Balsamo, G., Bechtold, P., Biavati, G., Bidlot, J., Bonavita, M., … Thépaut, J. (2020). The ERA5 global reanalysis. Quarterly Journal of the Royal Meteorological Society, 146(730), 1999–2049. https://doi.org/10.1002/qj.3803

Hijmans, R. J., Cameron, S. E., Parra, J. L., Jones, P. G., & Jarvis, A. (2005). Very high resolution interpolated climate surfaces for global land areas. International Journal of Climatology, 25(15), 1965–1978. https://doi.org/10.1002/joc.1276

Holdridge, L. R. (1947). Determination of World Plant Formations From Simple Climatic Data. Science, 105(2727), 367–368. https://doi.org/10.1126/science.105.2727.367

Huber, P., & Ronchetti, E. (2009). Robust Statistics (2nd ed.). Wiley.

Ippolito, M., De Caro, D., Cannarozzo, M., Provenzano, G., & Ciraolo, G. (2024). Evaluation of daily crop reference evapotranspiration and sensitivity analysis of FAO Penman-Monteith equation using ERA5-Land reanalysis database in Sicily, Italy. Agricultural Water Management, 295, 108732. https://doi.org/10.1016/j.agwat.2024.108732

Kassambara, A. (2017). Multivariate Analysis. Practical Guide To Cluster Analysis in R. Unsupervised Machine Learning. STHDA. http://www.sthda.com

Kistler, R., Collins, W., Saha, S., White, G., Woollen, J., Kalnay, E., Chelliah, M., Ebisuzaki, W., Kanamitsu, M., Kousky, V., van den Dool, H., Jenne, R., & Fiorino, M. (2001). The NCEP–NCAR 50–Year Reanalysis: Monthly Means CD–ROM and Documentation. Bulletin of the American Meteorological Society, 82(2), 247–267. https://doi.org/10.1175/1520-0477(2001)082<0247:TNNYRM>2.3.CO;2

Kottek, M., Grieser, J., Beck, C., Rudolf, B., & Rubel, F. (2006). World map of the Köppen-Geiger climate classification updated. Meteorologische Zeitschrift, 15(3), 259–263. https://doi.org/10.1127/0941-2948/2006/0130

Koudahe, K., Djaman, K., & Adewumi, J. K. (2018). Evaluation of the Penman–Monteith reference evapotranspiration under limited data and its sensitivity to key climatic variables under humid and semiarid conditions. Modeling Earth Systems and Environment, 4(3), 1239–1257. https://doi.org/10.1007/s40808-018-0497-y

Kovsted, J., & Tarp, F. (1999). Guinea-Bissau: War, Reconstruction and Reform (168). https://www.wider.unu.edu/sites/default/files/wp168.pdf

Kruger, J. A., Roffe, S. J., & van der Walt, A. J. (2024). AgERA5 representation of seasonal mean and extreme temperatures in the Northern Cape, South Africa.

South African Journal of Science, 120(3/4). https://doi.org/10.17159/sajs.2024/16043

Landeras, G., Bekoe, E., Ampofo, J., Logah, F., Diop, M., Cisse, M., & Shiri, J. (2018). New alternatives for reference evapotranspiration estimation in West Africa using limited weather data and ancillary data supply strategies. Theoretical and Applied Climatology, 132(3–4), 701–716. https://doi.org/10.1007/s00704-017-2120-y

Levene, H. (1960). Robust tests for the equality of variance. In I. Olkin (Ed.), Contributions to probability and statistics (pp. 278–292). Stanford University Press.

Linares, O. F. (2002). African rice (Oryza glaberrima): History and future potential. Proceedings of the National Academy of Sciences, 99(25), 16360–16365. https://doi.org/10.1073/pnas.252604599

Liu, M., Paredes, P., Shi, H., Ramos, T. B., Dou, X., Dai, L., & Pereira, L. S. (2022). Impacts of a shallow saline water table on maize evapotranspiration and groundwater contribution using static water table lysimeters and the dual Kc water balance model SIMDualKc. Agricultural Water Management, 273(June), 107887. https://doi.org/10.1016/j.agwat.2022.107887

Liu, M., Shi, H., Paredes, P., Ramos, T. B., Dai, L., Feng, Z., & Pereira, L. S. (2022). Estimating and partitioning maize evapotranspiration as affected by salinity using weighing lysimeters and the SIMDualKc model. Agricultural Water Management, 261(June 2021), 107362. https://doi.org/10.1016/j.agwat.2021.107362

Lopez-Guerrero, A., Cabello-Leblic, A., Fereres, E., Vallee, D., Steduto, P., Jomaa, I., Owaneh, O., Alaya, I., Bsharat, M., Ibrahim, A., Abla, K., Mosad, A., Omari, A., Zitouna-Chebbi, R., & Jimenez-Berni, J. A. (2023). Developing a Regional Network for the Assessment of Evapotranspiration. Agronomy, 13(11), 2756. https://doi.org/10.3390/agronomy13112756

Mardia, K. V. ., Kent, J. T. ., & Bibby, J. M. . (1979). Multivariate analysis. Academic Press.

Martins, Paredes, P., Raziei, T., Pires, C., Cadima, J., & Pereira, L. S. (2017). Assessing reference evapotranspiration estimation from reanalysis weather products. An application to the Iberian Peninsula. International Journal of Climatology, 37(5), 2378–2397. https://doi.org/10.1002/joc.4852

Mendes, O., Correia, E., & Fragoso, M. (2025). Variability and trends of the rainy season in West Africa with a special focus on Guinea-Bissau. Theoretical and Applied Climatology, 156(5), 242. https://doi.org/10.1007/s00704-025-05471-6

Mendes, O., & Fragoso, M. (2023). Assessment of the Record-Breaking 2020 Rainfall in Guinea-Bissau and Impacts of Associated Floods. Geosciences, 13(2), 25. https://doi.org/10.3390/geosciences13020025

Mendes, O., & Fragoso, M. (2024). Recent changes in climate extremes in Guinea-Bissau. African Geographical Review, 1–19. https://doi.org/10.1080/19376812.2024.2359997

Meng, X., Guo, H., Cheng, J., & Yao, B. (2022). Can the ERA5 Reanalysis Product Improve the Atmospheric Correction Accuracy of Landsat Series Thermal Infrared Data? IEEE Geoscience and Remote Sensing Letters, 19, 1–5. https://doi.org/10.1109/LGRS.2022.3167388

Montgomery, D. C., & Runger, G. C. (2011). Applied Statistics and Probability for Engineers (5th ed.). John Wiley & Sons, Inc.

Moratiel, R., Bravo, R., Saa, A., Tarquis, A. M., & Almorox, J. (2020). Estimation of evapotranspiration by the Food and Agricultural Organization of the United Nations (FAO) Penman–Monteith temperature (PMT) and Hargreaves–Samani (HS) models under temporal and spatial criteria – a case study in Duero basin (Spain). Natural Hazards and Earth System Sciences, 20(3), 859–875. https://doi.org/10.5194/nhess-20-859-2020

Musa, A. A., & Elagib, N. A. (2025). Extra Dimensions to the Calibration of Hargreaves-Samani Equation Under Data-Scarce Environment. Water Resources Management. https://doi.org/10.1007/s11269-025-04151-4

Nouri, M., & Homaee, M. (2022). Reference crop evapotranspiration for data-sparse regions using reanalysis products. Agricultural Water Management, 262, 107319. https://doi.org/10.1016/j.agwat.2021.107319

Paredes, P., Fontes, J. C., Azevedo, E. B., & Pereira, L. S. (2018). Daily reference crop evapotranspiration with reduced data sets in the humid environments of Azores islands using estimates of actual vapor pressure, solar radiation, and wind speed. Theoretical and Applied Climatology, 134(3–4), 1115–1133. https://doi.org/10.1007/s00704-017-2329-9

Paredes, P., Martins, D., Pereira, L., Cadima, J., & Pires, C. (2018). Accuracy of daily estimation of grass reference evapotranspiration using ERA-Interim reanalysis products with assessment of alternative bias correction schemes. Agricultural Water Management, 210, 340–353. https://doi.org/10.1016/j.agwat.2018.08.003

Paredes, P., & Pereira, L. S. (2019). Computing FAO56 reference grass evapotranspiration PM-ETo from temperature with focus on solar radiation. Agricultural Water Management, 215, 86–102. https://doi.org/10.1016/j.agwat.2018.12.014

Paredes, P., Pereira, L. S., Almorox, J., & Darouich, H. (2020). Reference grass evapotranspiration with reduced data sets: Parameterization of the FAO Penman-Monteith temperature approach and the Hargeaves-Samani equation using local climatic variables. Agricultural Water Management, 240, 106210. https://doi.org/10.1016/j.agwat.2020.106210

Paredes, P., Trigo, I., de Bruin, H., Simões, N., & Pereira, L. S. (2021). Daily grass reference evapotranspiration with Meteosat Second Generation shortwave

radiation and reference ET products. Agricultural Water Management, 248, 106543. https://doi.org/10.1016/j.agwat.2020.106543

Pelosi, A. (2023). Performance of the Copernicus European Regional Reanalysis (CERRA) dataset as proxy of ground-based agrometeorological data. Agricultural Water Management, 289, 108556. https://doi.org/10.1016/j.agwat.2023.108556

Pelosi, A., & Chirico, G. B. (2021). Regional assessment of daily reference evapotranspiration: Can ground observations be replaced by blending ERA5-Land meteorological reanalysis and CM-SAF satellite-based radiation data? Agricultural Water Management, 258, 107169. https://doi.org/10.1016/j.agwat.2021.107169

Pelosi, A., Medina, H., Van den Bergh, J., Vannitsem, S., & Chirico, G. B. (2017). Adaptive Kalman Filtering for Postprocessing Ensemble Numerical Weather Predictions. Monthly Weather Review, 145(12), 4837–4854. https://doi.org/10.1175/MWR-D-17-0084.1

Pelosi, A., Terribile, F., D'Urso, G., & Chirico, G. (2020). Comparison of ERA5-Land and UERRA MESCAN-SURFEX Reanalysis Data with Spatially Interpolated Weather Observations for the Regional Assessment of Reference Evapotranspiration. Water, 12(6), 1669. https://doi.org/10.3390/w12061669

Pereira, L. S., Allen, R. G., Smith, M., & Raes, D. (2015). Crop evapotranspiration estimation with FAO56: Past and future. Agricultural Water Management, 147, 4–20. https://doi.org/10.1016/j.agwat.2014.07.031

Pereira, L. S., Allen, R., Paredes, P., Smith, M., Raes, D., & Salman, M. (2025). Crop evapotranspiration. guidelines for computing crop water requirements. FAO Irrig. Drain. Pap. 56rev. (Rome (In Press).

Pereira, L. S., Paredes, P., & Espírito-Santo, D. (2024). Crop coefficients of natural wetlands and riparian vegetation to compute ecosystem evapotranspiration and the water balance. Irrigation Science, 42(6), 1171–1197. https://doi.org/10.1007/s00271-024-00923-9

Popova, Z., Kercheva, M., & Pereira, L. S. (2006). Validation of the FAO methodology for computing ET o with limited data. Application to south Bulgaria. Irrigation and Drainage, 55(2), 201–215. https://doi.org/10.1002/ird.228

Qiu, R., Li, L., Kang, S., Liu, C., Wang, Z., Cajucom, E. P., Zhang, B., & Agathokleous, E. (2021). An improved method to estimate actual vapor pressure without relative humidity data. Agricultural and Forest Meteorology, 298–299, 108306. https://doi.org/10.1016/j.agrformet.2020.108306

R Core Team. (2024). R: A Language and Environment for Statistical Computing. R Foundation for Statistical Computing, Vienna, Austria.; Posit Software, PBC, Boston. https://www.R-project.org

Ramos, T. B., Gonçalves, M. C., & van Genuchten, M. Th. (2024). Soil salinization in Portugal: An in-depth exploration of impact, advancements, and future

considerations. Vadose Zone Journal, 23(4). https://doi.org/10.1002/vzj2.20314

Raziei, T., & Pereira, L. S. (2013). Estimation of ETo with Hargreaves–Samani and FAO-PM temperature methods for a wide range of climates in Iran. Agricultural Water Management, 121, 1–18. https://doi.org/10.1016/j.agwat.2012.12.019

Republic of Guinea Bissau. (2014). Fifth National Report to the Convention on Biological Diversity. https://www.cbd.int/doc/world/gw/gw-nr-05-en.pdf

Republic of Guinea Bissau. (2018). Framework Convention on Climate Change. National Communication. (Issue January). http://environment.gov.gb

Rienecker, M. M., Suarez, M. J., Gelaro, R., Todling, R., Bacmeister, J., Liu, E., Bosilovich, M. G., Schubert, S. D., Takacs, L., Kim, G.-K., Bloom, S., Chen, J., Collins, D., Conaty, A., da Silva, A., Gu, W., Joiner, J., Koster, R. D., Lucchesi, R., … Woollen, J. (2011). MERRA: NASA's Modern-Era Retrospective Analysis for Research and Applications. Journal of Climate, 24(14), 3624–3648. https://doi.org/10.1175/JCLI-D-11-00015.1

Rosa, R. D., Ramos, T. B., & Pereira, L. S. (2016). The dual Kc approach to assess maize and sweet sorghum transpiration and soil evaporation under saline conditions: Application of the SIMDualKc model. Agricultural Water Management, 177, 77–94. https://doi.org/10.1016/j.agwat.2016.06.028

Ruane, A. C., Goldberg, R., & Chryssanthacopoulos, J. (2015). Climate forcing datasets for agricultural modeling: Merged products for gap-filling and historical climate series estimation. Agricultural and Forest Meteorology, 200, 233–248. https://doi.org/10.1016/j.agrformet.2014.09.016

Samuel, N., Lonatchedná, J., Mendes, O., & Mendes, C. (2019). A comparative investigation of evapotranspiration (ET) obtained from two methods and determining a best cultivation period. case of Bafata - Guinea Bissau. International Journal of Current Research, 11(02), 1468–1470. https://doi.org/https://doi.org/10.24941/ijcr.34115.02.2019

Soulis, K., Dosiadis, E., Nikitakis, E., Charalambopoulos, I., Kairis, O., Katsogiannou, A., Palli Gravani, S., & Kalivas, D. (2025). Assessing AgERA5 and MERRA-2 Global Climate Datasets for Small-Scale Agricultural Applications. Atmosphere, 16(3), 263. https://doi.org/10.3390/atmos16030263

Syakur, M. A., Khotimah, B. K., Rochman, E. M. S., & Satoto, B. D. (2018). Integration K-Means Clustering Method and Elbow Method For Identification of The Best Customer Profile Cluster. IOP Conference Series: Materials Science and Engineering, 336(1), 012017. https://doi.org/10.1088/1757-899X/336/1/012017

Temudo, M. P., & Cabral, A. I. R. (2023). Climate change as the last trigger in a long-lasting conflict: the production of vulnerability in northern Guinea-Bissau, West Africa. The Journal of Peasant Studies, 50(1), 315–338. https://doi.org/10.1080/03066150.2021.1996355

Thorndike, R. L. (1953). Who Belongs in the Family? Psychometrika, 18(4), 267–276. https://doi.org/10.1007/BF02289263

Thornthwaite, C. W. (1948). An Approach toward a Rational Classification of Climate. Geographical Review, 38(1), 55. https://doi.org/10.2307/210739

Tiruye, A., Ditthakit, P., Linh, N. T. T., Wipulanusat, W., Weesakul, U., & Thongkao, S. (2024). Comparing WaPOR and ERA5-Land: Innovative Estimations of Precipitation and Evapotranspiration in the Tana Basin, Ethiopia. Earth Systems and Environment, 8(4), 1225–1246. https://doi.org/10.1007/s41748-024-00446-5

Todorovic, M., Karic, B., & Pereira, L. S. (2013). Reference evapotranspiration estimate with limited weather data across a range of Mediterranean climates. Journal of Hydrology, 481, 166–176. https://doi.org/10.1016/j.jhydrol.2012.12.034

Toreti, A., Maiorano, A., De Sanctis, G., Webber, H., Ruane, A. C., Fumagalli, D., Ceglar, A., Niemeyer, S., & Zampieri, M. (2019). Using reanalysis in crop monitoring and forecasting systems. Agricultural Systems, 168, 144–153. https://doi.org/10.1016/j.agsy.2018.07.001

Trajkovic, S., Gocic, M., Pongracz, R., Bartholy, J., & Milanovic, M. (2020). Assessment of Reference Evapotranspiration by Regionally Calibrated Temperature-Based Equations. KSCE Journal of Civil Engineering, 24(3), 1020–1027. https://doi.org/10.1007/s12205-020-1698-2

Trigo, I. F., de Bruin, H., Beyrich, F., Bosveld, F. C., Gavilán, P., Groh, J., & López-Urrea, R. (2018). Validation of reference evapotranspiration from Meteosat Second Generation (MSG) observations. Agricultural and Forest Meteorology, 259, 271–285. https://doi.org/10.1016/j.agrformet.2018.05.008

UNEP. (1997). World atlas of desertification (Nick. Middleton, D. Thomas, & UNEP, Eds.). United Nations.

Van Rossum, G., & Drake, F. (2009). Python 3 Reference Manual. CreateSpace. https://www.python.org/

Van Tricht, K., Degerickx, J., Gilliams, S., Zanaga, D., Battude, M., Grosu, A., Brombacher, J., Lesiv, M., Bayas, J. C. L., Karanam, S., Fritz, S., Becker-Reshef, I., Franch, B., Mollà-Bononad, B., Boogaard, H., Pratihast, A. K., Koetz, B., & Szantoi, Z. (2023). WorldCereal: a dynamic open-source system for global-scale, seasonal, and reproducible crop and irrigation mapping. Earth System Science Data, 15(12), 5491–5515. https://doi.org/10.5194/essd-15-5491-2023

Vanella, D., Longo-Minnolo, G., Belfiore, O. R., Ramírez-Cuesta, J. M., Pappalardo, S., Consoli, S., D'Urso, G., Chirico, G. B., Coppola, A., Comegna, A., Toscano, A., Quarta, R., Provenzano, G., Ippolito, M., Castagna, A., & Gandolfi, C. (2022). Comparing the use of ERA5 reanalysis dataset and ground-based agrometeorological data under different climates and topography in Italy. Journal of Hydrology: Regional Studies, 42, 101182. https://doi.org/10.1016/j.ejrh.2022.101182

Vicente-Serrano, S. M., Domínguez-Castro, F., Reig, F., Tomas-Burguera, M., Peña-Angulo, D., Latorre, B., Beguería, S., Rabanaque, I., Noguera, I., Lorenzo-Lacruz, J., & El Kenawy, A. (2023). A global drought monitoring system and dataset based on ERA5 reanalysis: A focus on crop-growing regions. Geoscience Data Journal, 10(4), 505–518. https://doi.org/10.1002/gdj3.178

Viggiano, M., Busetto, L., Cimini, D., Di Paola, F., Geraldi, E., Ranghetti, L., Ricciardelli, E., & Romano, F. (2019). A new spatial modeling and interpolation approach for high-resolution temperature maps combining reanalysis data and ground measurements. Agricultural and Forest Meteorology, 276–277, 107590. https://doi.org/10.1016/j.agrformet.2019.05.021

Wu, L., Zhou, H., Ma, X., Fan, J., & Zhang, F. (2019). Daily reference evapotranspiration prediction based on hybridized extreme learning machine model with bio-inspired optimization algorithms: Application in contrasting climates of China. Journal of Hydrology, 577, 123960. https://doi.org/10.1016/j.jhydrol.2019.123960

Xavier, A. C., Scanlon, B. R., King, C. W., & Alves, A. I. (2022). New improved Brazilian daily weather gridded data (1961–2020). International Journal of Climatology, 42(16), 8390–8404. https://doi.org/10.1002/joc.7731

Xi, X., Zhuang, Q., Kim, S., & Gentine, P. (2023). Evaluating the Effects of Precipitation and Evapotranspiration on Soil Moisture Variability Within CMIP5 Using SMAP and ERA5 Data. Water Resources Research, 59(5). https://doi.org/10.1029/2022WR034225

Xue, C., Niu, L., Wu, H., Jiang, X., & Fan, D. (2019). Drought Assessment in Belt and Road Area Based on ERA5 Reanalyses. IGARSS 2019 - 2019 IEEE International Geoscience and Remote Sensing Symposium, 7737–7740. https://doi.org/10.1109/IGARSS.2019.8897863

Yonaba, R., Tazen, F., Cissé, M., Mounirou, L. A., Belemtougri, A., Ouedraogo, V. A., Koïta, M., Niang, D., Karambiri, H., & Yacouba, H. (2023). Trends, sensitivity and estimation of daily reference evapotranspiration ET0 using limited climate data: regional focus on Burkina Faso in the West African Sahel. Theoretical and Applied Climatology, 153(1–2), 947–974. https://doi.org/10.1007/s00704-023-04507-z

Zereg, S., & Belouz, K. (2023). Modeling daily reference evapotranspiration using SVR machine learning algorithm with limited meteorological data in Dar-el-Beidha, Algeria. Acta Geophysica, 72(3), 2009–2025. https://doi.org/10.1007/s11600-023-01107-3

Zhang, Y., Mao, G., Chen, C., Shen, L., & Xiao, B. (2021). Population Exposure to Compound Droughts and Heatwaves in the Observations and ERA5 Reanalysis Data in the Gan River Basin, China. Land, 10(10), 1021. https://doi.org/10.3390/land10101021

Zhu, B., Feng, Y., Gong, D., Jiang, S., Zhao, L., & Cui, N. (2020). Hybrid particle swarm optimization with extreme learning machine for daily reference

evapotranspiration prediction from limited climatic data. Computers and Electronics in Agriculture, 173, 105430. https://doi.org/10.1016/j.compag.2020.105430

References for Chapter 6

Allen, R.G., Pereira, L.S., Raes, D., Smith, M., 1998. Crop Evapotranspiration. Guidelines for computing crop water requirements, FAO irrigation and drainage paper 56. Rome.

Ayers, R.S., Westcot, D.W., 1985. Water Quality for Agriculture. Irrigation and Drainage Paper 29. 174 p.

Baggie, I., Sumah, F., Zwart, S.J., Sawyerr, P., Bandabla, T., Kamara, C.S., 2018. Characterization of the mangrove swamp rice soils along the Great Scarcies River in Sierra Leone using principal component analysis. Catena (Amst) 163, 54–62. https://doi.org/10.1016/j.catena.2017.11.026

Balasubramanian, V., Sie, M., Hijmans, R.J., Otsuka, K., 2007. Increasing Rice Production in Sub-Saharan Africa: Challenges and Opportunities. Advances in Agronomy 94, 55–133. https://doi.org/10.1016/S0065-2113(06)94002-4

Beck, H.E., Zimmermann, N.E., McVicar, T.R., Vergopolan, N., Berg, A., Wood, E.F., 2018. Present and future Köppen-Geiger climate classification maps at 1-km resolution. Sci Data 5, 180214. https://doi.org/10.1038/sdata.2018.214

Boogaard, H., Schubert, J., De Wit, A., Lazebnik, J., Hutjes, R., Van der Grijn, G., 2020. Agrometeorological indicators from 1979 to present derived from reanalysis. Copernicus Climate Change Service (C3S) Climate Data Store (CDS). [WWW Document]. https://doi.org/10.24381/cds.6c68c9bb

Bos, D., Grigoras, I., Ndiaye, A., 2006. Land cover and avian biodiversity in rice fields and mangroves of West Africa. Altenburg & Wymenga, Dakar.

Corwin, D.L., Lesch, S.M., 2005. Apparent soil electrical conductivity measurements in agriculture. Comput Electron Agric 46, 11–43. https://doi.org/10.1016/j.compag.2004.10.005

Cossa, V., 2023. Experimentação com variedades e densidades de sementeira de arroz no agroecossistema de mangal de bolanha salgada no Sul de Guiné-Bissau (Workshop). Malmon, Project EU_DESIRA: Bissau, Guinea Bissau.

D'Amico, M.E., Barbieri, M., Khair, D.A. El, Comolli, R., 2024. Mangrove rice productivity and pedogenic trends in Guinea Bissau, West Africa. J Soils Sediments 24, 244–258. https://doi.org/10.1007/s11368-023-03608-6

Doorenbos, J., Kassam, A.H., 1979. Yield Response to water. FAO Irrigation and Drainage Paper No. 33. 193 p.

Fageria, N.K., 1985. Salt tolerance of rice cultivars. Plant Soil 88, 237–243. https://doi.org/10.1007/BF02182450

FAO, 2023. With major processing by Our World in Data. "Rice yields – FAO" [dataset]. Food and Agriculture Organization of the United Nations, "Production: Crops and livestock products" [original data]. [WWW Document]. URL https://ourworldindata.org/grapher/rice-yields (accessed 2.6.25).

Feddes, R., Kowalik, P., Zaradny, H., 1978. Simulation of field water use and crop yield, in: Penning de Vries, F.W.T., van Laar, H.H. (Eds.), Simulation of Plant Growth and Crop Production. Wageningen : Pudoc, The Netherlands, pp. 194–209.

Forkutsa, I., Sommer, R., Shirokova, Y.I., Lamers, J.P.A., Kienzler, K., Tischbein, B., Martius, C., Vlek, P.L.G., 2009. Modeling irrigated cotton with shallow groundwater in the Aral Sea Basin of Uzbekistan: II. Soil salinity dynamics. Irrig Sci 27, 319–330. https://doi.org/10.1007/s00271-009-0149-0

Garbanzo, Cespedes, J., Temudo, M., Cameria, M., Paredes, P., Ramos, T., 2025b. Addressing weather data scarcity in estimating reference crop evapotranspiration: A case study from Guinea Bissau, West Africa . Submitted to Climate. .

Garbanzo, G., Cameira, M., Paredes, P., 2024a. The Mangrove Swamp Rice Production System of Guinea Bissau: Identification of the Main Constraints Associated with Soil Salinity and Rainfall Variability. Agronomy 14, 468. https://doi.org/10.3390/agronomy14030468

Garbanzo, G., Céspedes, J., Sandoval, J., Temudo, M., Paredes, P., Cameira, M. do R., 2024b. Moving toward the Biophysical Characterization of the Mangrove Swamp Rice Production System in Guinea Bissau: Exploring Tools to Improve Soil- and Water-Use Efficiencies. Agronomy 14, 335. https://doi.org/10.3390/agronomy14020335

Garbanzo, G., Cespedes, J., Temudo, M., Cameria, M., Paredes, P., Ramos, T., 2025a. Advances in soil salinity diagnosis for mangrove swamp rice production in Guinea Bissau, West Africa. Submitted to Science of Remote Sensing.

González, M.G., Ramos, T.B., Carlesso, R., Paredes, P., Petry, M.T., Martins, J.D., Aires, N.P., Pereira, L.S., 2015. Modelling soil water dynamics of full and deficit drip irrigated maize cultivated under a rain shelter. Biosyst Eng 132, 1–18. https://doi.org/10.1016/j.biosystemseng.2015.02.001

Guei, R.G., Dixon, C.A., Sampong, M.A., 1997. Strategies and approaches to mangrove swamp rice varietal improvement in West Africa. Afr Crop Sci J 5, 209–217. https://doi.org/10.4314/acsj.v5i2.27863

Guo, S., Li, X., Šimůnek, J., Wang, J., Zhang, Y., Wang, Y., Zhen, Z., He, R., 2024. Experimental and numerical evaluation of soil water and salt dynamics in a corn field with shallow saline groundwater and crop-season drip and autumn post-harvest irrigations. Agric Water Manag 305, 109119. https://doi.org/10.1016/j.agwat.2024.109119

Haque, M.A., Rafii, M.Y., Yusoff, M.M., Ali, N.S., Yusuff, O., Datta, D.R., Anisuzzaman, M., Ikbal, M.F., 2021. Advanced Breeding Strategies and Future Perspectives of Salinity Tolerance in Rice. Agronomy 11, 1631. https://doi.org/10.3390/agronomy11081631

Heinen, M., Mulder, M., Kroes, J., 2020. SWAP 4 – Technical addendum to the SWAP documentation.

Heinen, M., Mulder, M., van Dam, J., Bartholomeus, R., de Jong van Lier, Q., de Wit, J., de Wit, A., Hack - ten Broeke, M., 2024. SWAP 50 years: Advances in modelling soil-water-atmosphere-plant interactions. Agric Water Manag 298, 108883. https://doi.org/10.1016/j.agwat.2024.108883

Hilhorst, M.A., 2000. A Pore Water Conductivity Sensor. Soil Science Society of America Journal 64, 1922–1925. https://doi.org/10.2136/sssaj2000.6461922x

Hodson, T.O., 2022. Root-mean-square error (RMSE) or mean absolute error (MAE): when to use them or not. Geosci Model Dev 15, 5481–5487. https://doi.org/10.5194/gmd-15-5481-2022

Hopmans, J.W., Qureshi, A.S., Kisekka, I., Munns, R., Grattan, S.R., Rengasamy, P., Ben-Gal, A., Assouline, S., Javaux, M., Minhas, P.S., Raats, P.A.C., Skaggs, T.H., Wang, G., De Jong van Lier, Q., Jiao, H., Lavado, R.S., Lazarovitch, N., Li, B., Taleisnik, E., 2021. Critical knowledge gaps and research priorities in global soil salinity, in: Advances in Agronomy. Academic Press Inc., pp. 1–191. https://doi.org/10.1016/bs.agron.2021.03.001

Huber, P., Ronchetti, E., 2009. Robust Statistics, 2nd ed. Wiley, New-Jersey.

IRRI, n.d. Salinity-tolerant rice variety set to boost rice yield in stress-prone areas in Kenya [WWW Document]. 2023. URL https://www.irri.org/news-and-events/news/salinity-tolerant-rice-variety-set-boost-rice-yield-stress-prone-areas-kenya (accessed 1.6.25).

Jnr, S.D., 2014. Land degradation and agriculture in the Sahel of Africa: causes, impacts and recommendations. Journal of Agricultural Science and Applications 03, 67–73. https://doi.org/10.14511/jasa.2014.030303

Kanzari, S., Šimůnek, J., Daghari, I., Younes, A., Ali, K., Mariem, S., Ghannem, S., 2024. Modeling Irrigation of Tomatoes with Saline Water in Semi-Arid Conditions Using Hydrus-1D. Land (Basel) 13, 739. https://doi.org/10.3390/land13060739

Karimov, A.Kh., Šimůnek, J., Hanjra, M.A., Avliyakulov, M., Forkutsa, I., 2014. Effects of the shallow water table on water use of winter wheat and ecosystem health: Implications for unlocking the potential of groundwater in the Fergana Valley (Central Asia). Agric Water Manag 131, 57–69. https://doi.org/10.1016/j.agwat.2013.09.010

Kitamura, Y., Yano, T., Honna, T., Yamamoto, S., Inosako, K., 2006. Causes of farmland salinization and remedial measures in the Aral Sea basin—Research on water management to prevent secondary salinization in rice-based cropping system in arid land. Agric Water Manag 85, 1–14. https://doi.org/10.1016/j.agwat.2006.03.007

Letey, J., Hoffman, G.J., Hopmans, J.W., Grattan, S.R., Suarez, D., Corwin, D.L., Oster, J.D., Wu, L., Amrhein, C., 2011. Evaluation of soil salinity leaching requirement guidelines. Agric Water Manag 98, 502–506. https://doi.org/10.1016/j.agwat.2010.08.009

Li, Y., Šimůnek, J., Jing, L., Zhang, Z., Ni, L., 2014. Evaluation of water movement and water losses in a direct-seeded-rice field experiment using Hydrus-1D. Agric Water Manag 142, 38–46. https://doi.org/10.1016/j.agwat.2014.04.021

Li, Y., Šimůnek, J., Zhang, Z., Jing, L., Ni, L., 2015. Evaluation of nitrogen balance in a direct-seeded-rice field experiment using Hydrus-1D. Agric Water Manag 148, 213–222. https://doi.org/10.1016/j.agwat.2014.10.010

Liu, M., Paredes, P., Shi, H., Ramos, T.B., Dou, X., Dai, L., Pereira, L.S., 2022. Impacts of a shallow saline water table on maize evapotranspiration and groundwater contribution using static water table lysimeters and the dual Kc water balance model SIMDualKc. Agric Water Manag 273, 107887. https://doi.org/10.1016/j.agwat.2022.107887

Ma, L., Ahuja, L.R., Ascough, J.C., Shaffer, M.J., Rojas, K.W., Malone, R.W., Cameira, M.R., 2001. Integrating system modeling with field research in agriculture: applications of the root zone water quality model (RZWQM), in: Advances in Agronomy. pp. 233–292. https://doi.org/10.1016/S0065-2113(01)71016-4

Maas, E.V., 1990. Crop Salt Tolerance, in: Tanji, K.K. (Ed.), Agricultural Salinity Assessment and Management, ASCE Manual Reports on Engineering Practices. ASCE, New York, pp. 262–304.

Marcos, M., Sharifi, H., Grattan, S.R., Linquist, B.A., 2018. Spatio-temporal salinity dynamics and yield response of rice in water-seeded rice fields. Agric Water Manag 195, 37–46. https://doi.org/10.1016/j.agwat.2017.09.016

Martiarena, M.L., Temudo, M.P., 2023. Endogenous learning and innovation in African smallholder agriculture: lessons from Guinea-Bissau. The Journal of Agricultural Education and Extension 1–19. https://doi.org/10.1080/1389224X.2023.2169480

Mendes, O., Fragoso, M., 2023. Assessment of the Record-Breaking 2020 Rainfall in Guinea-Bissau and Impacts of Associated Floods. Geosciences (Basel) 13, 25. https://doi.org/10.3390/geosciences13020025

Merkohasanaj, M., Garbanzo, G., Cortez, N., Jose, F., Peinado, M., Andreetta, A., Cunha-Queda, C., 2025. Catena Soil physicochemical characterization and suitability assessment for the coastal mangrove swamp rice production system in Guinea-Bissau (Sumited to Catena). Catena (Amst).

Minhas, P.S., Ramos, T.B., Ben-Gal, A., Pereira, L.S., 2020. Coping with salinity in irrigated agriculture: Crop evapotranspiration and water management issues. Agric Water Manag 227, 105832. https://doi.org/10.1016/j.agwat.2019.105832

Mo'allim, A.A., Kamal, M.R., Muhammed, H.H., Yahaya, N.K.E.M., Zawawe, M.A. b. M., Man, H. bt. C., Wayayok, A., 2018. An Assessment of the Vertical Movement of Water in a Flooded Paddy Rice Field Experiment Using Hydrus-1D. Water (Basel) 10, 783. https://doi.org/10.3390/w10060783

Monteiro, J.E.B. de A., Azevedo, L. da C., Assad, E.D., Sentelhas, P.C., 2013. Rice yield estimation based on weather conditions and on technological level of production systems in Brazil. Pesqui Agropecu Bras 48, 123–131. https://doi.org/10.1590/S0100-204X2013000200001

Montgomery, D.C., Runger, G.C., 2011. Applied Statistics and Probability for Engineers, 5th ed. John Wiley & Sons, Inc., Arizona,USA.

Mualem, Y., 1976. A new model for predicting the hydraulic conductivity of unsaturated porous media. Water Resour Res 12, 513–522. https://doi.org/10.1029/WR012i003p00513

Narjary, B., Kumar, S., Meena, M.D., Kamra, S.K., Sharma, D.K., 2021. Effects of Shallow Saline Groundwater Table Depth and Evaporative Flux on Soil Salinity Dynamics using Hydrus-1D. Agricultural Research 10, 105–115. https://doi.org/10.1007/s40003-020-00484-1

Pereira, L.S., Paredes, P., Hunsaker, D.J., López-Urrea, R., Mohammadi Shad, Z., 2021. Standard single and basal crop coefficients for field crops. Updates and advances to the FAO56 crop water requirements method. Agric Water Manag 243, 106466. https://doi.org/10.1016/j.agwat.2020.106466

Phogat, V., Pitt, T., Cox, J.W., Šimůnek, J., Skewes, M.A., 2018. Soil water and salinity dynamics under sprinkler irrigated almond exposed to a varied salinity stress at different growth stages. Agric Water Manag 201, 70–82. https://doi.org/10.1016/j.agwat.2018.01.018

Phogat, V., Yadav, A.K., Malik, R.S., Kumar, S., Cox, J., 2010. Simulation of salt and water movement and estimation of water productivity of rice crop irrigated with saline water. Paddy and Water Environment 8, 333–346. https://doi.org/10.1007/s10333-010-0213-7

Plevris, V., Solorzano, G., Bakas, N., Ben Seghier, M., 2022. Investigation of performance metrics in regression analysis and machine learning-based prediction models, in: 8th European Congress on Computational Methods in Applied Sciences and Engineering. CIMNE. https://doi.org/10.23967/eccomas.2022.155

R Core Team, 2024. R: A Language and Environment for Statistical Computing [WWW Document]. R Foundation for Statistical Computing, Vienna, Austria. URL https://www.R-project.org (accessed 3.30.24).

Ragab, R., 2002. A holistic generic integrated approach for irrigation, crop and field management: the SALTMED model. Environmental Modelling & Software 17, 345–361. https://doi.org/10.1016/S1364-8152(01)00079-2

Ramos, T.B., Liu, M., Paredes, P., Shi, H., Feng, Z., Lei, H., Pereira, L.S., 2023. Salts dynamics in maize irrigation in the Hetao plateau using static water table lysimeters and HYDRUS-1D with focus on the autumn leaching irrigation. Agric Water Manag 283, 108306. https://doi.org/10.1016/j.agwat.2023.108306

Ramos, T.B., Šimůnek, J., Gonçalves, M.C., Martins, J.C., Prazeres, A., Castanheira, N.L., Pereira, L.S., 2011. Field evaluation of a multicomponent solute transport model in soils irrigated with saline waters. J Hydrol (Amst) 407, 129–144. https://doi.org/10.1016/j.jhydrol.2011.07.016

Reddy, I.N.B.L., Kim, B.-K., Yoon, I.-S., Kim, K.-H., Kwon, T.-R., 2017. Salt Tolerance in Rice: Focus on Mechanisms and Approaches. Rice Sci 24, 123–144. https://doi.org/10.1016/j.rsci.2016.09.004

Shekhar, S., Mailapalli, D.R., Raghuwanshi, N.S., Das, B.S., 2020. Hydrus-1D model for simulating water flow through paddy soils under alternate wetting and drying irrigation practice. Paddy and Water Environment 18, 73–85. https://doi.org/10.1007/s10333-019-00765-8

Šimůnek, J., Brunetti, G., Jacques, D., van Genuchten, M.Th., Šejna, M., 2024. Developments and applications of the HYDRUS computer software packages since 2016. Vadose Zone Journal 23. https://doi.org/10.1002/vzj2.20310

Šimůnek, J., van Genuchten, M.T., 1996. Estimating Unsaturated Soil Hydraulic Properties from Tension Disc Infiltrometer Data by Numerical Inversion. Water Resour Res 32, 2683–2696. https://doi.org/10.1029/96WR01525

Šimůnek, J., van Genuchten, M.Th., Šejna, M., 2016. Recent Developments and Applications of the HYDRUS Computer Software Packages. Vadose Zone Journal 15, 1–25. https://doi.org/10.2136/vzj2016.04.0033

Skaggs, T.H., Shouse, P.J., Poss, J.A., 2006. Irrigating Forage Crops with Saline Waters: 2. Modeling Root Uptake and Drainage. Vadose Zone Journal 5, 824–837. https://doi.org/10.2136/vzj2005.0120

Sonmez, S., Buyuktas, D., Okturen, F., Citak, S., 2008. Assessment of different soil to water ratios (1:1, 1:2.5, 1:5) in soil salinity studies. Geoderma 144, 361–369. https://doi.org/10.1016/j.geoderma.2007.12.005

Steurer, M., Hill, R.J., Pfeifer, N., 2021. Metrics for evaluating the performance of machine learning based automated valuation models. Journal of Property Research 38, 99–129. https://doi.org/10.1080/09599916.2020.1858937

Stulina, G., Cameira, M.R., Pereira, L.S., 2005. Using RZWQM to search improved practices for irrigated maize in Fergana, Uzbekistan. Agric Water Manag 77, 263–281. https://doi.org/10.1016/j.agwat.2004.09.040

Sugimori, Y., Funakawa, S., Pachikin, K.M., Ishida, N., Kosaki, T., 2008. Soil salinity dynamics in irrigated fields and its effects on paddy-based rotation systems in southern Kazakhstan. Land Degrad Dev 19, 305–320. https://doi.org/10.1002/ldr.843

Sylla, M., Stein, A., van Breemen, N., Fresco, L.O., 1995. Spatial variability of soil salinity at different scales in the mangrove rice agro-ecosystem in West Africa. Agric Ecosyst Environ 54, 1–15. https://doi.org/10.1016/0167-8809(95)00594-I

Taylor, R., 1990. Interpretation of the Correlation Coefficient: A Basic Review. Journal of Diagnostic Medical Sonography 6, 35–39. https://doi.org/10.1177/875647939000600106

Teixeira, D.S., 1962. Os solos da Guiné Portuguesa. Carta general caracteristicas, formação e utilização, 1st ed, Junta de investigaçoes do ultramar. Junta de Investigações do Ultramar, Lisboa.

Temudo, M.P., 2011. Planting Knowledge, Harvesting Agro-Biodiversity: A Case Study of Southern Guinea-Bissau Rice Farming. Hum Ecol 39, 309–321. https://doi.org/10.1007/s10745-011-9404-0

Temudo, M.P., Cabral, A.I.R., 2023. Climate change as the last trigger in a long-lasting conflict: the production of vulnerability in northern Guinea-Bissau, West Africa. J Peasant Stud 50, 315–338. https://doi.org/10.1080/03066150.2021.1996355

Temudo, M.P., Cabral, A.I.R., Reis, P., 2022. The Sea Swallowed our Houses and Rice Fields: The Vulnerability to Climate Change of Coastal People in Guinea-Bissau, West Africa. Hum Ecol 50, 835–850. https://doi.org/10.1007/s10745-022-00352-2

Teutschbein, C., Seibert, J., 2012. Bias correction of regional climate model simulations for hydrological climate-change impact studies: Review and evaluation of different methods. J Hydrol (Amst) 456–457, 12–29. https://doi.org/10.1016/j.jhydrol.2012.05.052

The Republic of Guinea-Bissau, 2018. Framework Convention on Climate Change. National Communication. Bissau, Guinea Bissau.

USDA, 2024. Guinea-Bissau Rice Area, Yield and Production [WWW Document]. International Production Assessment Division. URL https://ipad.fas.usda.gov/countrysummary/Default.aspx?id=PU&crop=Rice (accessed 12.25.24).

van Genuchten, M.Th., 1997. A Numerical Model for Water and Solute Movement in and below the Root Zone. U.S. Salinity Laboratory, USDA, ARS, Riverside, California.

van Genuchten, M.Th., 1980. A Closed-form Equation for Predicting the Hydraulic Conductivity of Unsaturated Soils. Soil Science Society of America Journal 44, 892–898. https://doi.org/10.2136/sssaj1980.03615995004400050002x

Van Ghent, P.A.M., Ukkerman, R., 1993. The Balanta rice farming system in Guinea Bissau, Projet PRIVAT. WUR, Wageningen, The Netherlands. https://doi.org/http://content.alterra.wur.nl/Internet/webdocs/ilri-publicaties/publicaties/Pub53/pub53-h6.pdf

Xu, X., Huang, G., Sun, C., Pereira, L.S., Ramos, T.B., Huang, Q., Hao, Y., 2013. Assessing the effects of water table depth on water use, soil salinity and wheat yield: Searching for a target depth for irrigated areas in the upper Yellow

River basin. Agric Water Manag 125, 46–60. https://doi.org/10.1016/j.agwat.2013.04.004

Yu, Q., Kang, S., Hu, S., Zhang, L., Zhang, X., 2021. Modeling soil water-salt dynamics and crop response under severely saline condition using WAVES: Searching for a target irrigation volume for saline water irrigation. Agric Water Manag 256, 107100. https://doi.org/10.1016/j.agwat.2021.107100

Zeng, L., Lesch, S.M., Grieve, C.M., 2003. Rice growth and yield respond to changes in water depth and salinity stress. Agric Water Manag 59, 67–75. https://doi.org/10.1016/S0378-3774(02)00088-4

References for Chapter 7

Andreetta, A., Huertas, A. D., Lotti, M., & Cerise, S. (2016). Land use changes affecting soil organic carbon storage along a mangrove swamp rice chronosequence in the Cacheu and Oio regions (northern Guinea-Bissau). Agriculture, Ecosystems & Environment, 216, 314–321. https://doi.org/10.1016/j.agee.2015.10.017

Byrd, R. H., Lu, P., Nocedal, J., & Zhu, C. (1995). A Limited Memory Algorithm for Bound Constrained Optimization. SIAM Journal on Scientific Computing, 16(5), 1190–1208. https://doi.org/10.1137/0916069

Céspedes, J., Garbanzo, G., Cabral, A., Temudo, M., & Campagnolo, M. (2025). An approach to monitoring rice development in the mangrove swamp rice production system of Guinea-Bissau. (Submitted to Science of The Total Environmental). Science of The Total Environmental.

D'Amico, M. E., Barbieri, M., Khair, D. A. El, & Comolli, R. (2024). Mangrove rice productivity and pedogenic trends in Guinea Bissau, West Africa. Journal of Soils and Sediments, 24(1), 244–258. https://doi.org/10.1007/s11368-023-03608-6

Fayrap, A., & Koç, C. (2012). Comparison of Drainage Water Quality and Soil Salinity in Irrigated Areas with Surface and Subsurface Drainage Systems. Agricultural Research, 1(3), 280–284. https://doi.org/10.1007/s40003-012-0032-8

Guei, R. G., Dixon, C. A., & Sampong, M. A. (1997). Strategies and approaches to mangrove swamp rice varietal improvement in West Africa. African Crop Science Journal, 5(2), 209–217. https://doi.org/10.4314/acsj.v5i2.27863

Kaplan, G., Gašparović, M., Alqasemi, A. S., Aldhaheri, A., Abuelgasim, A., & Ibrahim, M. (2023). Soil salinity prediction using Machine Learning and Sentinel – 2 Remote Sensing Data in Hyper – Arid areas. Physics and Chemistry of the Earth, Parts A/B/C, 130, 103400. https://doi.org/10.1016/j.pce.2023.103400

Merkohasanaj, M., Cortez, N., Goulao, L., & Andreetta, A. (2022). Characterisation of physical-chemical and fertility dynamics of mangrove soils from Guinea-Bissau in different agroecological conditions underlying paddy rice cultivation ao cultivo do arroz. Revista de Ciencias Agrarias, 45(4), 267–271. https://doi.org/https://doi.org/10.19084/rca.28424

Merkohasanaj, M., Garbanzo, G., Cortez, N., Jose, F., Peinado, M., Andreetta, A., & Cunha-Queda, C. (2025). Soil physicochemical characterization and suitability assessment for the coastal mangrove swamp rice production system in Guinea-Bissau (Sumited to Catena). Catena. www.malmon-desira.com

Minhas, P. S., Ramos, T. B., Ben-Gal, A., & Pereira, L. S. (2020). Coping with salinity in irrigated agriculture: Crop evapotranspiration and water management

issues. Agricultural Water Management, 227(May 2019), 105832. https://doi.org/10.1016/j.agwat.2019.105832

Paredes, P., Fontes, J. C., Azevedo, E. B., & Pereira, L. S. (2018). Daily reference crop evapotranspiration with reduced data sets in the humid environments of Azores islands using estimates of actual vapor pressure, solar radiation, and wind speed. Theoretical and Applied Climatology, 134(3–4), 1115–1133. https://doi.org/10.1007/s00704-017-2329-9

Paredes, P., & Pereira, L. S. (2019). Computing FAO56 reference grass evapotranspiration PM-ETo from temperature with focus on solar radiation. Agricultural Water Management, 215, 86–102. https://doi.org/10.1016/j.agwat.2018.12.014

Paredes, P., Pereira, L. S., Almorox, J., & Darouich, H. (2020). Reference grass evapotranspiration with reduced data sets: Parameterization of the FAO Penman-Monteith temperature approach and the Hargeaves-Samani equation using local climatic variables. Agricultural Water Management, 240, 106210. https://doi.org/10.1016/j.agwat.2020.106210

Ramos, T. B., Darouich, H., Oliveira, A. R., Farzamian, M., Monteiro, T., Castanheira, N., Paz, A., Alexandre, C., Gonçalves, M. C., & Pereira, L. S. (2023). Water use, soil water balance and soil salinization risks of Mediterranean tree orchards in southern Portugal under current climate variability: Issues for salinity control and irrigation management. Agricultural Water Management, 283, 108319. https://doi.org/10.1016/j.agwat.2023.108319

Ramos, T. B., Gonçalves, M. C., & van Genuchten, M. Th. (2024). Soil salinization in Portugal: An in-depth exploration of impact, advancements, and future considerations. Vadose Zone Journal, 23(4). https://doi.org/10.1002/vzj2.20314

Sonmez, S., Buyuktas, D., Okturen, F., & Citak, S. (2008). Assessment of different soil to water ratios (1:1, 1:2.5, 1:5) in soil salinity studies. Geoderma, 144(1–2), 361–369. https://doi.org/10.1016/j.geoderma.2007.12.005

Sylla, M. (1994). Soil salinity and acidity: spatial variability and effects on rice production in West Africa's mangrove zone [Wageningen University and Research: Wageningen, The Netherlands]. https://edepot.wur.nl/202352

Sylla, M., Stein, A., van Breemen, N., & Fresco, L. O. (1995). Spatial variability of soil salinity at different scales in the mangrove rice agro-ecosystem in West Africa. Agriculture, Ecosystems & Environment, 54(1–2), 1–15. https://doi.org/10.1016/0167-8809(95)00594-I

Xiao Pang, Xinhua Jia, Thomas M DeSutter, Thomas F Scherer, Dean D Steele, & Ishara Rijal. (2010). Effect of Subsurface Drainage on Water Availability in the Red River Valley of the North. 2010 Pittsburgh, Pennsylvania, June 20 - June 23, 2010. https://doi.org/10.13031/2013.30017

Yang, H., Wang, Z., Cao, J., Wu, Q., & Zhang, B. (2023). Estimating soil salinity using Gaofen-2 imagery: A novel application of combined spectral and textural

features. Environmental Research, 217, 114870. https://doi.org/10.1016/j.envres.2022.114870

Zhao, W., Ma, F., Yu, H., & Li, Z. (2023). Inversion Model of Salt Content in Alfalfa-Covered Soil Based on a Combination of UAV Spectral and Texture Information. Agriculture, 13(8), 1530. https://doi.org/10.3390/agriculture13081530